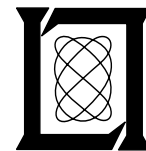# Description and Performance Evaluation of the Moving Target Detector

**L. Cartledge
R. M. O'Donnell**

8 March 1977

Lincoln Laboratory

MASSACHUSETTS INSTITUTE OF TECHNOLOGY

LEXINGTON, MASSACHUSETTS

1. Report No. FAA-RD-76-190	2. Government Accession No.	3. Recipient's Catalog No.	
4. Title and Subtitle Description and Performance Evaluation of the Moving Target Detector		5. Report Date 8 March 1977	
		6. Performing Organization Code	
7. Author(s) L. Cartledge R. M. O'Donnell		8. Performing Organization Report No. ATC-69	
9. Performing Organization Name and Address Massachusetts Institute of Technology Lincoln Laboratory Post Office Box 73 Lexington, Massachusetts 02173		10. Work Unit No. (TRAIS)	
		11. Contract or Grant No.	
		13. Type of Report and Period Covered	
12. Sponsoring Agency Name and Address Department of Transportation Federal Aviation Administration Systems Research and Development Service Washington, D. C. 20591		Final Project Report	
		14. Sponsoring Agency Code	

15. Supplementary Notes

16. Abstract

Under FAA sponsorship, MIT, Lincoln Laboratory has developed new techniques which significantly enhance automated aircraft detection in all forms of clutter. These techniques are embodied in a digital signal processor called the Moving Target Detector (MTD). This processor has been integrated into the ARTS-III system at the National Aviation Facilities Experimental Center, Atlantic City, New Jersey (NAFEC) and has undergone testing during the summer of 1975. This report contains a description of the MTD design and its evaluation tests. A detailed discussion of the significance of the results is also presented.

The detection performance of the MTD was excellent in the clear, in rain and ground clutter, and false alarms were under complete control. The MTD processed range and azimuth data was very accurate, and the MTD did not suffer from track dropouts as did the conventional MTI when the aircraft track became tangential to the radar. Performance was excellent on magnetron as well as klystron-type radars with the exception of second-time-around clutter cancellation.

17. Key Words Air Traffic Control Doppler Processor Radar Signal Processor Moving Target Indicator Moving Target Detection Adaptive Thresholding Airport Surveillance Radar	18. Distribution Statement Document is available to the public through the National Technical Information Service, Springfield, Virginia 22151.

19. Security Classif. (of this report) Unclassified	20. Security Classif. (of this page) Unclassified	21. No. of Pages 224	

Form DOT F 1700.7 (8-72)   Reproduction of completed page authorized

TABLE OF CONTENTS

iii

LIST OF ILLUSTRATIONS

DESCRIPTIOM'AND PERFORMANCE EVALUATION OF THE MOVING TARGET DETECTOR

I. INTRODUCTION

Utilization of primary radar data in the FAA automated air traffic control system has been impeded by the inability of existing signal processors to reliably detect aircraft in regions of strong ground and precipitation clutter, particularly when the aircraft are moving tangentially to the radar. During the past four years, under FAA sponsorship, M.I.T. Lincoln Laboratory has developed new techniques which significantly enhance automated aircraft detection in all forms of clutter. These techniques are embodied in a digital signal processor called the Moving Target Detector (MTD). This processor has been integrated into the ARTS-III system at the National Aviation Facilities Experimental Center, Atlantic City, New Jersey (NAFEC) and has undergone careful testing during the summer of 1975.

The purpose of these tests was to confirm the suitability of the MTD radar processor in automated and manual terminal radar control systems. Measurements included:

(1) Collection of false alarm and detection statistics using calibrated coherent signal generators.

(2) Measurements of the MTI improvement factor and radar sensitivity in the presence of ground and weather clutter.

(3) Measurement of blip-scan ratios and position reporting accuracies in flight tests using controlled aircraft in various clutter environments.

An ideal primary radar sensor for a terminal radar control system allows automatic radar-only acquisition and tracking of all aircraft in the system's field of view. Such a sensor should provide'consistent, reliable detection of small low-flying aircraft and should do this in all expected clutter conditions. Departures from this ideal occur when the radar sensor has inadequate subclutter visibility or produces excessive false tracks. Accordingly, these tests of the MTD were designed to measure the radar signal processor's ability to resolve aircraft from clutter backgrounds while providing adequate sensitivity in detecting small low-flying aircraft at longer ranges.

The basic approach to the test program was to make unbiased, direct comparisons between the MTD processor with its radar (a modified FPS-18) and an RVD-4 (Radar Video Digitizer) processor combined with an ASR-7 radar. The two radar systems were installed at the ASR-5 site at NAFEC and operated simultaneously by use of a diplexer through the ASR-5 antenna. Data recording and extraction, as well as operation of both systems, was done in conjunction with existing ARTS-III digital equipment.

Whenever it was both practical and meaningful, simultaneous measurements of both radars' detection and tracking performance were made against dedicated aircraft targets in various clutter environments. In order to make the comparisons easier to evaluate, free space sensitivities of the two radars were equalized.

The actual evaluation tests were preceded by an equipment check-out phase. During this phase the radars and signal processors were tested to ascertain that they met the design specifications. This equipment check-out included measurements of the radar's noise figure, power output and doppler frequency stability along with checks and adjustments of the sensitivity time control functions. The sensitivity of the radar processor was measured as a function of the ratio of signal energy-to-noise power density.

Finally, the two systems were operated simultaneously against dedicated aircraft. Specific tests were run to check the system's coverage both at high elevations and at long ranges. Other tests were flown to check position reporting accuracy. Test flights were made in various environments including clear areas, over ground clutter and areas of weather clutter. During this last evaluation phase, periodic checks of the noise figure, power and stability were made along with checks for malfunctions in digital portions of the system.

The remainder of this report is organized into four sections. Section II contains a summary of the MTD design, the test facilities and procedures and the measured MTD performance. A complete description of the MTD and the philosophy of its design is contained in Section III. Section IV presents the details of the radars used in the tests and the data collection and reduction system. A detailed description of the tests which were performed and their results are presented in Section V. A number of appendices are added for completeness.

II. SUMMARY

A. The MTD Radar System

Until the present time there has been difficulty incorporating radar data from the Airport Surveillance Radars (ASR's) into an automated environment such as the ARTS-III system. These problems have been caused by the radar's inability to reject ground clutter, precipitation clutter and angels while still maintaining good detectability on all aircraft in the desired coverage pattern. A new processor called the Moving Target Detector (MTD) has been developed. This processor makes reliable, automated aircraft detection in all forms of clutter a reality. The MTD is a special-purpose, hard-wired, digital signal processor (see Figure II-1) which provides near-optimum target detection over the entire ASR coverage out to 48 nmi. The MTD[1-3] differs from previous ASR processors in that it employs coherent linear filtering with adaptive threshalding techniques. For each scan the output of the radar receiver is sorted into approximately three million range-azimuth-velocity cells; the detection threshold of each cell is independently adjusted during each scan. The system is completely adaptive and there are no knobs or parameters to set which are time-dependent.

A block diagram of the processor is presented in Figure 11-2. The processor incorporates a digital ground clutter map which establishes the thresholds for the zero radial velocity cells. The clutter level in the ground clutter map continually adapts- to a value based on the average level in the previous eight scans (32 seconds). Thresholding against ground clutter in this manner eliminates the usual MTI blind speed at zero radial velocity and permits the detection of tangential (zero radial velocity) aircraft over clutter if they have sufficiently large cross-sections.

The non-zero radial velocity cells are thresholded using the mean level of the signals in the same velocity filter averaged over one-half mile in range on either side of the cell of interest. The echoes from weather and/or receiver noise are averaged to establish a threshold. With this method of thresholding, the radar has subweather visibility; i.e., aircraft with radial velocity different than the rain can be seen even if their returns are substantially less than the total weather returns.
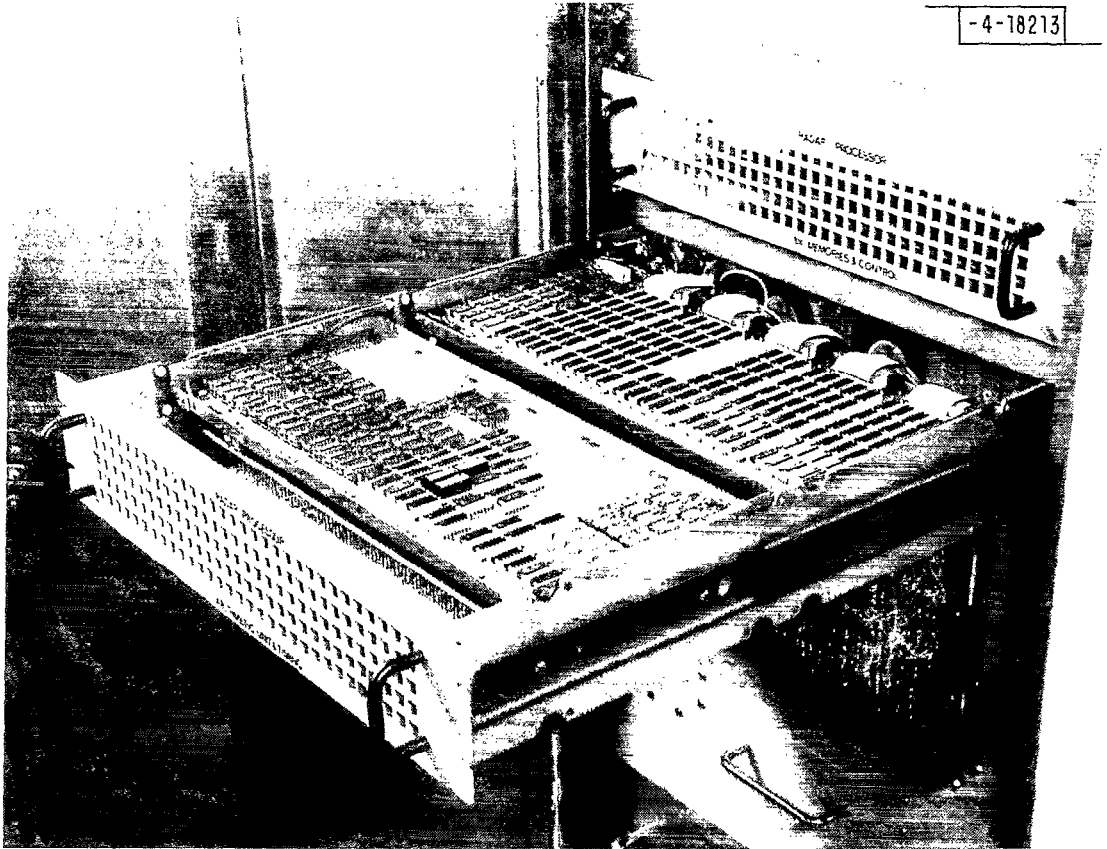
THIS PHOTOGRAPH SHOWS THE MTD PROCESSOR WITH ONE DRAWER OPEN.
THE MTD IS A HARD-WIRED, DIGITAL SIGNAL PROCESSOR WHICH UTILIZES
APPROXIMATELY 900 INTEGRATED CIRCUITS. ABOUT 450 ARE CONTAINED
IN EACH OF THE TWO DRAWERS. INCLUDING THE DISC MEMORY ON
WHICH THE GROUND CLUTTER MAP IS STORED, THE PROCESSOR OCCUPIES
A VOLUME OF ABOUT SIX CUBIC FEET.

Fig. II-1, MTD processor.
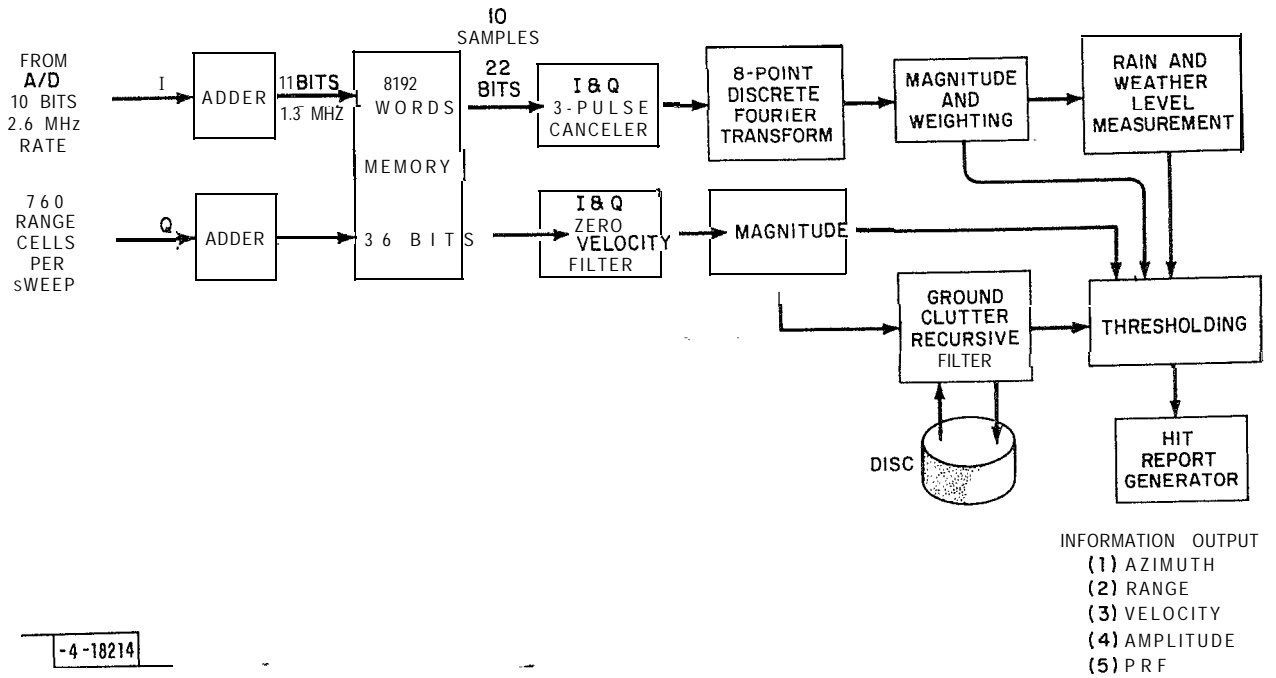
Fig. 11-2.   MTD processor block diagram.

To eliminate blind speeds the pulse repetition rate is varied for each group of 10 pulses. This technique, when used with a coherent transmitter, also eliminates second-time-around ground clutter returns.

B. Test Facilities and Instrumentation

The MTD and RVD-4 processors have been integrated into the ARTS-III system at NAFEC. There they have undergone simultaneous testing during the summer of 1975 under a variety of environmental conditions. During the series of tests, controlled aircraft were flown in the NAFEC area. The MTD was operated with an FPS-18 which is a coherent S-band radar with-properties almost the same as the coherent ASR-8, while the RVD-4 was tested with an ASR-7. The sensitivity of the ASR-7 and FPS-18 were adjusted so that both systems had equal signal-to-noise ratio per scan in receiver noise, During these tests the FPS-18 and ASR-7 were operated while sharing the same antenna; in this case an ASR-5 antenna. A block diagram of the test setup is presented in Figure 11-3. Data consisting of radar reports, beacon reports, radar/beacon correlated reports and track reports for the MTD and RVD-4 processors are output to the magnetic tapes shown in Figure II-3. Data from the test flights have been analyzed. These tests measured detection performance on controlled aircraft and false alarm performance in the clear, while flying in heavy precipitation (rain- level about 40 dB above noise level) and in ground clutter near Atlantic City, New Jersey.

C. Performance in the Clear

The false alarm performance of the MTD in Gaussian noise agrees well with extensive theoretical calculations of its performance. To illustrate the detectability of targets of opportunity in the clear, a time-exposure photograph of about 30 scans of radar data from the ARTS-III tracker is presented in Figure II-4 using data input from the MTD at NAFEC. Note the absence of false tracks. The aircraft tracks are accurate and without gaps. This is true for aircraft flying radially (see Track #1) as well as tangentially (see Track #2).

On 2 September 1975, in a two-hour test (1200 radar scans), a Piper Cherokee Arrow and an Aero Commander were flown in clutter-free regions using separate and criss-crossing paths. The MTD processed radar data displayed a measured average blip-scan ratio of .97.

6

18-4-17247

ASR-4/BEACON ANTENNA

BEACON XMTR / RCVR → BDAS

ASR-7 XMTR / RCVR → RVD-4

MODIFIED AN/FPS-18 XMTR / RCVR → MTD

A R T S III   IOP

. BEACON PROCESSOR
• RADAR CORRELATOR AND INTERPOLATOR
• R/B CORRELATOR
• TRACKER
• DISPLAY INTERFACE

DEDS

DISPLAY

MAGNETIC TAPE
MTD DATA

MAGNETIC TAPE
RVD-4 DATA
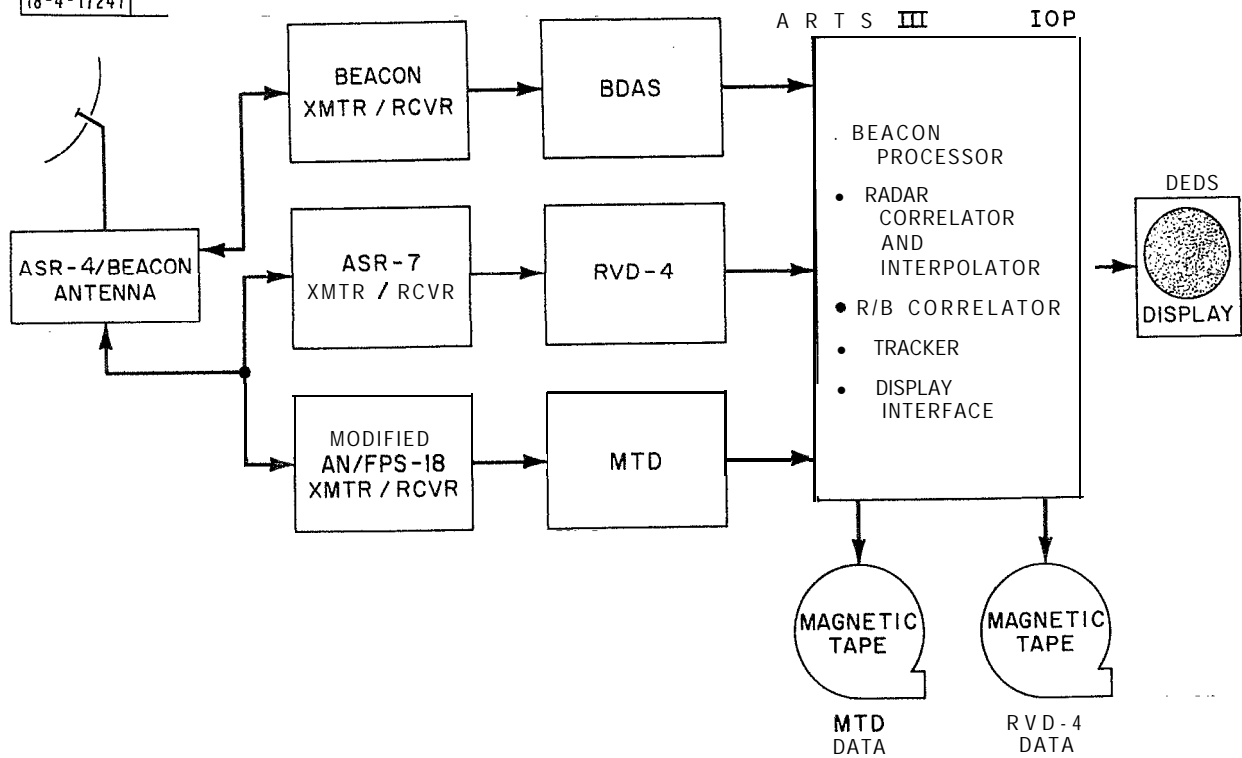
Fig. 11-3.   MTD/RVD-4 experimental test set-up.
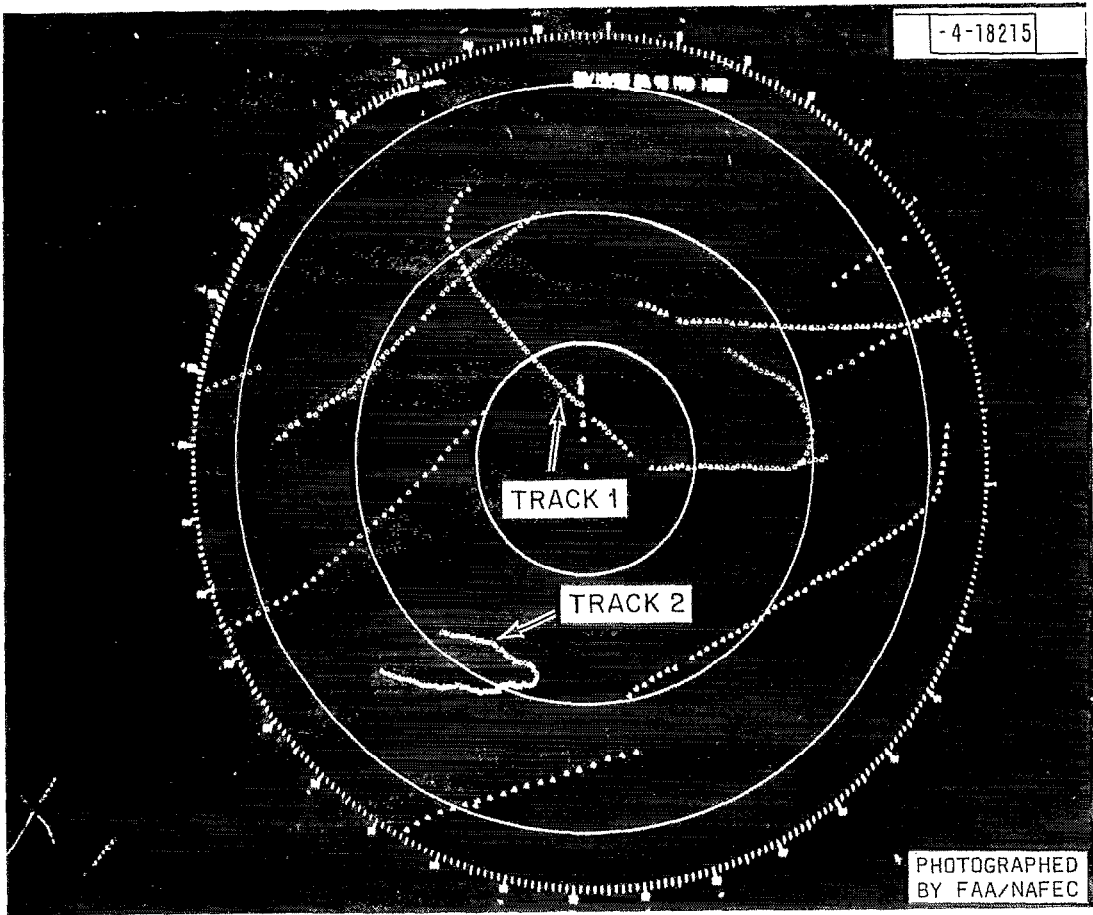
A TIME EXPOSURE PHOTOGRAPH OF ABOUT 40 SCANS OF RADAR DATA FROM ARTS-III
TRACKER IS PRESENTED USING DATA INPUT FROM THE MTD AT NAFEC. NOTE THE
ABSENCE OF FALSE AND GROUND CLUTTER DETECTIONS. THE AIRCRAFT TRACKS ARE
ACCURATE AND WITHOUT GAPS. THIS IS TRUE FOR AIRCRAFT FLYING RADIALLY (SEE
TRACK 1) AS WELL AS TANGENTIALLY (SEE TRACK 2). FIVE-MILE RANGE RINGS ARE
DISPLAYED.

Fig. 1X-4. ARTS III output using MTD processor.

The random range and azimuth error of the MTD processed radar reports was measured using the method of least squares to be $.14^{\circ}$ and .022 nmi (see Section V-H). These errors are approximately one-half of the errors measured with conventional, noncoherent radar digitizers.

D.   Performance in Ground Clutter

The MTI improvement factor of the MTD is consistent with theoretical calculations. It represents a 20-db (100 times) improvement over existing ASR radars' ability to detect aircraft in strong clutter.

On 12 August 1975 a Piper Cherokee single-engine aircraft was flown back and forth over a patch of ground clutter near Atlantic City. This ground clutter consists of some moderately distributed clutter and many very large discrete scatterers (large buildings). The 1200 scans in this two-hour flight test were examined in detail. The blip-scan ratio for the MTD was measured to be .99. A long-exposure photograph of 50 scans of ARTS-III track data is presented in Figure II-5. A digital map of the ground clutter is superimposed on the ARTS-III tracker output. During this block of data, a radar-only target of opportunity crossed back and forth over the controlled aircraft's track. Presented in Figure II-6 are 30 scan averages of the blip-scan ratio during the ground clutter test. In over 1200 scans there were only five missed detections of the test aircraft. A set of long exposure photographs of 40 *scans* of ARTS-III track data are presented in Figure II-7 with radar/beacon tracking and radar-only tracking. With or without the ATCRBS beacon data, the MTD track data is solid and accurate.

E.   MTD Performance in Rain

On 6 August 1975 a Piper Cherokee single-engine aircraft was flown in and out of heavy precipitation for about two hours ($\sim$1200 scans). The MTD radar report data had an average blip-scan ratio of .98 while the aircraft flew through the rain. In Figure II-8, nine scans of track data from the MTD are presented with the normal video superimposed to show the rain cloud's location. The strongest rain clutter return was measured to be 40 dB above the radar receiver noise level. Even in the presence of this heavy rain, the MTD detected the tangentially flying aircraft almost every scan of the radar while maintaining excellent false alarm performance. The MTD eliminated entirely the false-alarm-in-weather problem.

MTD

° RADAR/BEACON
0 RADAR ONLY
B BEACON ONLY
? COAST

TEST AIRCRAFT

TEST AIRCRAFT

-4-17826

TWO MILE RANGE RINGS
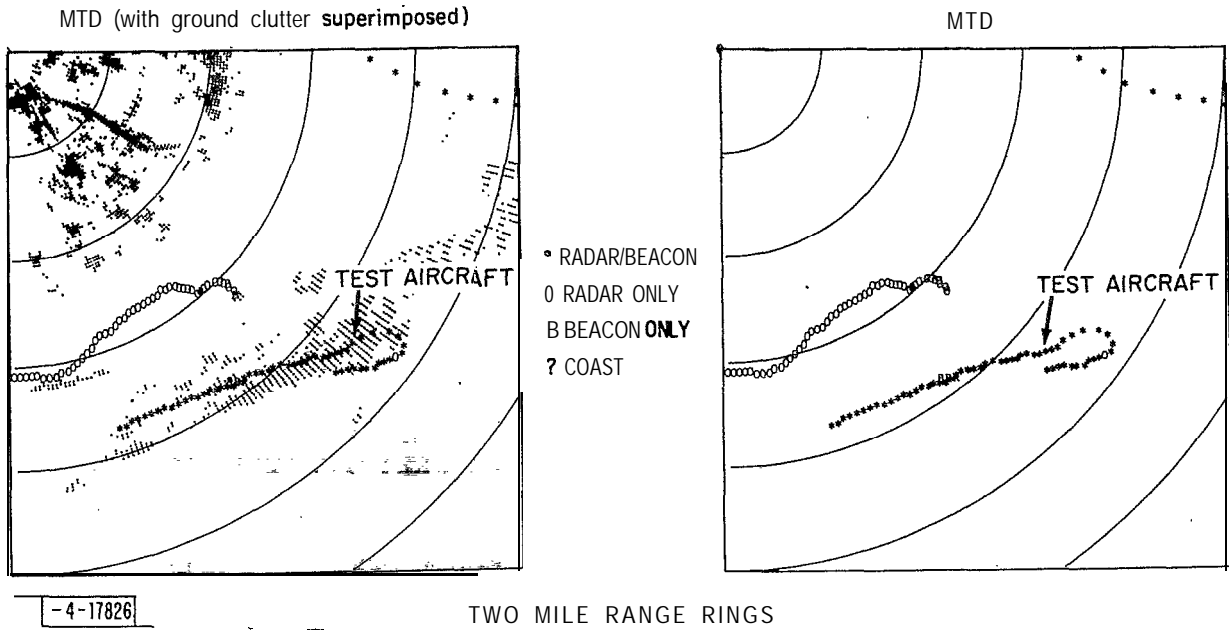
Fig. II-5. MTD tracking performance in clutter.

18-D0-11237

MTD

P_D (30 scan averages)

1.0

0.8

0.6

0

700   900   1100   1300   1500   1700   1900   2100   2300

SCAN NUMBER
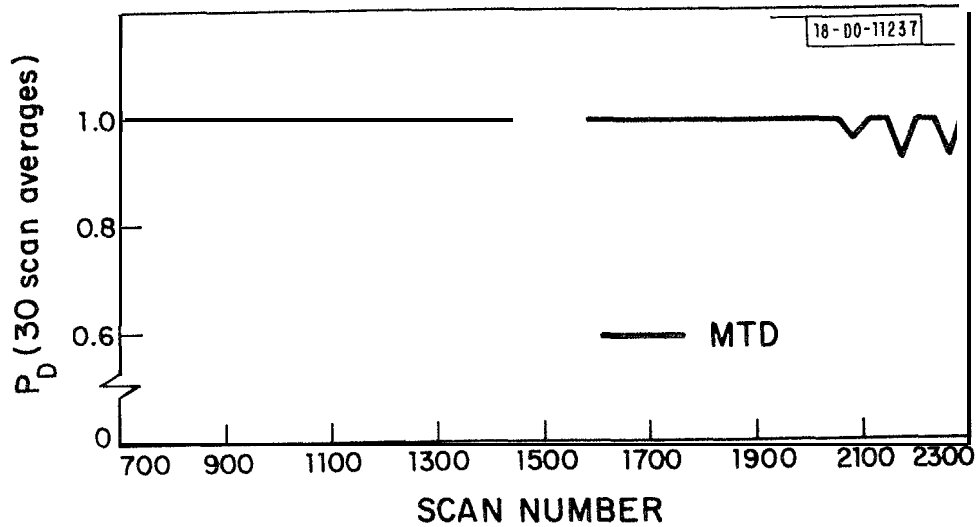
Fig. II-6. MTD blip/scan ratio during clutter test (12 August 1975).

MTD (Radar and Beacon)

MTD (Radar only)

4 NMI

6

8

10

12

5 NMI

TEST
AIRCRAFT

10 NMI

DISPLAY CODE

O RADAR ONLY
B BEACON ONLY
° RADAR AND
  BEACON
? COAST

TEST
AIRCRAFT

MTD (Radar and Beacon)

MTD (Radar only)

4NMI

6

8

10

12

5NMI

10NMI
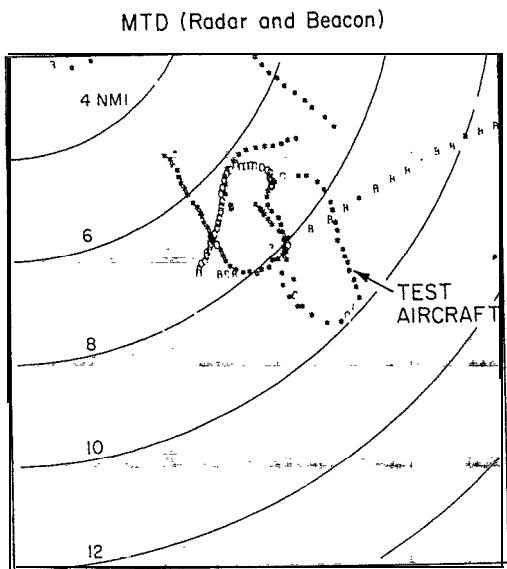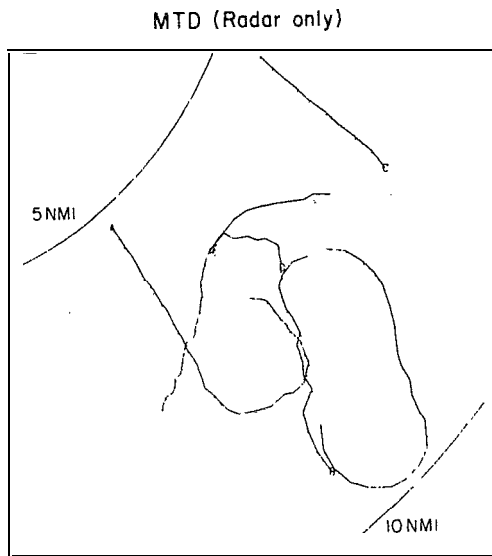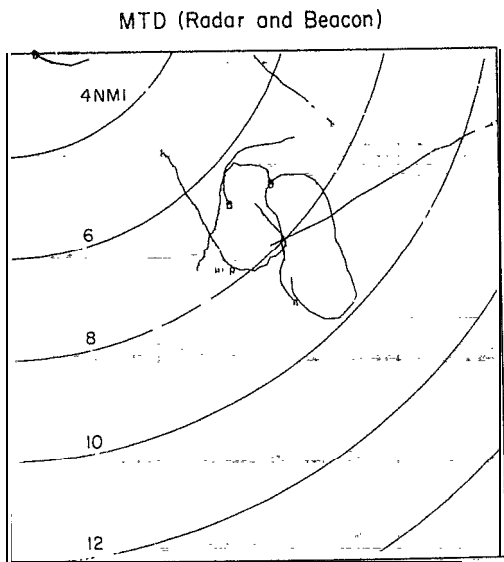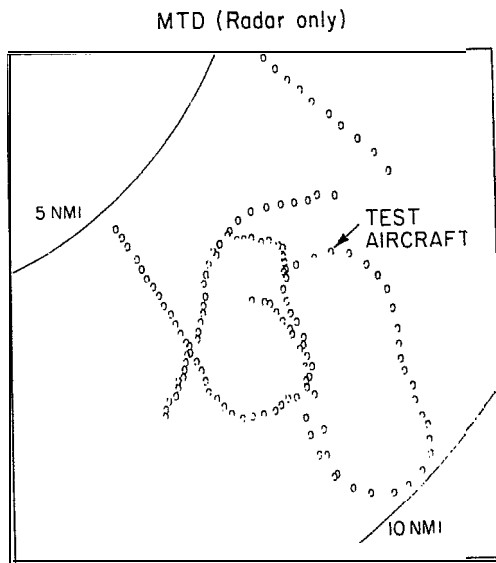
Fig . MTI-subclutter performance: radar/beacon tracking and radar only
compared.
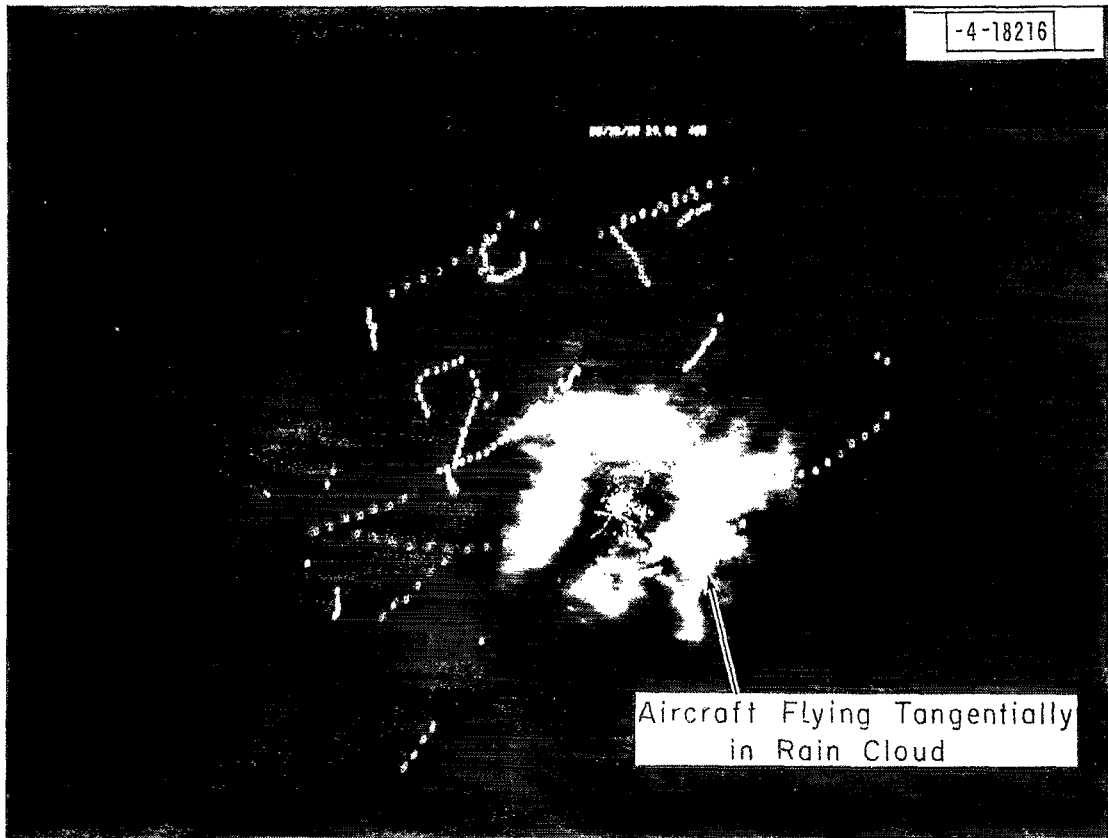
HEAVY RAIN CLUTTER FROM THE NORMAL VIDEO OF THE RADAR AT NAFEC
IS SUPERIMPOSED ON A TIME EXPOSURE PHOTOGRAPH (9 RADAR SCANS)
OF MTD/ARTS-III TRACK OUTPUT. NOTE THAT THERE ARE NO MTD FALSE
DETECTIONS CAUSED BY THE RAIN OR GROUND CLUTTER. THE AIRCRAFT
MARKED IS FLYING TANGENTIALLY IN A RAIN STORM AND IS CLEARLY
AND CLEANLY DETECTED ON EVERY SCAN OF THE RADAR.

Fig. II-8.   MTD performance in presence of rain clutter.

Most sliding-window detectors such as the RVD-4 experience an increase in false alarms in weather because the weather returns are partially correlated from pulse to pulse. Previous processors have ignored this correlation. The MTD circumvents this problem by coherent filtering so as to achieve subweather visibility on aircraft and it estimates the threshold by averaging in range over statistically independent, uncorrelated weather samples.

F.   Use of MTD with ASR-5 and ASR-7

Because of the similarity of the modified FPS-18 klystron transmitter used in these tests and the klystron transmitter used in the ASR-8, the MTD processor could be used with the coherent ASR-8 radar with only minor modifications (a different IF amplifier and 10-bit A/D converter). In addition, the MTD has been operated at NAFEC with an ASR-5 and ASR-7 transmitter. The MTD gave excellent performance with these radars after minor modifications were made to improve the radars' stability. With these noncoherent radars (ASR-5 and ASR-7) the MTD exhibits essentially the same performance as when operated with the coherent ASR-8 or FPS-18, with the exception of the cancellation of second-time-around ground clutter echoes. There is a random phase relationship between the last pulse and the second-to-last pulse transmitted by a magnetron transmitter.

G.   Tangential Aircraft Detection Performance

The detection performance of the MTD was measured and found to be excellent whether the aircraft is moving radially or tangentially. The detection. of aircraft flying tangential to the radar is accomplished by the action of the adaptive zero velocity threshold and the fine grained clutter map. It is further enhanced because at broadside aspect angles, aircraft cross sections are usually 15 to 20 dB above their nose-on values. A comparison of the MTD and the ASR-7 in the MTI mode is presented in Figure II-9.

H.   Conclusions

The detection performance of the MTD is excellent in the clear, in rain and ground clutter and the false alarms are under complete control. The MTD processed range and azimuth data are very accurate and the MTD does not suffer from track dropouts that the conventional MTI does when the aircraft track is tangential to the radar. Performance is excellent on magnetron as well as klystron-type radars with the exception of second-time-around clutter cancellation.
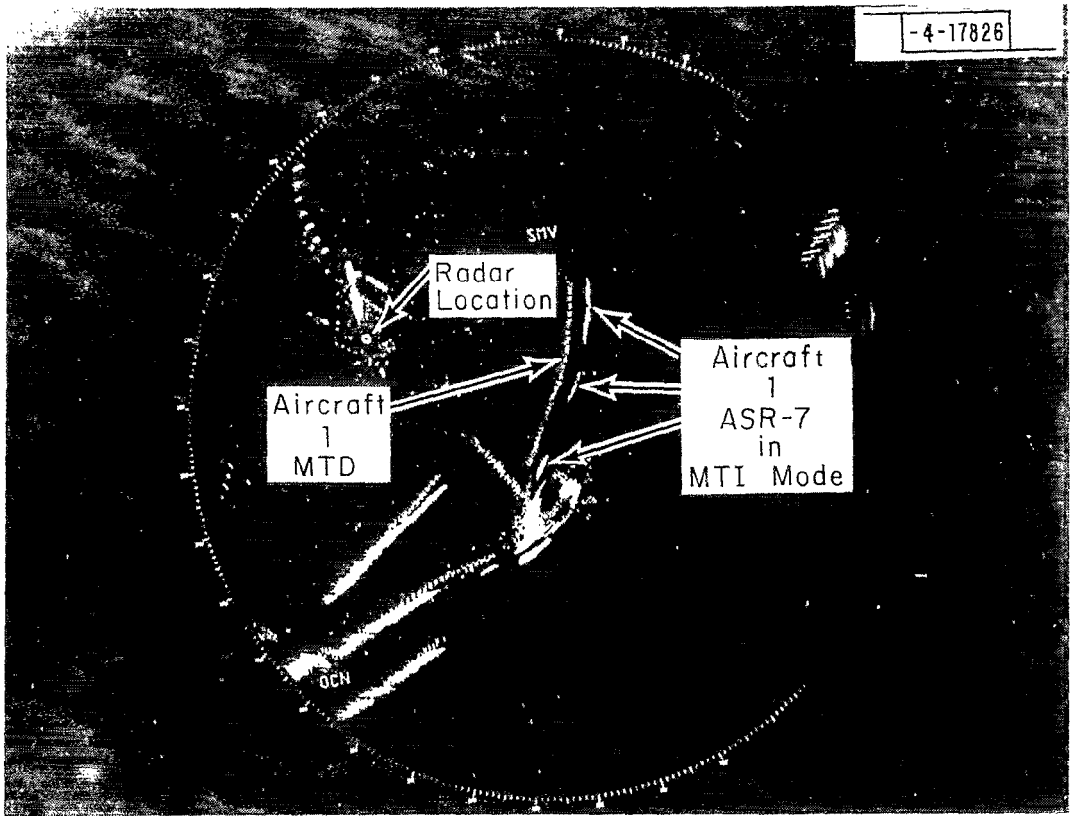
THIS LONG EXPOSURE PHOTOGRAPH SHOWS THE RELATIVE PERFORMANCE OF THE FPS-18/MTD SYSTEM AND THE ASR-7 IN THE MTI MODE. THE TWO RADARS ARE CO-LOCATED IN THE UPPER LEFT PORTION OF THE DISPLAY. THE OUTPUT OF THE TWO RADARS IS SLIGHTLY OFFSET ON THE PPI TO FACILITATE EXAMINATION OF THE TRACKS. THE MTD PROCESSOR CLEARLY DETECTS THE TANGENTIALLY FLYING AIRCRAFT (MARKED 1), WHILE THE TRACK FROM THE ASR-7 IN THE MTI MODE CONTAINS LONG GAPS WHEN THE AIRCRAFT IS IN THE ZERO RADIAL VELOCITY NOTCH OF THE MTI CIRCUIT. SINCE THE RVD OPERATES ON THE MTI VIDEO DATA IT CAN-NOT PERFORM BETTER THAN THE DATA PROVIDED TO IT BY RADAR.

Fig. II-9. Comparison of MTD with ASR-7 in MTI mode.

Finally, work is underway on a second generation Moving Target Detector with similar signal processing algorithms but with digital implementation techniques which are optimized for operational use.   This MTD-II will use parallel structure and be microprogrammable.   Its design will be detailed in future reports.

III. <u>DESCRIPTION OF THE MTD AND THE PHILOSOPHY OF ITS DESIGN</u>*

    A.   <u>Introduction</u>

    Airport Surveillance Radars (ASR's) generally give good service in a manual control environment. However, until the present time there has not been a "solution" to the problem of providing high probability of detection with low false alarm rate in an automated aircraft surveillance system. The principal difficulties are an excessive number of false alarms, which will overload the automation computers of the ARTS-III system, and aircraft detection which is so spotty that the computer cannot make long continuous tracks of all aircraft.

    To be truly useful any solution which is chosen must work not only when a single type of clutter or background is present, but also when several types of clutter are present simultaneously; for example, both in ground clutter and precipitation. In addition, the false alarms sent to the tracker must be spatially and temporally uncorrelated, or even a relatively small number of false alarms will give rise to an excessive false track rate out of the tracking computer.

    We will discuss the basic radar problems along with the techniques to solve them and, finally, describe the MTD (Moving Target Detector) digital signal processor whose design incorporates features which attack all of the radar problems simultaneously.

    B.   <u>Radar Problems and Solutions</u>

    The poor performance previously mentioned is due to competition of aircraft returns with the so called "clutter" returns and the response, of the circuits used in the radar to overcome these clutter returns. It is convenient to classify the problems according to the types of the return. These problems are fixed ground clutter, second-time-around ground clutter, precipitation clutter, angels and surface vehicles, and interference from other radars.

    1.   <u>Fixed Ground Clutter</u>

    By far the largest undesired radar reflections come from fixed objects on the ground. Ground clutter usually extends out to about 20 nmi. In very hilly or mountainous areas it may extend out to the maximum radar range ($\sim$60 nmi). In ASR radars its natural or intrinsic spectrum is very narrow compared to the spectral spread caused by antenna scanning motion.

---

*Portions of this section are taken from References 1, 2, and 3.

Ground clutter varies appreciably from spot to spot in the area of coverage. Typical distributions of the mean backscatter coefficient σ_o are shown in Figure 111-1. It tends to be highest from cities.

In the present ASR radars, ground clutter is reduced by three mechanisms: MTI filtering, antenna tilt and by mounting the antenna close to the ground to take advantage of the shielding effect of nearby objects. Figure III-2 shows the MTI filtering performance achievable using two cascaded delay line cancellers with and without limiting. Previous ASR radars have all employed limiting in the IF followed by a phase detector. The purpose of the limiting is to normalize the video output so that clutter residue from the MTI filter is reduced to the average noise level. This allows the video gain to be adjusted so the clutter will not show up on the controller's scope. Unfortunately, this limiting action spreads the clutter spectrum so that considerably poorer subclutter visibility (SCV) is achieved than if the normalization had been done by some other mechanism not involving nonlinearities.

If we consider the parameters of a typical terminal radar (ASR-7, see Table III-1) at 15 nmi and σ_o from Figure III-1 that is exceeded only 5 percent of the time, we find that for a 1 m^2 target (typical small aircraft) the input signal-to-clutter ratio is -31 dB. Since an output signal-to-clutter ratio of about 15 dB is needed for-adequate target visibility, an improvement factor of about 46 dB is required. We see from Figure III-2 that this is not achievable with the present configuration. It is, thus, common practice to achieve greater signal-to-clutter advantage by tilting the antenna upward (see Figure III-3) by 2° to 5° depending on the local clutter situation. If tilted, as shown in Figure III-3, there is a 17-dB advantage (maximum range divided by zero elevation range to the fourth power) in input signal to clutter for an aircraft flying in the peak of the antenna pattern. This advantage is degraded as the aircraft gets out of the peak of the antenna patterns so that, typically, detection gets spotty due to competition with ground-clutter for small aircraft below about 1.5^o or above 9°. These angles change depending on the antenna tilt and ground clutter intensity.

Another undesirable feature of the improvement curves in Figure III-2 is the very wide notch around the blind speeds. The effects of higher order blind speeds are usually reduced by using a staggered PRF. However the wide notch around zero
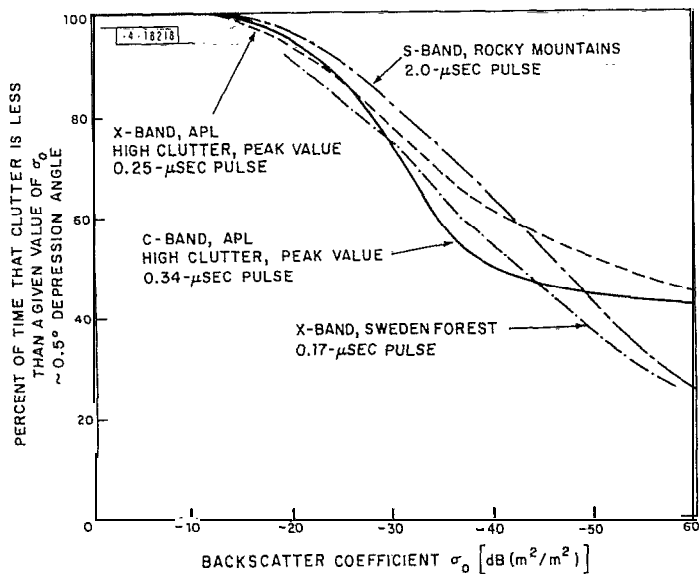
Fig. 111-1. Land clutter backscatter distribution from surface radars (from Reference 4).
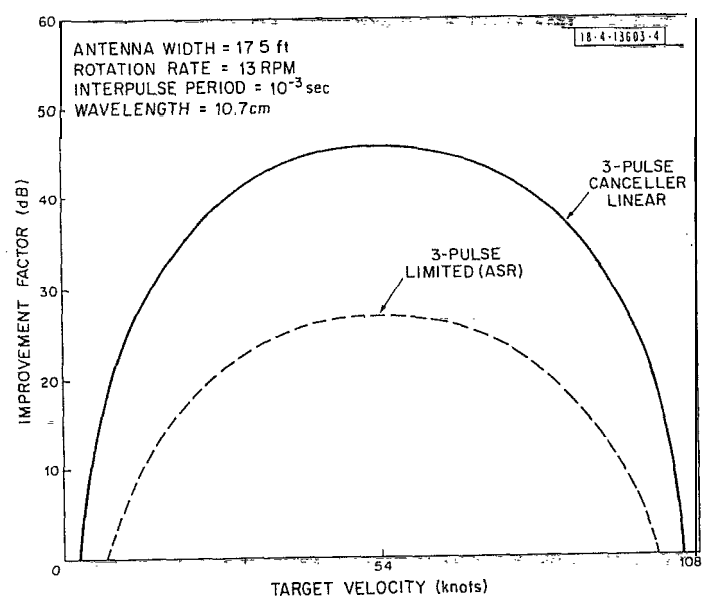
Fig. III-2. Performance of S-Band 3-pulse cancellers.
(Improvement factor is the ratio of signal-to-clutter out of the canceller to signal-to-clutter in. The latter ASR radars use 3-pulse cancellers following a limiter shown above by the curve "3-pulse limited (ASR)").

18
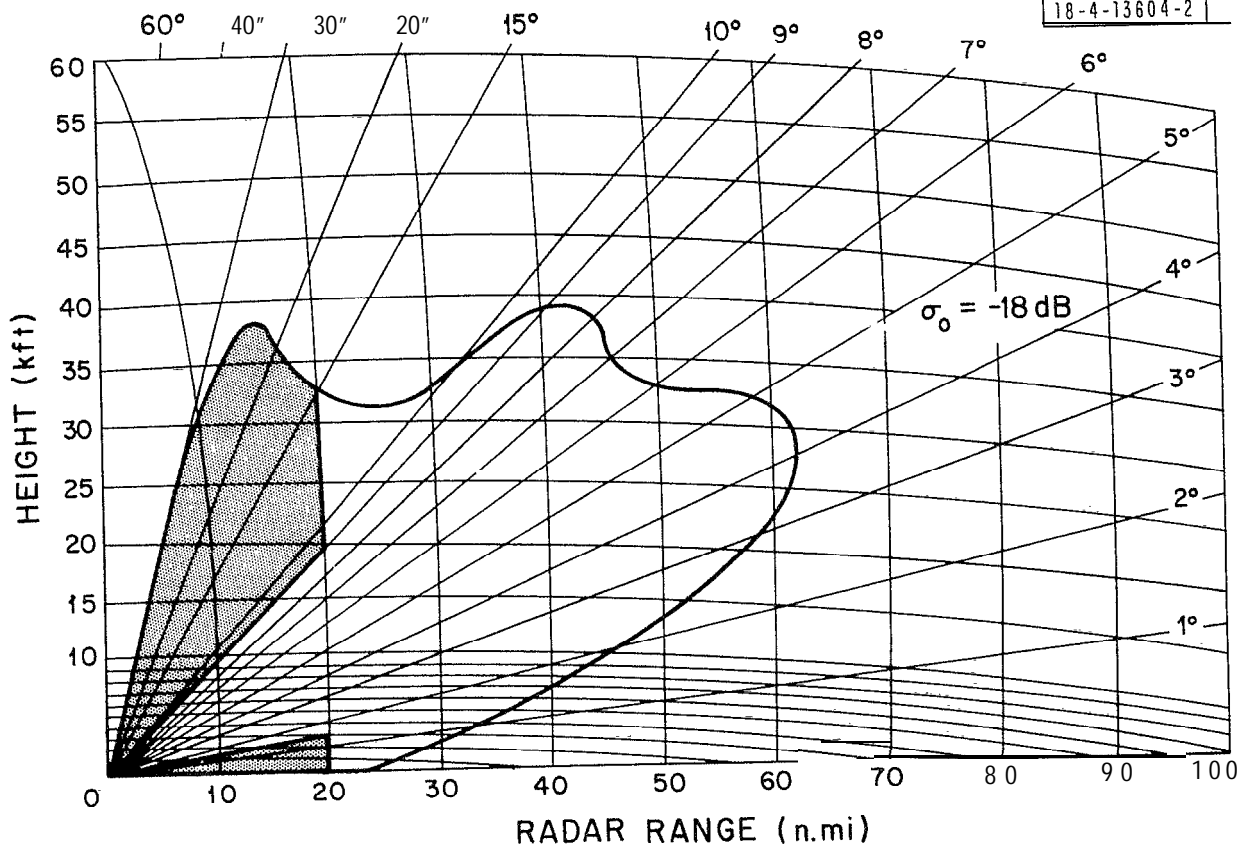
Fig. III-3. Coverage of ASR-7 radar against a 2-M^2 target.

means that targets will be lost for a considerable distance on the scope when the aircraft flies tangential to the radar. The 3-pulse canceller with limiting is worse in this respect than the 2-pulse canceller with limiting.

A further limitation in performance of existing ASR's is the presence at many sites of buildings or hills which limit the minimum elevation visible to the radar. Increasing the height of the antenna to overcome this limitation causes an undesirable increase in ground clutter level which could be overcome by improvement in SCV.

To give complete flexibility in siting and tilting the antenna while still rejecting ground clutter, an approximate 20-dB improvement in performance over that of existing ASR radars-is needed. It is obvious that this requires linear processing of clutter and target signals. Hence, one must avoid all nonlinearities in the receiver. To narrow the blind speed region, one should process coherently groups of many pulses.

In order to assess quantitatively what could be considered a "good" MTI Processor for improving the performance of ASR radars against fixed ground clutter, calculations were made of the performance of the so called "optimum processor". Given the initial conditions, the optimum processor has by definition the highest improvement in target-to-interference (interference is defined as clutter plus front-end noise) ratio of any processor, By knowing the performance of such a processor, one can judge how closely any other (i.e., suboptimum) processor approaches the theoretical limit,

The processor considered here can be defined as a device that takes M complex signal returns V_i, multiplies these returns by a complex filter weight $\bar{W}_i$, adds them and then takes the square of the amplitude

$$R = \left| \sum_{i=1}^{M} \bar{W}_i \, V_i \right|^2$$

V_i is composed of target, noise and clutter. The theory of optimization will not be shown here but follows that of DeLong and Hofstetter[11]. The clutter spectrum, which in this case is essentially all caused by the antenna scanning motion, is modeled by an antenna having a Gaussian beam shape as in Emerson[12].

Figure III-4 shows the target-to-interference improvement in decibels that is possible (optimum) for the mechanically rotating ASR antenna whose parameters are given in Table 111-1. These results assume the use of a sufficiently stable coherent transmitter. Results. almost this good have been obtained in tests using the magnetron-type transmitters in the ASR-5 and ASR-7. These results are reported in Section V-J.

The maximum clutter-to-noise ratio which can be handled will be set by the dynamic range of available analog-to-digital converters. Under the assumption that the rms thermal noise level is set at one lsb (least significant bit) the maximum improvement ratio that can be obtained is given by the relationship

$$IR_{max} = 6(n-1) + 10 \log_{10} (N)$$

where

IR_{max} = the best obtainable improvement ratio in dB

n   = the number of bits in each of the two A/D converters used

N   = the number of radar pulses integrated per decision

Clearly,. the A/D limited level of performance will not be achieved if the analog hardware preceding the A/D converters limits the dynamic range of the system. The usable dynamic range can be reduced by nonlinearity or spurious modulations anywhere in the radar system. Usable dynamic range may also be limited by the effects of truncation or round-off in the digital computations.

The solid curve in Figure III-4 is the improvement obtained when the optimum filter is tuned to the doppler frequency of the target as the target doppler is varied. The dashed curve represents the frequency response of the particular optimum filter tuned to 300 Hz.

The following general characteristics of the optimum processor should be noted:

(a) The upper curve (Figure III-4) levels out at about M x C/N = 10^5 where M is the number of pulses processed and C/N is the clutter-to-noise ratio, unless M is small. This points up the need for wide dynamic range A/D converters as explained above.
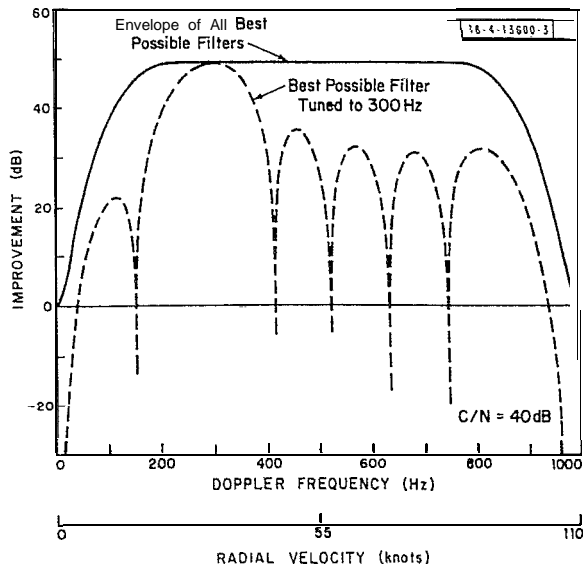
Fig. III-4. Improvement of target-to-interference ratio, scanning antenna.

TABLE III-1

ASR RADAR PARAMETERS

Antenna Width	5.25 m
Antenna Rotational Speed	1.36 m/sec
Wavelength	0.107 m
PRF	1000 pulses/sec
Number of Pulses Processed Per Look	10
Clutter-to-Noise Ratio	40 dB

(b) At the so called "blind speeds" 0 and 1000 Hz), there is no improvement but there is no deterioration either, thus, a target whose cross section is sufficiently above that of the clutter can be seen.

(c) For filters that are not tuned on or close to blind speeds, there are very deep nulls at the blind speeds.

(d) The width of the notch about the blind speeds increases with antenna rotational speed when all other parameters are held constant.

(e) The filter can be approximated by a discrete Fourier transform (DFT) only in certain special cases.

(f) Because the optimum weights, W_i, are a function of clutter-to-noise ratio, the optimum processor requires some a priori knowledge. However, this ratio can be determined in principle by the application of a proper algorithm in the receiver together with ground clutter memory from scan to scan.

In Figure III-5 we compare the optimum processor results with those of conventional MTI processors (Figure III-Z). We see that the amount of clutter rejection achieved in conventional MTI systems is far less than the best that can be done.

The implementation of the optimum processor for every range-azimuth cell calls for M complex multiplications for each target velocity examined. Usually, if M pulses are being processed, a filter bank with M filters will give adequate coverage for all target velocities. Thus, M^2 complex multiplications must be performed for every range cell. For a typical ASR, 800 range cells per sweep must be sampled on 10 sweeps and processed every 10 ms. If optimum filters were used, 8,000,000 complex multiplications per second would be required or 32 million simple multiplications.

A simpler processor can be built. The optimum processor can be broken into two parts; a clutter filter followed by a target filter. The filter used to reduce clutter multiplies the signal vector by the antenna weighting and by the inverse of the interference covariance matrix. The target filter used to enhance the target is a DFT. The near-optimum processor could consist of a digital filter which approximates as closely as possible the frequency response of the clutter filter followed by a DFT for the target filter. This combination gives an improvement factor within a few decibels of the optimum shown in Figure III-4 and
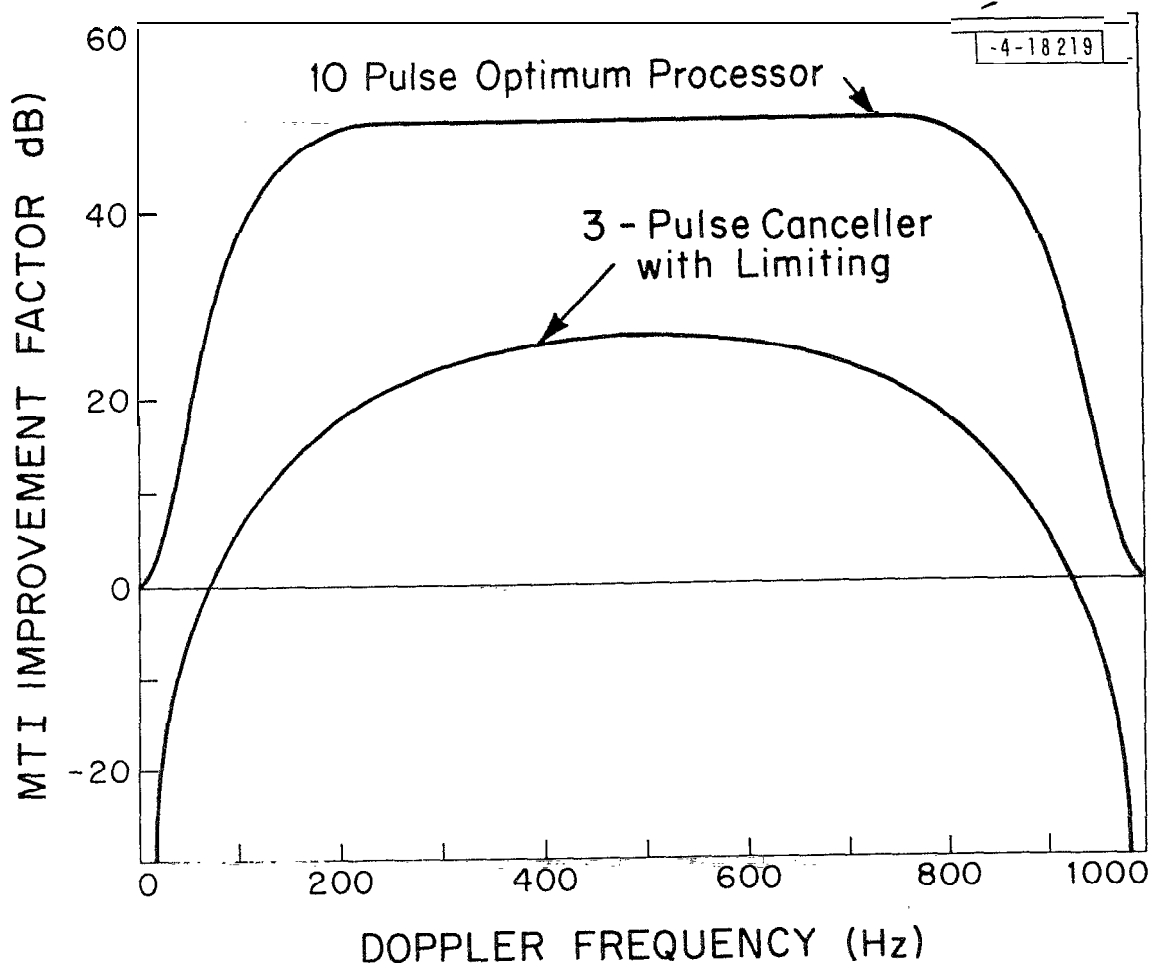
Fig. III-5. Comparison of optimum processor with conventional 3-pulse canceller.

is much less complex than implementation of the optimum processor. It should be noted that either processor provides target doppler information.

Through direct comparison it has been found that a simple three-pulse canceller without feedback forms the clutter filter portion of a near-optimum processor for the scanning antenna.

The near-optimum ground clutter processor would not be complete without adequate thresholding. For a typical ASR utilizing a near-optimum processor, ground clutter will appear only in the zero doppler filter and the filters immediately adjacent on each side. Geometrically ground clutter is very heterogeneous in character. It varies greatly in size from one resolution cell to the next. Thus, averaging nearby cells will not give a good estimate for thresholding purposes. A practical way to accurately set ground clutter thresholds is to use a digital ground clutter map which remembers the ground clutter in every range-azimuth resolution cell averaged over a sufficient time period (number of scans). Whenever an aircraft's cross section is sufficiently larger than the clutter over which it is flying, it will be seen even if it has zero radial velocity (tangential target).

2.   Second-Time-Around Ground Clutter

The so called "second-time-around" clutter effect is caused by radar returns from ground clutter which is illuminated by the next-to-last radar pulse which was transmitted. This ground clutter is beyond the unambiguous range of the radar. These returns are prevalent where conditions of anomalous propagation exist such that the radar waves intercept the ground at great distances (greater than that corresponding to the interpulse period). This effect is also prevalent in mountainous regions where clutter normally extends beyond the unambiguous range.

The presently deployed ASR 3,4,5,6 and 7's use magnetron transmitters which transmit pulses with random phase from pulse to pulse. With this type of radar it is impossible to maintain the phase relation between the first- and second-time-around clutter returns and the two cannot be filtered out simultaneously.

Further, the present ASR's use pulse trains with staggered interpulse periods so as to avoid blind speeds. This causes the second-time-around clutter return to

25

fall in different-range cells on succeeding returns so there is no hope of filtering it out. To effectively filter out second-tine-around clutter, a fully coherent transmitter (one coherent from pulse to pulse) and a constant PRF must be used. The PRF need not be constant forever, but only over an interval sufficient to collect a group of pulses for processing. If the PRF is changed from group to group of pulses, the radar is said to use "multiple PRF".

The ASR-8, which will be entering service soon, has a klystron transmitter that transmits pulses which are coherent from pulse to pulse. Thus, if a "multiple PRF were used with the ASR-8, second-time-around ground clutter could be filtered out adequately. This will be the *case* when MTD processors are used with the ASR-8's.

3. Precipitation Clutter

The backscatter from precipitation has been studied extensively. Figure III-6 shows the mean volume reflectivity from rain at 15 mm/hr. This is considered a heavy rain found only 0.04 percent of the tine at New Orleans[4]. This heavy rainfall is usually found only in relatively small size cells in the center of storms. The radar should be designed to reject at least this level and as much higher *a* level as possible.

Also marked on Figure III-6 is the point where the volume reflectivity is such as to cause a 1 m^2 return at 30 miles in an ASR radar (rain return from a typical cell with precipitation extending from the surface to 10,000 ft). Rain at 15 mm/hr is about 13 dB above this value. Remembering that these are average reflectivities and that ∿15 dB signal-to-noise ratio is required for automatic detection, we need about 30-dB rain rejection for good performance.

The rain clutter spectrum is spread around some mean value determined by the wind velocity. The spectral spread observed by the radar is fixed by wind shear conditions[4]. The standard deviation of the rain velocity spectrum typically reaches *values* of 25 knots at 30 nni and increases with range. This spread is due chiefly to wind shear. A typical heavy rain storm spectrum is presented in Figure III-7. The center velocity of the storm may be anywhere from -60 to +60 knots depending on wind conditions relative to the pointing direction of the antenna. Because the mean velocity of the storm is not centered at zero radial velocity for most-antenna azimuths, the storm return will leak through the MTI filter for many azimuth angles of the antenna.

26
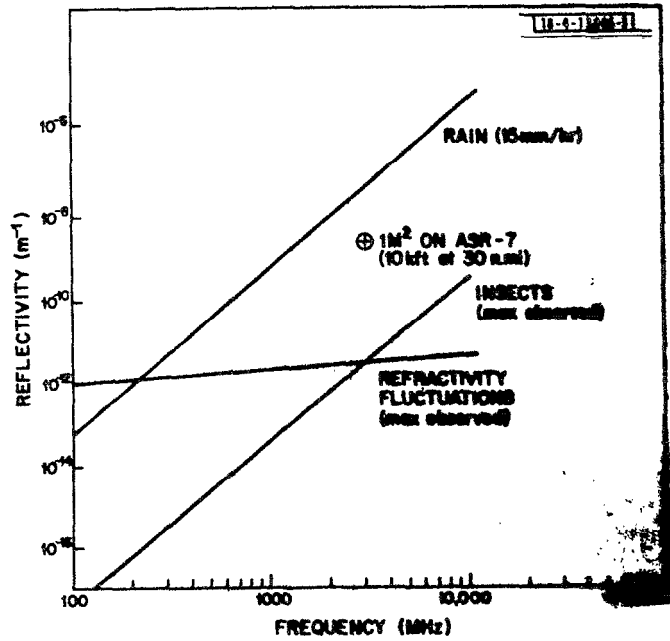
Fig. III-6. Reflectivity of various moving clutter sources.
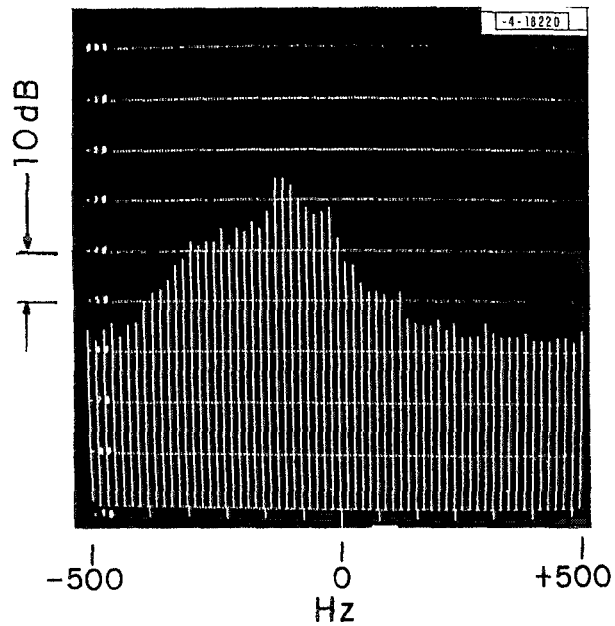
Fig. III-7. Typical spectrum from a heavy rainstorm taken using an S-Band radar (receiver noise level is -57 dB).

27

Circular polarization is normally used to reduce rain clutter by about 15 dB while reducing the aircraft signal level to a much lesser extent. The use of MTI helps reduce rain clutter except when the antenna is looking toward or away from the wind direction. In these directions the rain clutter spectrum is such that all of the rain clutter signals may pass through the MTI filters.

Log-FTC-antilog circuits[5,6] reduce the receiver gain in proportion to the average level of rain clutter for about a mile in range surrounding the cell of interest. This normalizes the rain clutter level, just as limiting is used to normalize ground clutter, at the output of the MTI circuit. Its purpose is to suppress the rain clutter on the scope. At the same time, of course, it suppresses the signal. For adequate detection, the signal amplitude must be appreciably above the clutter residue from the MTI filters.

Previous attempts to build a digitizer which works well in rain have failed due to a lack of recognition of the correlation properties of the clutter. Rain clutter signals are partially correlated from pulse to pulse so that noncoherent integration in the azimuth direction produces random signals whose variance is much greater than if the rain signals were noise-like[4] (uncorrelated). This greater variance requires a large increase in the detection threshold over that set for noise and a consequent loss in detectability of aircraft targets. If the threshold is not reset, a high false alarm rate in rain results. A typical correlation time for a rain storm is about 2 to 3 msec at S-band. This means that the coherent integration time should be significantly greater than 2 or 3 msec. This will insure that, after coherent integration, multiple threshold crossings from the same target may be added noncoherently without undue loss due to partial correlation of the samples.

It is easy to show that, since the detected rain clutter residue is partially correlated from azimuth to azimuth, the statistical spread of the noncoherently added returns is much greater than from receiver noise which is uncorrelated. This is shown diagramatically in Figure III-8. If a threshold is established as some multiple of the mean of the receiver noise (see Figure III-8) the probability of false alarm will be the area under the curve above the threshold. Correlated noise such as rain changes the curve to the one marked "correlated" without a
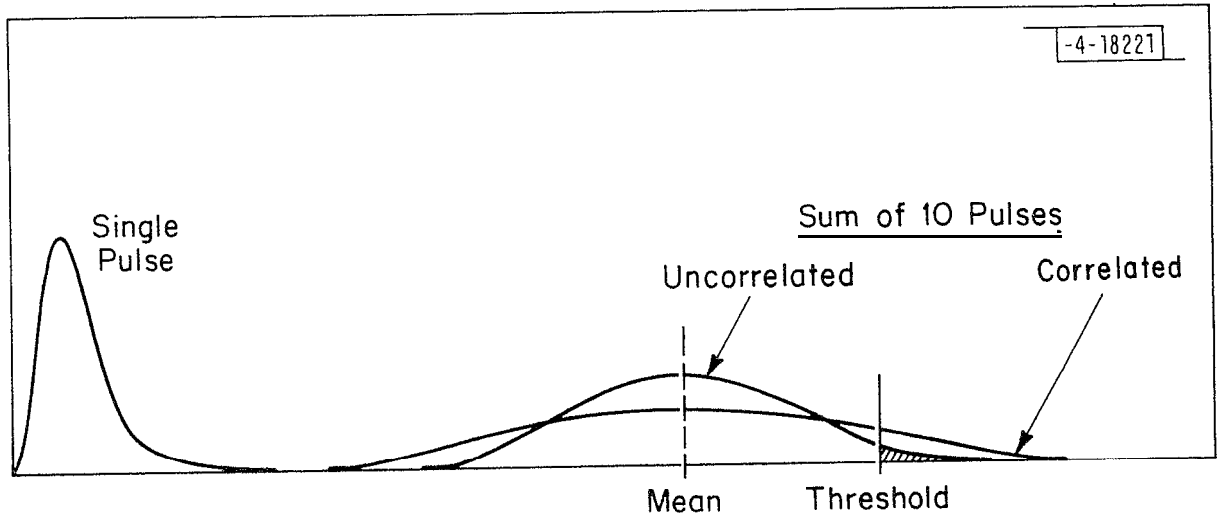
Fig. III-8. Noncoherent integration (probability distributions).

change in the mean so 'that the area above the threshold, and thus the probability of false alarm, goes up by orders of magnitudes. The correlation of the clutter can be measured adaptively and the threshold raised accordingly, but it has been shown by Nathanson (see reference 4, pages 88-92) that if this is done, most of the signal-to-noise improvement due to noncoherent integration is forfeited. Thus, it is clear that noncoherent integration in the presence of correlated clutter such as rain can only be done if the time between samples being non-coherently integrated is much greater than the correlation time of the correlated clutter.

It is fortunate that the optimum or near-optimum filtering against ground clutter described in the previous section utilizes a filter bank since this is a good approach to eliminating weather clutter. About 30 dB weather rejection is needed, 15 dB of which can be provided by circular polarization. Filtering of some sort is a viable solution to obtaining the remaining 15 dB. The filtering could be near-optimum as in the case of ground clutter except for the fact that the weather clutter spectrum (see Figure 111-7) changes with time. This change could be measured and the-filter adapted to the spectrum, but this would result in in-tolerable hardware complexity.

A good alternative is to use the filter bank produced by the near-optimum ground clutter filter. It is only necessary to set the threshold on each filter adaptively. A so called "mean-level" thresholding algorithm is employed. Since storms are rarely less than about one mile in extent, the moving clutter is averaged over a half mile on either side of the cell being examined for a target. Each velocity is averaged separately so that filters containing only noise will not be penalized.

Further, a multiple PRF system rather than a staggered PRF system[1] is used so that high speed aircraft typically fall in different filters in the filter bank on successive PRF's. There is a very high likelihood that the target return will be competing with noise only and not weather on one of two PRF's. Only for aircraft whose true (not aliased) radial velocity coincides with that of the rain will there be serious degradation in detection performance.

Precipitation clutter often appears in the zero radial velocity doppler filter. Sometimes relatively large zero velocity returns are received from a weather front which is moving quite rapidly through the radar's coverage. When this happens, changes in the zero velocity signal, for particular range azimuth cells, can occur faster than the ground clutter map can react. In this situation, large numbers of zero velocity threshold crossings can occur in areas which are spatially correlated from *scan to* scan. This, in turn, would give rise to false tracks if nothing were done about it. At NAFEC this problem was solved by adding instructions in the post-MTD software which prevents the tracker from initiating tracks on target reports whose radial velocity is zero.

4. Angel Clutter

The so called "angel clutter" refers to all returns which cannot be explained as being ground or precipitation clutter or targets.. Much effort has been spent in studying angels. It is now believed that nearly all, if not all, angels are caused by bird flocks.

Returns-from single birds[7,8] at S-band range in size between 10^{-4} and 10^{-2} m^2. A typical distribution of angel radar cross section is shown in Figure III-9. The radar return is principally from the body with very little from the wings. For *large* birds, the body is resonant near L-band (1300 MHz) and is in the Rayleigh region at UHF. Typically, there may be anywhere from one to several hundred birds in a resolution cell. Although the mean return from a typical flock of birds may be low ($\sim 10^{-2}$ m^2), the tail of the distribution has been observed to return up to 10 m^2. Birds have been seen as high as 12,000 ft altitude, but they usually fly less than 7,000 ft. The usual appearance on the scope is as so called "dot angels". "Ring angels" are also caused by birds as a large group leaves their nesting place at sunrise.

Of particular interest are the bird migrations in spring and fall. These have been described as "night effect", "falling leaves", "seasonal AP angel clutter", and have been reported by many terminals in the eastern section of the United States. The appearance on the scope when the radar is using MTI is that of two well defined lobes.

These migrations occur at night when there is a favorable wind. Migration will be very heavy on favorable nights so that most of the migration occurs on
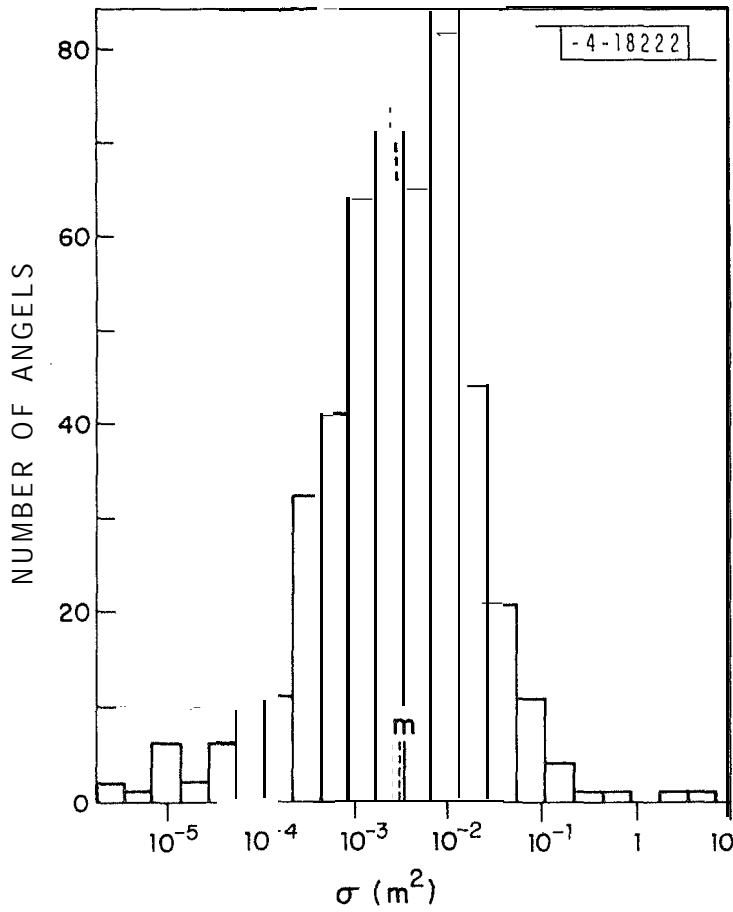
Fig. III-9. Distribution of "angel" cross sections (from Reference 7).

relatively few nights (5 to 15) each spring and fall. The number of birds associated with these migrations may be very large. One author estimated that a few million birds crossed a 100-mi front during one of the busy nights of the autumn migration over the Cape Cod region[9].

Birds fly between 15 and 45 knots true air speed. Taking into account winds, radial velocities over the range-f 80 knpts or so may be observed.

A fairly effective radar improvement used against bird clutter is a carefully tailor-ed sensitivity time control (STC)[9]. The STC varies the radar gain with range and is adjusted so that the minimum detectable target is a specific value, say 1 m^2. This calls for an R^{-4} attenuation law. Even with an R^4 STC applied, during the migratory season flocks of birds have caused many short false tracks in ASR radars (see reference 10).

The R^4 STC is most effective when the antenna provides uniform gain over the elevation coverage. However ASR radar antennas generally have cosecant-squared elevation patterns. Under this conditon STC applied to reduce bird return has the undesired effect of reducing the short range coverage against high altitude airplanes. The MTD processor provides target amplitude as well as range, azimuth and doppler of the target. The target amplitude output can be used to set a secondary (post-MTD) threshold for each doppler channel. Schemes using such thresholds in post-MTD software were developed at NAFEC. These have proven to be quite effective at filtering out bird returns while operating with no observable degradation in detection sensitivity of high altitude aircraft.

It was noticed empirically that most of the radar returns from birds fall in the lower radial velocity doppler filters and give rise to a single threshold crossing as the radar antenna scanned by. By contrast, aircraft returns mainly consist of multiple threshold crossings, usually with all doppler filters being equally likely. The area-CFAR (Constant False Alarm Rate) adaptive thresholding scheme which is used at NAFEC is described in Section 111-C-3,

5. Surface Vehicles

The cross section of ground vehicles is in the same range as aircraft; namely, from 1 to 100 m^2. Radial-velocities can range over $\pm$ 60 knots.

Some reduction in ground vehicle returns is achieved by tilting the antenna upward. One solution is to censor areas on the scope known to contain visible

roads carrying cars with radial velocities outside the notch at zero velocity. The ARTS-III system-starts these detections in track and by measuring the velocity of the target while in tentative track applies a speed threshold of-about 50 knots before declaring it a firm track. This technique has proven reasonably effective and results, at worst, in a few false tracks from surface vehicles.

In summary, a radar which is used for air traffic control and uses a scanning beam antenna should have a fully coherent transmitter; a linear, large dynamic range receiver; a signal processor containing a near-optimum ground clutter filter bank; a fine-grained ground clutter map to set ground clutter thresholds; mean-level thresholding on weather. It would employ multiple PRF's for elimination of blind speeds and would output target range, azimuth, doppler velocity and amplitude for-use-in higher level thresholding and other software for filtering clutter and interference. These are the signal processing and adaptive threshold-ing techniques which are employed in the MTD processor.

C. Moving Target Detector (MTD) Description*

1. Implementation of Processing Algorithms

The MTD processor is implemented as a hard-wired, pipeline digital signal processor. It processes the full 360° coverage of an ASR radar out to a nominal range of about 48 nmi**. The azimuth coverage of the radar is broken into 480 Coherent Processing Intervals (CPI's) each about one half an antenna beam width ($3/4^{\circ}$) in extent. The range cell size is 1/16 nmi. During one CPI, ten pulsesare transmitted at a constant PRF. These are processed by the MTD into eight doppler cells. Thus, there are about 2,900,000 range-azimuth-doppler cells in the MTD's coverage (see Figure III-10).

A block diagram of the processor was presented in Figure 11-2. The I and Q (In-phase and Quadrature) signals are sampled *at* a 2.6-MHz rate by 10-bit A/D converters. The I and Q channels are then added coherently, two at a time, to

---

*A detailed description of the MTD hardware can be found in reference 13.

**The 48-nmi range was chosen for convenience. The MTD could have been im-plemented out to a range of 60 nmi.

34
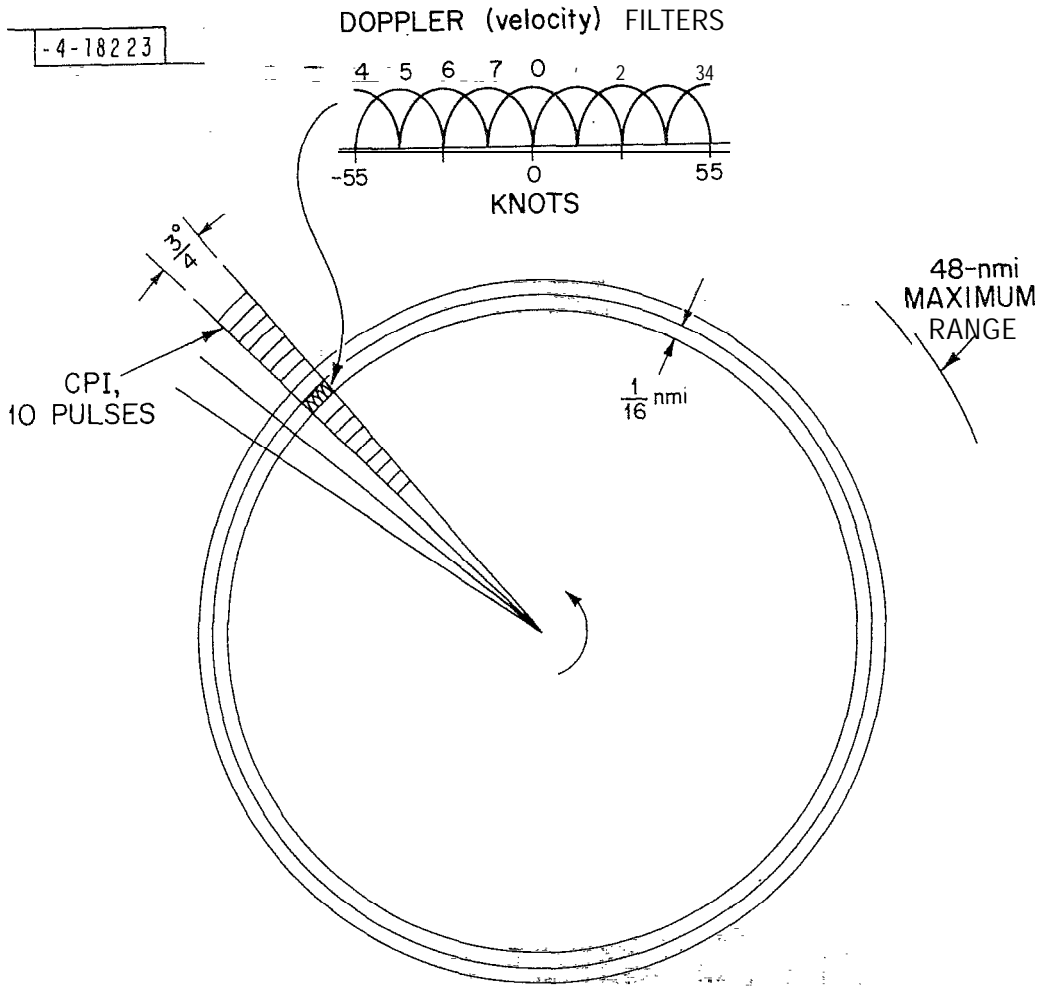
Fig. III-10. MTD resolution.

produce 11-bit I and Q channel words at a 1.3-MHz rate. Samples of both the I and Q channels for each of 760 range gates (47.5 miles of range) from each of 10 consecutive radar pulses are stored in a 8192-word memory. These 7600 words of memory are then processed sequentially (ten samples for each range cell) by a 3-pulse MTI canceller. The I and Q channels are each processed by separate hardware in the 3-pulse canceller section of the processor. Note that the ten samples of U-bit I and Q channel samples are transformed by the 3-pulse canceller to eight 13-bit words. The output of the 3-pulse canceller for both the I and Q channels (real and imaginary parts of the signal) is fed into an 8-point Discrete Fourier Transform (DFT). The DFT produces a complex frequency coefficient for each of eight doppler cells.

The 8-point Fast Fourier Transform algorithm requires four real multiplications by $1/\sqrt{2}$. They are performed in a fixed-wired multiplier which approximates $1/\sqrt{2}$ as $1/2 + 1/8 + 1/16 + 1/64 + 1/256$ and requires only four adders. The remainder of the MTD is configured so that all multiplications are by integral powers of 2 and can be computed by simply shifting the binary *data.*

Weighting of the I and Q channel signals to reduce the side lobe level is done after the DFT. Subtracting $1/4$ of the output of the two doppler filters adjacent to the one of interest is equivalent to a cosine on *a* pedestal weighting in the time domain.

Since the 3-pulse canceller has poor low doppler frequency response, a zero velocity filter (ZVF) is employed to see low radial velocity targets. This low-pass filter is implemented by coherently adding the first five samples of each of the I and Q channels, respectively, taking their magnitude and adding to this the magnitude of the sum of the last five samples. This gives a broader frequency response than simply adding coherently all ten samples and then taking the magnitude. The magnitudes of the signals which come out of the 3-pulse canceller-DFT-weighting chain are then taken.

After magnitudes are taken, adaptive thresholds are set and threshold crossings (detections) are noted and output. The adaptive thresholds are set depending on the clutter phenomena which are present. The doppler domain is divided into three domains: doppler cell 0, doppler cells 2 through 6 and doppler cells 1 and 7.

In doppler cell 0, the clutter is generally due to ground backscatter. The
average ground backscatter cross section varies from range-azimuth cell to range-
azimuth cell. The average backscatter signal level for each cell is measured and
stored on a disc memory (see Figure II-Z). To build up an accurate map, careful
registration of the clutter map with the true pointing direction of the antenna
is essential. This is achieved by breaking up each revolution of the antenna,
marked by 4096 Azimuth Change Pulses (ACP's) into 240 units containing 17 or 18
ACP's each. Each unit contains two CPI's. The disc is accessed every two units
(34 to 36 ACP's, approximately 44 msecs), during which time four CPI's worth of
ground clutter data is read onto and off of the disc. The disc has a maximum
access time of 18 msecs. Two, 3000-word MOS buffers are used to store the data
for use in the processor. A recursive filter is used to update on a scan-to-scan
basis the average signal level stared on the disc. This disc holds 480 x 768 =
368,640 clutter words, one for each range-azimuth (CPI) cell in the coverage.
The words are stored in 10-bit floating point format to preserve the large dynamic
range of the clutter signal.

On each scan, 1/8 of the stored clutter level is subtracted from the stored
level. One-eighth of the signal level output from the ZVF is added to the value
remaining after subtraction. This new level is then stored on the disc for thresh-
olding in the next scan. The threshold for the zero doppler cell is a fixed value
between 4 and 7 1/2 times the level stored on the disc. This fixed value may be
altered by changing a plug.

In the doppler cells 2 through 6 the clutter is due chiefly to rain. For
each doppler and range cell, the average signal level is measured by averaging the
received signal over 14 range cells centered on the range cell of interest. This
average is multiplied by a constant "a" to form the threshold for that range-
azimuth-doppler cell for that scan. Since only coherent integration has been
performed, the 14 outputs are statistically independent Rayleigh distributed
numbers regardless of whether from noise or rain clutter so that the false alarm
rate associated with multiplying constant "a" doesn't change as weather comes into
the area. Figure III-11 shows the false alarm rate as a function of threshold
setting when averaging over various numbers of statistically independent samples.
Note that for 14 samples and a probability of false alarm of 10^{-6} the threshold is
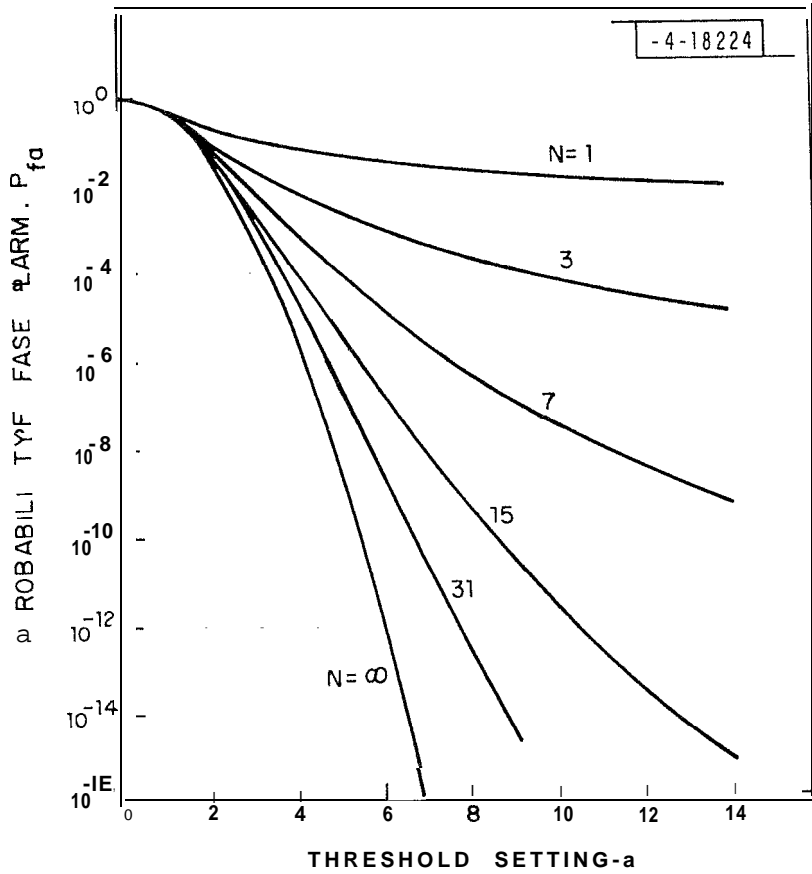
Fig. III-11. False alarm rate as a function of threshold setting. (Parameter N is the number of uncorrelated samples averaged to determine the threshold).

38

only about 2 dB above that derived assuming perfect knowledge (N = ∞) of the rain or noise conditions. The use of this type of mean-level threshold assumes that the rain level is constant over **14** cells (∿ 1 nmi) of interest. The experience with rain to date indicates an inconsequential increase in the false alarm rate when rain enters the region of interest.

In the actual implementation of the MTD the PRF is changed by about 20% between groups of 10 pulses so that a higher velocity target will be aliased into a different filter on each PRF (see Figure 111-12). Thus, it is highly probable that all targets will be free of weather clutter on at least one of the two PRF's, except for those whose true radial velocity is equal within about 25 knots to that of the rain.

Doppler cells 1 and 7 can contain clutter due to rain or spillover from the ground backscatter in cell 0. The threshold set in these cells is the greater of two thresholds: (a) the -threshold set as in doppler cells 2 through 6, or (b) a fixed binary fraction ∿ $(1/2)^n$ n = integer − of the threshold set in cell 0, n is set by changing a plug.

Finally, note that if any I and Q channel sample is noted to have all the bits on (i.e., be in saturation), any target detections for that range cell are deleted.

An interference eliminator circuit has been hard-wired into the MTD to eliminate non-synchronous pulsed interference. The magnitude of each of the 10 pulses in each CPI is taken by adding the absolute values of I and Q. This algorithm though primitive is accurate to within 3 dB. The average is multiplied by five and stored. The 10 magnitudes are also stored until the average has been computed. They are then compared sequentially with five times the average. If any one exceeds this number any threshold crossings that might have occurred in that range gate during that CPI interval are inhibited.

The output message of circuitry-of the MTD contains double buffering for up to 38 detections per CPI. Double buffering is required because the MTD and the Input/ Output Processor (IOP) are asynchronous devices. At the start of each CPI, a PRF/ azimuth (PAZ) word is entered into the first buffer. When a threshold crossing takes place a velocity/range/strength (VRS) word for that detection is entered in the first buffer. At the end of each CPI the PAZ word and any VRS words for that

Filter Number 4 5 6 7 0 1 2 3 4

PRF 1

4 5 6 7 0 1 2 3 4

PRF 2

Aircraft Aliases

Rain

TRUE
AIRCRAFT →
VELOCITY

0

RADIAL VELOCITY

Fig. III-12. Detection in rain using two PRF's.
(Schematic diagram of multiple PRF response to rain and aircraft. The
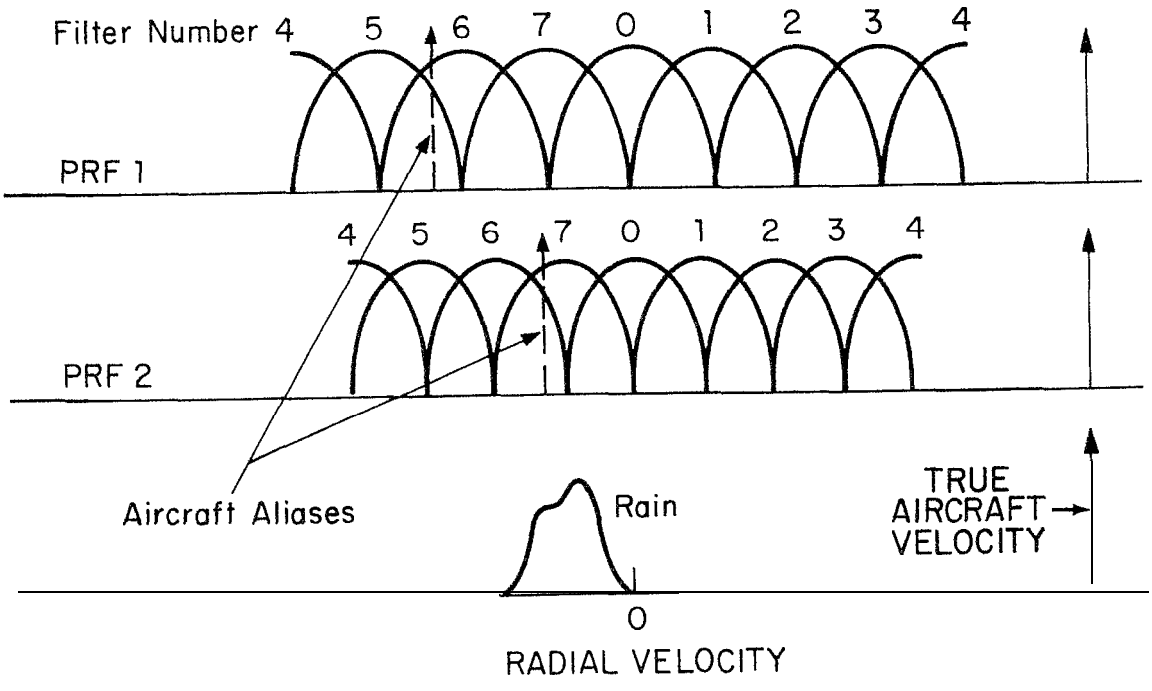doppler foldover occurs whenever the sampling rate is too low).

CPI are transferred from the first to the second buffer. During the next CPI the contents of the second buffer are transferred to the IOP. A NOVA minicomputer is also connected to this output and receives the data in parallel with the IOP.

Figure II-1 presents a picture of the MTD hardware. Standard TTL circuits are used except for the MOS buffer to the disc memory. The construction utilizes wire-wrap boards to hold the integrated circuits. Besides the input core memory and the clutter map disc memory, the MTD consists of approximately 1000 integrated circuits. The MTD includes all of the digital timing for the radar and generates a 31-MHz, 1.0 μsec pulse which is up-converted in the transmitter to S-band to become the transmitted pulse.

2. Report Correlation and Interpolation Software-

A single aircraft target will typically result in threshold crossings in many range, azimuth and doppler cells. These multiple threshold crossings must be associated as belonging to the same target. This process has become known as report correlation*. Also, a more accurate measurement of the target range, azimuth and doppler may be obtained by averaging amplitudes over the multiple threshold crossings. This is called report interpolation. These two functions are performed at NAFEC in the ARTS-III software. In addition, the target doppler returns received at the two different PRF's are used to calculate the aircraft's unambiguous radial velocity, If the threshold crossings are from only one PRF, then an ambiguous velocity flag-is set.

Range and azimuth adjacency are the sole criteria 'used to correlate target reports. Doppler adjacency was not used as a criteria because it was found that amplitude modulation of the target cross section can give rise to split target reports.

For each range-azimuth cell (CPI) doppler report consolidation is performed. The doppler filter number with the largest strength response is noted. Since different doppler filters have different gains, the amplitude of each threshold crossing is divided by a specific normalization factor [15]. After range and

---

*A detailed description of the radar report'correlation and -interpolation algorithms used is given in references 15 and 16.

41

azimuth adjacency are-used to consolidate in range and azimuth, target interpolation is performed. The range of the target is reported as the range cell of the largest response. The azimuth of the target report is calculated by taking the first moment of target intensity-averaged-over azimuth. The doppler interpolation is performed by taking the ratio of the strengths of the doppler filter with the largest strength and the-adjacent doppler filter with the second largest strength. This ratio forms an estimate of the target's radial velocity. It is made with a precision of 1/64 of the PRF. This interpolation is done using a look-up table[15,16]. If there are no threshold crossings from a doppler filter adjacent to the doppler filter with the largest strength, then doppler interpolation is bypassed and the doppler is assumed to be the center frequency of the filter with the largest strength. Doppler interpolation is done separately for each PRF. The interpolated doppler numbers at each of the PRF's are then used to calculate the unambiguous radial velocity of the target.

3. Post-MTD Thresholding Software.

a. Introduction

Early in the testing of the MTD at NAFEC it became evident that several environmental-phenomena were causing more false alarms than initially predicted. Furthermore, these false alarms were partially correlated both spatially and temporally and, thus, were causing false tracks to be initiated by the ARTS-III tracker. Typically there were 50 to 100 false alarms per scan due to noise and as many as several hundred false alarms per scan from all environmental phenomena when they were present.

A series of thresholding algorithms, developed by W. Goodchild at NAFEC, have been particularly- successful in eliminating almost all of the non-noiselike false alarms. These algorithms have been incorporated in the ARTS-III software before the radar reports are sent to the tracker.

b. Environmental Phenomena

As noted previously the zero velocity returns from fast moving weather systems can give rise to threshold crossings which are spatially and temporally correlated and thus cause false tracks. These zero velocity false alarms occur along the leading edge of a rain cloud which happens to be passing tangentially

42

to the radar. The threshold crossings occur when the weather moves from one range azimuth cell to another faster than the clutter map can react.

Threshold crossings in the non-zero doppler channels are prevented by the mean-level threshold. The zero radial-velocity cell has no mean-level threshold however. Implementation of a mean-level threshold in the zero-doppler channel would result in a 1-mile band of reduced sensitivity around each isolated ground clutter return. This, in turn, would drastically impair the detection performance of tangential aircraft in areas of ground clutter.

A second source of unwanted threshold crossings is the combination of non-synchronous pulsed interference with various forms of clutter. The interference detection circuits in the MTD operate by calculating the average amplitude of the returns from the 10 pulses in each range gate for each CPI. If any single return exceeds the average by some preset multiple, the large pulse is declared to be interference, and threshold crossings from that range gate are ignored. This system works well when the background is white noise, but it breaks down when the background is clutter (i.e., colored noise). In the latter situation, the total clutter energy is not equally divided among the doppler filters, whereas the single interfering pulse energy is non-synchronous interference which passes the amplitude threshold and may be detected in a doppler cell which is subject to low background power spectral density (receiver noise).

Finally, the bird problem is exacerbated by the requirement of maximum sensitivity in the high elevation portions of the CSC^2 antenna pattern. In effect this leads to excess sensitivity at the lower elevations. A consequence is large numbers of threshold crossings from bird echoes.

        c. Threshold Algorithms

The post-MTD thresholding algorithms as implemented at NAFEC are as follows:

      1.   The coverage is divided into 22.5' x 4 nmi sectors.

      2.   From 0 to 16 nmi, and filters 0-7:

          a.   Prior to correlation and interpolation, any replies are discarded which exceed the sector threshold for its corresponding doppler filter.

b.   Following correlation and interpolation 1.99
     is added to the sector threshold of each filter
     which contains a single CPI report.   (Nominal
     threshold is 0).

C.   If no single CPI reports occur in a sector on
     the following scan(s), the threshold is decre-
     mented for-each filter by 1/4.

d.   Single CPI reports passing the threshold test
     are sent to the tracker for possible track
     updating but not for track initialization.

3.   From 16 to 48 nmi:

a.   Correlation and interpolation is performed first.

b.   Single CPI reports are discarded if they do not
     exceed the threshold.

C.   Single CPI reports increment and lack of them
     decrement the threshold as above.

d.   Single CPI reports passing the threshold test,
     are sent to the tracker for either track updating
     or track initialization.

4.   Interference is removed from azimuthal sectors 5$^{\text{o}}$
     wide and with range extent of 0 to 48 nmi as follows:

a.   If there is an excess of 10 single CPI reports
     in a sector, they are prevented from initiating
     or updating tracks.

b.   Once interference is detected, the single CPI
     reports involved are not used to increment the
     thresholds.

This set of four thresholding algorithms adequately controls the number of false
alarms input to the tracker.   Careful study has revealed no noticeable degrada-
tion in detection performance due to the use of these algorithms.

44

IV. EXPERIMENTAL TEST SETUP AT NAFEC

    A. Introduction

        The MTD was integrated into an existing-experimental facility; namely, the Terminal Facility-for Automated Surveillance Testing (TFAST) at NAFEC. This facility is used by the FAA for testing various facets of the augmented ARTS development and other radar programs. The facility was reconfigured so that the MTD could be operated either alone or simultaneously with the RVD-4. When operated alone the MTD could process intermediate frequency signals from any one of the three radars at the site (an ASR-5, ASR-7 or FPS-18). When the MTD and the RVD-4 were operated simultaneously, it was necessary for the MTD to operate with the FPS-18 and the RVD-4 to process video from the ASR-7. The RVD-4 could process video from the ASR-5, however, contact with the radar environment via the antenna is only available to the ASR-5 when the FPS-18/ASR-7 complex is connected to the dummy load and vice versa. The normal mode of operation for the MTD is in conjunction with the modified FPS-18. A schematic diagram showing this arrangement is presented in Figure IV-1.

    B. MTD System-

        1. General

        A functional schematic diagram of the MTD system is presented in Figure IV-2. The system has been partitioned in that figure to represent the packaging of the system. The MTD hardware is contained in a single cabinet rack (see Figure IV-3). The FPS-18 radar occupies a number of large cabinets as shown in Figure IV-4. The IOP is a medium-size digital computer (64K of 30-bit words) and is shown in Figure IV-5. The NOVA-1220 minicomputer which was used at NAFEC is shown along with some of its peripherals in Figure IV-6. Finally, the DEDS display from the ARTS-III system which was used as display for both analog and digital signals from the MTD system is shown in Figure IV-7.

        2. FPS-18

        The FPS-18 is a ground-based, S-band, air surveillance radar. It was designed in the early 1950's as a gap filler radar in the SAGE system. In many ways it is typical of the S-band airport surveillance radars, but it is unique among them in that it has a fully coherent master oscillator-power amplifier transmitter. The FPS-18 uses a continuous wave intermediate frequency oscillator to provide a coherent phase reference. The transmitted pulse is derived from this

18-4-17781

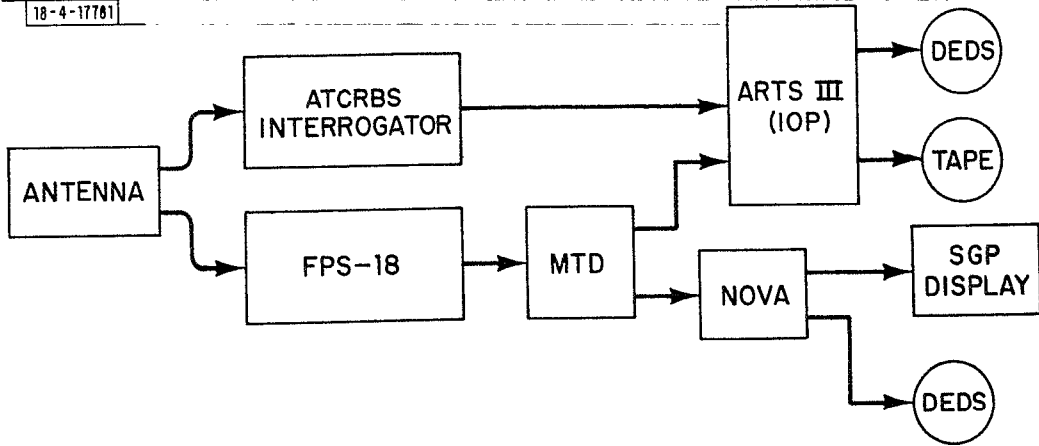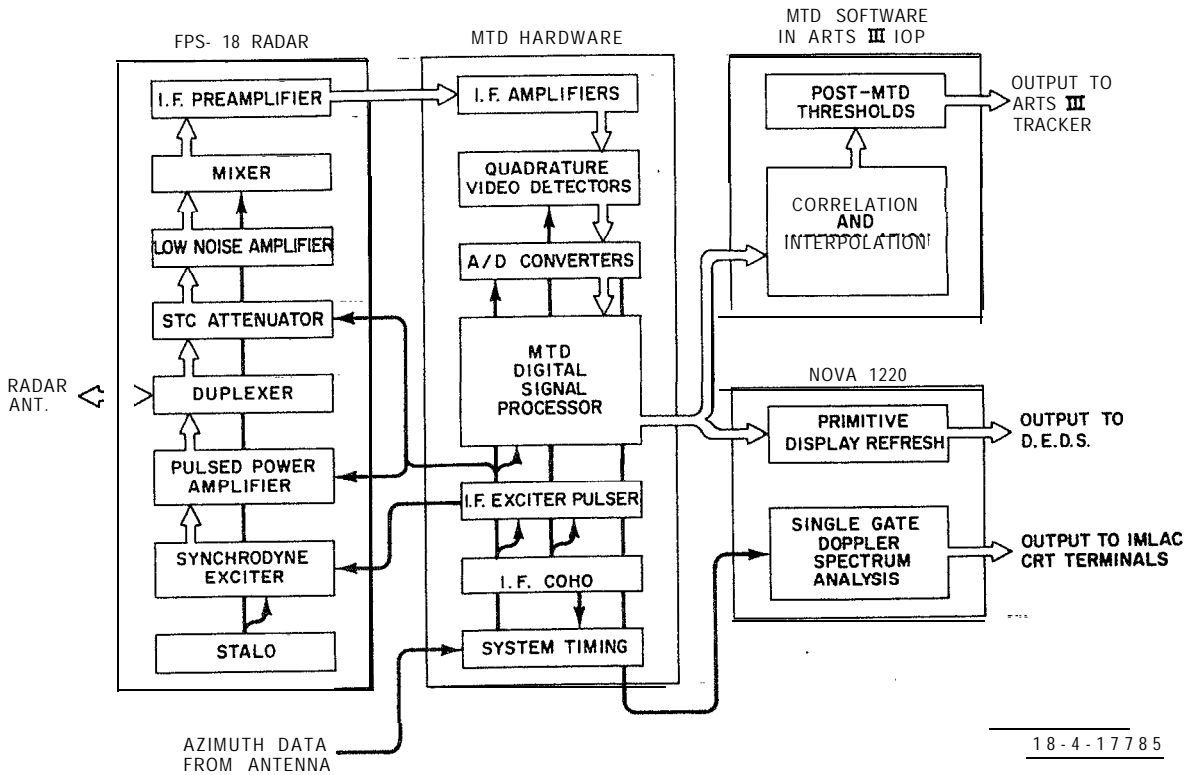Fig. IV-1. MTD — normal set-up:

18-4-17785

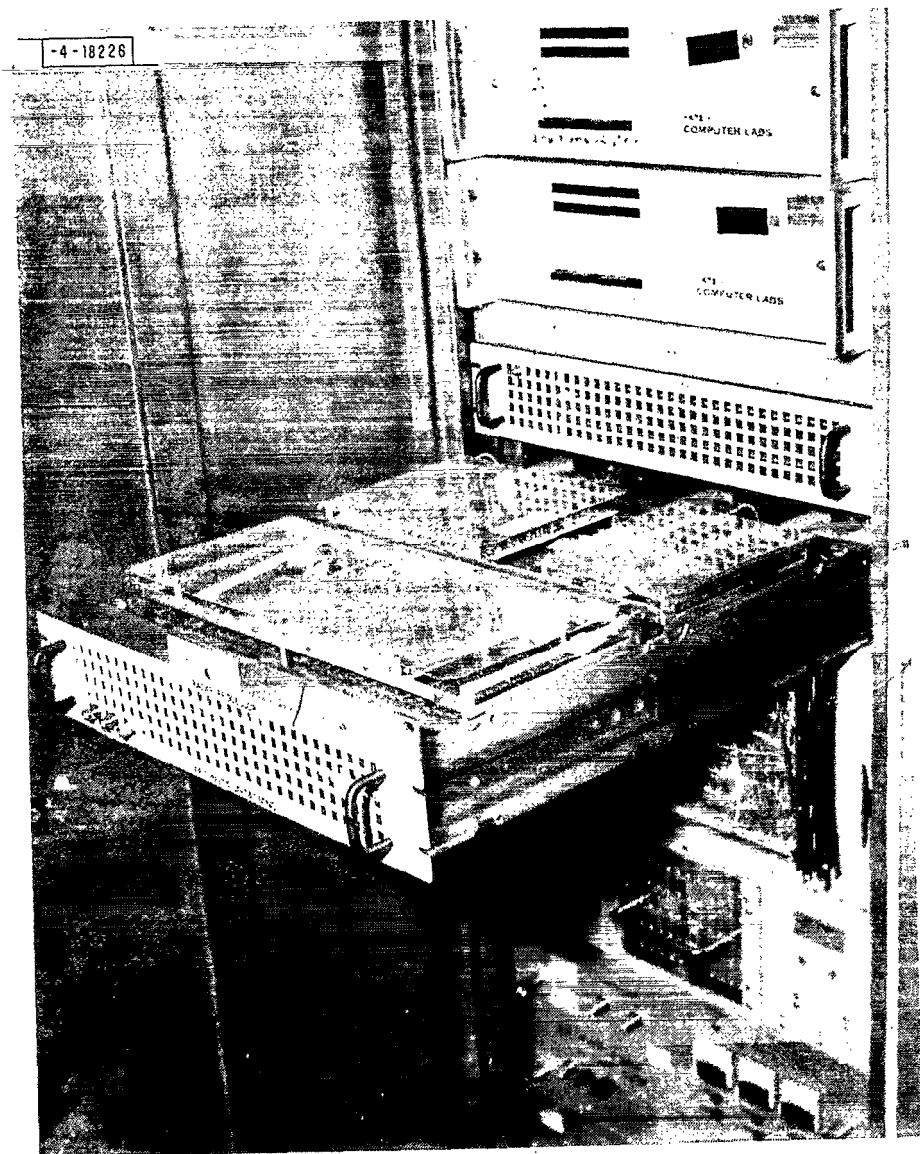Fig. IV-Z. MTD — system functional schematic.

46
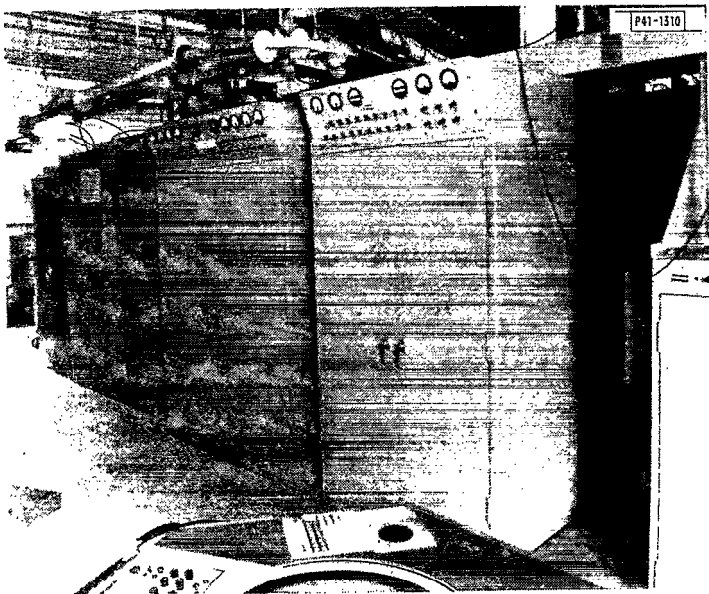
Fig. m-3. **MTD** cabinet.

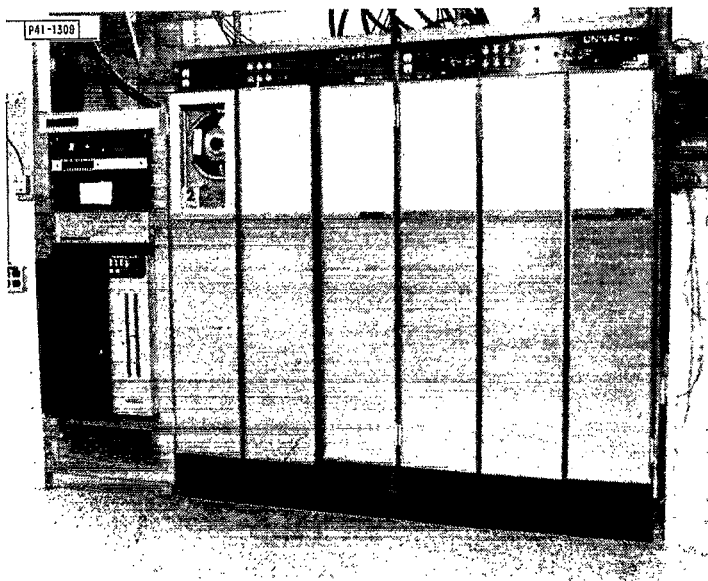Fig. IV-4. FPS-18 radar.

Fig. W-5. Input-output processor (IOP).

Fig. IV-6.   NOVA-SGP set-up.

Fig. IV-7.   DEDS display.

oscillator via the S-band stalo and a synchrodyne exciter. The resulting S-band
pulse is amplified through a (VA-87) pulsed klystron power amplifier. Most S-band
surveillance radars on the other hand use a pulsed magnetron power oscillator
to provide the transmitted pulse and derive a coherent reference waveform by
locking the phase of a keyed intermediate frequency oscillator to the random
starting phase of the magnetron.

The coherent klystron type of radar has the advantage that coherency is
maintained from pulse to pulse. Thus, second-time-around echoes will be treated
the same way as returns from shorter ranges, Because of this advantage and because
a system was readily available, it was decided to use an FPS-18 radar as a test
bed for the MTD development. Some characteristics of the FPS-18, both as originally
designed and as modified for the MTD, are listed in Table IV-1.

TABLE IV-1

FPS-18 PARAMETERS

PARAMETER.	AS DESIGNED	WITH MTD
Peak Power	2 Mw	.9 Mw
Pulse Width	1 µsec	1 µsec
PRF	1200 PPS (fixed)	Variable, 1245 average
Noise Figure	. 10 dB	8 dB
System Dynamic Range	2 5 dB	55 dB

Ultimately the analog portion of the MTD system hardware used only the trans-
mitter and duplexer from the FPS-18. Originally it had been hoped that some of
the FPS-18 exciter and receiver could be used, but it turned out that the necessary
system dynamic range -could not be achieved with the old vacuum tube electronics.
Accordingly, the original FPS-18, RF front end and intermediate amplifiers were
all replaced with solid-state units. The new receiver front end included a para-
metric amplifier and a PIN diode RF attenuator for improved STC. These changes
were made to provide adequate, linear dynamic range in the receiver circuits.

Further, it was found necessary to replace the FPS-18 stalo and exciter
circuits with solid-state units and to modify the higher power modulator circuits

50

extensively.   These latter changes were necessary in order to reduce the spurious modulation products in the doppler bandwidth to an acceptable level.   The problem of pulse-to-pulse phase modulation of the transmitted signal is unusually severe because-of the MTD's requirements for non-uniform pulse repetition rates and very low spurious sideband levels.   Modifications to the FPS-18 transmitter included the addition of holdoff diodes in the resonant charging circuits, raising of the natural resonant frequency of these charging circuits, installation of additional high voltage filter capacitors and the implementation of an active regulator which compensated for the varying load imposed by the MTD waveform.

The details of these FPS-18 modifications are not a principal issue for this report.   However, additional discussion of the modification of the FPS-18 and other radars for use with the MTD processor will be found in Section V-J.

When interfacing with magnetron-type radars, the MTD accepts intermediate frequency signal and coho waveforms from the radar and delivers such triggers to the radar as are needed for operation of the high power modulator, coho gating and STC circuits.   Practice to date has been to use the intermediate frequency signal from the existing preamplifier in the radar and to use the coho signal, *at* a level of a few milliwatts, from the most convenient output port on the coho oscillator/ amplifier chain in the radar.

3.   MTD Hardware

Figure IV-8 depicts the analog portion of the MTD. This hardware was assembled almost- entirely from readily available shelf items.   All the amplifiers, attenuators, power dividers and mixers are catalog items.   The bandpass filter in the IF channel was made to order but is now a catalog item and the two low-pass filters which follow the double balanced mixers were designed and constructed at Lincoln Laboratory.

Both the IF and the coho amplifiers are capable of delivering approximately 7 volts signal output.   The double balanced mixers are high power types rated at 1-watt total continuous input.   The end result is that the MTD IF channels and quadrature video detectors are linear up to peak video output levels of about 2 volts.   The A/D converters limit at a level of 1.024 volts.   Hence, the upper limita-tion on linear dynamic range is still the A/D converters (see Section V-A-l for a discussion of the dynamic range actually realized).

O-12dB

BANDPASS
FILTER
2.6MHz BW

30dB

30dB

I.F.

INPUTS
FROM
RADAR

0°
POWER
DIVIDER

DOUBLE
BALANCED
MIXER

O-30dB

COHO

30dB

QUADRATURE
HYBRID

DOUBLE
BALANCED
MIXER

LOW PASS
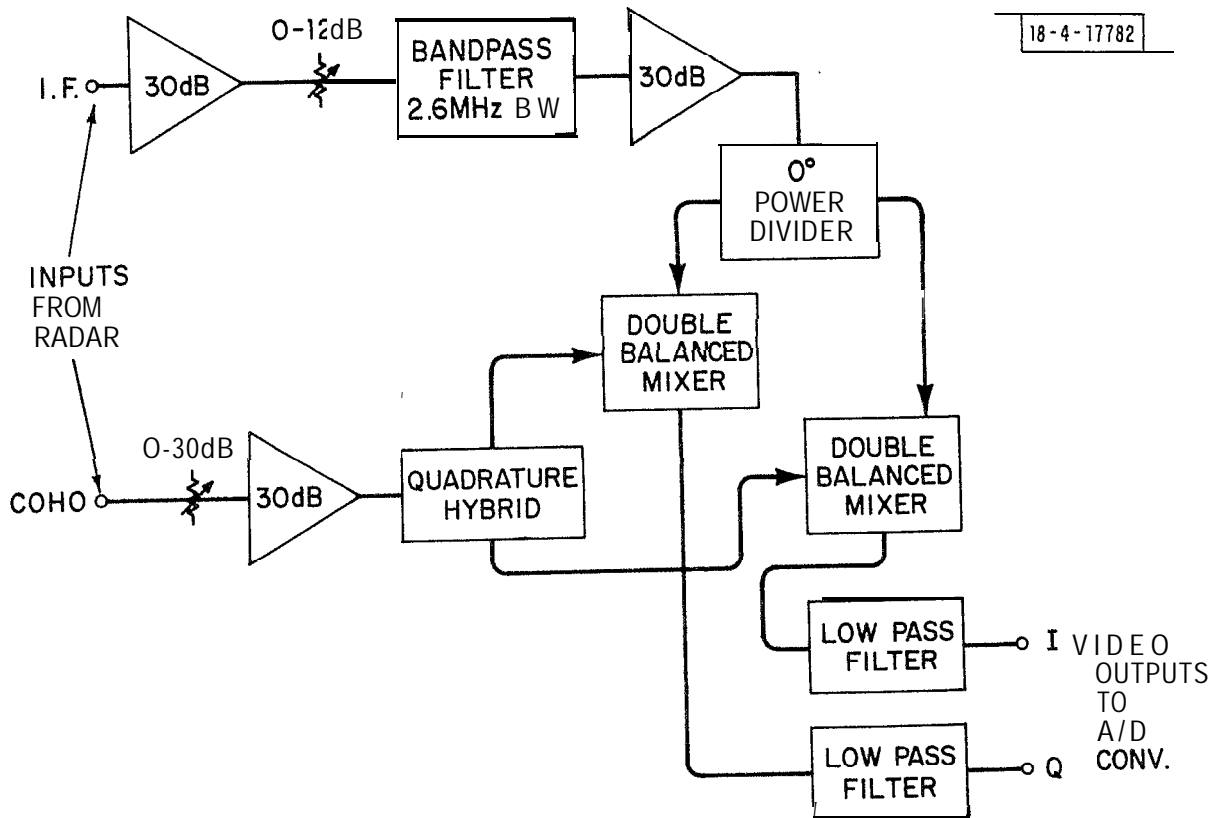FILTER

I VIDEO
OUTPUTS
TO
A/D
CONV.

LOW PASS
FILTER

Q

Fig. IV-8. MTD analog hardware block diagram.

52

The MTD digital hardware is described in detail in Section III-C-3 and in reference 1.5.

4. MTD ARTS-III System

For flight tests and for some of the other performance measurements, detections from the MTD are sent to the ARTS-III IOP (Input/Output Processor) for further processing. The threshold crossings for each scan are correlated and target centroids are found by interpolation as described in Section III and in references 15 and 16. In addition, the IOP takes single-pulse threshold crossings from the BDAS (Beacon Data Acquisition System) hardware and performs correlation and interpolation on these reports. The IOP also performs in software the sliding-window detector portion (second threshold) of the RVD-4 processing. Next, the radar and beacon reports are correlated together if they are close enough together in range and azimuth. The radar only, beacon only, and radar/beacon correlated reports are then sent to an automatic tracker where scan-to-scan correlation, smoothing of target position and-estimation of target velocity are performed by the track oriented α-β tracker. The tracker updates the smoothing parameters (based on a "firmness" table which weights tracks according to their history. The tracker used is the ARBTL (Augmented Radar-Beacon Tracking Level). The RBTL, the ARTS-III tracker presently employed in the field does not use radar data for automatic trackingAll tracking in the RBTL is done with beacon data. The ARBTL uses both radar and beacon, but it should be noted that the track initiation and track dropping constants weigh the beacon data much more heavily than the radar data. In fact the parameters assume the radar data is poor and is quite noisy. Thus radar-only tracks will be dropped more quickly than beacon-only tracks of the same detectability. In addition, the IOP performs a data interface function with the DEDS (Data Entry Display System) display upon which the ARTS-III tracker output is displayed and from which the controller interacts with the track file via a keyboard and track ball. A complete description of the ARTS-III software and tracker is contained in references 18 and 19.

5. The NOVA-DEDS Display

In normal operation the output from the MTD digital hardware is available both to the IOP computer and to the NOVA 1220 minicomputer which is located adjacent to the MTD digital hardware. The NOVA is interfaced with a second DEDS display

53

system and can be programmed to present the output from the MTD as alphanumerics on the DEDS plan position indicator. The display arrangement allows observation of the MTD system at times when the ARTS-III IOP computer and associated displays may not be available. The NOVA software used in this subsystem has features which make it particularly useful for measuring false alarm rates and probability of detection of the MTD.

In this system (Figure IV-9) MTD threshold crossing data is delivered to the NOVA via an MTD-NOVA interface. This data consists of the range, azimuth, doppler channel number, and strength of the signal which caused the threshold crossing along with the PRF at which the radar was operating at the time.

Any combination of the eight doppler channels may be selected for display. A particular doppler channel is selected by throwing the associated sense switch on the NOVA minicomputer. Coordinates of selected threshold crossings are passed through a routine which converts them from range and azimuth to X-Y for display on the DEDS. The information gets to the DEDS through a cascade of three refresher/buffer routines and, finally, through a NOVA/DEDS interface chassis which is physically located in the NOVA chassis.

Each of the three buffers can hold the same number of targets, nominally 100. When the system is started the target's coordinates are stored in the first buffer (and displayed on the DEDS if the brightness control for that buffer has been turned up). When the firstbuffer is filled its contents are emptied into the second buffer and it begins to fill again. Thus, the 101st threshold crossing causes threshold crossings 1 through 100 to be shifted into the second buffer, and initiates the next filling of the first buffer. Similarly, the 201st threshold crossing causes threshold crossings 1 through 100 to be placed in buffer number three and threshold crossings 101 through 200 to be shifted into buffer number two, while it is placed in buffer number one and so on. The 301st threshold crossing after the system is started causes threshold crossings 1 through 100 to be discarded while subsequent threshold crossings are stepped down through the three buffers.

This system was devised to provide a scan-history-type of display. The idea was that proper adjustment of the individual brightness controls could provide moving targets with decaying tails so that the direction of motion would be immediately obvious. This technique was found to be unsuccessful primarily because the data
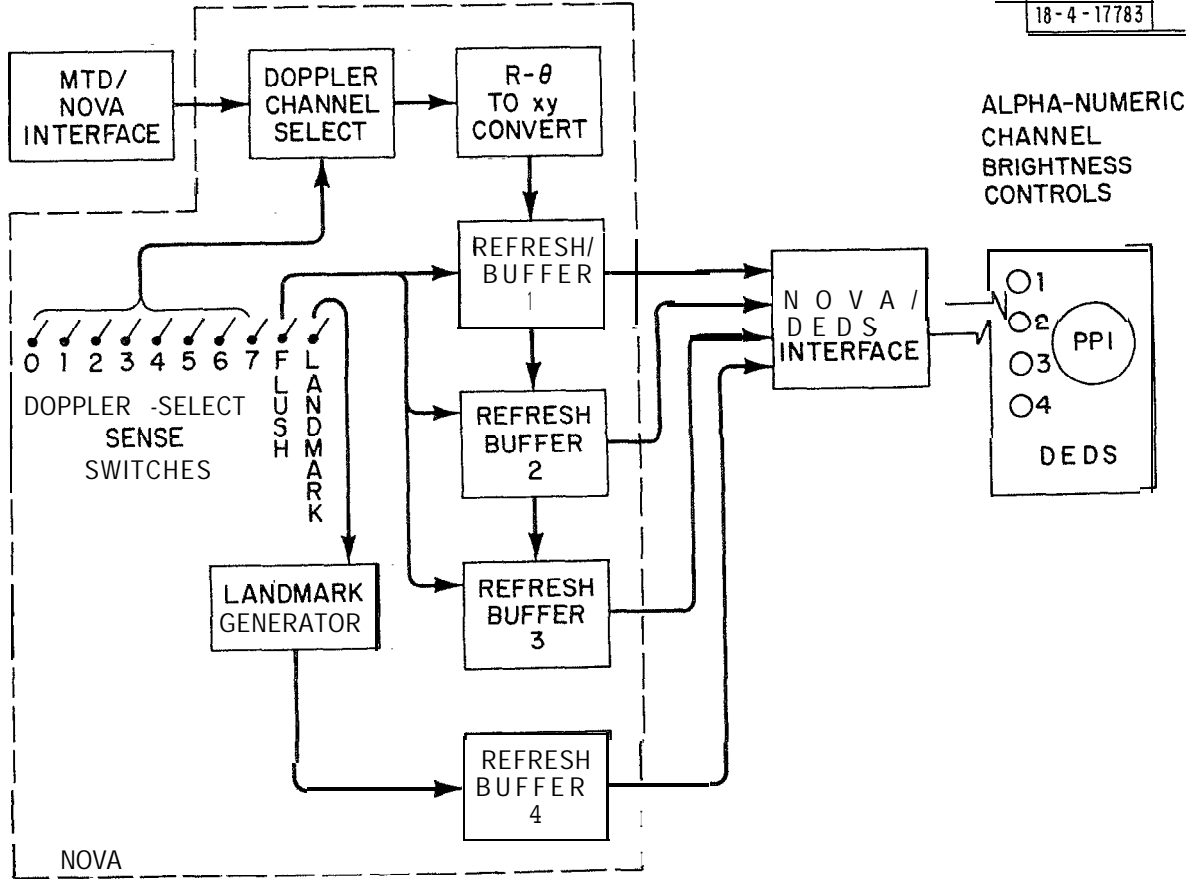
Fig. :v-9. NOVA-DEDS display subsystem.

rate at that point in the system is too high. However, when only one of the brightness controls is-turned up the very obvious filling and emptying of a single buffer provides a convenient way to count such things as false alarms.

A "landmark" section of the subsystem is available for preprogrammed display of the positions of airports and aircraft navigation aids in the area.

In addition to the digital outputs from the NOVA or the IOP, analog video signals from the various radars can be displayed on the DEDS. Figure IV-10 shows a typical display of combined digital and analog outputs,

6. NOVA-Single Gate Processor (SGP)

a. Description

To provide a means of examining the spectrum of the radar output, a real-time Fourier analysis program called SGP (Single Gate Processor) has been written. The program, which is not compatible with normal ARTS-III/NOVA DEDS opera-tion, accepts data from a single, selectable-, radar range cell. Complex video samples are delivered to the NOVA minicomputer from the MTD input circuitry every repetition period. These data are processe-d in a 64-point Fast Fourier Transform (FFT) for conversion to log power spectral density. The output is presented on a graphic display in the form of a graph giving relative decibel levels of spectral power density (see Figures IV-11 to IV-13).

The subprograms required for this function are shown in block diagram form in Figure IV-14. Input data from the radar are presummed over an adjustable number of points to control the duration and, hence, the resolution of the output periodo-gram. Typical resolution values vary from about 15.75 Hz per line for no pre-summing to about 3/4 Hz per line when 64 points are presummed. Each presummed data point is placed in an appropriate buffer area in core until 64 samples are accumulated.

These samples are averaged, real and imaginary parts separately, to obtain the DC component of the input data. The resultant value is subtracted from each data point. Since radar signals returned from ground clutter (the main component here) are largely stationary in time, the DC removal process eliminates much of the signal magnitude. This-reduces the dynamic range required in the processing and, consequently, simplifies the subsequent calculations. The DC having been removed, a multiplicative gain factor is applied to the signal.
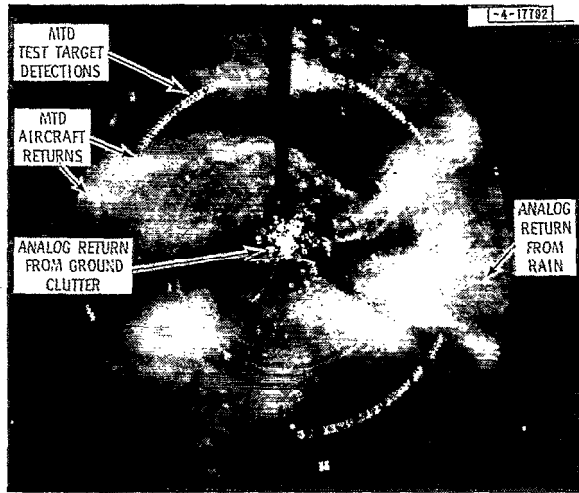
BOTH ANALOG AND MTD DIGITAL SIGNAL'S DISPLAYED NOTE THAT
THE NUMBERS INDICATE SIGNAL'S DOPPLER CELL

Fig. IV-10. NOVA-DEDS PPI display.
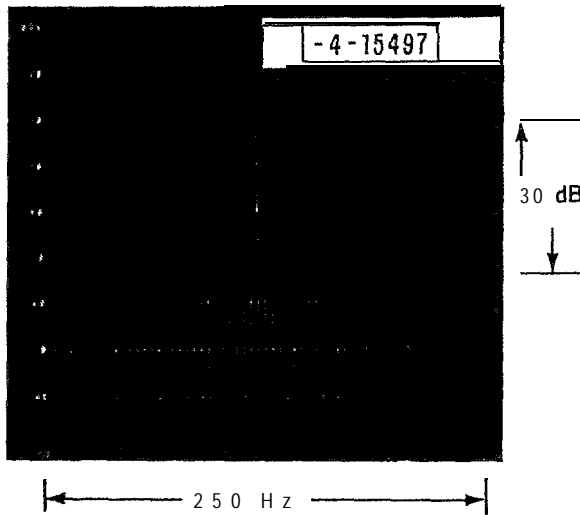(Both analog and MTD digital signals displayed; numbers indicate signal's
doppler cell).

Fig. w-11. Fixed target at 35 nmi.
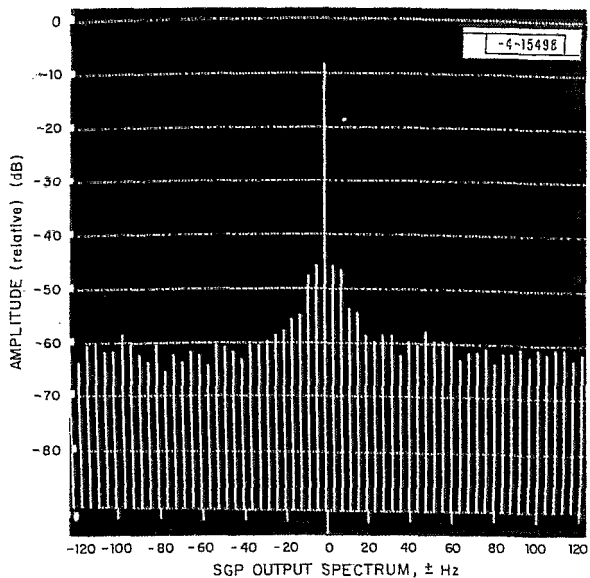(Output of FPS-18 with SGP; note balanced sidebands at ± 30 Hz,)

57

Fig. IV-12. Fixed target at 15 nmi.
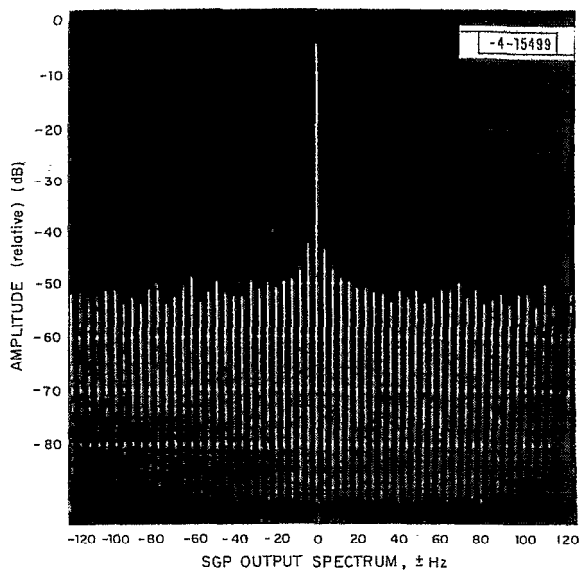(Output of FPS-18 with SGP; note absence of balanced sidebands at ± 30 Hz.;
horizontal scale to ± 125 Hz.)

Fig. IV-13.   Fixed target at 31 nmi.
(Output of FPS-18 with SGP; horizontal scale to ± 125 Hz.)

SAMPLING
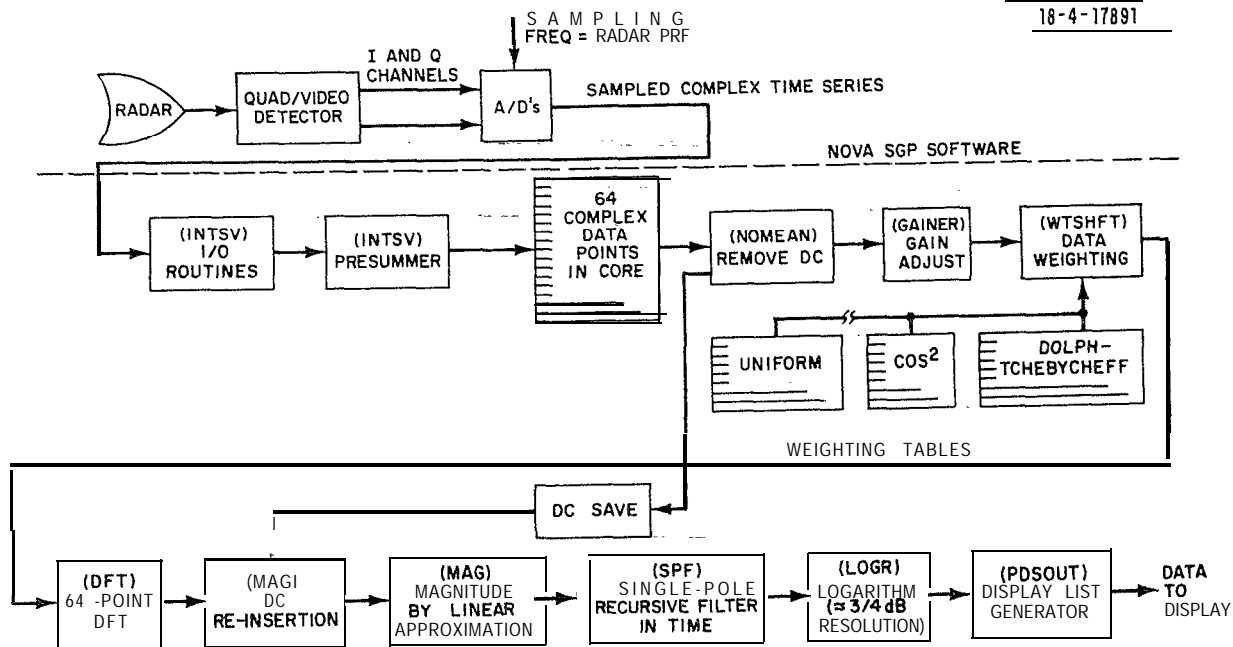FREQ = **RADAR PRF**

I AND Q
CHANNELS

SAMPLED COMPLEX TIME SERIES

RADAR → QUAD/VIDEO DETECTOR → A/D's

NOVA SGP SOFTWARE

(INTSV) I/O ROUTINES → (INTSV) PRESUMMER → 64 COMPLEX DATA POINTS IN CORE → (NOMEAN) REMOVE DC → (GAINER) GAIN ADJUST → (WTSHFT) DATA WEIGHTING

UNIFORM   cos^2 DOLPH-TCHEBYCHEFF

WEIGHTING TABLES

DC SAVE

(DFT) 64-POINT DFT → (MAGI) DC RE-INSERTION → (MAG) MAGNITUDE BY LINEAR APPROXIMATION → (SPF) SINGLE-POLE RECURSIVE FILTER IN TIME → (LOGR) LOGARITHM (≈3/4 dB RESOLUTION) → (PDSOUT) DISPLAY LIST GENERATOR → DATA TO DISPLAY

Fig. IV-14.   SGP system block diagram.

These modified data are then windowed to control side lobe levels. An assortment of weighting functions is available, including cosine squared, Tchebycheff (60 dB), and uniform-weighting. The weighted data are passed through a conventional FFT routine and the DC component, suitably scaled, is reinserted. The Fourier coefficients are then detected linearly giving a data set corresponding to the square root of the power density.

In order to provide a better spectral estimate, the output spectra are averaged. The amplitude of each line in successive spectral estimates is put through a separate recursive filter. The filtered data are then converted to logarithms and delivered to the display generating routines for final processing.

The resultant periodograms have proved to be useful not only for diagnostic purposes but for evaluation of proposed processing systems.

b. Radar Stability Measurements

The maximum clutter-to-target ratio at which a radar will give good detection must be somewhat less than the dynamic range of the radar. Nominally, the dynamic range extends from the receiver's thermal noise level upward to the receiver's limit level. However, if doppler domain sidebands due to spurious modulations are larger than the thermal noise level, these sidebands will limit the dynamic range to some smaller value. Spurious sidebands can be generated by angle modulation of the stalo and coho signals, angle or amplitude modulation of the transmitted signal, or jitter in timing waveforms.

The dynamic range requirement for the modified FPS-18 has been estimated to be 54 dB. This implies that the total spurious sideband energy in any doppler resolution cell must be more than 54 dB below the zero doppler "carrier" signal reflected from a fixed echo in the same range cell.

Theoretically, one can think of working up a spurious sideband budget and assigning an allowable index of modulation to each signal. For instance, more or less arbitrarily, we might ask that each source contribute no more than 60 dB of spurious sideband energy, where 0 dB is the level of the fixed echo return. This would require the short-term frequency stability of the stalo to be on the order of one part in 10^{10}, the rms timing jitter to be on the order of 1.1 nsec, and peak phase deviation of the transmitted pulse to be on the order of 1 milliradian.

60

Measurement of the individual signals is difficult, tedious, and involves cumbersome, specialized equipment. In effect, the spectral purities demanded of the radar signals are close to the state of the art and, if signal generators were available for measurement purposes which had greater spectral purity, one would be tempted to use them in the radar. Thus, the radar itself in conjunction with the SGP diagnostic subsystem described above, is a convenient instrument for measuring its own stability. The radar/SGP combination is used to present periodograms from either fixed ground clutter or artificial echoes from passive delay devices.

The SGP display does not indicate the source af various spurious disturbances directly, but these can be identified by a process of elimination. For example, Figure IV-11 shows a periodogram from a fixed echo at a range of about 35 nmi. There are sidebands displaced 30 Hz on either side of the main (zero doppler) return. These sidebands are only about 30 dB weaker than the carrier--clearly unacceptable performance. It was found that the 30-Hz sidebands were less intense at shorter ranges, hence, it was assumed that they were originating in the stalo.

Since the spurious frequency was less than the line frequency, it was postulated that the disturbance was caused by vibration, and this proved to be the case. Investigation with a vibration analyzer disclosed a 30-Hz mechanical vibration of the stalo. This vibration was generated by blowers in another cabinet and was coupled into the stalo through the floor and through a rigid cable trough. Mechanical isolation of the stalo cabinet eliminated the offensive sidebands as can be seen in Figures IV-12 and IV-13.

The lower frequency sidebands out to ± 16 Hz are believed to be due to tower motion. In both Figures IV-12 and IV-13 the signal strength is well below the limit level of the receiver.

C. RVD-4 System

1. General

The MTD and the RVD-4 processors were both integrated into the ARTS-III system at NAFEC where they have undergone simultaneous testing during the summer of 1975. The RVD-4 was tested with an ASR-7. The ASR-7 and RVD-4 will be described briefly to illustrate the mutual constraints imposed by simultaneous testing of the two processors.

2.   ASR-7

The ASR-7 is an S-band, solid-state, airport surveillance radar. It uses a staggered PRF, a 3-pulse MTI canceller for clutter rejection and log-FTC circuit and circular polarization for weather rejection.   Details of the ASR-7 are given in References 20 and 21.

3.   RVD-4 Processor

The RVD-4 utilizes a double thresholding technique to examine the radar's video output for targets.   The first threshold, a rank-order quantizer, converts the video into zeros or ones.   The second threshold, a sliding-window detector, declares the presence or absence of an aircraft.   This is a form of non-coherent integration.   The RVD-4 differs from previous models in that it measures the degree of correlation of the clutter signals over a coverage sector (2 nmi x 32 ACPs) and uses this information in an adaptive way to set the sliding-window detector threshold for-constant false alarm rate.   The RVD-4 also adaptively chooses log-normal or MTI video signals, depending on whether receiver noise, weather or ground clutter predominates in any particular geographic sector of the coverage.   When used with the RVD-4, the ASR employs a staggered PRF in order to eliminate blind speed problems.

A complete description of the RVD-4 is given in Reference 22.

D.   Test Target Generator

The TFAST site is-equipped with a solid-state, coherent test target generator (TTG).   This equipment was designed to FAA specifications and built by Westinghouse. It is a stable and very versatile source of radar test signals and was used extensively in the MTD test program at NAFEC.

The TTG accepts coho and stalo signals along with triggers and azimuth data from the radar with which it is being used.   The coho signal is passed through an intermediate frequency channel which contains a doppler simulation modulator and a range gate.   The former can impose a random phase shift or a simulated doppler shift on the IF signal.   The latter can be set up to match the pulse width of the radar under test.   The range gated and doppler shifted intermediate frequency signal is heterodyned against the stalo signal to produce a coherent test target signal at the radar's operating frequency.

Digital logic in the TTG accepts the azimuth data pulses from the radar and drives a digital attenuator to generate a simulated antenna pattern.

The amount and sense of the simulated doppler offset, the range delay, the range rate, the target azimuth and the antenna beam shape can be controlled from the front panel of the TTG. For the MTD tests a precision waveguide attenuator was added at the output of the TTG. The net result was that the TTG could supply coherent range-gated doppler-shifted test signals with any needed set of parameters. The signal amplitude, particularly the relative signal amplitudes, were known with good accuracy and precision. Table IV-Z lists the important characteristics of the TTG signals.

<div align="center">TABLE IV-2</div>

<div align="center">TTG TARGET CHARACTERISTICS</div>

Frequency	Same as transmit frequency (2.7 to 2.9 GHz)
Pulse Width	Two selectable pulse widths, each adjustable 0.2 to 6 microseconds
Phase	Selectable random phase or coherent phase operation
Range Start	Selectable 1 to 60 nmi in 1-microsecond steps
Range Rate	Continuously variable 0 to 1000 knots. Minimum range step 0.2 microseconds
Simulated Doppler	Sweep-to-sweep phase change to simulate optimum speed target or continuously adjustable to simulate any velocity 0 to +1000 knots
Azimuth Position	Selectable 0 to 360 degrees in .088 degree (one azimuth change pulse) steps
Antenna Scan Modulation	Amplitude modulation fully programmable by manual pin board for a maximum of 99 steps. Dynamic range = 40 dB minimum
Target Scintillation __	Random amplitude modulation. Modulation percentage can be adjusted
Radar Cross Section	Target amplitude adjustable with precision waveguide attenuator

E. Recording of Test Data

In order to analyze the data from the tests of the MTD the output track position data as well as much data at several other places in the data analysis was output onto

<div align="center">63</div>

magnetic tape for later analysis. First, threshold crossings from the MTD and beacon threshold crossings as well as timing and scan number information are written on a magnetic tape transport manufactured by the BUCODE Corp. This bulk data was then processed through the ARTS-III tracker. Two forms of output tapes are available; a "primitive" extraction tape and a "system" extraction tape.

1.   Primitive Data Extraction

The primitive extraction tape contains the following information:

a.   Preamble

The initial words of each data block contain descriptive information to define the run/extraction mode. The information consists of the following:

1.   Scan number

ii.   Block Number and record number

iii.   Number of Words Containing Data

iv.   Clock Time

v.   Data Extraction Type Indicator

b.   Data

The data extracted consists of the following information collected within *a* specified range-azimuth gate:

i.   MTD Output – PAZ and VRS Words

ii.   Radar *Target* Reports

iii.   Target Records used in Forming Target Reports

iv.   Noise Responses

2.   MTD System Data Extraction

This data is utilized to determine MTD radar and IOP performance. Radar, beacon and track information is extracted for subsequent data reduction and analysis.

a.   Preamble

The initial words of each block contain descriptive information to define the run-extraction mode. The information consists of the following:

1.   Scan Number

ii.   Block Number and Record Number

iii.   Number of Words Containing Data

iv.   Clock Time

v.   Data Extraction Type Indicator

b.   Data Extraction

The data extracted consists of the following information on a scan basis. The first four items are collected only within an operator specified range-azimuth gate or via a unique beacon code.

 i.   MTD Radar Reports

 ii.   Beacon Reports

 iii.   Radar/Beacon Correlated Reports

 iv.   Tracking Data

 v.   Counters of the Number of Tentative Tracks

beacon
radar
initiating beacon
initiating radar
terminating beacon
terminating radar

 vi.   Counters of the Number of Firm Tracks

beacon
radar only
initiating beacon
initiating radar only
terminating beacon
terminating radar only
coasts beacon
coasts radar
coasts both beacon and radar

On-line recording of raw MTD and beacon replies on the BUCODE 4025 tape transport allows subsequent playback of the recorded data to insure compatibility in performance comparisons. The data is available for processing in subsequent MTD radar and IOP performance runs. A complete description of the radar, beacon and track data that is produced as well as the tape and data formats is given in references 15 and 25.

F.   Data Analysis

1.   General

In order to carefully analyze the performance of the MTD during the tests at NAFEC, a set of interactive graphics computer programs were written in FORTRAN for the Laboratory's IBM 370/Model 168 computer. A Tektronix 4014 graphic terminal with a keyboard and cursor was employed. The purpose of these programs is to read the MTD/IOP data tapes generated at NAFEC and display interactively any

plots of aircraft position. From these displays, blip/scan ratios and position accuracy studies were made. By correlation with ground clutter maps, data was analyzed for detection performance and both range and azimuth accuracy. A block diagram of this interactive graphics system is shown in Figure IV-15.

These programs use as input either the primitive or the system extraction data tapes generated by the ARTS-III system at NAFEC. A set of programs was written to take the 7-track 200-BPI density tapes generated at NAFEC and repack them onto a data format (g-track, 800-BPI density) which could be read quickly and cost effectively on the IBM 370. The primitive tape contains MTD threshold crossings and the radar reports after single-scan correlation and interpolation and after post-MTD thresholding (see Section IV-D). The system tape contains radar and beacon reports which are input to the ARTS-III tracker and also the ARTS-III tracking output. Tables IV-3 and 4 contain a list of radar observables on each tape. Both of these tapes together contain all the information necessary to analyze the whole sensor system from MTD output through the ARTS-III tracker for a given flight test. The interactive graphics program allows one to quickly and thoroughly analyze the data*. Areas of interest may be magnified on-the graphics terminal to carefully examine a small geographical area of the radar's coverage. Also, any data displayed may be written to disk storage and later printed for careful examination or for a permanent record. A cursor which is available on the Tektronix 4014-l graphics display can be used to selectively examine a particular track or target report and display its radar observables such as range, azimuth, scan number, velocity, etc. Hard copy of all plots presented on the graphics display can be obtained.

In addition, the interactive graphics software was modified to *allow* the fitting of a polynomial to range vs. scan number or azimuth vs. scan number using the method of least squares. The details of this work are presented in Section V-H.

The interactive graphics programs were first used to examine carefully the performance of the ARTS-III software in the IOP. Many software bugs and design errors were found and were then fixed by Univac who had responsibility for maintaining

_____

* The data from any specified number of adjacent scans and from geographically rectangular regions of the coverage may be displayed.

66

IBM 370/
MODEL 168

MTD
PRIMITIVE DATA
TAPE

MTD
SYSTEM SUMMARY
DATA TAPE

TEKTRONIX
4014
GRAPHICS
TERMINAL

TEKTRONIX
4014
GRAPHICS
TERMINAL
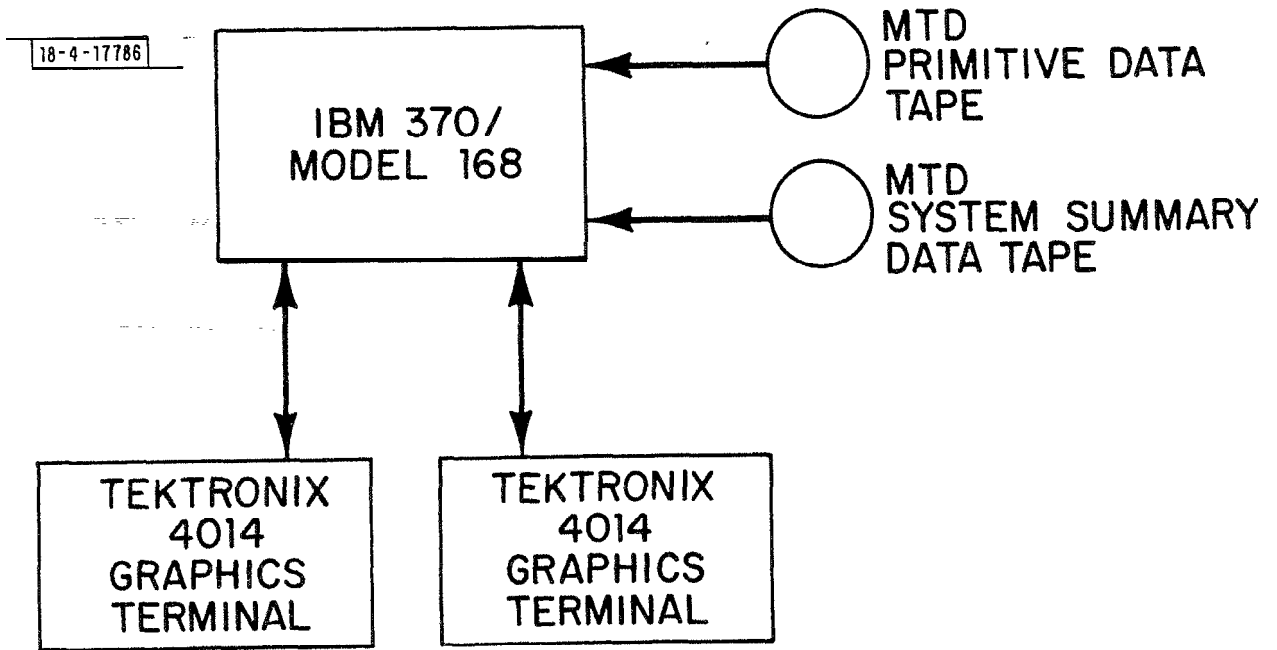
Fig. IV-15.   Interactive graphics system.

TABLE IV-3

LIST OF DATA ON PRIMITIVE EXTRACTION TAPE

For each radar threshold crossing

1. Scan number
2. Range
3. Azimuth-
4. Doppler filter number
5. PRF
6. Amplitude

TABLE IV-4

LIST OF DATA ON SYSTEM EXTRACTION TAPE

A. For each radar report
   1. Range
   2. Azimuth
   3. Radial velocity
   4. Amplitude
   5. Scan number

B. For each beacon report
   1. Range
   2. Azimuth
   3. Altitude
   4. Beacon code
   5. Scan number

C. For each radar/beacon track report
   1. Predicted azimuth
   2. Predicted range
   3. Predicted velocity
   4. Altitude   ⎫
   5. Beacon code   ⎬ if needed
   6. Radar/beacon hit history for last 10 scans
   7. Scan number

68

the IOP software.   Some of these problems included split radar targets, missing data, tracker malfunctioning, etc.

Once the ARTS-III software had been checked the interactive graphics system was used to measure the performance of the MTD.   During the flight tests the RVD-4 test flight data was written by the IOP onto tapes with essentially the same format.   The IBM programs have been modified so that data from either or both of the radar processors could be displayed;   A later report will document the comparison between the RVD-4 and the MTD.

2.   Examples of Displays

a.   General

In order to acquaint the reader with the display nomenclature and the flexibility of the interactive graphics system, a series of displays of data taken at NAFEC will be presented.   They will include single and multiple scan displays, examples of magnified displays, displays of-multiple radar observables and, finally, short examples of printed output.

b.   Single Scan Displays

Displays are presented for raw threshold crossings from the MTD radar processor (Figure IV-16a), MTD radar reports after single-scan correlation and interpolation (Figure IV-16b) which are input to the tracker, beacon reports which are input to the tracker (Figure IV-16c), and track position reports after the ARTS-III tracker (Figure IV-16d). The symbols 0, B, *, ? in Figure IV-16d stand for radar-only track reports, beacon-only track reports, radar/beacon correlated track reports and coasting track (no report for that scan for an active track) respectively.   Two-mile range rings are displayed.

c.   Multiple-Scan Displays

In Figures IV-17 we present 40 scans of data to highlight the uses and information content of many of the multiple scan displays.   The raw MTD threshold crossings (a dot for detection in each range-azimuth cell) are displayed as data, while the MTD radar, beacon and MTD radar/beacon correlated reports input to the tracker are displayed.   In Figures IV-16a and IV-17a it is evident that typically an aircraft is detected-in several CPI's and one or two range cells on each scan. The display symbology in Figures IV-17b, c and d is used to sense the time flow of an aircraft data and to make sure there is one and only one report for each target

69

RAW MTD THRESHOLD CROSSINGS

MTD TARGET REPORTS AFTER CORRELATION AND INTERPOLATION

(a)

(b)

BEACON REPORTS

AUTOMATED TRACKER OUTPUT

(c)

(d)

DISPLAY CODE

0 RADAR ONLY

B BEACON ONLY

* RADAR AND
   BEACON

(TWO MILE RANGE RINGS)
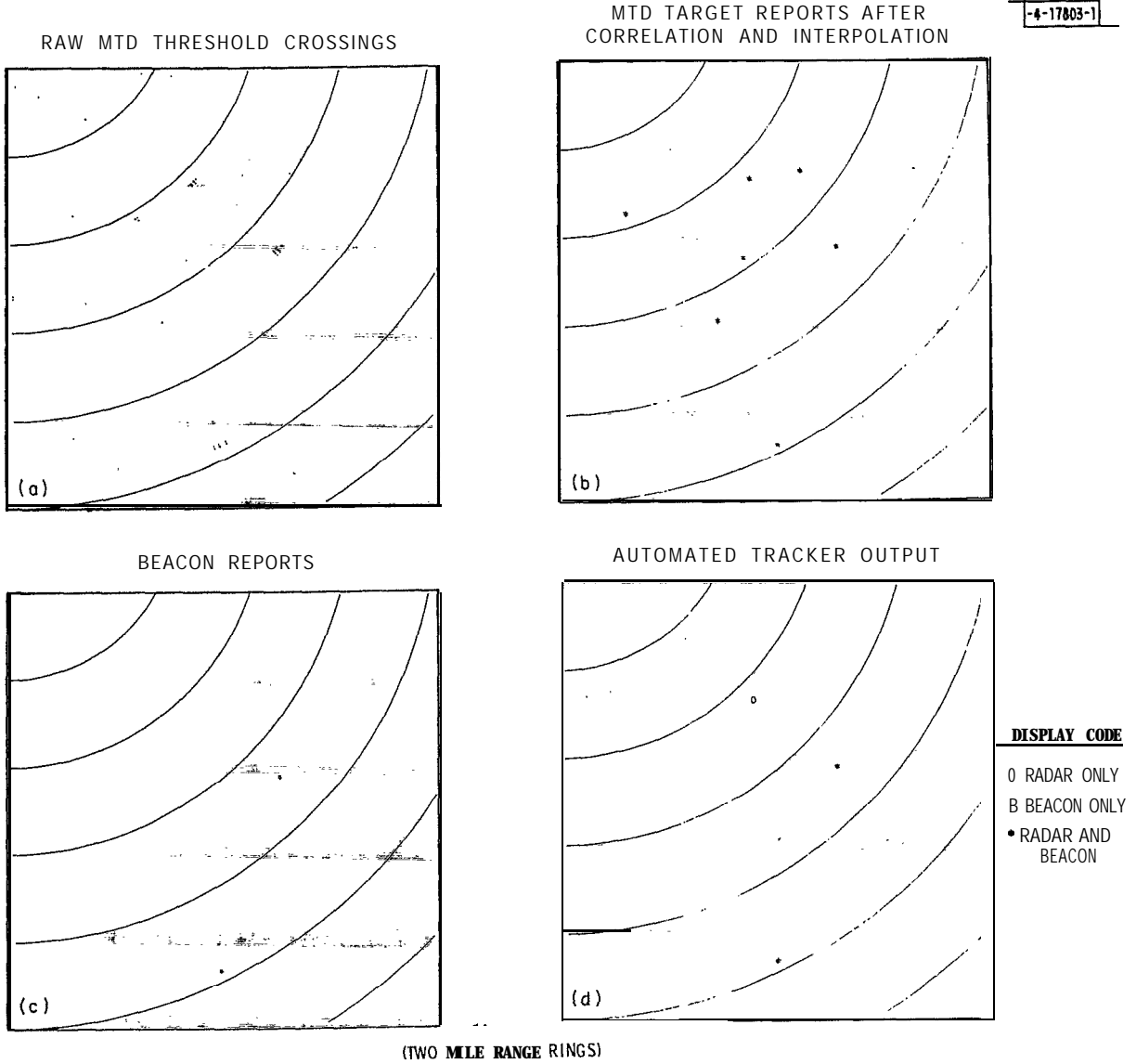
Fig. IV-16. Single scan displays of MTD data (0:radar only; B:beacon only; *:radar and beacon).

RAW MTD THRESHOLD CROSSINGS
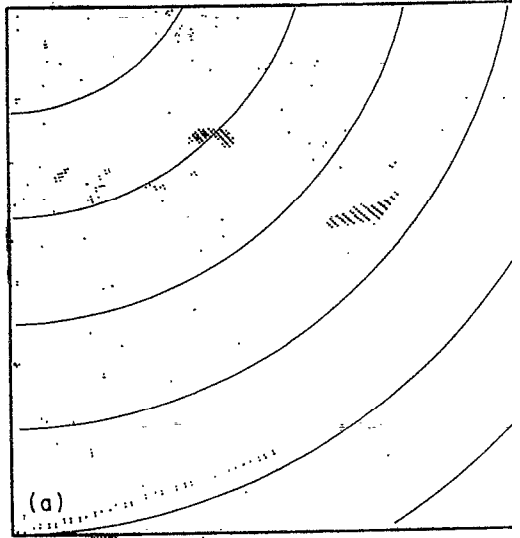
MTD REPORTS AFTER CORRELATION AND INTERPOLATION
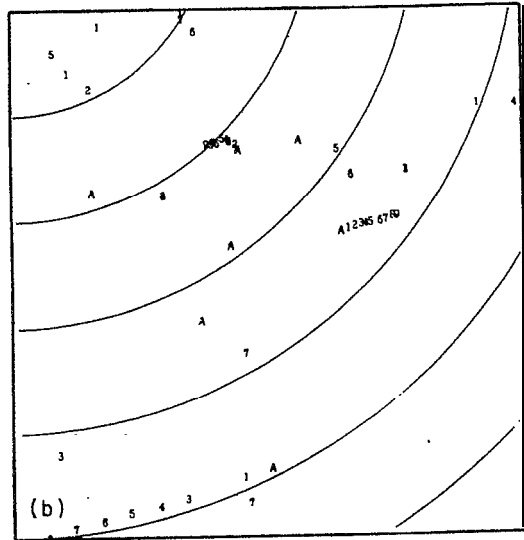
BEACON REPORTS
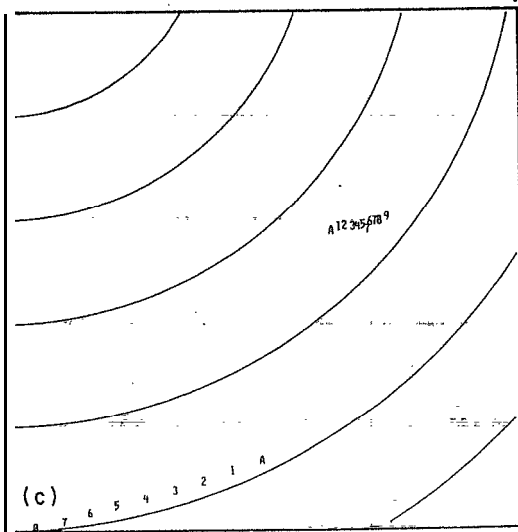
MTD RADAR /BEACON CORRELATED REPORTS
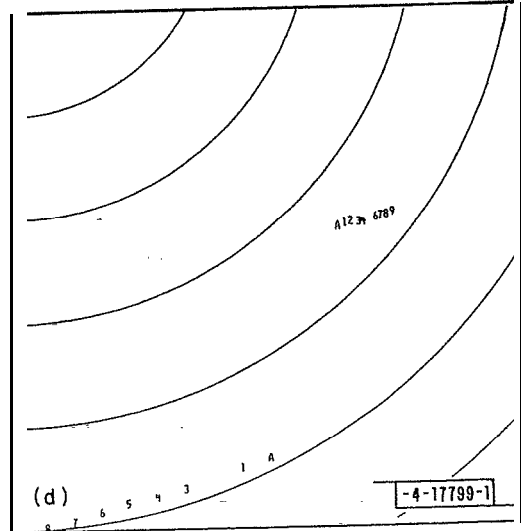
(TWO MILE RANGE RINGS)

Fig. IV-17. Multiple scan displays of MTD data.

71

each scan. With this display symbology, each report from first, second, third, . . tenth, eleventh, twelfth, thirteenth, etc. scan is displayed as a A, 1, 2, 3, . . 9, B, 1, 2, etc. Thus, there is a single alphanumeric code for the report from each scan. In Figure IV-18 data output from the ARTS-III tracker is presented using several formats. In Figure IV-18a, the symbols 0, B, *, ? represent radar-only track reports, beacon-only track reports, radar/beacon correlated track reports and no report (coasting tracks), while in Figure IV-18b all reports belong-ing to the same track index number are connected together with a line in time sequence of increasing scan number. All track reports which have the same track index number are given the same alphanumeric symbol in the data presented in Figure IV-18c. The symbology of Figure IV-18d is the same as that of Figures IV-17b through 17d. To illustrate the usefulness of these symbologies, the data in Figure IV-18 was rerun through the ARTS-III tracker when the data from the beacon was inhibited. The resulting long exposure displays of the automated tracker out-put for the same geographical region and time interval are presented in Figure IV-19. Two-mile range rings are shown for the displays in Figures IV-16 through IV-19.

d.   Magnification of Displays

The interactive graphics programs have the capability of magnifying any display an arbitrary amount. Figure IV-20 presents several magnifications of track data as an illustration of this feature.

e.   Overlay of Different Types of Data

Any or all different types of data from the same geographical region and same scan intervals may be overlayed for comparative analysis. Figure IV-21 presents three types of data; raw MTD reports, MTD radar reports after cor-relation and interpolation and track report data both individually and the three overlayed.

f.   Displays of Ground Clutter

A map of the clutter at NAFEC is stored on discs in the IBM 370. This digital map may be displayed alone or overlayed on any report data. A display of all of the ground clutter at NAFEC is presented in Figure IV-22. Figure IV-23 presents ARTS-III track output with and without clutter superimposed. With this display option it is possible to tell when test aircraft are flying through ground clutter on a scan-by-scan basis.

DISPLAY CODE

O RADAR ONLY

B BEACON ONLY

* RADAR AND
    BEACON

? COAST

TRACK REPORTS
WITH SAME
TRACK INDEX
NUMBER
CONNECTED
WITH LINE

(a)

(b)

TRACK REPORTS
WITH SAME
TRACK INDEX
HAVE SAME
SYMBOL

TRACK REPORTS
FOR A GIVEN
SCAN HAVE
THE SAME
ALPHA-NUMERIC
SYMBOL

(c)

(d)

(TWO MILE RANGE RINGS)

Fig. IV-18. Multiple scan displays of automated tracker output.

73

DISPLAY CODE

0 RADAR ONLY

B BEACON ONLY

· RADAR AND BEACON

? COAST

(a)

(b)
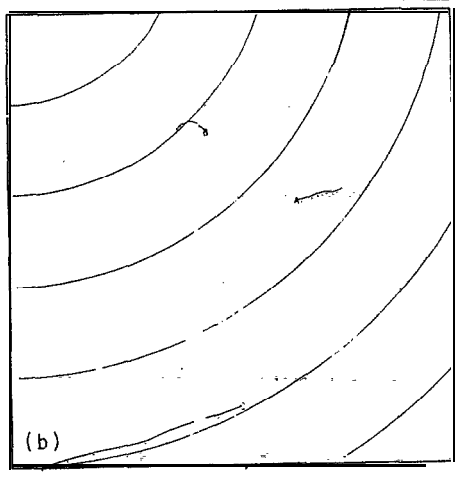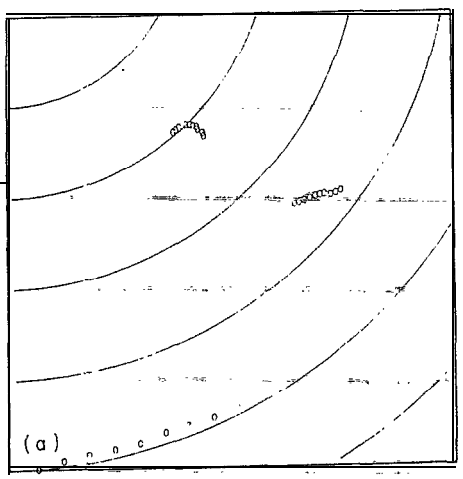
TRACK REPORTS WITH SAME TRACK INDEX NUMBER CONNECTED WITH LINE

TRACK REPORTS WITH SAME TRACK INDEX HAVE SAME SYMBOL

(c)

(d)
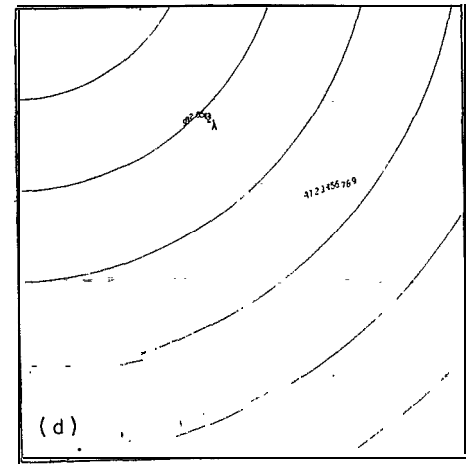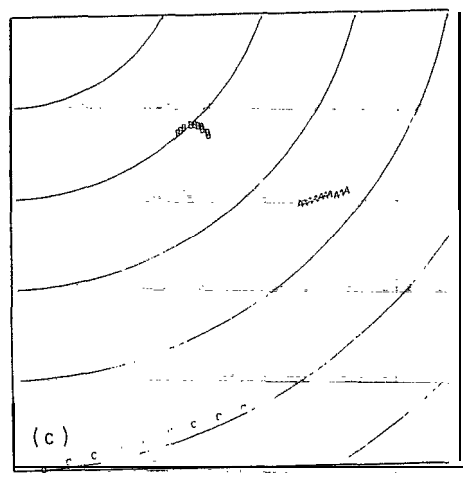
TRACK REPORTS FOR A GIVEN SCAN HAVE ME SAME ALPHA-NUMERIC SYMBOL

(TWO MILE RANGE RINGS)

Fig. IV-19. Multiple scan displays of automated tracker output (radar only data).
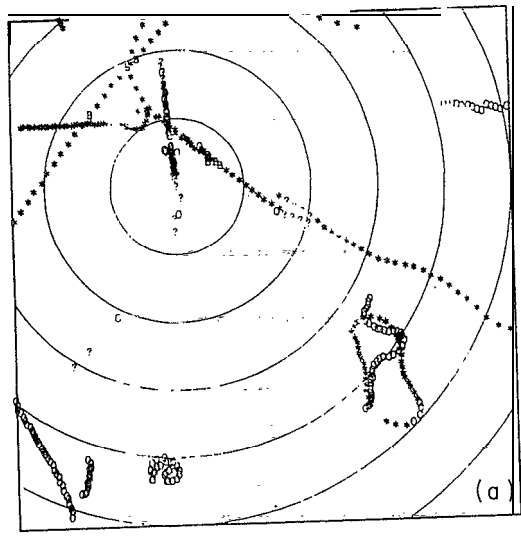
DISPLAY CODE

O RADAR ONLY

B BEACON ONLY

⚬ RADAR AND
  BEACON

? COAST
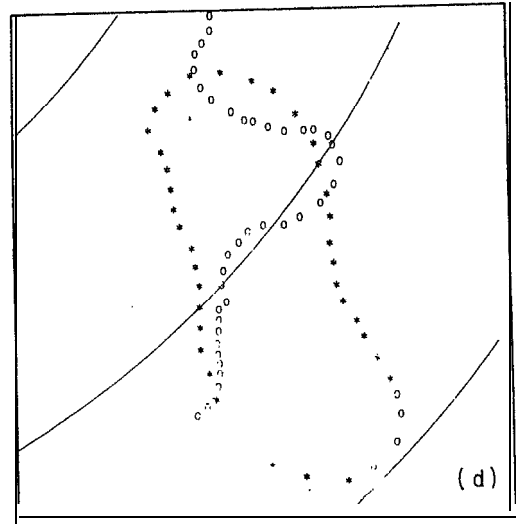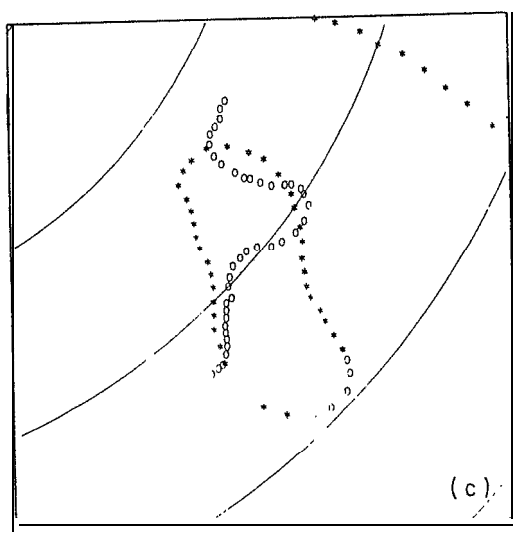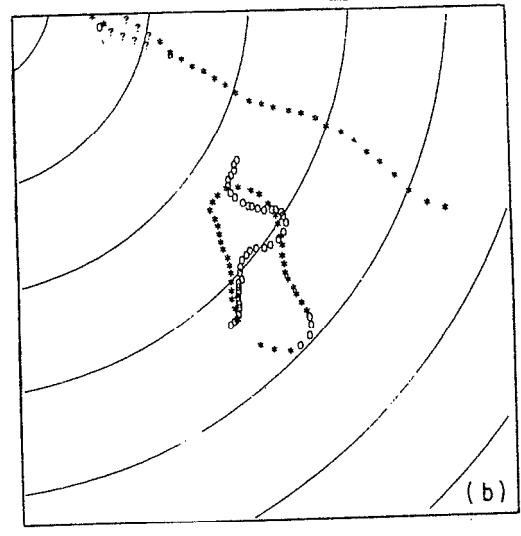
(FIVE MILE RANGE RINGS)

Fig. IV-20. Automated tracker output with different degrees of magnification.

RAW MTD THRESHOLD CROSSINGS

MTD REPORTS AFTER CORRELATION AND INTERPOLATION

AUTOMATED TRACKER OUTPUT

ALL THREE DISPLAYS OVERLAYED

(a)

(b)

(c)

(d)

-4-17801-1

(TWO MILE RANGE RINGS)
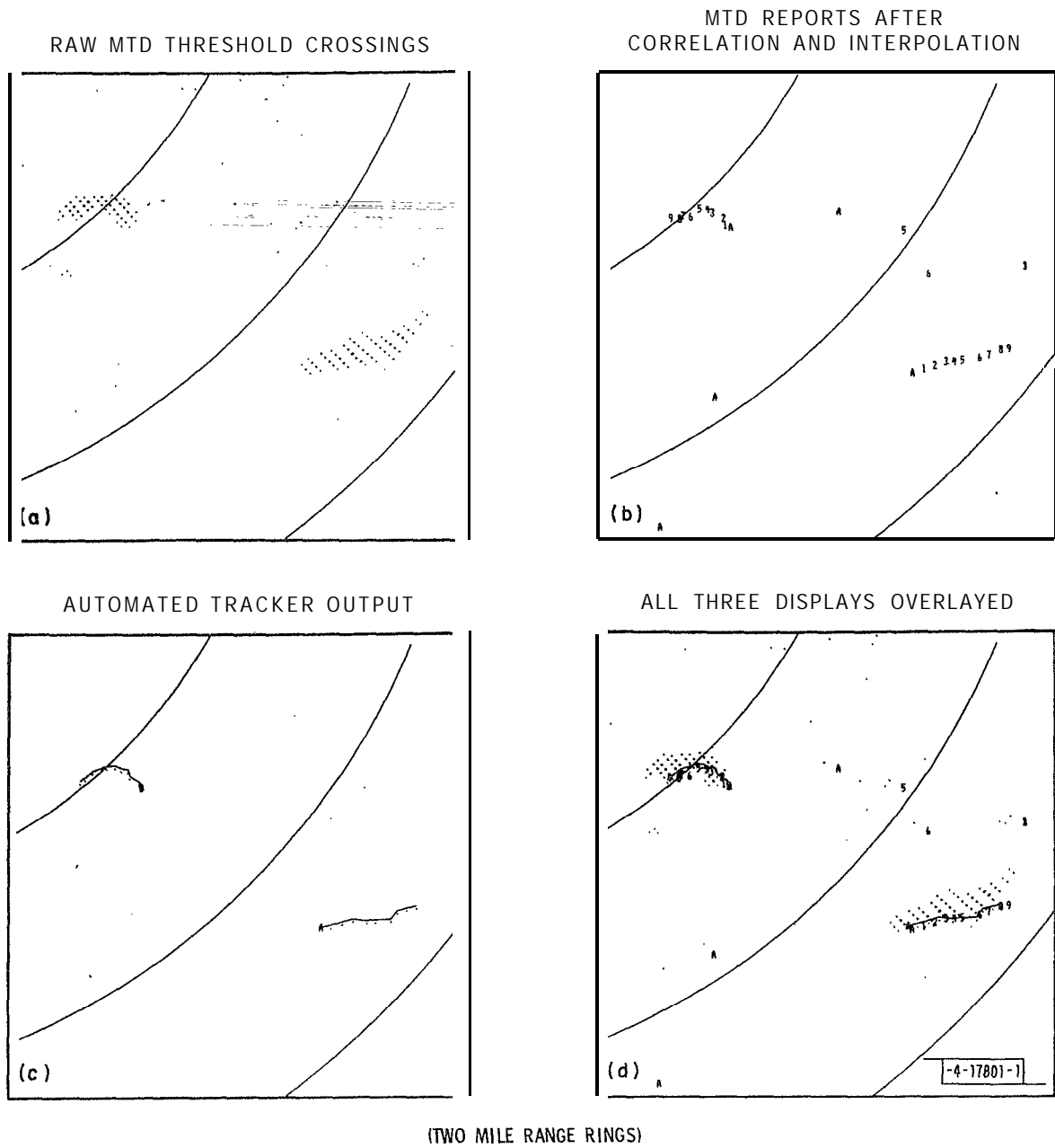
Fig. IV-21.   Different types of MTD data displayed singularly and overlayed.

76

**FIVE MILE
RANGE RINGS**

AREA USED **FOR
GROUND CLUTTER
FLIGHT TESTS**

Fig. IV-22. **MTD** automated tracker output with and wfthout ground clutter superimposed.

MTD (with ground clutter superimposed)

MTD

TEST AIRCRAFT

TEST AIRCRAFT

• BACON/BEACON
O RADAR ONLY
B BEACON ONLY
? COAST

TWO MILE RANGE RINGS
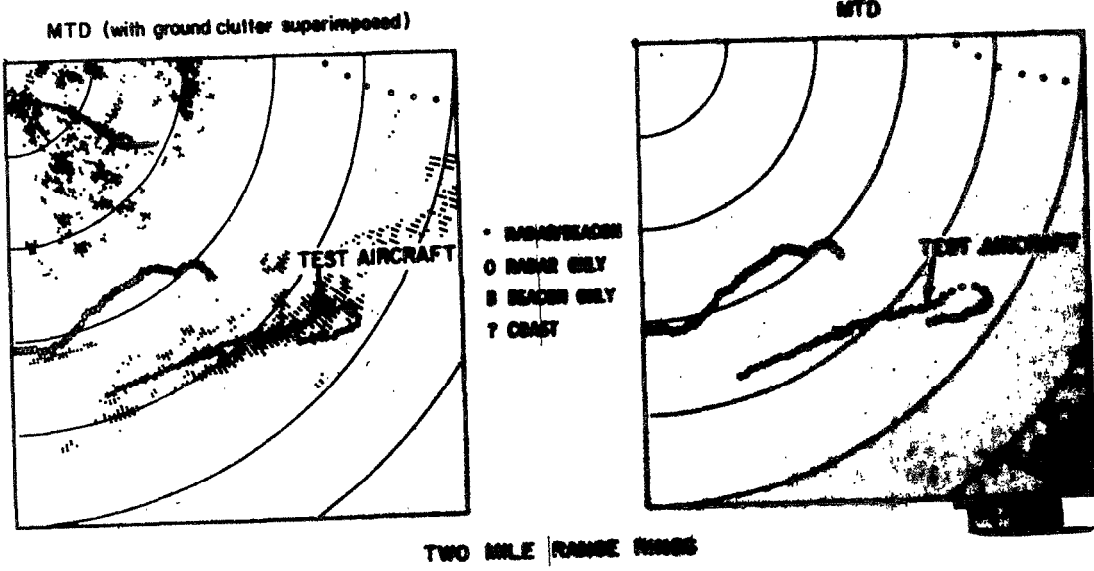
Fig. TV-23.   Performance of **MTD** in ground clutter.

g. <u>Printed Output</u>

Finally, there are options to print out all the data on any one report type or on any or all of the report types within the display.

V. DETAILS OF SPECIFIC TESTS

A. MTD Performance in Thermal Noise Environment

1. P_{FA} vs. RMS Thermal Noise Level

a. General

An important step in system testing is the determination of the dynamic range over which the system is in fact linear. The upper end of the linear dynamic range of signal strength is the level at which the A/D converters saturate (or a level which is simply related to it). As signal and noise levels are reduced, the lower end of the linear dynamic range may be encountered when quantizing noise and the effects of round-off and truncation cause an increase in the false alarm rate of the processor. To experimentally establish the lower end of the linear dynamic range, the probability of false alarm was measured as a function of the thermal noise level at the A/D converters. These measurements are made individually for each of the seven non-zero doppler channels in the system.

The weather thresholds are described by Drury (reference 13) and analyzed by Labitt (reference 26) and O'Donnell-(reference 27). Labitt's calculations were made earlier for an analog model of the digital system. O'Donnell's later analysis takes into account the effects of quantization in the digital realization of the system.

In this analysis,. Gaussian noise distributions of known RMS voltage are sampled in the A/D converters and propagated through the MTD using digital convolution techniques. A functional diagram of the MTD is presented in Figure V-1 showing the parts of the MTD that are linear operations and those that are not. The probabilities of false alarm as a function of RMS noise level, doppler filter number and threshold setting were calculated. The details of this analytical work are described in detail in Appendix C.

b. Experimental Measurement

Measurements of the false alarm rates due to noise are made with the transmitter off and the system disconnected from the antenna and connected to a waveguide dummy load; Attenuators in the intermediate frequency amplifier train are adjusted to produce the desired noise level at the A/D converter input. This noise level is measured with a true RMS voltmeter. The desired

Ⓐ

I-CHANNEL
ANALOG
VOLTAGE

A/D
CONVERTER

σ_I

Ⓑ
LINEAR

ADDER

σ_S

Ⓒ
LINEAR

THREE-PULSE
CANCELLER
AND
8-POINT FFT
AND
WEIGHTING

2σ
SAMPLES/CPI

10
SAMPLES/CPI

I

Ⓓ
NONLINEAR

MAGNITUDE
ALGORITHM

Ⓔ
LINEAR

CALCULATION
OF
MEAN LEVEL

Ⓕ
NONLINEAR

THRESHOLDING

P_{FA}
vs

RMS NOISE
LEVEL

DOPPLER
FILTER NO.

THRESHOLD
SETTING

Ⓐ

Q-CHANNEL
ANALOG
VOLTAGE

A/D
CONVERTER

Ⓑ
LINEAR

ADDER

Ⓒ
LINEAR

THREE-PULSE
CANCELLER
AND
8-POINT FFT
AND
WEIGHTING

Q

2σ
SAMPLES/CPI

10
SAMPLES/CPI

*ZERO VELOCITY FILTER, CLUTTER MAP, AND ITS THRESHOLDING ARE DELETED.

Fig. V-1.   MTD processor: functional diagram.

80

threshold multiplier can be selected by inserting one of a set of prewired plugs into a certain socket on the MTD chassis. The occurrence of false alarms is observed using the NOVA/DEDS subsystem. The time for 100 false alarms (or 1000) is obtained easily using a stopwatch and observing the time interval between subsequent fillings and emptyings of a single buffer.

Graphs of data measured this way along with calculated false alarm time are presented in Figures V-2 through V-6. At high noise levels the agreement between all measured data and both calculations is good. In filters 2, 3 and 4 there is good qualitative agreement between calculated and measured data, i.e., the false alarm rates increase with decreasing noise level. Quantitatively the measured increase in false alarm rate occurs at higher noise levels than predicted. It has been found that the A/D converters are probably at least partly the cause of the discrepancy. The A/D converters are rated at 10 bits but perform closer to 9-bit converters, the least significant bit being in error part of the time (reference 28). Thus, if the least count of the A/D converters had been 4 milli-volts rather than 2 millivolts, the agreement between theory and measurement would have been quite good for filters 2 through 6.

The net result is that the MTD processor can produce the expected false alarm rates at RMS noise levels of three or more A/D converter least counts. It *was* originally anticipated that the system would operate well at RMS noise levels as low as one least count. The difference means, a 9.5 dB reduction in dynamic range. Thus, the dynamic range that we realize is less than 45 dB. We had expected it to be 54 dB.

Because of the symmetry between filters 1 and 7, 2 and 6, and 3 and 5 only data from filters 1 through 4 are presented here, although all seven filters were measured.

In the case of the 1 (and 7) filter, the discrepancy between theory and measurement is even larger. The least count would have to represent 8 milli-volts rather than 2 to explain the difference. An exact explanation of the higher false alarm rates in the 1 and 7 filters is not available. Note, however, that these filters are unique in at least two respects. First, the 1 and 7 filters fall in pbrtions of the doppler passband at which the gain of the 3-pulse canceller is quite low. Secondly, the 1 and 7 filters are the only ones which use the $1/\sqrt{2}$ multiplier approximation in the DFT.
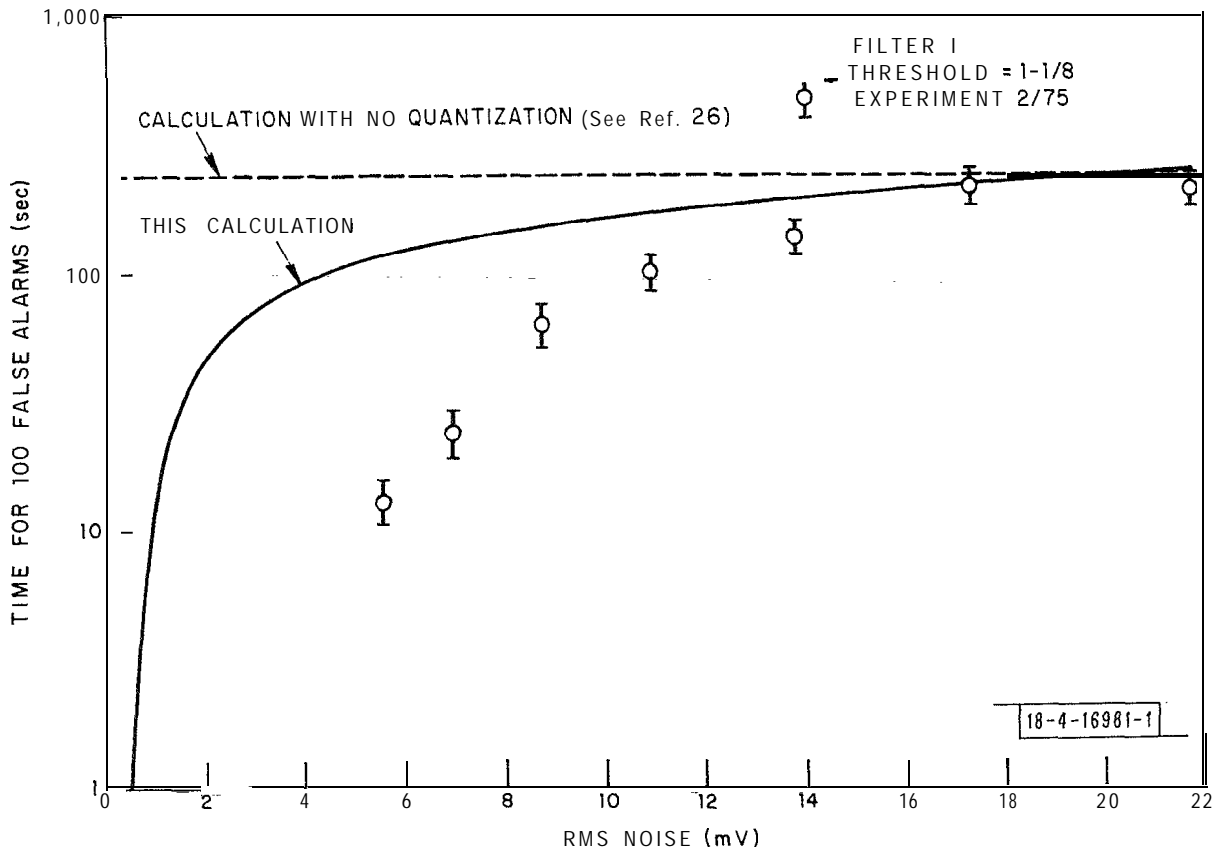
Fig. V-2.   False alarm time vs. rms noise level.

82
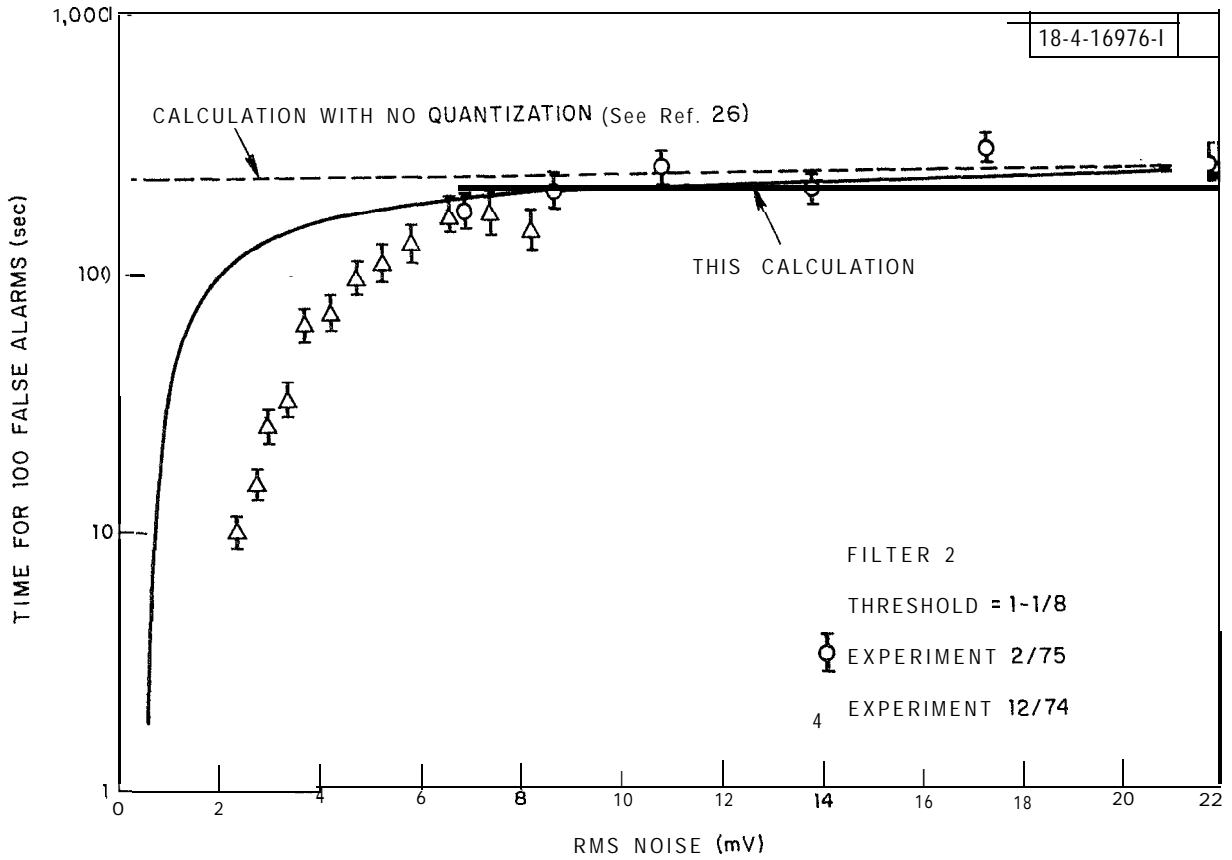
Fig. v-3. False alarm time vs. rms noise level.
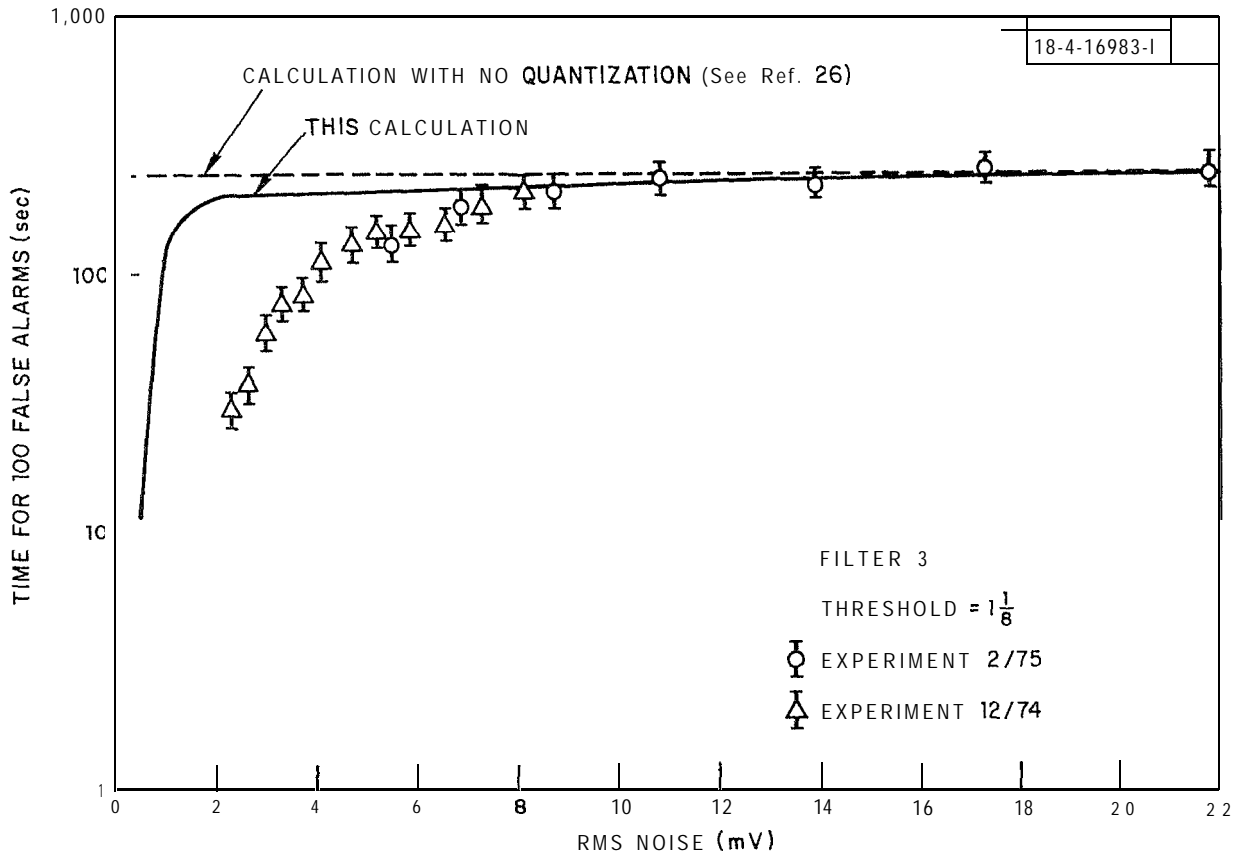
Fig. V-4.   False alarm time vs. rms noise level.
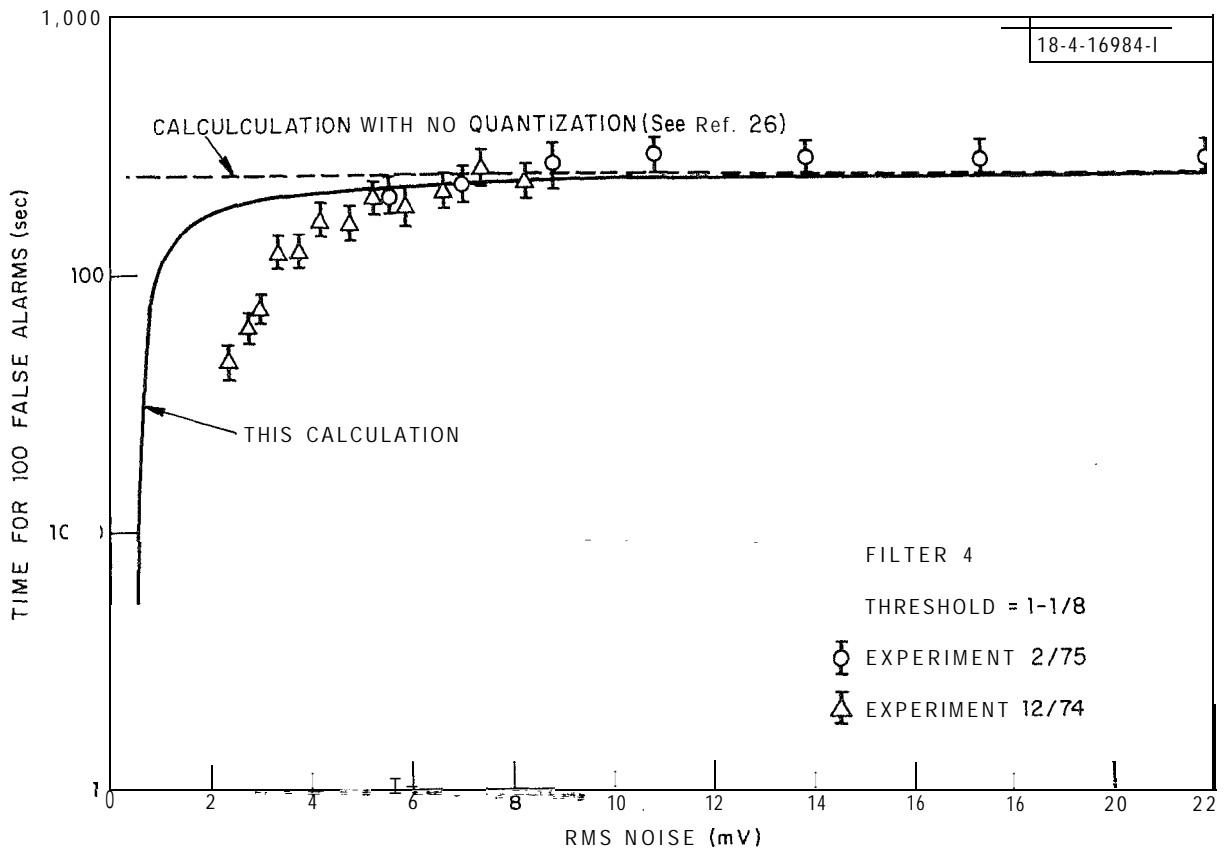
Fig. V-5.   False alarm time vs. rms noise level.
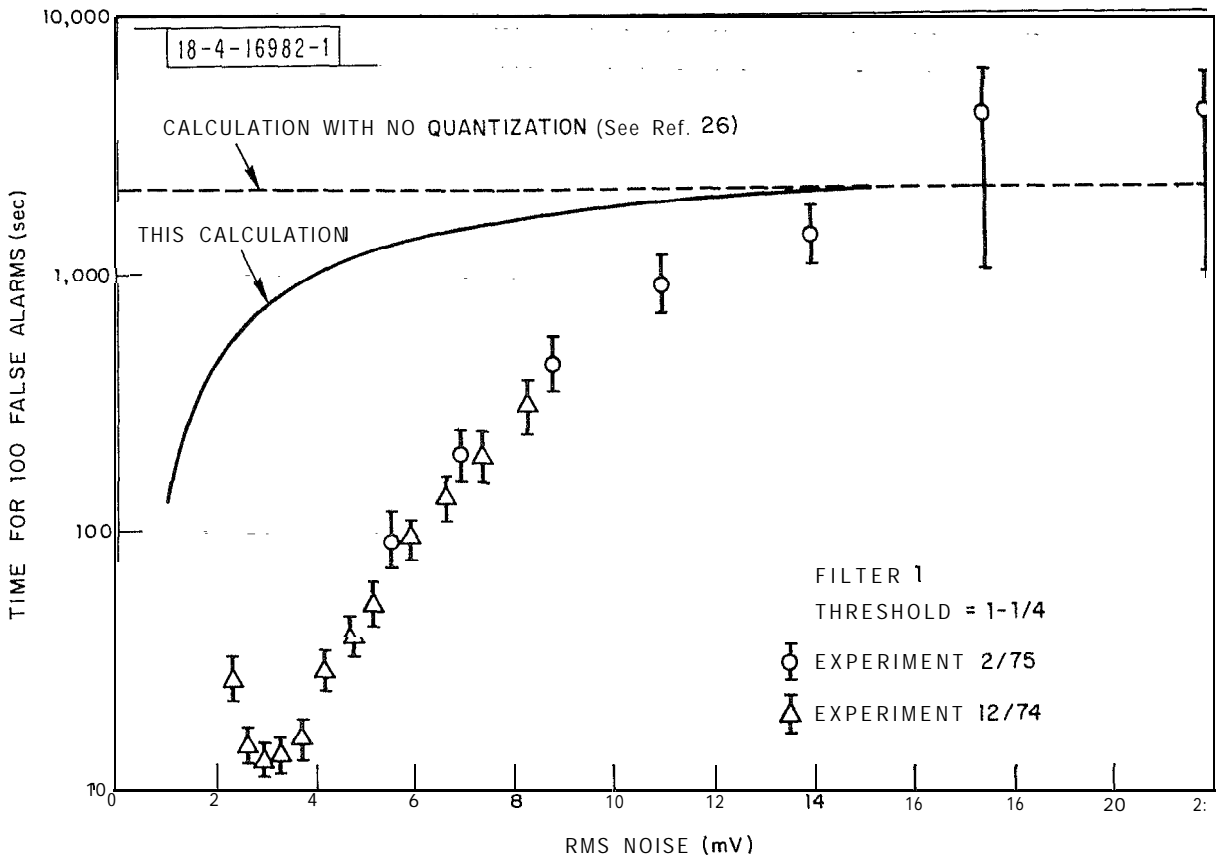
Fig. V-6.   False alarm time vs. rms noise level.

In view of the above measurements, it was decided that the normal operation of the system would be with the RMS noise level at 3 A/D converter counts (approximately 6 millivolts). Filters 2 through 6 would operate normally with a threshold ratio of 1 1/8 and filters 1 and 7 would operate normally with a threshold ratio of 1 1/4. This increase in the noise level from that designed for 2 millivolts up to 6 millivolts represents a decrease in dynamic range of slightly more than 9.5 dB. The higher threshold an the 1 and 7 doppler channels causes a loss in sensitivity of slightly less than 0.46 dB in those channels relative to the other doppler channels.

Techniques to reduce or remove the quantization errors due to truncation of bits within the processor have been analyzed and indicate that significant dynamic range (8-10 dB) can be added to the processor by use of these techniques. These techniques are described in Appendix C.

2. P_d vs. P_{fa} in Thermal Noise

Throughout the MTD testing effort, signal-to-noise ratios were expressed in terms of signal energy and noise power spectral density. This was done so that comparison of results between systems with different waveforms would be normalized.

The sensitivity of a radar receiver is defined in terms of the ratio of signal energy to noise power density required to produce a given probability of detection at a given false alarm rate. A wealth of theory exists. Predictions of probability of detection, P_d, and probability of false alarm, P_{fa}, to be expected for almost every imaginable situation are available in the literature (references 29 and 30). An example of these P_d vs. P_{fa} curves is presented in Figure V-7. In the preceding section we described measurements of the false alarm rate as a function of the receiver noise level. These results define the lower end of the system dynamic range. Next, we describe *measurements* made to determine if the system is in fact delivering the expected sensitivity at those noise levels.

The first tests of sensitivity may be regarded as the final stage of the system debugging process. Insofar as possible, the signals were arranged to eliminate losses caused by doppler filter splitting, range gate splitting, or
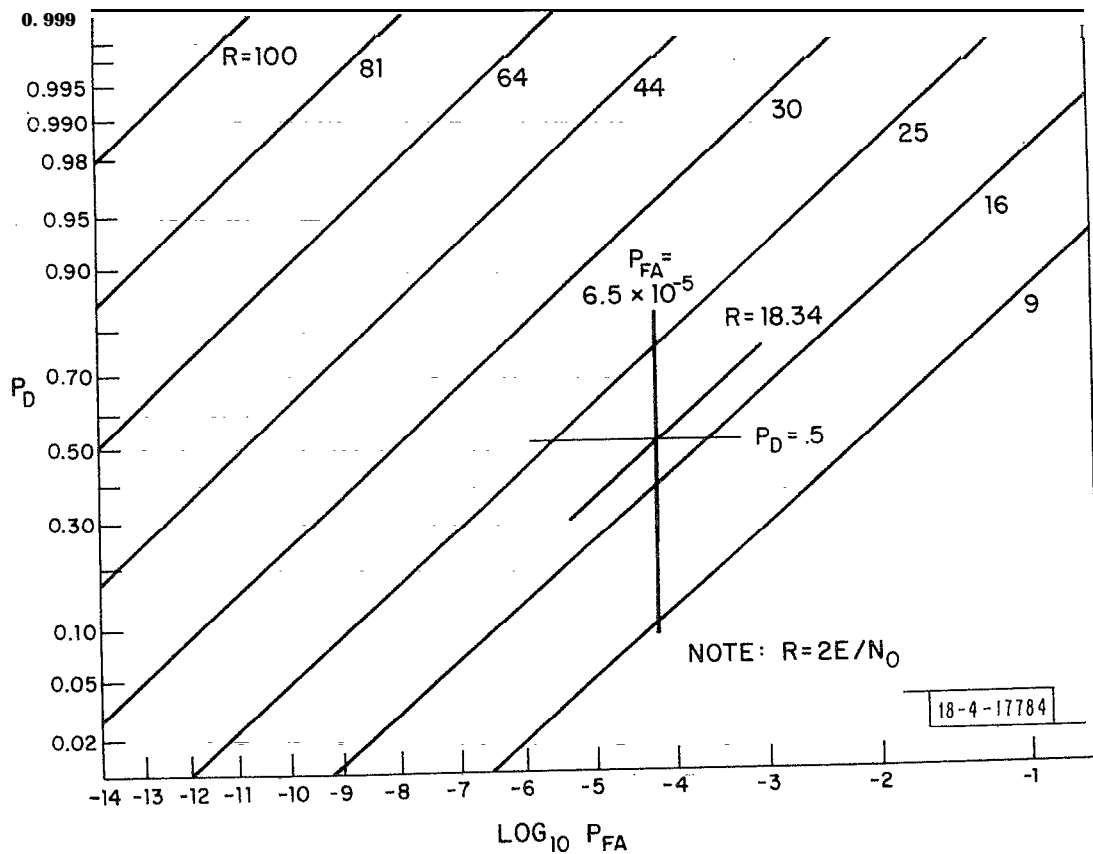
Fig. V-7. P_D vs. P_{FA} for known signal and unknown phase.

antenna pattern effects. The remaining losses include those associated with receiver mismatch and with the CFAR threshold which uses a finite number of samples in estimating the noise level. With this relatively simple loss structure, the performance of the MTD receiver was compared to that predicted by theory.

The experimental setup used *to* make these sensitivity measurements is shown in Figure V-8. The precision waveguide attenuator was calibrated in terms of signal-to-noise ratio with the TTG (Test Target Generator) in the CW position. The STC was turned off and the attenuator setting which caused the $(S+N)/N$ ratio to be exactly 3 dB as observed on a calibrated RMS voltmeter was noted. This is the attenuator setting at which the IF signal-to-noise is unity.

In these initial measurements a P_d of either 0.5 or 0.75 was used. The P_d was observed on the DEDS PPI display. To do this a NOVA DEDS display program was modified so that each of the target buffers contained 120 targets rather than the nominal value of 100. Each range gate received exactly 480 opportunities for a threshold crossing in a scan of the radar. The range of the test target was adjusted so that only a single range gate was involved and the azimuth modulation was turned off so the TTG made a continuous ring of test targets. Thus, when we observed only one of the target buffers in the NOVA DEDS display, the 50 percent probability of detection point was indicated when the 120 target buffer filled and emptied exactly twice per scan. Similarly, 75 percent detection was indicated when the buffer filled and emptied exactly three times per scan. The value of the signal-to-noise ratio in the IF bandwidth that produced the observed probability of detection was set with the precision waveguide attenuator.

Finally, the effective ratio E/N_o at the threshold *was* calculated from the relation

$$E/N_o = \left[(\tau\beta)\frac{S}{N}\right] \bullet \quad [n\, L]$$

where (S/N) = the IF signal-to-noise ratio measured as described above

τ = the radar (or TTG) pulse width

β = the 3-dB bandwidth of the receiver

n = the number of radar pulses integrated in the processor

L = the signal processing losses.
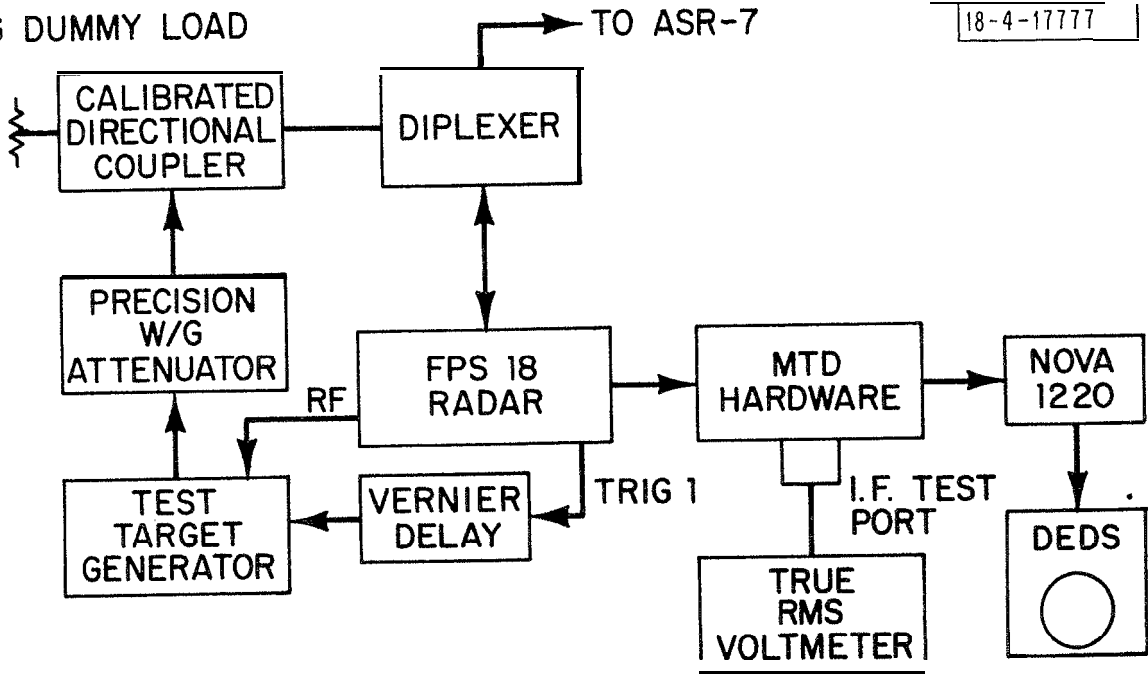
Fig. V-8.   MTD sensitivity test set-up.

The first factor relates the single pulse E/N_o ratio in the intermediate frequency amplifier to the signal-to-noise ratio measured there. It is based on the assumptions that the TTG pulse was rectangular and that the noise bandwidth of the radar receiver was, in fact, the nominal 3-dB bandwidth of the 3-pole Butterworth filter which was used to set the IF pass band.

The second factor in the equation above accounts for the improvement in signal-to-noise ratio which is expected from the processor. For this measurement, losses associated with antenna scanning, azimuth straddling, range gate straddling and doppler filter straddling have been eliminated. Losses that must be considered are pulse mismatch loss, doppler filter mismatch loss and threshold estimating loss. The latter arises from the fact that the mean-level threshold can use only a finite number of noise samples.

Except for those losses, the MTD as operated in this test is exactly the case "signal known except for phase" that was analyzed by Manasse[30]. In that reference Manasse calculated the detectability in various situations assuming receivers optimized for each situation. His results for this case are reproduced in Figure V- 7.

With 760 range gates in each of 480 CPI's, a single doppler channel of the MTD has 364,800 opportunities to produce a false alarm for each 360-degree scan of the antenna. At 12.75 antenna revolutions per minute, this corresponds to 77,520 target/no-target decisions per second. Thus, the probability of a false alarm when observing a single.doppler channel is given by

$$P_{fa} = 1.29 \times 10^{-3}/FAT$$

where FAT is the time for 100 false alarms in seconds.

In normal operation with the RMS noise level at the A/D converters set at 6 millivolts and the threshold ratio at 1 1/8, the time for 100 false alarms from the doppler filter number 4 is slightly more than 200 seconds (see Figure V-5). By the relationship above, this represents a P_{fa} on the order of 6.5×10^{-5}.

Interpolating from Figure V-7 we find that an ideal receiver operating on signals which are known except for phase would produce $P_d = .5$ and $P_{fa} = 6.5 \times 10^{-5}$ when the ratio E/N_o was about 9.6 dB and there were no losses. It is expected that the pulse mismatch loss will be on the order of 0.8 dB. The doppler

filter mismatch loss calculated for the particular weighting used in the MTD is approximately 0.9 dB. The loss associated with a CFAR threshold which computes the noise level from 13 samples has been calculated to be approximately 2 dB (see Figure III-11). Hence,, it is expected that operating with the known losses, the MTD tested as outlined above should produce the observed detection statistics (P_d = .5 at P_{fa} = 6.5 x 10^{-5}) at an E/N_o ratio of about 13.3 dB.

The MTD system integrates 10 pulses with a nominal pulse width of one microsecond. If the IF bandwidth is assumed to be 2.6 MHz*, then the E/N_o before the signal processing losses will be

$$E/N_o = 10 \times 10^{-6} \times 2.6 \times 10^{6} \left(\frac{S}{N}\right) = 26 \left(\frac{S}{N}\right)$$

After repeated runs of the test described above with P_d = .5 and P_{fa} = 6.5 x 10^{-5} the average of the IF signal-to-noise.ratio turned out to be about 0.5 dB below unity. Thus, the equivalent E/N_o averaged out to be about 13.65 dB.

We conclude that at RMS noise levels of 6 millivolts or more this version of the MTD processor can provide sensitivity which is very close to that predicted theoretically.

    3. <u>Probability of Detection vs. Doppler Frequency</u>

        a. <u>Single Filters at Fixed Pulse Repetition Rate</u>

The sensitivity of individual doppler filters was measured as a function of the doppler frequency. The equipment setup of Figure V-8 was used for these tests. As described above, the NOVA display program with 120 target buffers was used in order to facilitate measurement of the 50 and 75 percent P_d points. Each doppler filter was tested individually.

---

*
After these measurements were made it was discovered that 'the IF filter in use at NAFEC has been designed with a bandwidth of 2.6 MHz at the 1-dB points rather than the 3-dB points as had been assumed. This discrepance caused the IF noise bandwidth of the radar to be about 1.5 dB greater than was anticipated. However, the sensitivity measurements made in this section were based on IF signal-to-noise measurements made at the output end of the filter. Various analog video filters were used at different times, hence the measurements reported above were probably optimistic by about 1.5 dB.

The measurements were made by first setting the desired doppler offset on the TTG and then adjusting the precision attenuator to produce 50 percent probability of detection as observed on the DEDS display.

Results for the non-zero doppler filters are displayed in Figure V-9. The measured doppler response was found to be essentially identical to that predicted in reference 26. Excellent symmetry was observed to exist between filter pairs 1-7, 2-6 and 3-5. In order to make the figure. easier to interpret, results are plotted in Figure V-9 only for filters 1 through 4.

The zero velocity filter response was measured the same way. Because of the action of the clutter map, the TTG doppler offset was set at a high blind speed. This was done to make the signal appear in different range-azimuth cells each scan. Otherwise the clutter map would have caused the threshold value to increase from scan to scan which would have made accurate measurements impossible. Results of this measurement are plotted in Figure V-10.

b. Overall Response at Variable PRF

The response of the seven non-zero doppler filters was measured with the radar operating at its normal variable pulse repetition rate. These measurements were made at the 75 percent P_d level. The zero velocity filter was not included because of the previously mentioned difficulties with the clutter map and clutter threshold. The results of this measurement are plotted in Figure V-11.

B. Sensitivity Measurements for Comparison with the RVD-4

1. Background

The motivation for these measurements is to obtain sensitivity measurements which are suitable for direct comparison with similar measurements made on the RVD-4. For meaningful comparisons, both sets of measurements must be averaged over range and azimuth as well as doppler. Further, signal-to-noise ratio settings of the TTG must be normalized.

The MTD range gates occur at 1/16 nmi (.7725 microsecond) intervals. The FPS-18 transmits-1-microsecond pulses. Hence, in the MTD/FPS-18 the received signal is oversampled by slightly less than 25% and the loss due to range gate splitting is quite small. The ASR-7/RVD-4 system, on the other-hand, operates at the same sampling rate with a pulsewidth of 0.833 microsecond, hence a greater gate splitting loss.

93
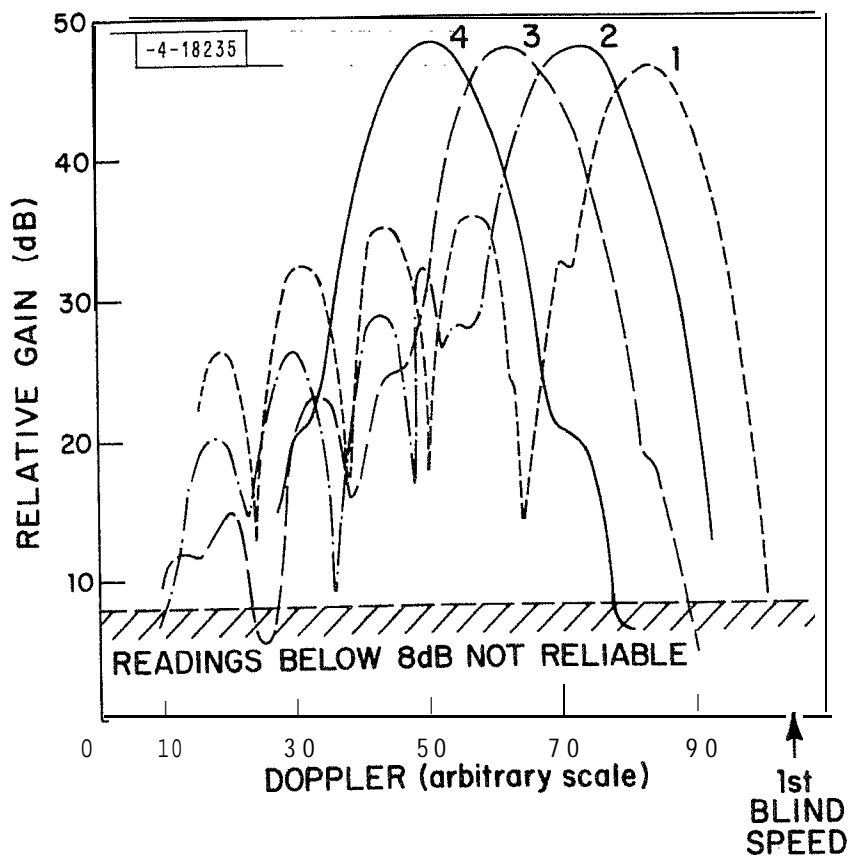
Fig. V-Y. Doppler response of MTD weather thresholded channels (measured).
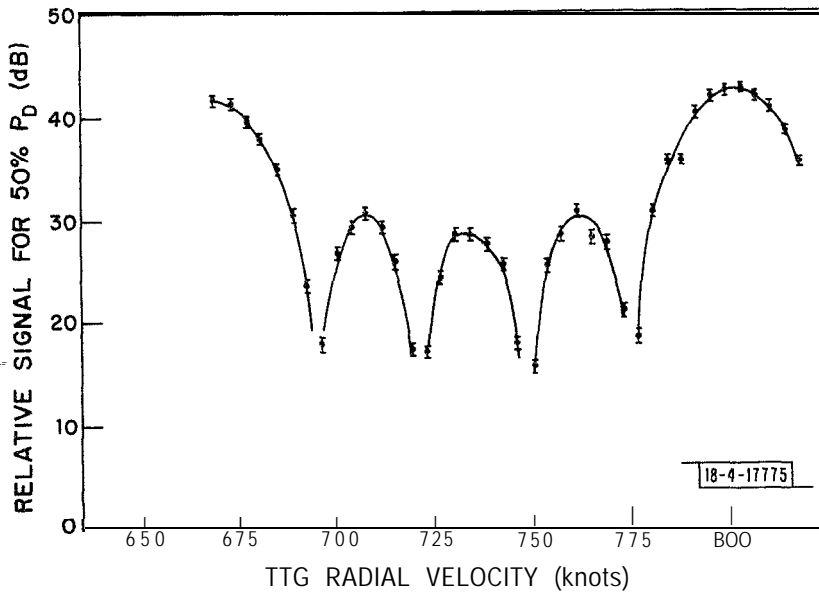
Fig. V-10. MTD zero velocity filter response.
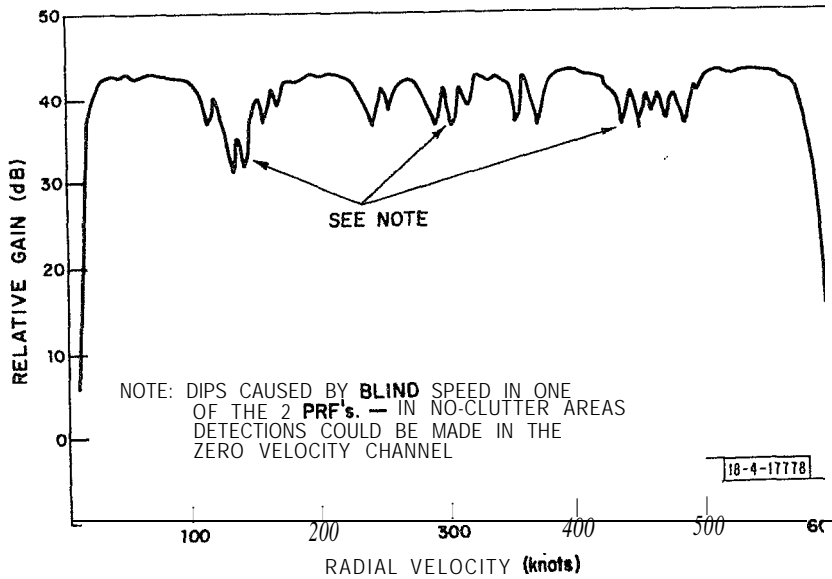
Fig. V-11. MTD weather thresholded doppler response.

Conventional radar video digitizers (including the RVD-4) make target thresholding decisions based on the history contained within an azimuth sliding window. This sliding window operates continuously in azimuth. Hence, the detection statistics should be independent of the target azimuth.

The MTD, on the other hand, divides the azimuth coverage into 480 fixed cells. Each of these cells, called a coherent processing interval (CPI), contains the information from 10 radar transmissions. Since the ground clutter map must register correctly from scan to scan, each of the 480 CPI's must be fixed in azimuth. The time duration of each CPI is set by the radar PRF. However, the antenna speed can vary with variations in wind loading. Thus, to keep the CPI's from overlapping each other at the higher antenna speeds it is necessary to allow extra time at the normal antenna speeds. This is done by leaving small segments during which no processing is done between pairs of CPI's at the nominal antenna speed (reference 13). Later versions of the MTD will probably use a varying PR?? which is slaved to the azimuth data so as to eliminate the need for dead zones.

For the purpose of estimating the beam shape and azimuth straddling, it was assumed that the antenna one-way voltage gain pattern could be represented by a function of the form (reference 31)

$$G(0) = \frac{\sin \left(\frac{2.783\ y}{\theta} \right)}{2.783\ \frac{y}{\theta}}$$

where y is the difference between the target and the antenna boresight azimuth and θ is the one-way 3-dB beamwidth.

The loss in received signal was then calculated as a function of target azimuth. These calculations are normalized to the signal that would be received from a stationary antenna with the nose of the beam aimed directly at the target. From these signal values the loss in probability of detection can be calculated for various situations. One important situation is that in which only a single threshold crossing is required of the MTD for a target detection to be declared. This is the way the MTD is operated at long ranges where sensitivity is important.

The time occupied by a single CPI is much less than the time the antenna takes to sweep out a 3-dB bandwidth. Hence detection is possible in more than one CPI and, if a target may be declared on the basis of a single threshold

crossing, the probability of detection on a single scan is the cumulative probability of detection as a- function of target azimuth. Under the assumption that the radar would provide 90 percent probability of detection with the antenna stopped and pointed directly at the target we find that the single scan probability of detection varies from a low .73 to a high of .91 as a function of azimuth position. Non-fluctuating targets were assumed. Averaged over all possible combinations of target azimuth vs. CPI position the probability of detection is .83.

Azimuth straddling loss is defined here as the increase in radar power (or the increased signal-to-noise ratio) that must be supplied to restore the average probability of detection when the antenna is scanning to the value that is realized when the antenna is stationary and aimed directly at the target. In this specific case the loss is estimated to be on the order of 0.6 dB for the MTD.

The RVD-4 sliding window occupies about 76% of the 3-dB one-way beamwidth.

As noted before the results from the RVD-4 should be essentially independent of the target azimuth. The beam shape loss of the ASR/RVD-4 system is estimated to be on the order of 1 dB.

2.   Normalizing

The sensitivity of a processor is defined in terms of detection statistics at its output and the ratio of signal energy to noise power density (E/N_o) at the processor input. For the purposes of these tests-, the processor input is defined as the radar's IF channel.

In the tests using controlled aircraft the signal (E/N_o) input to the two processors was equalized. This is done by normalizing the ratio of average power output to noise figure in each radar. For tests using the coherent test target direct measurements of average power were more difficult because of the low signal levels involved. E/N_o was controlled by adjusting the ratio of the peak of the pulsed signal power to the RMS noise voltage; This is done with a precision waveguide attenuator at the TTG output. This attenuator was calibrated with the TTG in the CW position. RMS noise voltage and RMS CW signal-plus-noise voltage were measured with a true RMS voltmeter at the IF frequency. These measurements were used to establish a unity signal-to-noise ratio point on the TTG attenuator. Normalization of the two processors was simplified because the IF bandwidth of the MTD and that of the ASR-7 were nominally equal.

3. Test Method

Averaging over range and azimuth was provided by a NAFEC modification to the TTG. With this modification the TTG produced 128 targets per scan. These are arranged in four-rings, each containing 32 targets. The targets move in range at a rate determined by the TTG target velocity setting. The azimuth of each target is increased one ACP per scan.

The spacing between the rings of targets was set at 65/16 nmi. With this setting the four target ranges tended to average over the range gate splitting possibilities. Additional averaging over the continuum of range gate splitting possibilities was provided by a uniform increase in the range of the entire target pattern.

Similarly, azimuth was averaged over the possible CPI splitting position both by the uniform spacing and the scan-to-scan stepping of the targets' azimuths. CPI pairs are spaced at an average of 17 ACP's while the test targets are spaced by 128 ACP's or 7 9/17 CPI pairs. An entire pattern of test targets is stepped clockwise one ACP in each scan.

The overall effect is to provide 128 TTG targets which describe a spiral path moving one ACP per scan while moving uniformly in range at a rate determined by the TTG control settings.

This-pattern of moving targets was observed for 17 scans. Different targets strength and/or velocity parameters were set in, the target pattern was reset to its start position and the process was repeated.

A subroutine in the IOP computer was used to record the number of detections in each of 15 scans every time the test target pattern was recycled. The IOP subroutine does not distinguish between false alarms and detections. Hence, the estimates of P_d collected this way are adulterated slightly by random variation in the false alarm rate.

The MTD probability of detection was measured by this method and the results are displayed graphically in Figure V-12.

C. Comparison Flight Testing — General

1. Objectives

The basic objective of the MTD development was to provide an effective primary radar sensor subsystem for automated terminal radar air traffic control systems. Accordingly, the objective of the flight tests was to demonstrate
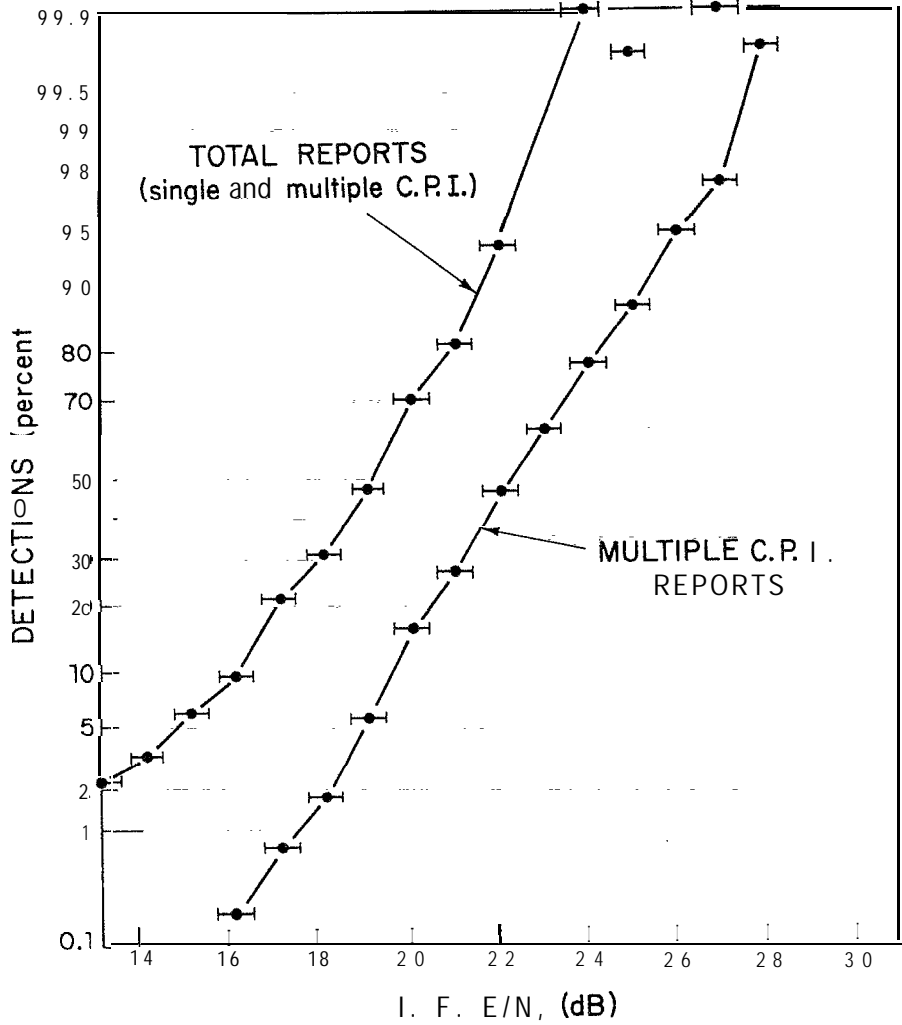
Fig. V-12. Detection percentages vs. i-f SNR (measured).

the effectiveness of the MTD radar as such a sensor subsystem. It was decided that the most effective way to do this would be by making a direct comparison between the MTD and the best available primary radar sensor subsystem, the RVD-4 operated in conjunction with an ASR-7 radar.

The absolute detection sensitivity in receiver noise obtainable from a given radar transmitter-receiver was not an issue in these flight tests. The primary basis for comparison between the two processors is their relative performance in detecting and reporting the position of aircraft whose echoes are competing with clutter returns from one or several sources (ground, weather, birds, etc.).

Many recent mid-air collisions involve at least one small. unequipped (with an ATCRBS transponder) aircraft. Therefore, a flight test objective is to demonstrate the radar processor's effectiveness against small general aviation airplanes operating at relatively low airspeeds.

2. Normalization

Ideally, the flight testing should be done with both processors (the MTD and the RVD-4) receiving radar information from the same radar. This approach was considered initially but rejected because the radar pulse repetition rates required by the different processors are very different. Major redesign of at least one of the processors would have been required to make single radar tests practical. The approach chosen was to operate the two radar processors through a common antenna by means of a diplexer. The two radar processors then were operated simultaneously while the test aircraft was flying.

Obviously, the results of the simultaneous flight tests made in this manner would be easier to interpret if the two radars were identical. Since the radars were not identical, their performance was normalized in terms of the quotient of average power divided by system noise figure. This quotient was adjusted to be the same for each of the radars. Average power and noise figure are measured on the antenna side of the diplexer (see Figure IV-l). Hence, differences in the waveguide losses between the antenna side of the diplexer and the different radars were accounted for, in the measurement*.

_____

*
 After these tests were made it was discovered that the IF bandwidth in the MTD was 2.6 MHz at the 1-dB points rather than the 3-dB points as has been assumed. Thus the E/N presented to the MTD during the flight tests was actually about 1.4 dB less ?han that calculated during the normalization process.

The difference in carrier frequency of the two radars necessitated by the diplexer remains as a potential source of error in the comparison of the two systems. Radar frequency can affect at least three parameters; namely, target cross section, antenna performance and the radar propagation.

On a single scan, target scintillation can cause large differences in the amplitude of radar returns *at* slightly different frequencies. However, when averaged over many scans, differences in aircraft cross section due to small differences in radar frequency are usually considered to be negligible.

When considered as a function of frequency, the behavior of ASR radar antennas varies somewhere between constant aperture and constant gain. Antennas which are designed for best aperture efficiency tend toward constant aperture, hence increasing gain as the frequency is raised. On the other hand, antennas which are designed for outstanding side lobe performance may tend toward constant gain, hence decreasing effective aperture with increasing frequency.

Two propagation mechanisms seem important in these flight tests. At shorter ranges and higher altitudes a free space model seems appropriate. At lower altitudes or longer ranges the radar propagation is probably better described by including the interference zone pattern propagation factor in the radar equation (reference 29).

The MTD *was* operated in conjunction with the FPS-18 radar at a radar frequency of 2710 MHz. The RVD-4 in turn processed video, from an ASR-7 which was operated 85 MHz higher in frequency. It can be shown that differences in received signal energy caused by that difference will be limited to less than 1 dB over all combinations of antenna performance and propagating mechanisms considered here:

3.   Aircraft

The primary target in all of the flight tests was one of three Piper Cherokees. A Piper Cherokee is a 4-place, low-wing airplane. It was originally introduced as a training plane and has a 150-horsepower engine and fixed landing gear. Over the years, variations of the basic design with higher horsepower and retractable landing gear have been developed and marketed. In size, speed and gross weight Cherokees are typical, small, general aviation aircraft. Detailed radar cross section measurements have been made on a 150-horsepower Cherokee

101

(reference 32). The specific aircraft that were used in the MTD flight tests
are as follows:

> N 35530 — a Cherokee Arrow with 200 horsepower and retractable landing
> 'gear,
>
> N 56639 — Cherokee Arrow similar to the one above,
>
> N 43403 — a Cherokee Warrior which is a later model with 150 horse-
> power, fixed landing gear and a somewhat longer wing than
> earlier Cherokees.

None of the aircraft used in the flight tests are the same model as the one
measured in the RATSCAT tests (reference 32). However, they are all very similar
and there seems to be no reason to suspect that the radar cross section of these
airplanes is significantly larger than that reported in that reference. There
is, conversely, reason to suspect that the Arrows with landing gear retracted
present somewhat smaller radar cross section for at least some aspect angles.

D. Coverage Comparison Flights

1. Low Altitude Flights

It was expected that, after normalization and in the absence of ground
clutter or precipitation, the two radar- systems would provide nearly identical
radar coverage. A few flight tests were run to verify that this was so and to
provide baseline data for comparison with later results obtained in clutter and
precipitation environments.

The test aircraft flew at an altitude of 1000 ft along courses which were
intended to be segments of radials from the TFAST site. The plane flew radially
out from the-site until it was no longer detectable and then was turned around
and flew radially in.

Results from these low altitude tests were essentially as expected. A
Cherokee Warrior was used and near unity blip-scan ratio was obtained out to a
range of approximately 23 nmi (see Figure V-13). No attempt was made to predict
the maximum range theoretically. However, the TFAST site has been in use testing
S-band radars for many years and the low altitude coverage achieved with the
FPS-18/MTD compares favorably with results that have been delivered at that site
by other radars of commensurate sensitivity using the same antenna.
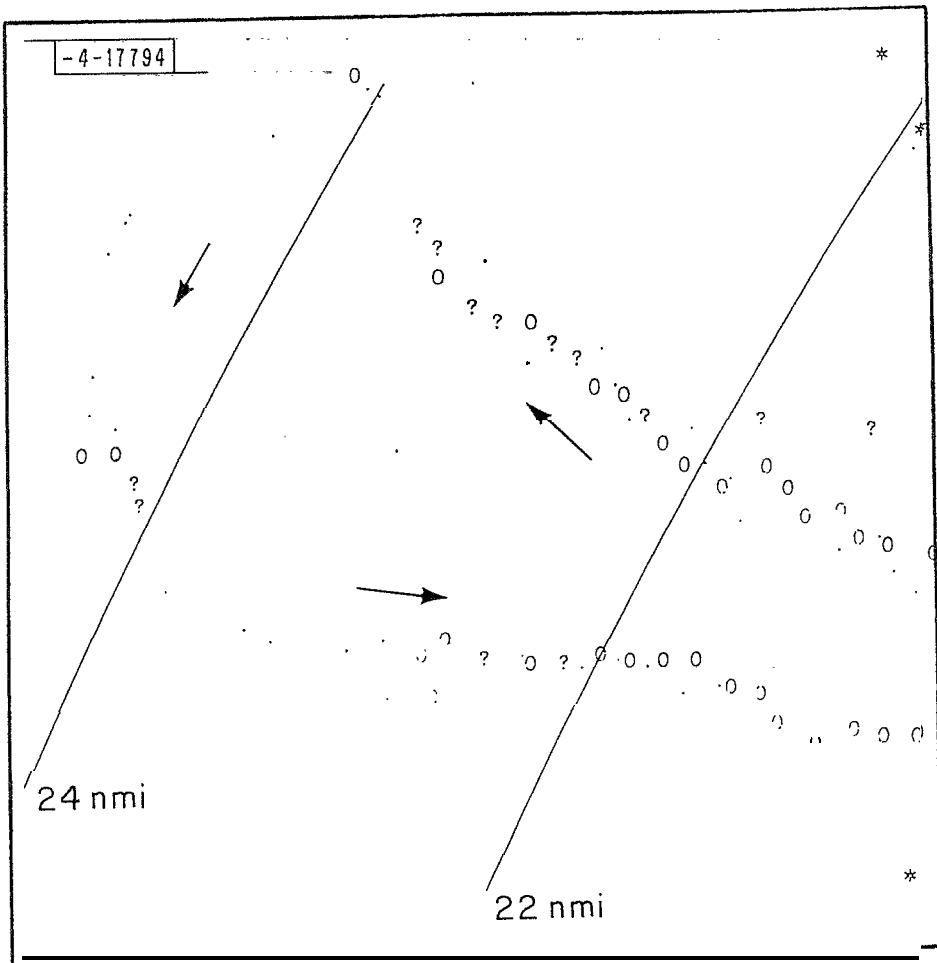
DISPLAY CODE

. MTD TARGET
REPORTS

0 ARTS III
PREDICTED
TRACK

? TRACKER
COAST

Fig. V-13.   Low altitude coverage.

2. Flight Tests at High Elevations

As originally conceived, the MTD system used a broad fan beam antenna pattern in the vertical plane. The ASR-5 antenna at the TFAST site provides a CSC^2 vertical pattern. In the original MTD system concept it was assumed that adequate sensitivity time control (STC) could reduce detection of clutter from birds and other weak moving-echoes to an acceptable level.

However, when a CSC^2 elevation pattern is used, the application of STC causes reduced sensitivity at higher elevations. Thus, if the MTD is to be used with existing CSC^2 antennas, the amount of STC used always represents a compromise. Desire for freedom from angel clutter must be traded off against the desire for good coverage at high elevation angles_". A few test radials were flown at higher altitudes in order to get some indication of how the STC in the MTD was affecting the coverage at these higher elevation angles.

The results (see Figure V-14) are corrupted somewhat by differences in target cross section at different aspects and by differences in the ground reflection pattern factor at different azimuths. However, a definite trend can be recognized. The upper limit of the elevation coverage was measured to be $22 \pm 2^{\circ}$ when the R^{-4} STC attenuation curve extended out to 16 1/2 nmi. When the STC attenuation was reduced so that the receiver recovered full gain at a range of 8 nmi, the vertical coverage angle increased to approximately 28 degrees.

This coverage compares very favorably with that measured previously by NAFEC using older radars on the TFAST antenna (reference 33). There is reason to suspect, however, that the improvement in short range, high angle coverage is related to improved subclutter visibility rather than sensitivity.

---

*Our experience at NAFEC has been that the angel clutter can be removed quite effectively by selective thresholding in the software that follows the MTD in an automatic system. The MTD provides both target doppler frequency and strength information for every threshold crossing it transmits to the automatic-tracking system. Software in the IOP and other ARTS hardware can make use of this information and discriminate between aircraft echoes and angel-echoes on the basis of doppler offset and target strength (see Section III-B).
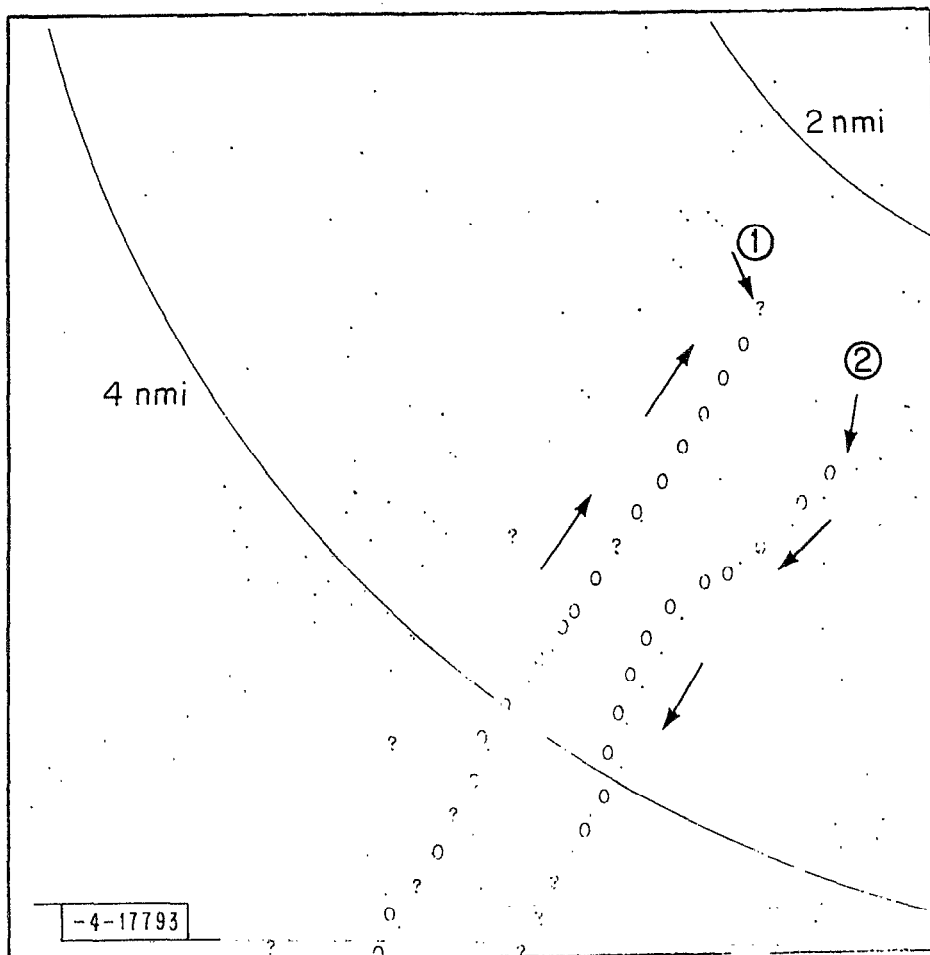
DISPLAY CODE

. MTD TARGET
    REPORTS

0   ARTS I II
     PREDI CJED
     TRACK

? TRACKER
   COAST

Fig. V-14.   High altitude coverage.

E.   Detection of Aircraft in Precipitation Areas

1.   Test Target Generator Tests

Expectations that the MTD processor will produce good detection statistics against aircraft flying in precipitation areas are based on certain assumptions about precipitation echoes. It is assumed that precipitation return may be approximated as colored Gaussian noise. Further, it is assumed that over the single azimuth resolution cell and the 16 range cells spanned by the samples used in setting the mean-level thresholds the precipitation clutter spectral power densities are relatively well correlated. Insofar as these assumptions are correct, the performance of the system in clutter environments can be predicted. Such predictions require knowledge of the precipitation echo power spectrum, the MTD threshold performance and the frequency response of the different MTD doppler channels. Threshold performance and doppler response have been measured and were presented in Section V-A.

Observations of precipitation spectra were made at NAFEC as often as the weather and other workload permitted. This activity is reported in Appendix A of this report. The observations are summarized in the following three statements:

(a) The strongest precipitation echoes observed did not exceed the linear dynamic range of the system.

(b) All precipitation echoes observed were spread in doppler over at least two adjacent doppler filter passbands.

(c) No precipitation echo was observed to affect more than four adjacent doppler filter passbands; i.e., in the worst case observed half of the unambiguous doppler passband was free of precipitation clutter.

Unfortunately, the test setup included no mechanism for simultaneous measurement of precipitation clutter spectra and detection statistics. Hence, direct quantitative measurements of system performance in precipitation could not be made. Qualitative assurance that the system was working as designed was obtained by injecting a moving target signal from the test target generator while operating in a precipitation environment.

Results of two such checks are presented as PPI photographs in Figures V-15 and V-16. The strongest precipitation echoes at the time those photographs were made were on the order of 30 dB above the thermal noise as observed at the input

to one of the A/D converters. The general weather drift at the time those photographs were made was from SW to NE (i.e., from the *lower* left to the upper right corner of the pictures).

As expected, the moving precipitation affected different doppler channels in different quadrants. Thus, in the lower left quadrant with the weather approaching the radar, detections of the TTG signal were in doppler channels 5 and 6. In the upper right quadrant where the weather was receding, detections occurred in doppler channel 3. In the segments which were free of precipitation, detections were observed in doppler channels 3, 5 and 6. This shows that the threshold level of the mean-level detector is increased in those range-azimuth doppler cells which contain precipitation clutter.

In most cases the mean-level threshold used with doppler channels 1 through 7 adapts to precipitation clutter with negligible increase in the false alarm rate. Occasionally dense precipitation cells with significant returns near zero doppler cause false alarms in the zero doppler channel. This can happen because the weather pattern is moving so fast that the time average zero velocity threshold (clutter map) does not have time enough to react adequately. This type of false alarm can be seen on Figures V-15 and V-16. These false alarms were eliminated by a test in the automatic track initiation routine which prohibits track initiation on target reports whose doppler offset is zero (see Section III-B-3).

2.   Test Flight — August 6, 1975

On August 6, 1975, the aircraft detection performance of the MTD was measured in a rain environment. A Piper Cherokee-Arrow aircraft was used for this test. The duration of the test was about two hours (1600 scans). The aircraft which was beacon equipped was vectored through heavy rain clouds during the tests. The intensity of the rain was measured on an A-scope. Its intensity varied from 0 to 40 dB above the receiver noise level. Data from the test was collected onto four Bucode tapes (see Section IV). Thirty scan blip-scan ratios of the radar reports after the correlator/interpolator were measured using the interactive graphics displays. A plot of the results is presented in Figure V-17. There are three gaps in the data caused by the rewinding and changing of the data tapes. The sharp dips in the detectability of the aircraft during the
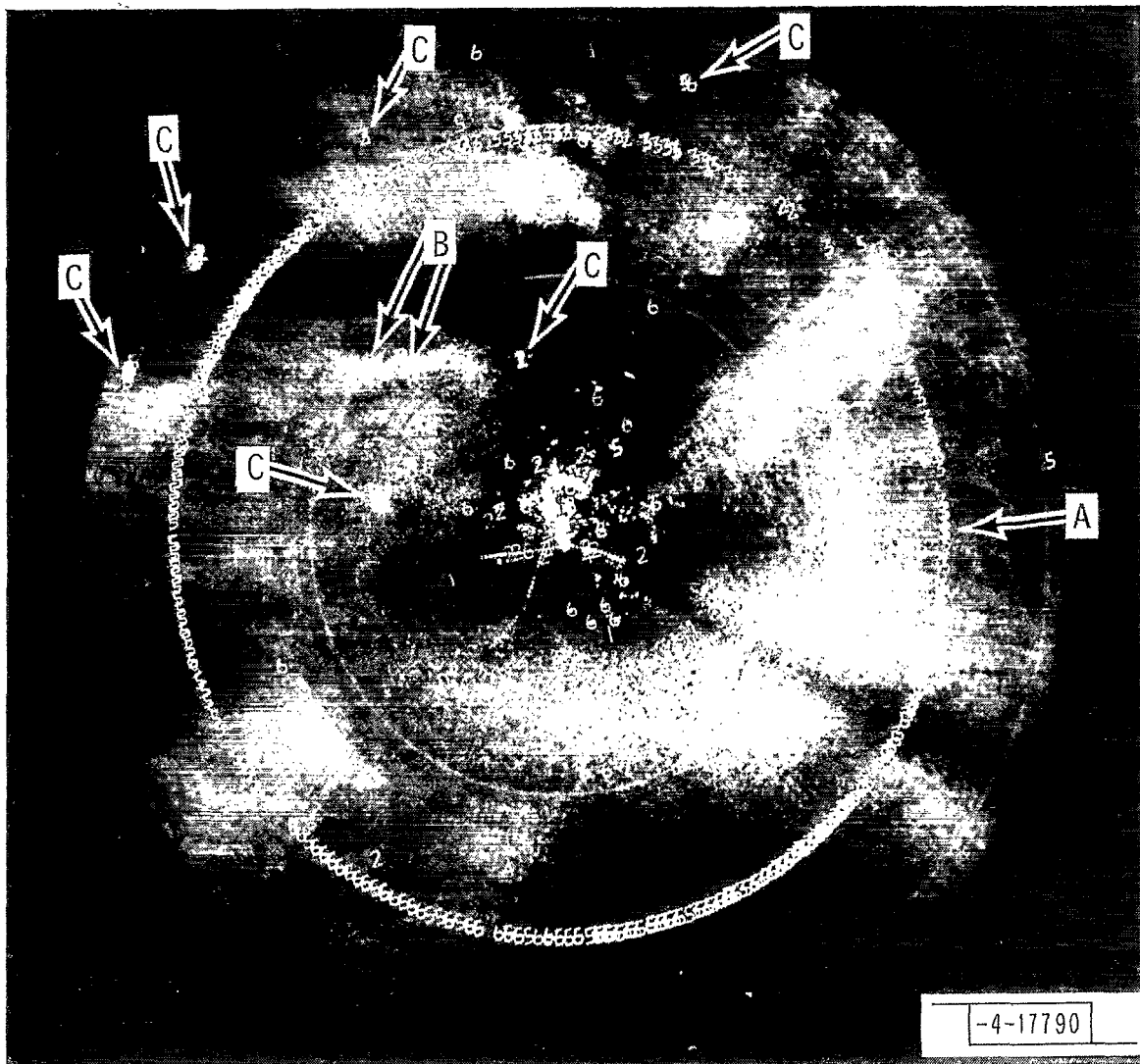
A = TEST TARGET GENERATOR
    TARGET RING
B = ZERO VELOCITY "LEADING EDGE" PRECIPITATION
    ECHOS
C = AIRCRAFT RETURNS

Fig. V-15. Test target generator detection in precipitation clutter.
(TTG set for 75% detection.)
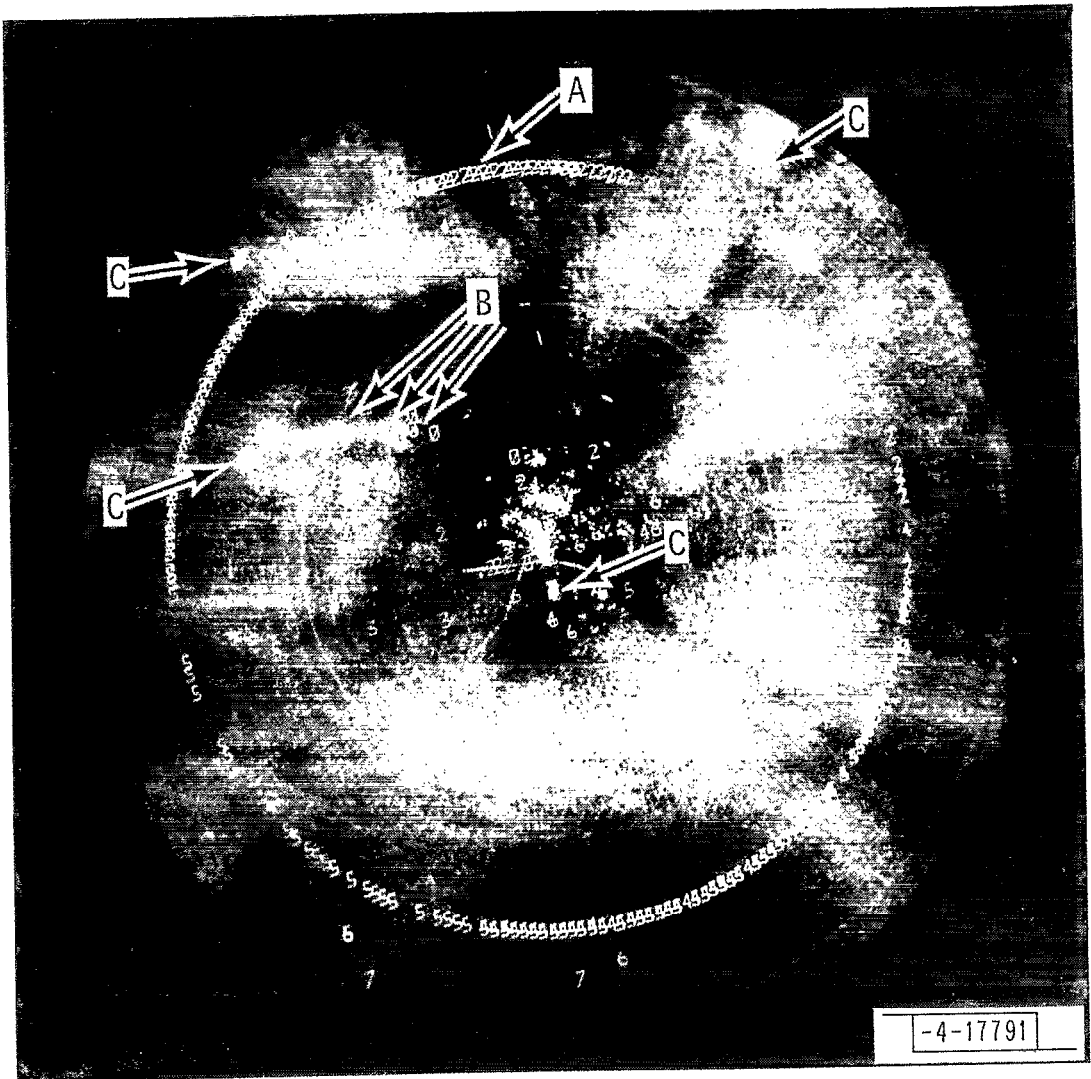
A = T.T.G. TARGET
      RING

B = ZERO VELOCITY LEADING
      EDGE PRECIPITATION
      ECHOS

C = AIRCRAFT
      RETURNS

Fig. v-16, Test target generator detection in precipitation clutter.
(TTG set for 50% detection.)

first hour were caused "by inadvertently vectoring the aircraft out of the radar coverage. The location of the aircraft during these periods was at a range of greater than 20 miles and an altitude of Less than 1500 ft. During significant portions of the last hour of the tethe test aircraft flew-through rain clouds whose backscatter intensity was 30 to 40 dB above receiver noise. As can be seen in Figure V-17, the detection performance in these heavy rain clouds is excellent. In Figure V-18 a photograph of the normal video of the radar is presented. The output of the ARTS-III tracker is presented for the entire test flight in Figures V-19 through V-26. In most cases, there are 60 scans of data per picture. The areas of flight through-heavy rain clouds (30-40 dB) were scans 1370-1400, 1500-1600, 1610-1700, 1720-1850. During these scans the MTD had a blip-scan ratio very close to unity. To obtain the tracking performance of the MTD data without beacon data, the recorded data was played back through the ARTS-III tracker with the beacon data inhibited. The radar-only track output data in Figures V-27a and b corresponds to Figure V-22a and V-23b. To give an indication of what the radar report data lookslike, MTD radar reports after correlation and interpolation and tracker output using two display types are displayed in Figure V-28 for an 80-scan segment of the rain test flight. data. The location of the test aircraft is noted on the figure. The data for a 40-scan segment in the northwest portion of the radar's coverage is displayed in Figure.V-29 to indicate the false alarm performance of the MTD data and the derived track data. There are few false alarms and negligible false tracks while the detectability of all aircraft in the coverage appears to be unity. Presented in Figure V-30 are the automatic tracker output for northwest portion of the radar coverage. These were obtained when the beacon--data was inhibited. Again, the tracks have essentially unity probability of detection and a negligible false track rate in the presence of heavy rain. Finally, in Figure V-31 a long exposure photograph (9 scans) of the ARTS-111 tracker output is superimposed on top of the normal video of the radar. The backscatter from the rain clouds and the ground clutter is visible. Note the excellent detectability of the aircraft flying through and around the rain clouds. In addition, false track reports from the rain are either few or nonexistent.
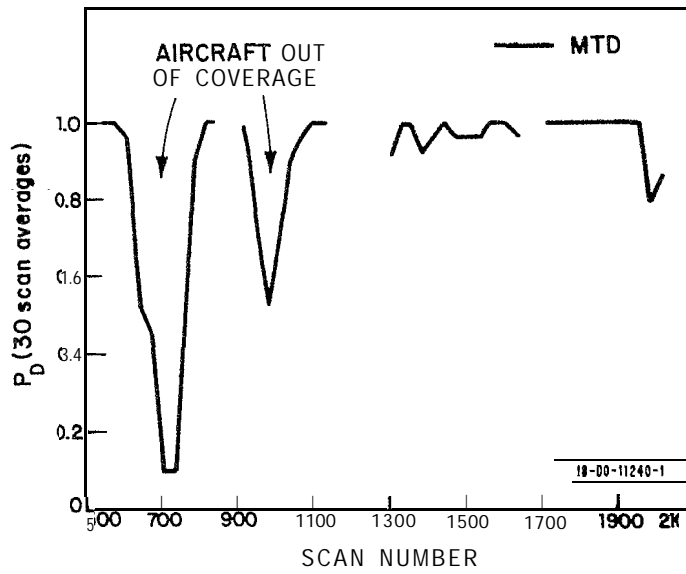
Fig. V-17. Blip/scan ratio during rain (6 August 1975).
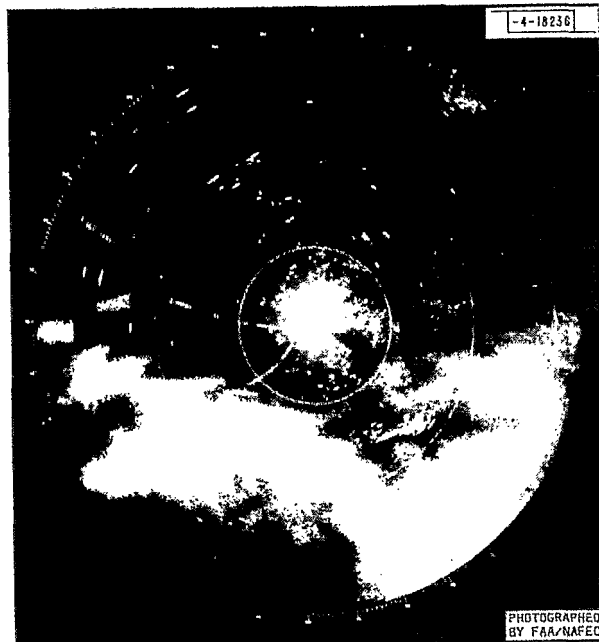
Fig. V-18. Normal video of rain (6 August 1975); 5-nmi range rings.

111

-4-17809-1

DISPLAY CODE

D RADAR ONLY
B BEACON ONLY
• RADAR AND
   BEACON
? COAST

(a) ALTITUDE = 1000 FT
SCAN 550 TO 589

(b) ALTITUDE = 1000 FT
SCAN 590 TO 629
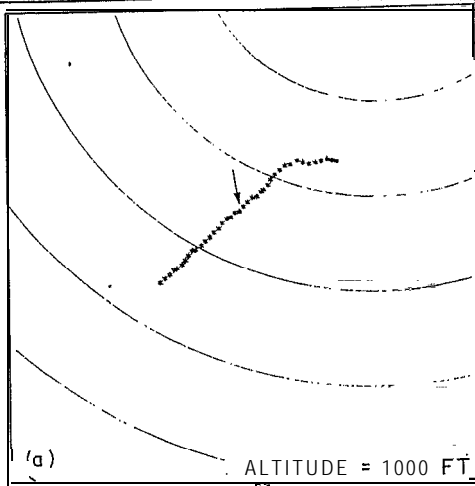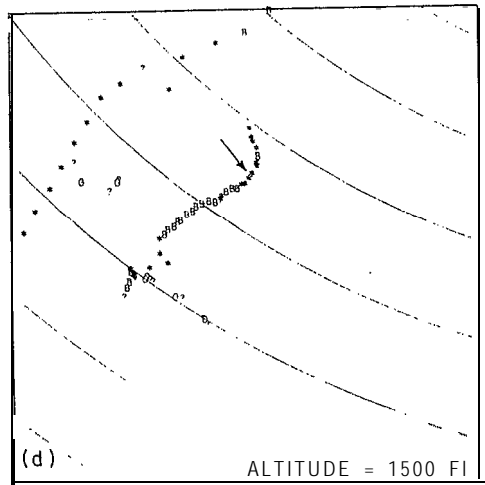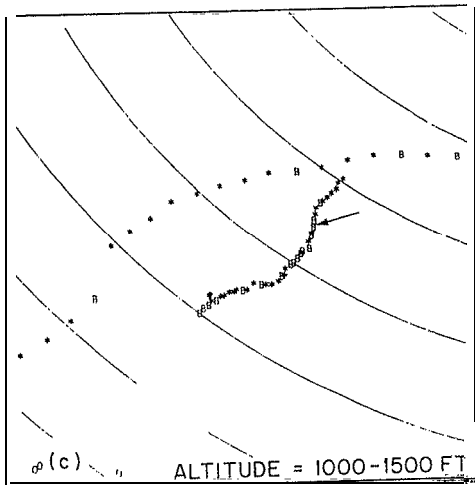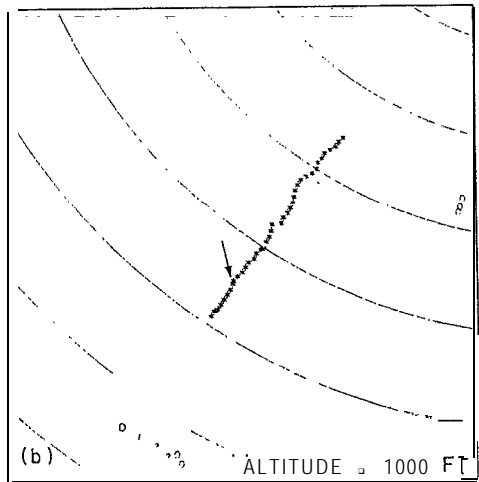
(c) ALTITUDE = 1000-1500 FT
SCAN 630 TO 669

(TWO MILE RANGE RINGS)

(d) ALTITUDE = 1500 FT
SCAN 670 TO 709

Fig. V-19. Test flight in rain (6 August 1975); automated tracker output.
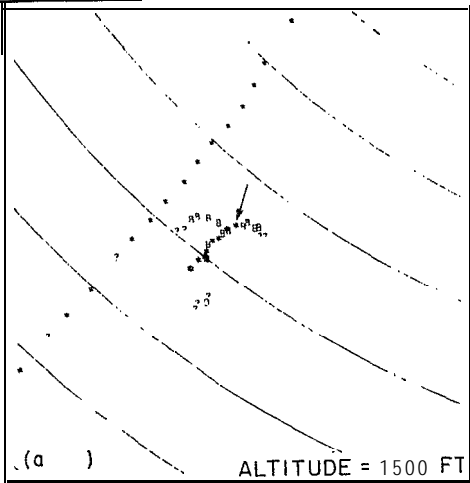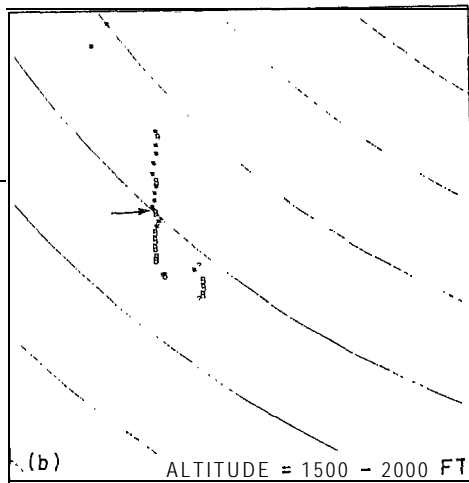
112

DISPLAY CODE

0 RADAR ONLY
B BEACON ONLY
• RADAR AND
    BEACON
? COAST

(a)   ALTITUDE = 1500 FT
SCAN 710 TO 749

(b)   ALTITUDE = 1500 – 2000 FT
SCAN 750 TO- 789
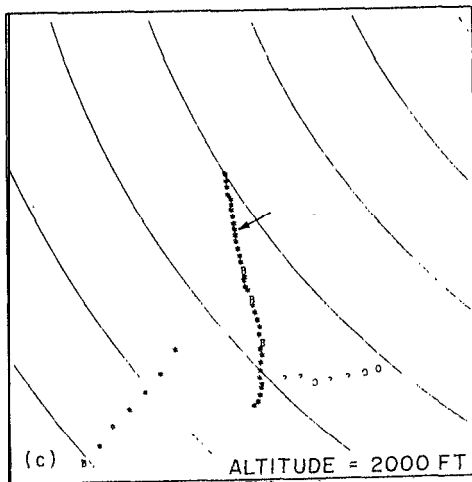
(c)   ALTITUDE = 2000 FT
SCAN 790 TO 829   (TWO MILE RANGE RINGS)
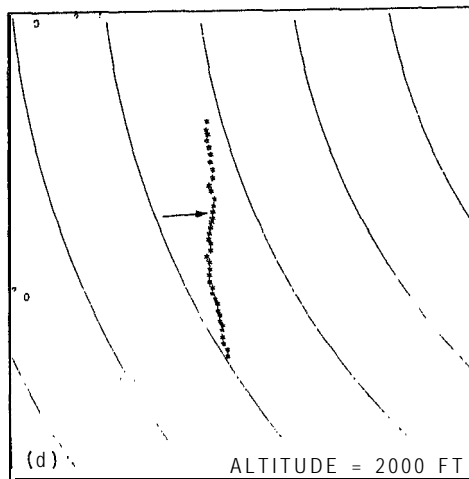
(d)   ALTITUDE = 2000 FT
SCAN 830 TO 869

Fig. V-20.   Test flight in rain (6 August 1975); automated tracker output.
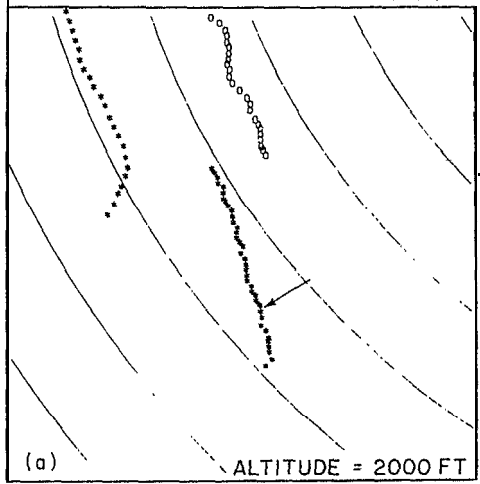
113

DISPLAY CODE

O RADAR ONLY

B BEACON ONLY

• RADAR AND
    BEACON

? COAST

(a) ALTITUDE = 2000 FT

SCAN 916 TO 954

(b) ALTITUDE = 2000 FT

SCAN 955 TO 994

(c) ALTITUDE ≈ 2000 FT

SCAN 995 TO 1034   (TWO MILE RANGE RINGS)

(d) ALTITUDE = 2000 FT

SCAN 1035 TO 1074
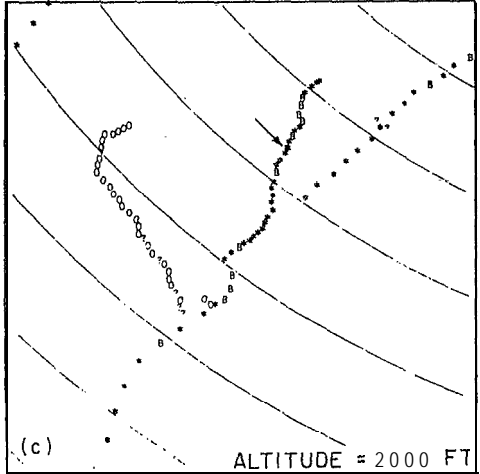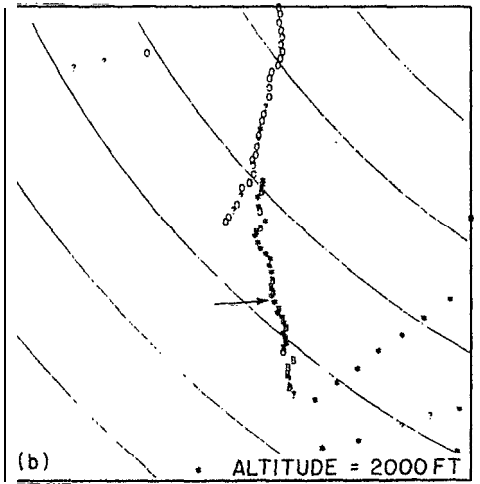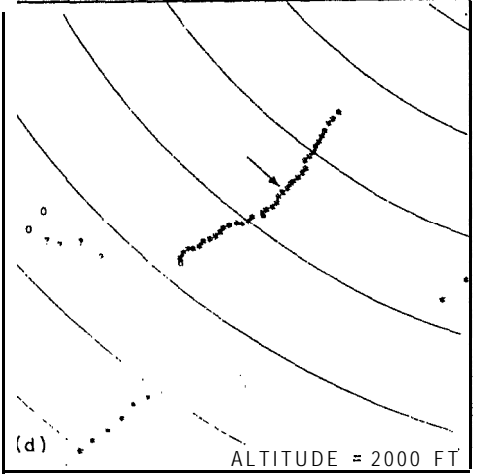
Fig. V-21.   Test flight in rain (6 August 1975); automated tracker output.

114

DISPLAY CODE

0 RADAR ONLY

B BEACON ONLY

• RADAR AND
    BEACON
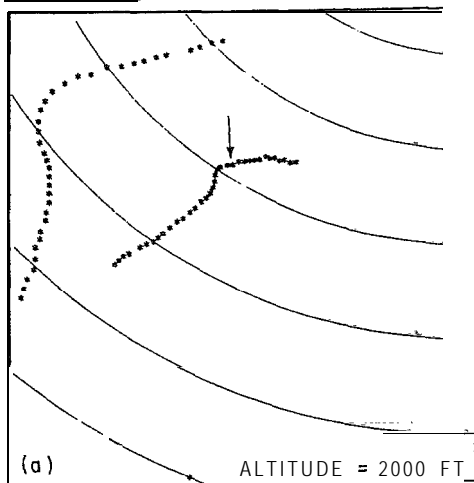
? COAST

(a)   ALTITUDE = 2000 FT

SCAN 1075 TO 1114
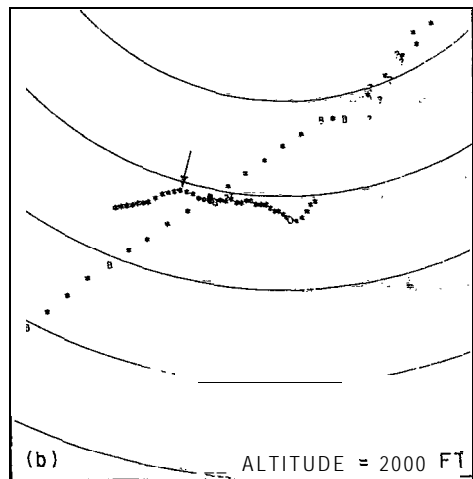
(b)   ALTITUDE = 2000 FT

SCAN 1115 TO 1154
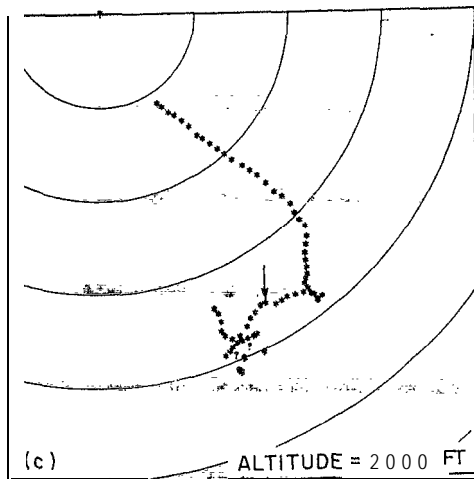
(c)   ALTITUDE = 2000 FT

SCAN 1315 TO 1354   (TWO MILE RANGE RINGS)
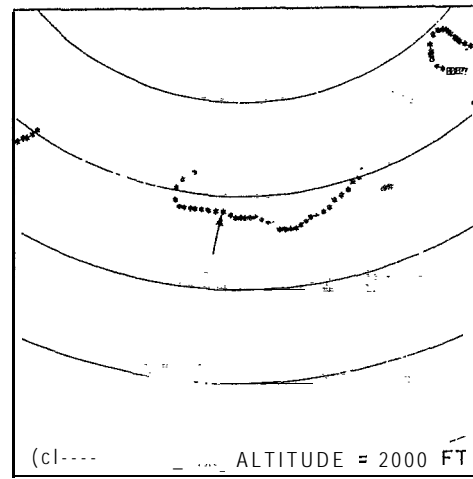
(cl----   _ ..._ ALTITUDE = 2000 FT

SCAN 1355 TO 1394

Fig. V-22.   Test flight in rain (6 August 1975); automated tracker output.
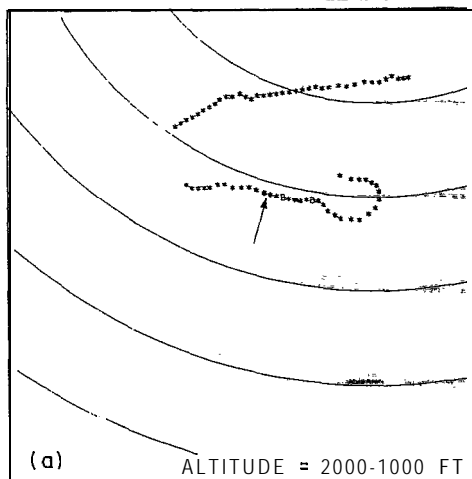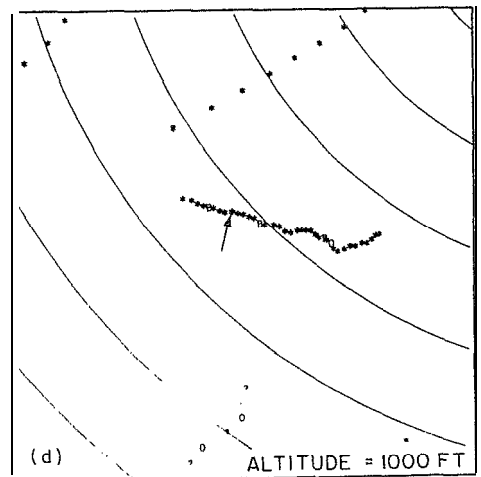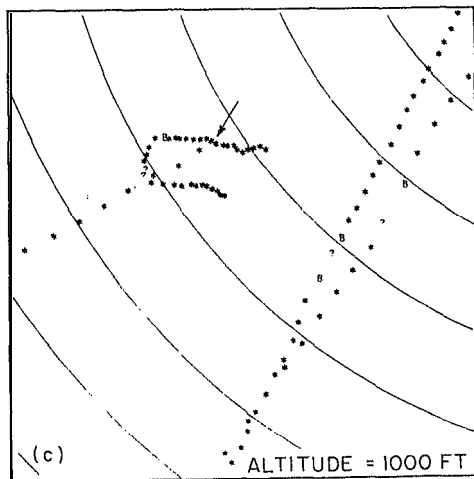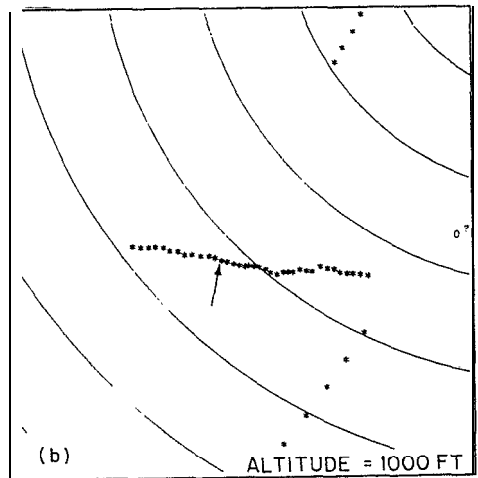
Fig. V-23.   Test flight in rain (6 August 1975); automated tracker output.
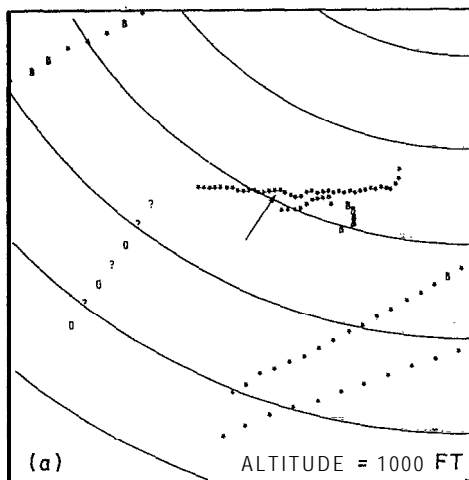
DISPLAY CODE

D RADAR ONLY

B BEACON ONLY

• RADAR AND BEACON

? COAST

(a) ALTITUDE = 1000 FT

SCAN 1555 TO 1594

(b) ALTITUDE = 1000-1200 FT

SCAN 1595 TO 1634

(c) ALTITUDE = 1200 FT
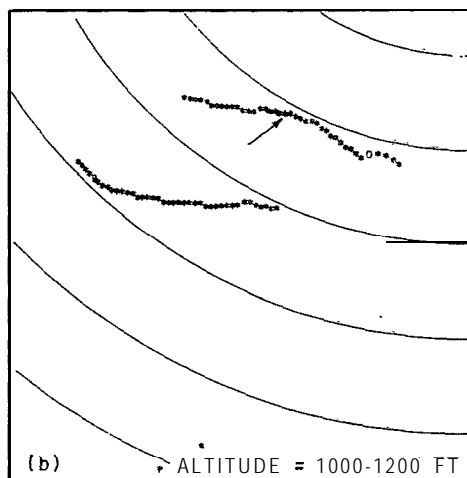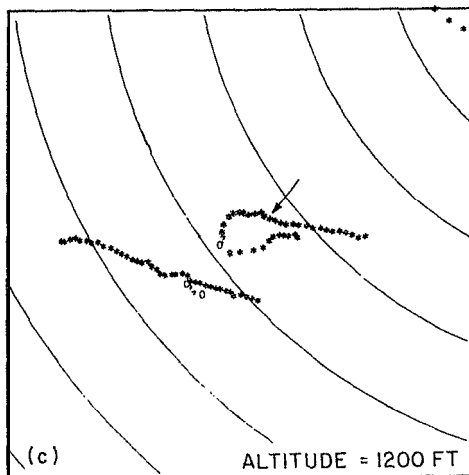
SCAN 1635 TO 1674   (TWO MILE RANGE RINGS)

(d) ALTITUDE = 1200 FT
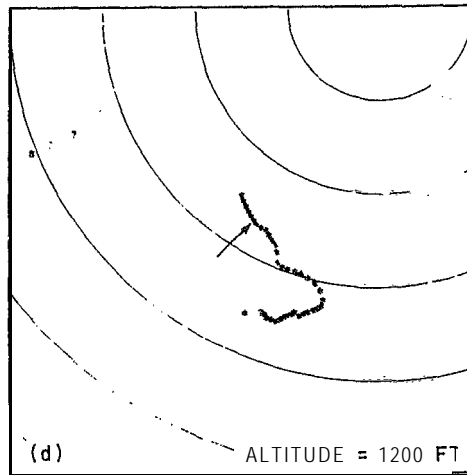
SCAN 1720 TO 1759

Fig. V-24.   Test flight in rain (6 August 1975); automated tracker output.
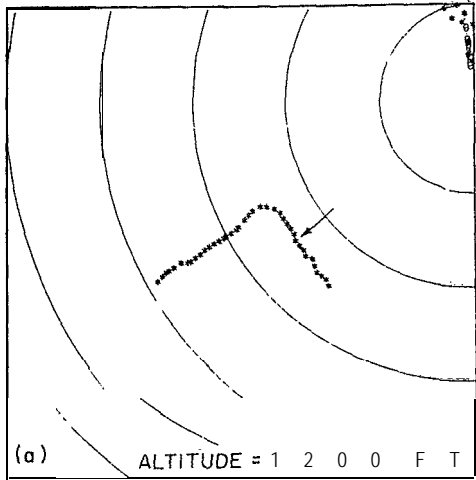
117

DISPLAY CODE

0 RADAR ONLY
B BEACON ONLY
° RADAR AND
  BEACON
? COAST

(a) ALTITUDE = 1 2 0 0 F T

SCAN 1760 TO 1799

(b) ALTITUDE = 1200 FT

SCAN 1800 TO 1839

(c) ALTITUDE = 1200 FT
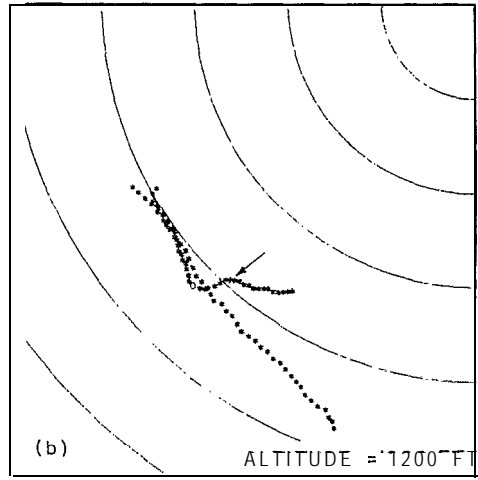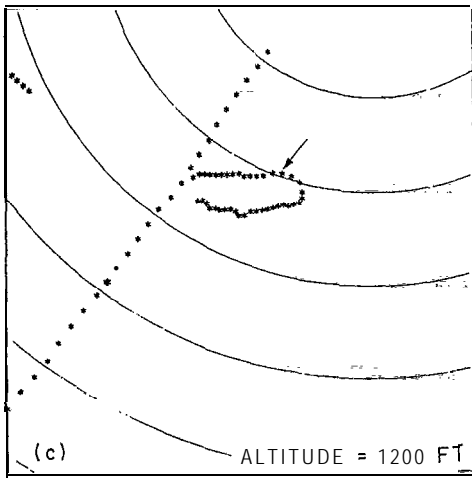
SCAN 1840 TO 1879

(TWO MILE RANGE RINGS)
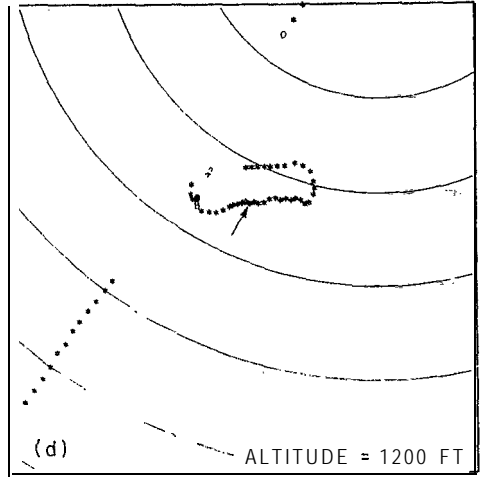
(d) ALTITUDE = 1200 FT

SCAN 1880 TO 1919

Fig. V-25. Test flight in rain (6 August 1975); automated tracker output.

118

DISPLAY CODE

0 RADAR ONLY

B BEACON ONLY

* RADAR AND
  BEACON

? COAST
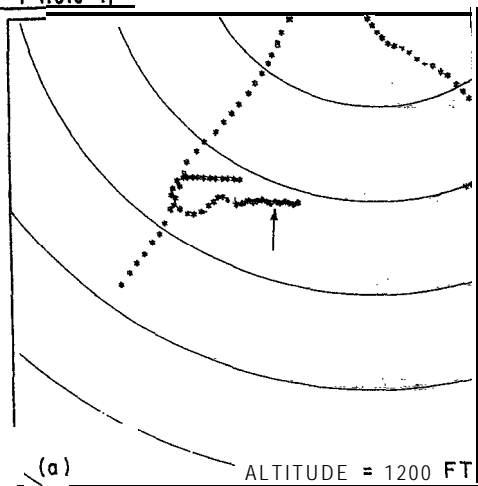
(a) ALTITUDE = 1200 FT

SCAN 1920 TO 1959   (TWO MILE RANGE RINGS)
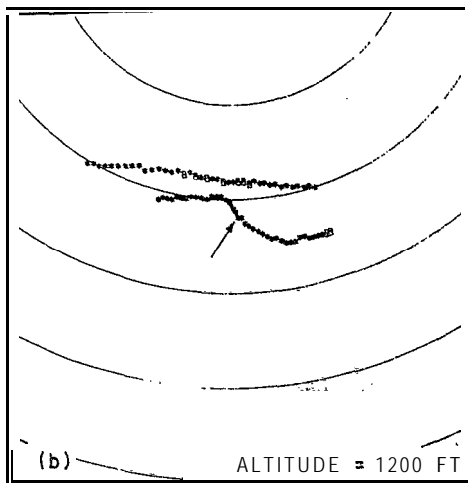
(b) ALTITUDE = 1200 FT

SCAN 1960 TO 1999
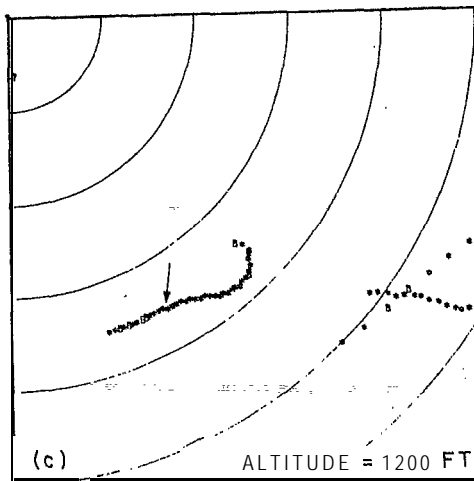
(c) ALTITUDE = 1200 FT

SCAN 2000 TO 2039

Fig. V-26. Test flight in rain (6 August 1975); automated tracker output.

119
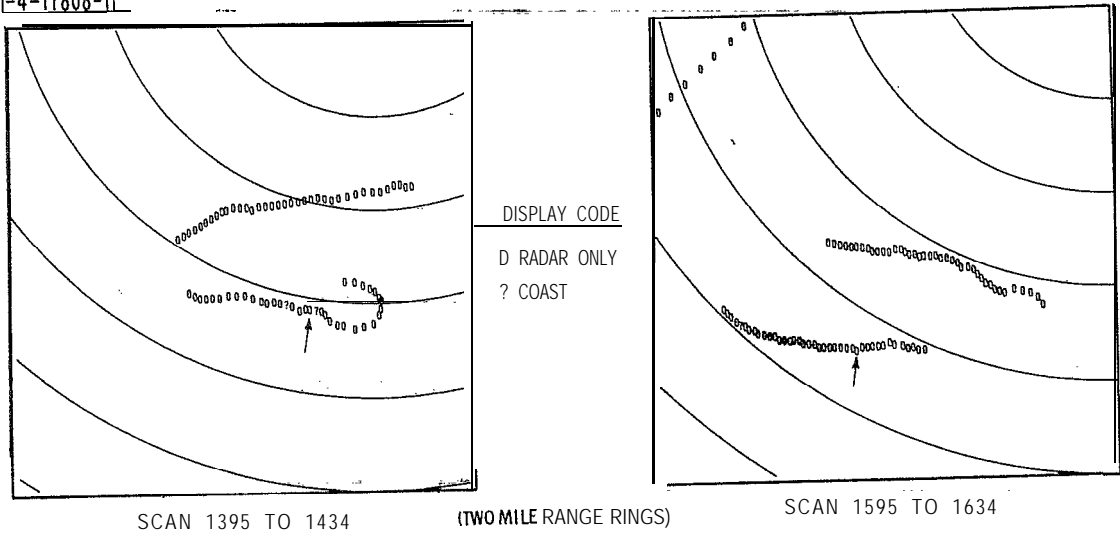
Fig. V-27. Test flight in rain (6 August 1975); automated tracker output.

MTD **RADAR REPORTS AFTER CORRELATION AND INTERPOLATION**
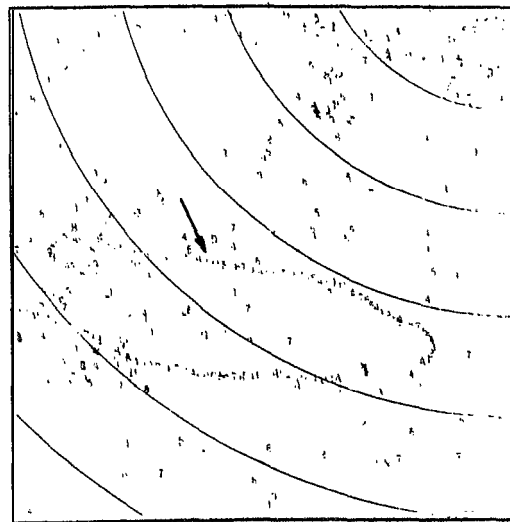
(TWO MILE RANGE RINGS)

AUTOMATED TRACKER OUTPUT
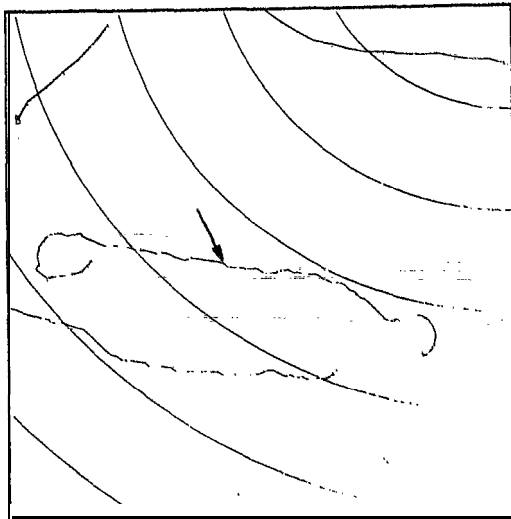
DISPLAY CODE

0 RADAR ONLY

B BEACON ONLY

⊕ RADAR AND
   BEACON

? COAST
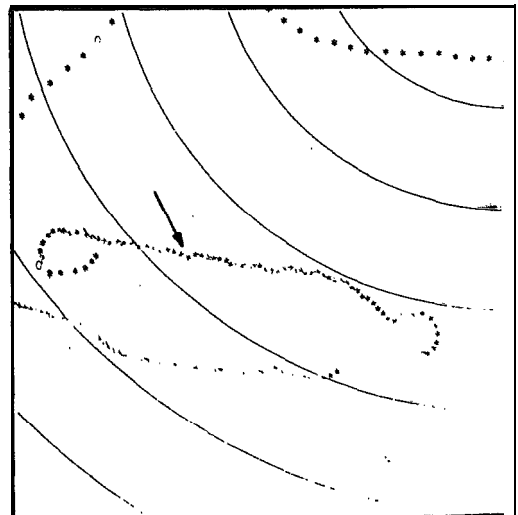
Fig. V-28. Test flight in rain (6 August 1975); MTD **data** — 80 scans.

MTD RADAR REPORTS

(TWO MILE RANGE RINGS)

AUTOMATED TRACKER OUTPUT

DISPLAY CODE

O RADAR ONLY

B BEACON ONLY

* RADAR AND BEACON
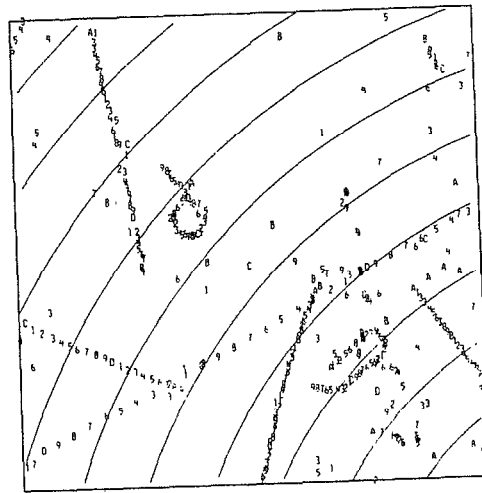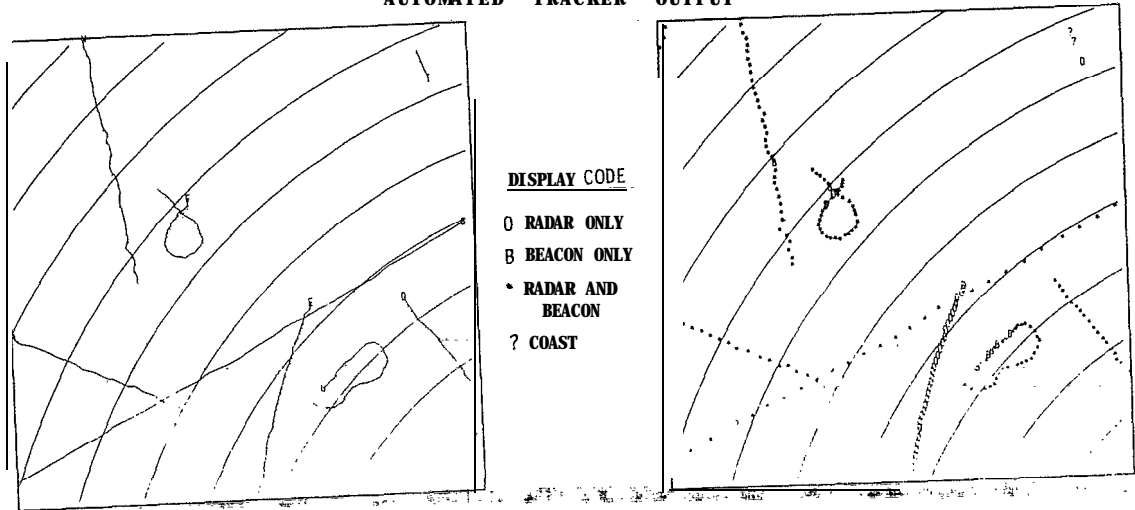
? COAST

Fig. V-29. MTD-automated tracker performance in rain; targets of opportunity.

122
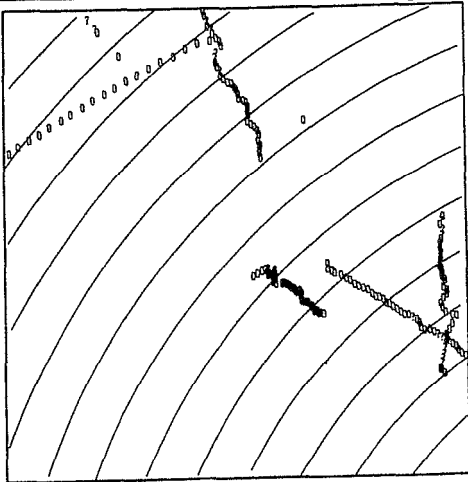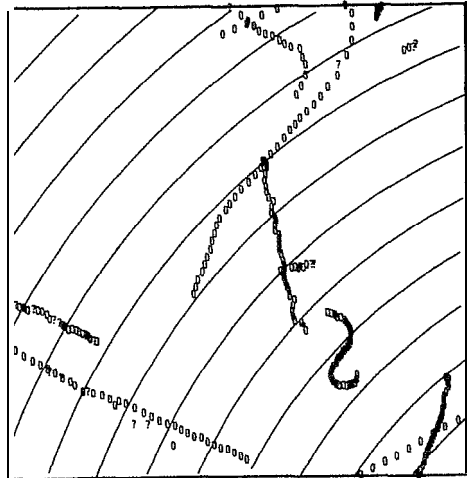
SCAN 1380 TO 1419

DISPLAY CODE

D RADAR ONLY

? COAST

SCAN 1421 TO 1459
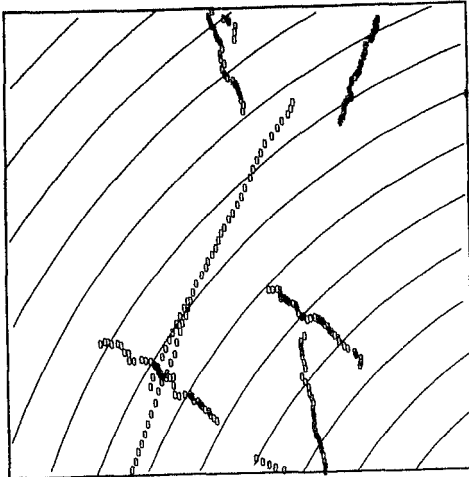
SCAN 1460 TO 1499   (TWO **MILE RANGE** RINGS)   **SCAN 1540 TO 1579**
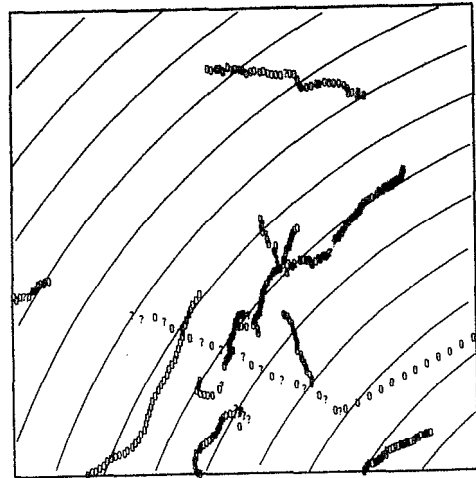
Fig. V-30. MTD-automated tracker performance in rain; "radar-only" targets of opportunity.
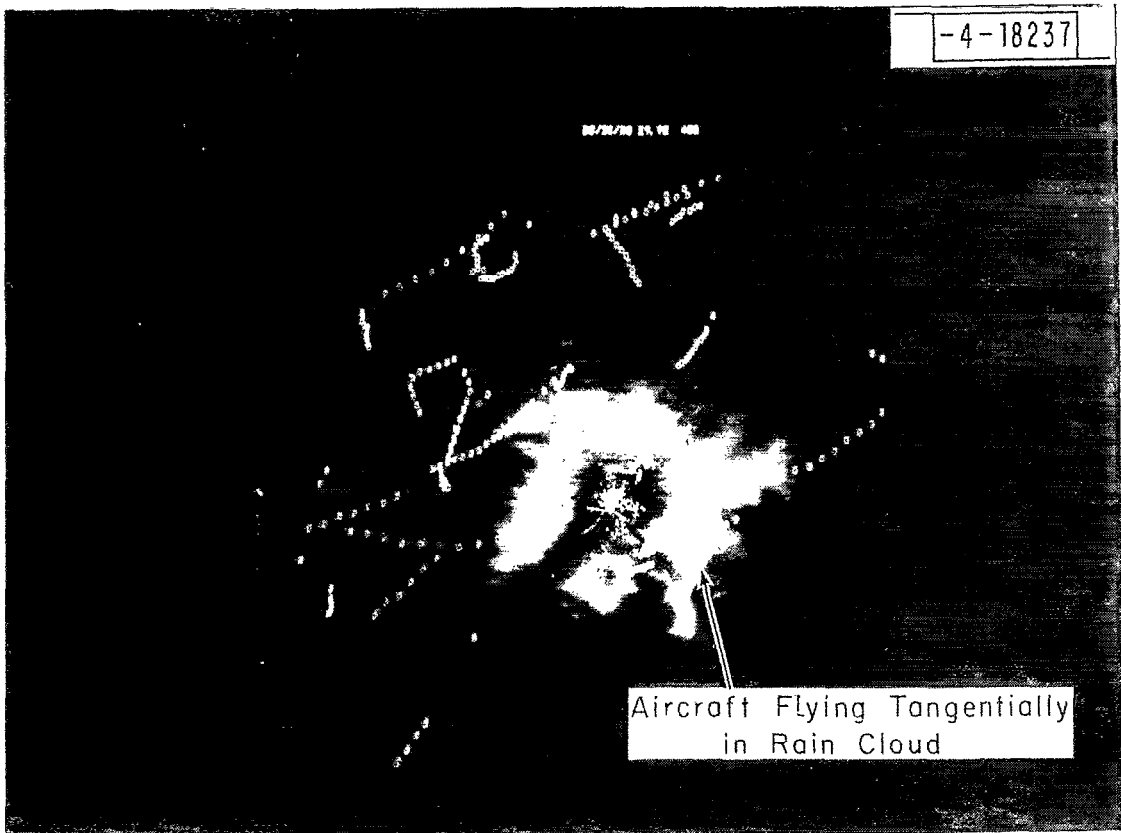
Fig. V-31.   MTD performance in the presence of rain clutter.

3. Conclusions

The MTD detected the Piper Cherokee Arrow (cross section ~ 1 m^2) with a blip-scan ratio approaching unity while the aircraft was flying through heavy weather whose backscatter was measured to be 30 to 40 dB above receiver noise. The *false alarm* rate of the MTD *was* constant and there were negligible false tracks output from the ARTS-III tracker caused by rain returns.

F. Subclutter Visibility Measurements with the Test Target Generator

1. Background

The TFAST site is a rather unfortunate one for demonstrating subclutter capability because there are only a few small areas from which ground clutter returns are observed. There are, however, a few isolated point returns which are relatively strong. These are known to be from some tall buildings in Atlantic City, Ventnor City and Margate. Echoes as strong as 70 dB above the system noise before STC are observed at ranges of 7 or 8 nmi.* The area of this patch of ground clutter is about 1 mi. x 6 mi. Figure V-32 presents a digital map of the ground clutter at NAFEC. The patch used for these tests is marked.

The MTD is a linear system. Hence, the sensitivity to moving targets should be independent of the presence or absence of ground clutter so long as the ground clutter echo amplitude remains within the linear dynamic range of the system. The linear dynamic range of the MTD system at NAFEC *was* approximately 44.6 dB as measured at the analog-to-digital converters. Results, presented in Section V-B, show that the MTD exhibits a probability of detection of 50 percent when the signal-to-noise ratio in the IF channel is between 2.0 and 3.4 dB. Thus, the MTD is expected to have a subclutter visibility** of 41.2 dB.

2. Test Methods

The subclutter visibility measurements (see Figure V-33) are made with the radar connected to the antenna, the transmitter on and the antenna scanning normally. Basically, the method was to:

---

*These echoes were attenuated to about 30 dB above system noise when the STC was applied.

**The subclutter visibility is defined as the ratio of clutter signal to target signal when the target signal was exactly superimposed on the clutter signal and producing a probability of detection of 0.5.
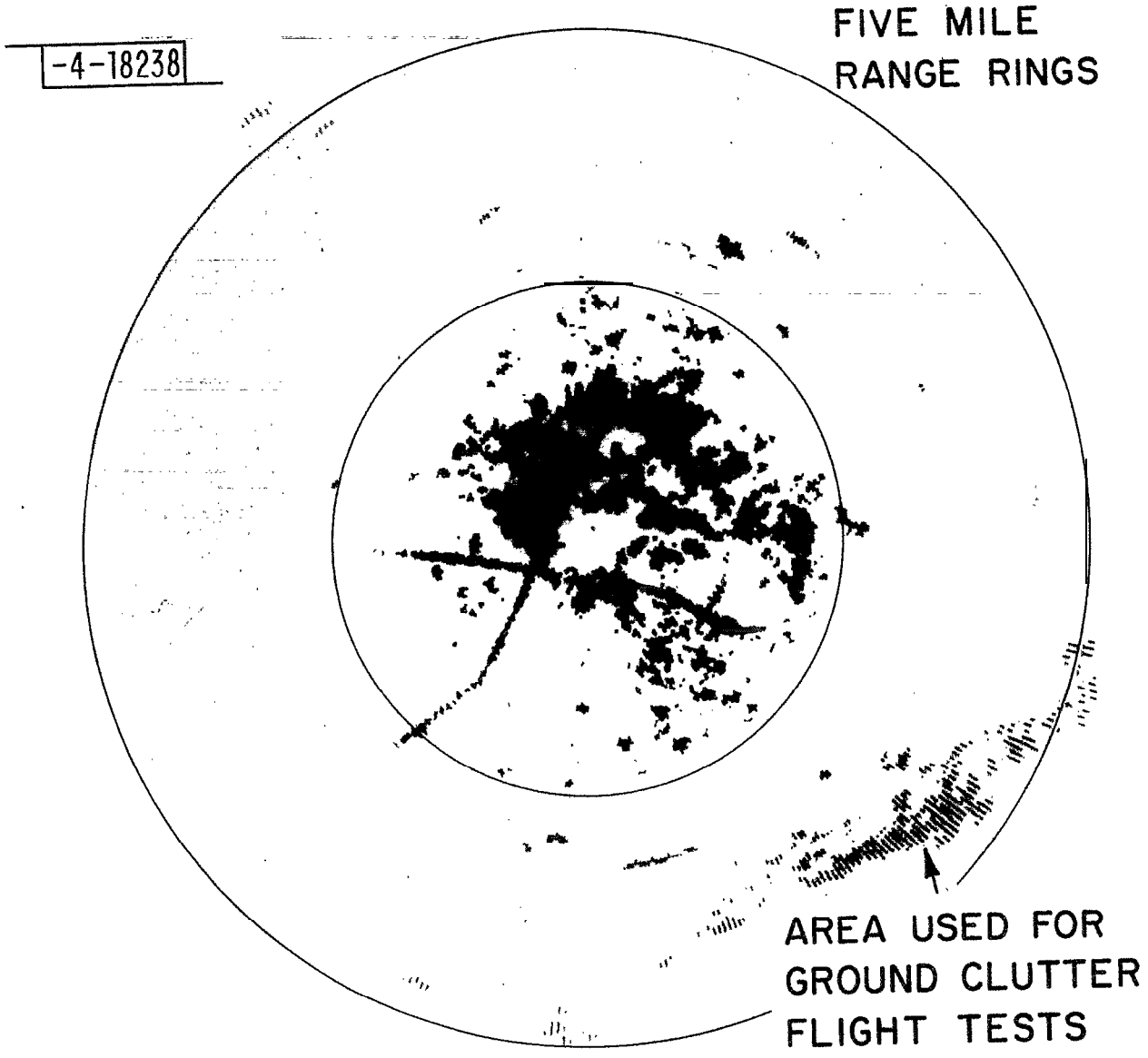
Fig. V-32.   Digital map of ground clutter at NAFEC (5 nmi range rings),
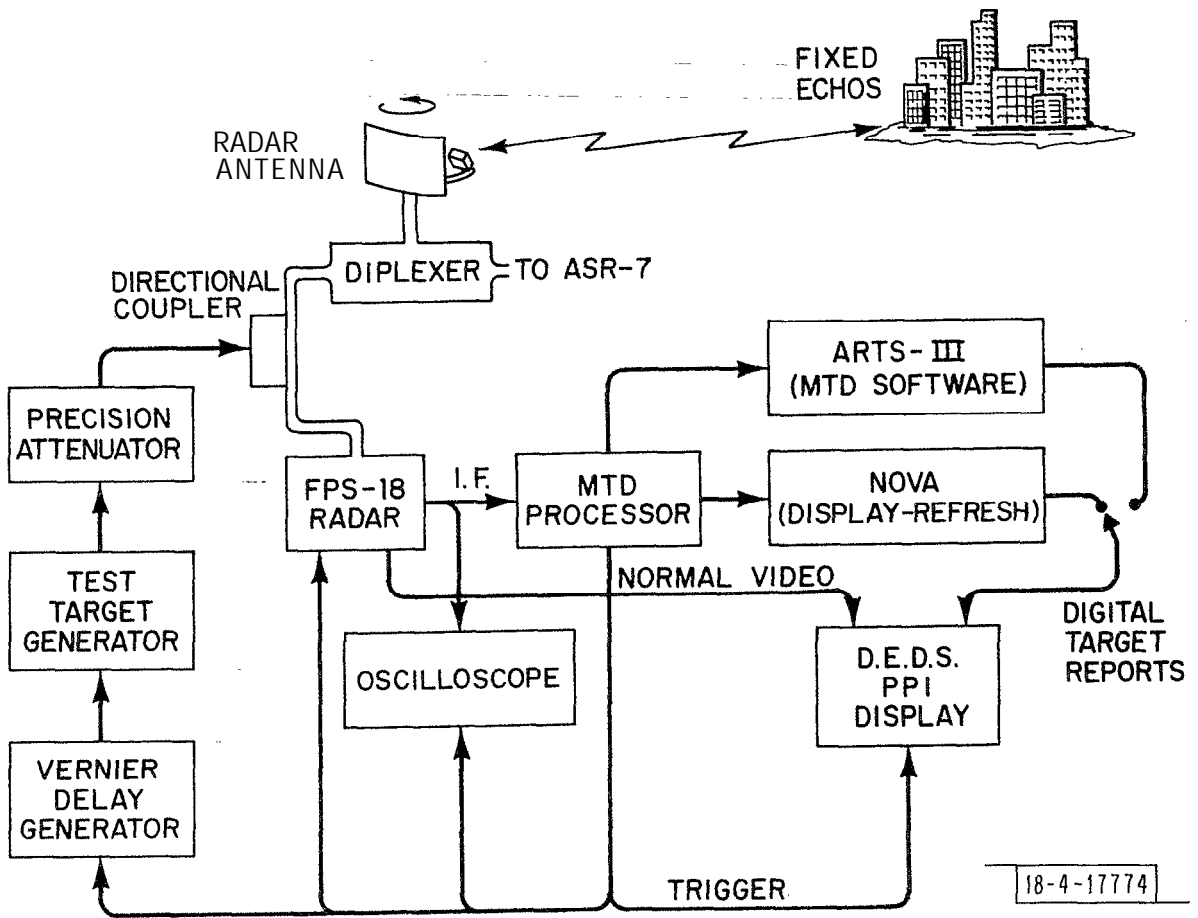
Fig. V-33. SCV test set-up.

(a) determine the range and azimuth of a large isolated fixed echo.

(b) adjust the STC or other front-end attenuator until that echo was on the verge of limiting the A/D converters

(c) superimpose the test target generator signal over the clutter signal.

(d) reduce the amplitude of the test target generator signal until the blip-scan ratio observed on the PPI display was 0.5. Observe the corresponding reading on the precision waveguide attenuator.

(e) increase the amplitude of the TTG signal by adjusting the 'precision attenuator until the TTG signal and the clutter signal were the same amplitude as observed on-an-expanded A-scope display of the IF amplifier output.

The measured subclutter visibility is the difference in dB between the attenuator readings taken in steps (d) and (e) above.

Precise measurement of subclutter capability using real radar returns is difficult because the amplitude and phase of even the most stable clutter echoes fluctuate slowly. These fluctuations, as observed on a bipolar video channel, are -estimated to cause variations in I or Q signals of as much as 2 dB during the time required to make a subclutter measurement.

There are other potential sources of error, particularly inaccurate position-ing of the TTG target over the clutter. During the NAFEC tests the procedure used was to offset the TTG target in range by a few pulse widths in order to set the azimuth of the test target exactly over that of the clutter while observing the analog PPI display. Once the azimuth was set exactly the two echoes were superimposed in range by varying the range of the TTG target while observing an expanded A-scope presentation of the IF signal. The TTG which was used for these tests did not have adequate resolution in the range setting circuitry, hence a vernier delay generator was added at the TTG trigger input.

Some MTI systems can be adjusted so as to produce clutter residue which may lead to optimistic subclutter readings in tests of this kind. In these NAFEC tests this possibility was eliminated as a possible source of-error. Checks were made with no target signal and in all the measurements the MTD produced no clutter residue detections.

3. Results

The procedure described above was carried out several times at each of a number of doppler offsets. The results, which are in agreement with theory, are presented graphically in Figure V-34.

G. Detection of Aircraft in Ground Clutter

1. Test Flight — August 12, 1975

As mentioned in Section V-F, there is a limited amount of ground clutter in the NAFEC area, the main region being a 1 mi. x 6-mi. strip along the New Jersey coastline about 8 miles SE of the TFAST site. On August 12, 1975, a Piper Cherokee was flown over this region of ground clutter far about two hours to test the detection performance of the MTD in a ground clutter environment. As with the precipitation tests, the interactive graphics programs were used to examine the data. Thirty scan blip-scan ratios of MTD radar reports are presented in Figure V-35.

The MTD detected the test aircraft on all but five of the more than 1200 scans of the test flight. This results in a blip-scan ratio of .996. In addition there were neither false tracks nor excessive false alarms caused by the ground clutter.

Figure V-36 presents-40 scans of ARTS-III: tracker output alone and superimposed on digital map of the ground clutter which was used for the test. In this segment of the data, the aircraft was flying tangentially through the ground clutter. ARTS-III radar/beacon tracker outputs for the test flight are presented in Figures V-36 through V-45. The test aircraft is marked in the figures.

The data was also processed through the ARTS-III tracker with the beacon data inhibited. The tracking results were equivalent to those obtained when the beacon data was used. Figure V-46 presents ARTS-III tracker output data for two particularly complex sections of the test flight rerun without beacon report data. The tracking performance is as good without the beacon data as with it.

2 Conclusions

The small test aircraft was detected solidly over the ground clutter near Atlantic City. The detection probability was measured to be .996 while the aircraft flew through the ground clutter repeatedly at many different aspect angles relative to the radar.
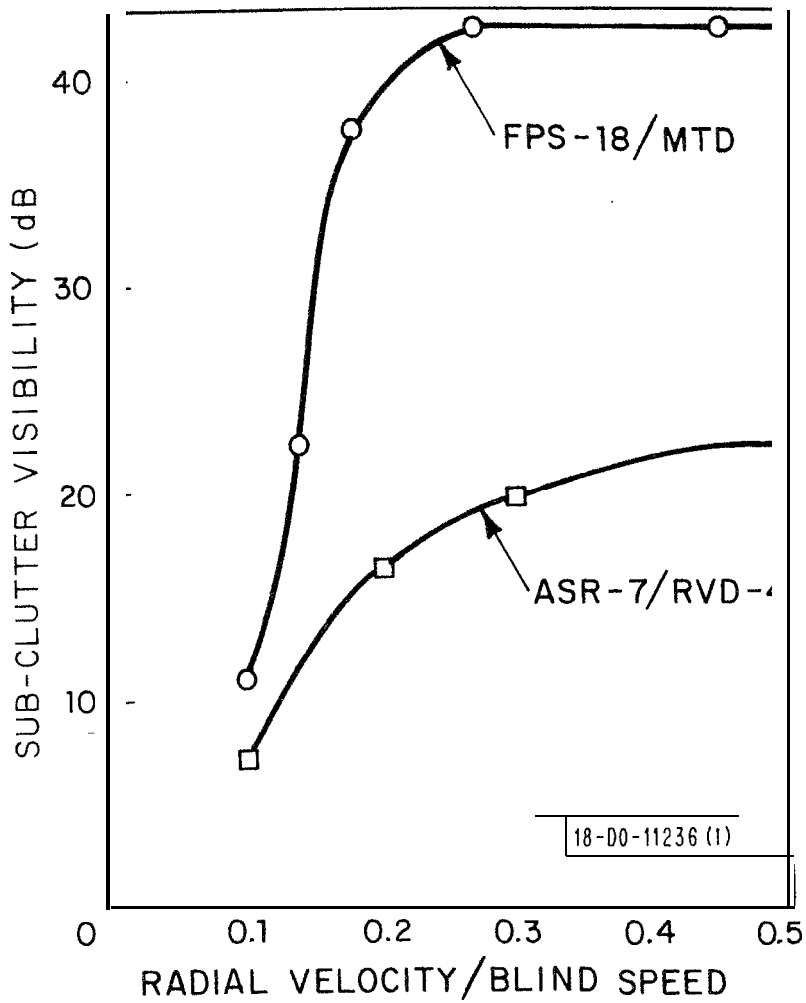
Fig. V-34.   Subclutter visibility for P_D = Cl.5 (measured).
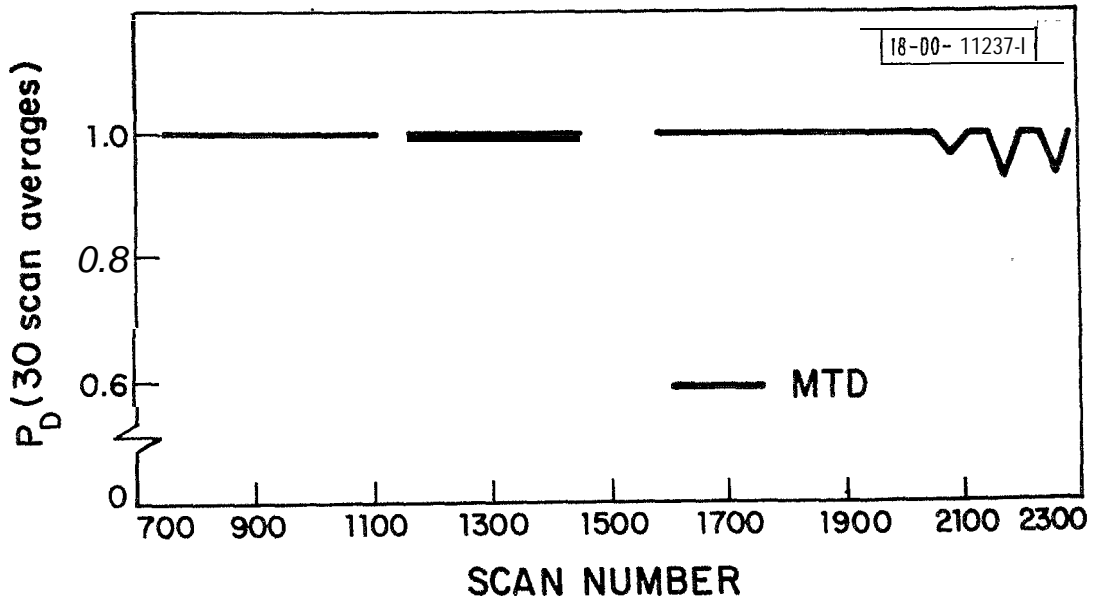
Fig. V-35.   Blip/scan ratio during clutter test (12 August 1975);
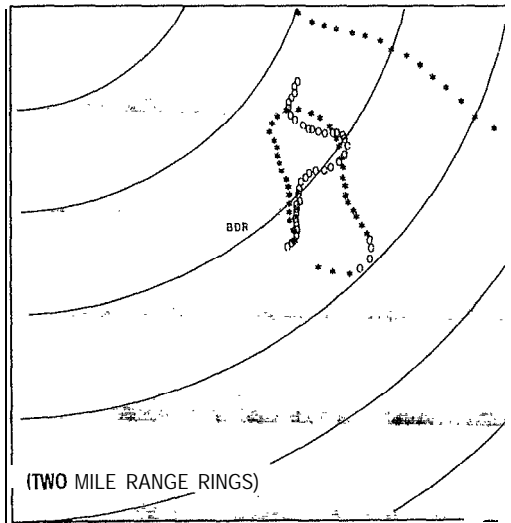
Fig. V-36.   MTD-automated tracker output for ground clutter test flight (12 August 1975).

131

DISPLAY CODE

0 RADAR ONLY

B BEACON ONLY

. RADAR AND BEACON

? COAST

(a)

SCAN 750 TO 789
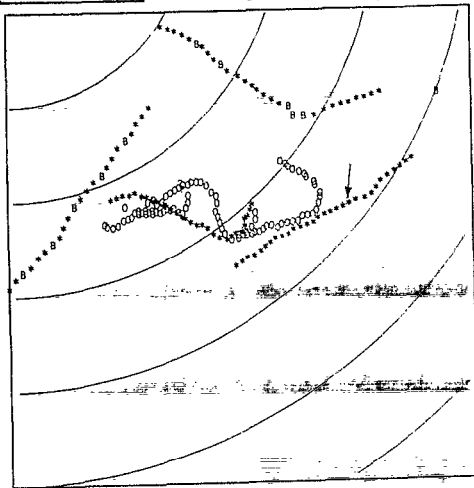
(b)

SCAN 790 TO 829

(c)
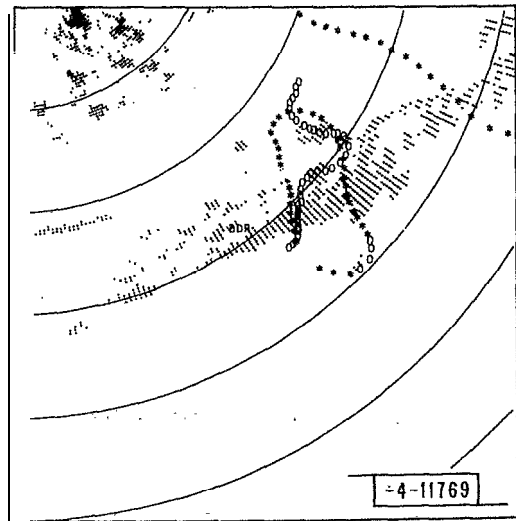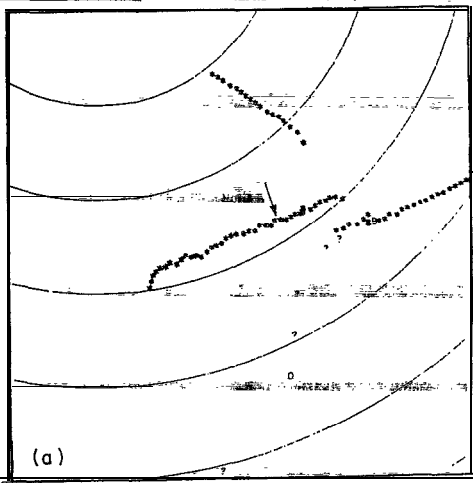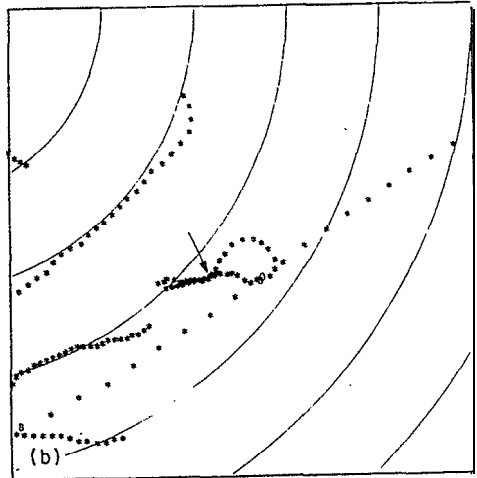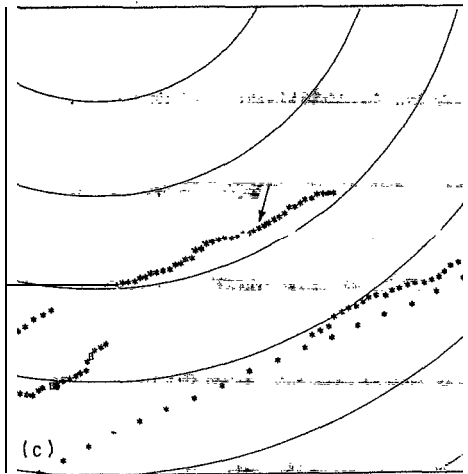
SCAN 830 TO 869   (TWO MILE RANGE RINGS)

(d)
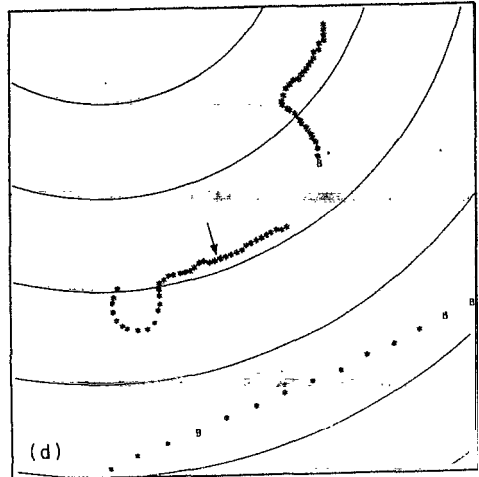
SCAN 870 TO 909

Fig. V-37. MTD-automated tracker output for ground clutter test flight (12 August 1975); altitude = 1000 ft.
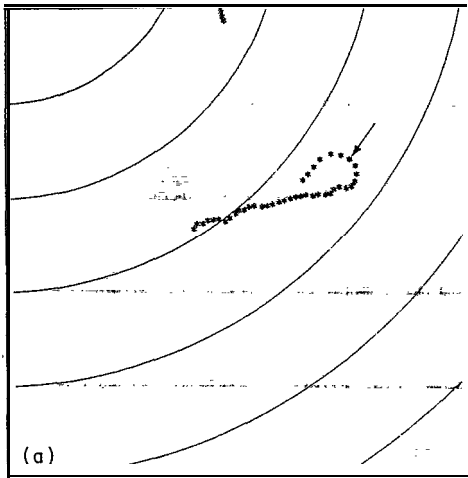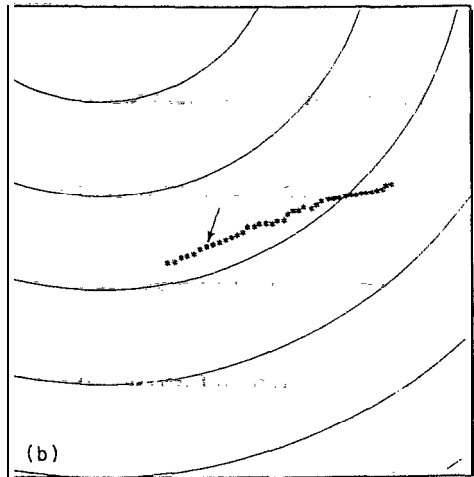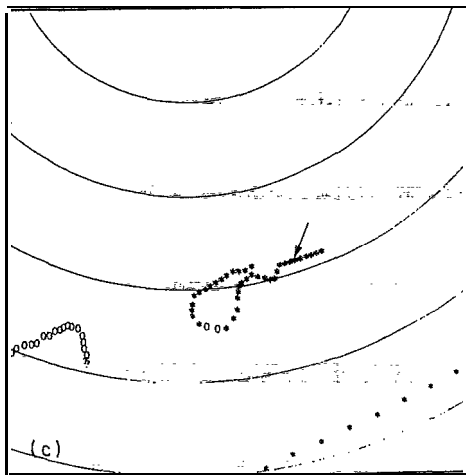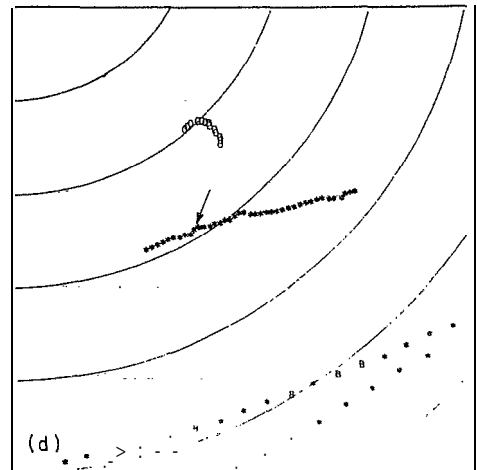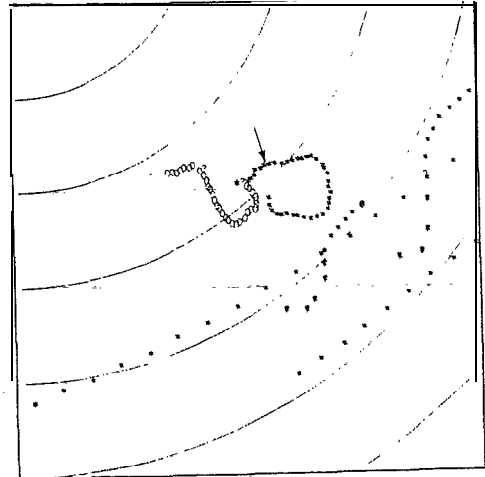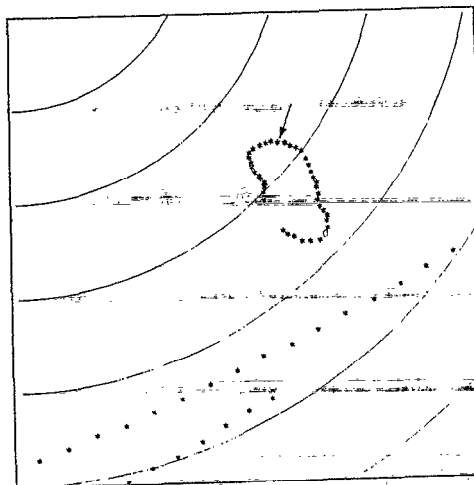
Fig. V-38. MTD-automated tracker output for ground clutter test flight (12 August 1975); altitude = 1000 ft.-

133
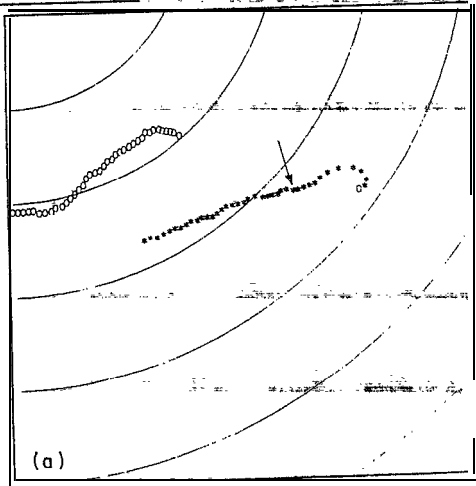
DISPLAY CODE

0 RADAR ONLY

B BEACON ONLY

• RADAR AND BEACON

? COAST

(a) SCAN 1070 TO 1109
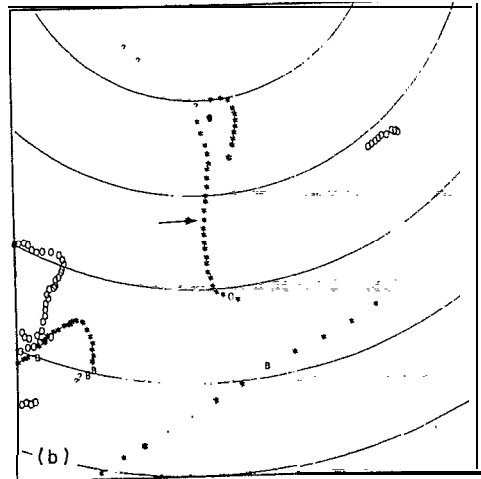
(b) SCAN 1161 TO 1199
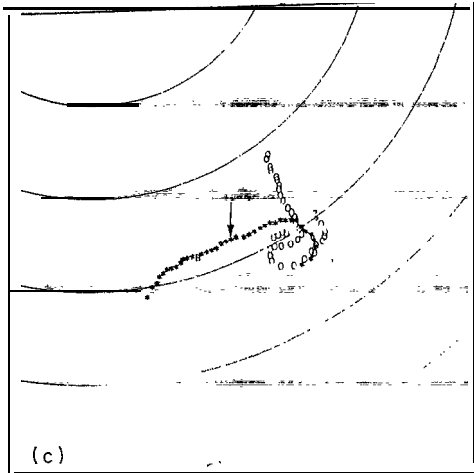
(c) SCAN 1200 TO 1239   (TWO MILE RANGE RINGS)
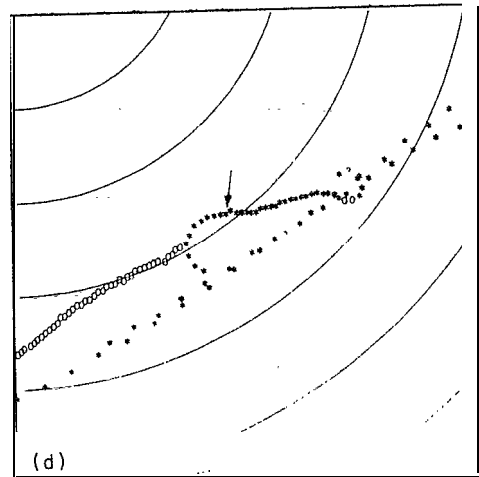
(d) SCAN 1240 TO 1279

Fig. V-39.   MTD-automated tracker output for ground clutter test flight (12 August 1975); altitude = 1000 ft.
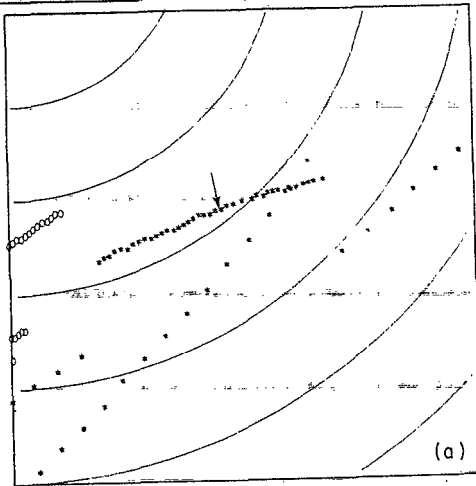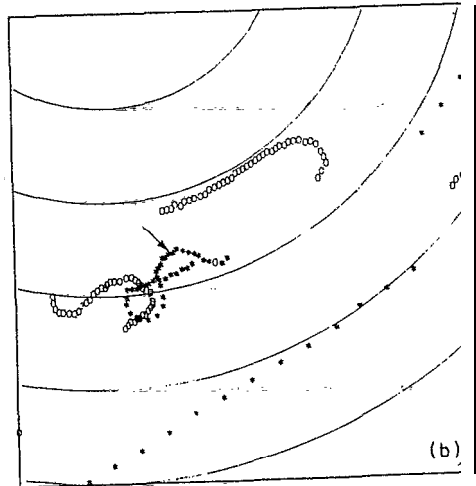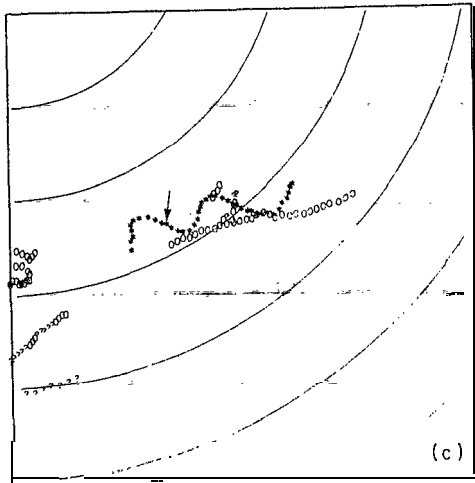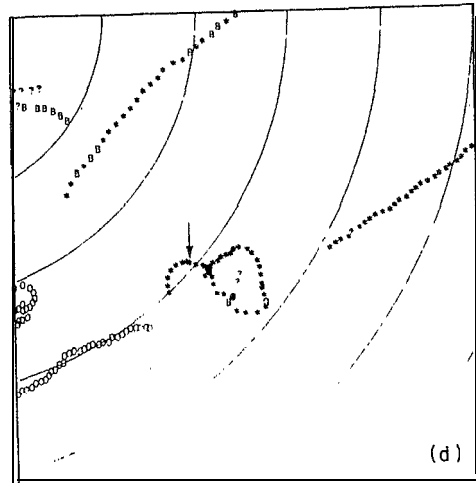
Fig. V-40. MTD-automated tracker output for ground clutter test flight (12 August 1975); altitude = 1000 ft.

-4-17822-1

DISPLAY CODE

0 RADAR ONLY

B BEACON ONLY

° RADAR AND
   BEACON

? COAST
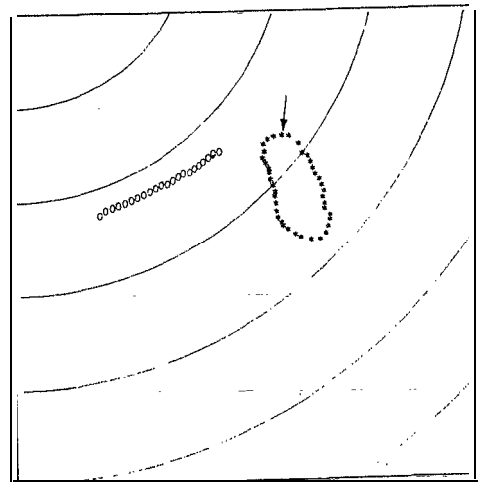
SCAN 1440 TO 1469

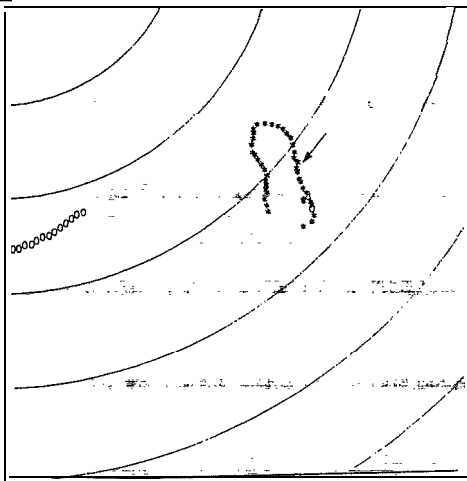SCAN 1580 TO 1619

SCAN 1620 TO 1659   (TWO MILE RANGE RINGS)   SCAN 1660 TO 1699
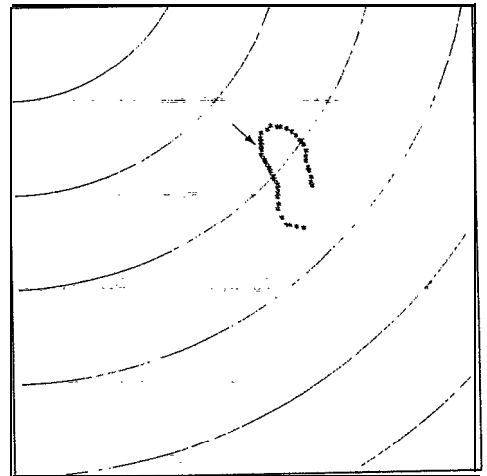
Fig. V-41.   MTD-automated tracker output for ground clutter test flight (12 August 1975); altitude = 1000 ft.
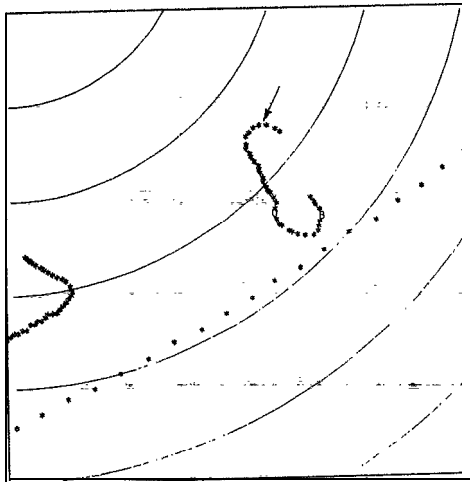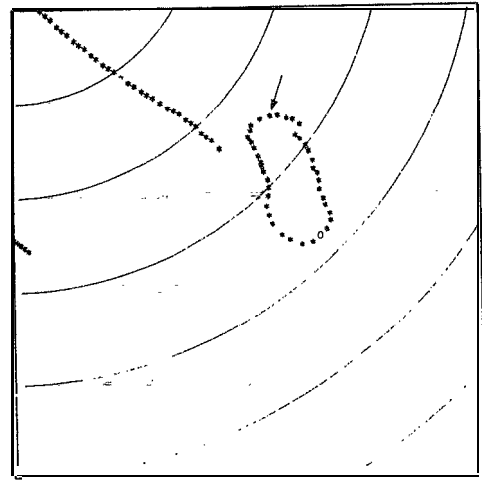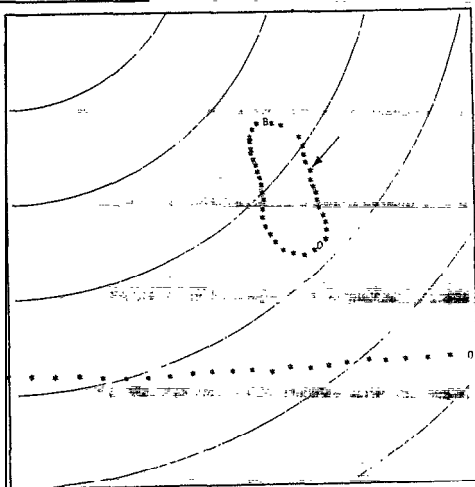
SCAN 1700 TO 1739

SCAN 1740 TO 1779

SCAN 1780 TO 1819 (TWO MILE RANGE RINGS)

SCAN 1820 TO 1859

DISPLAY CODE

0 RADAR ONLY

B BEACON ONLY

° RADAR AND BEACON

? COAST

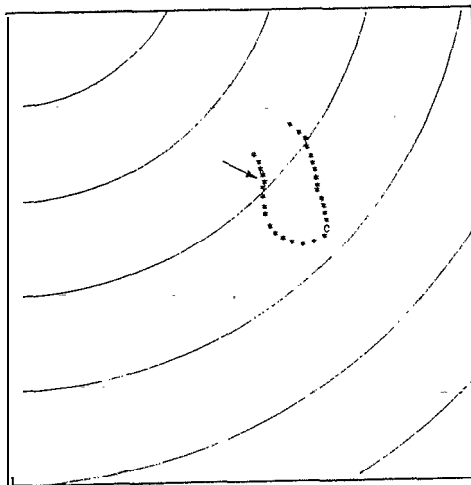Fig. V-42. MTD-automated tracker output for ground clutter test flight (12 August 1915); altitude = 1000 ft.

137
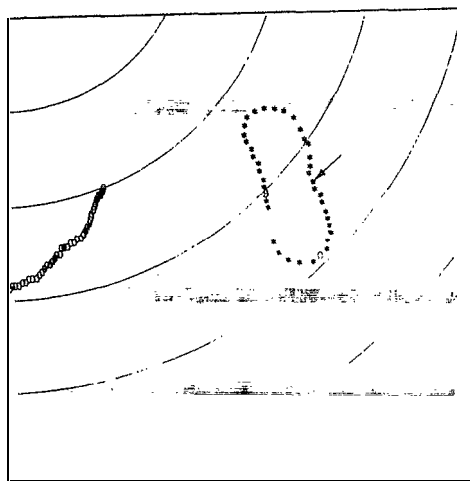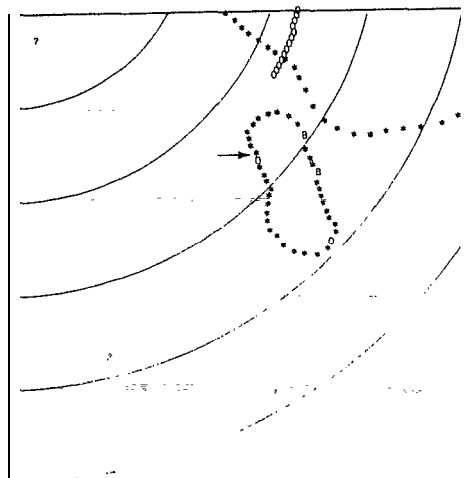
Fig. V-43. MTD-automated tracker output for ground clutter test flight (12 August 1975); altitude = 1000 ft.

SCAN 2100 TO 2139

SCAN 2140 TO 2179

SCAN 2180 TO 2219

(TWO MILE RANGE RINGS)

SCAN 2220 TO 2259

DISPLAY CODE

O RADAR ONLY
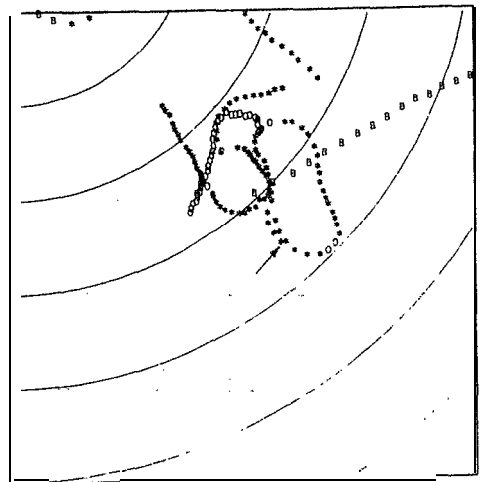
B BEACON ONLY

• RADAR AND BEACON

? COAST

Fig. V-44. MTD-automated tracker output for ground clutter test flight (12 August 1975); altitude = 1000 Et.

139

-4-17818-1

DISPLAY CODE

O RADAR ONLY

B BEACON ONLY

○ RADAR AND
--BEACON
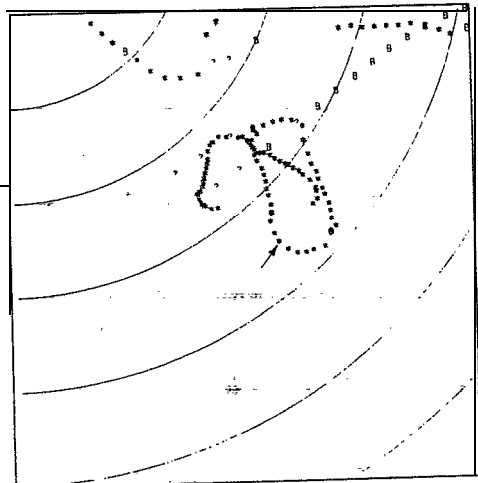
? COAST

SCAN 2260 TO 2299 (TWO MILE RANGE RINGS)

SCAN 2300 TO 2339

SCAN 2340 TO 2349

Fig. V-45. MTD-automated tracker output for-ground clutter test flight (12 Augusf 1975); altitude = 1000 ft.

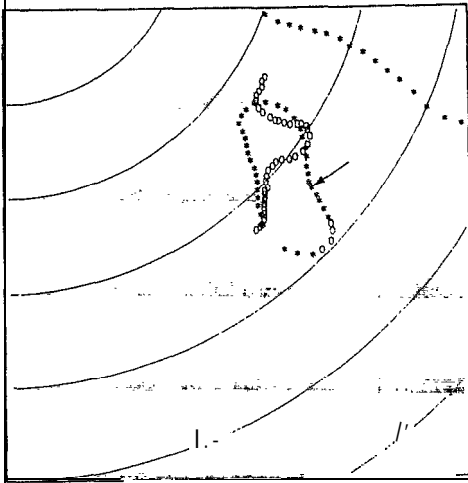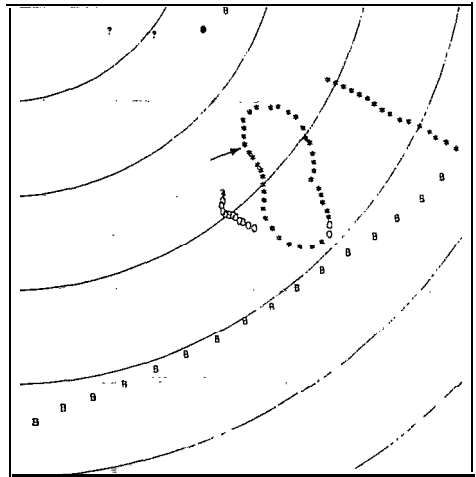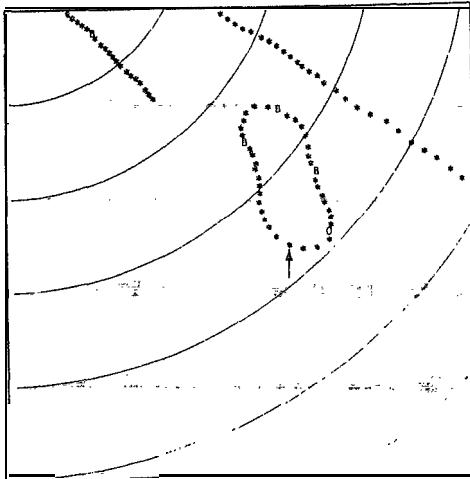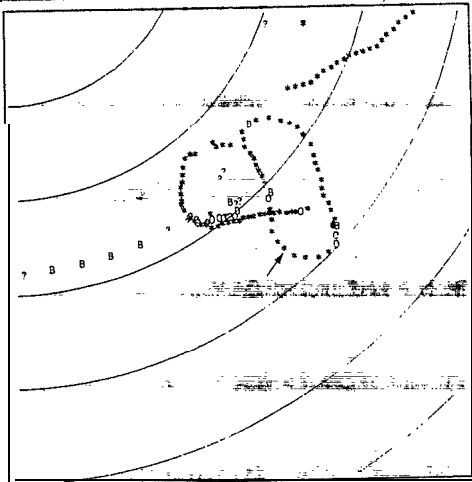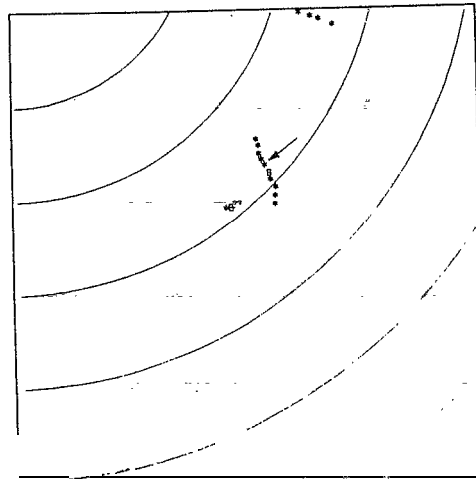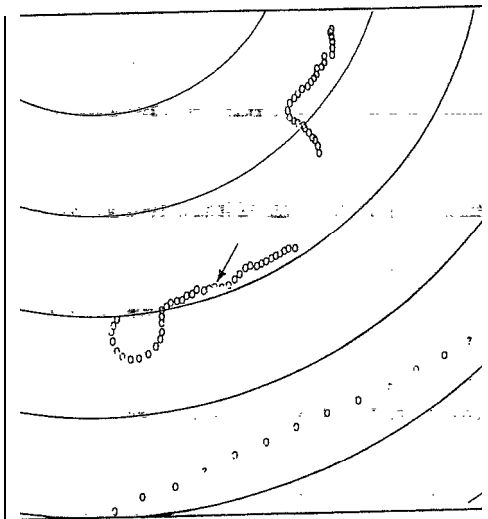SCAN 870 TO 909   (TWO MILE RANGE RINGS)   SCAN 1070 TO 1103

DISPLAY CODE

O RADAR ONLY

? COAST
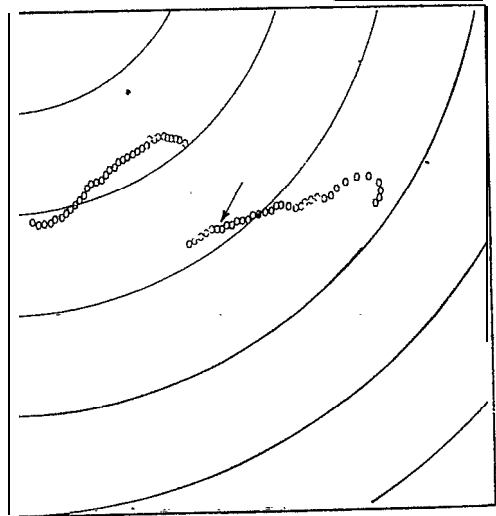
Fig. V-46. MTD-automated tracker output – radar only data (test flight of 12 August 1975).

H. Accuracy Studies

The accuracy of the radar report data input to the ARTS-III tracker has great bearing on the performance of the tracker. More accurate radar reports will allow the tracker's primary and secondary correlation search bins to be smaller and thus reduce false track initiations. In addition, better accuracy *will* allow the tracker to detect aircraft maneuvers sooner. With this in mind, a careful study of the range and azimuth accuracy of the MTD reports and tracks was made. One hundred aircraft targets of opportunity were selected from three clear day tests flown at NAFEC on August, 12, 21 and September 2, 1475. Selection of the aircraft tracks was performed according to the following criteria.

1. Of 30 successive scans of the radar, there were at least 27 MTD radar reports and 27 beacon reports successfully correlated and tracked.

2. All tracks chosen were nearly straight or had a gradual smooth curve. A variety of track orientations relative to the radar were chosen. For each selected track, three data types were used:

3. MTD radar report data after correlation and interpolation,

4. Beacon report data,

5. Predicted track position data for radar/beacon correlated tracks. For each data type a **least squares** fit to a fifth order polynomial was applied. independently to the range and azimuth vs. scan number. The equation for the polynomial   is

$$Y = A_1 + A_2X + A_3X^2 + A_4X^3 + A_5X^4 + A_6X^5$$

where: the A_i = the coefficients of the polynomial,

X = scan number

y = range or azimuth

The coefficients of the polynomial are given by:

$$A_1 = \frac{1}{D} \begin{bmatrix} b_1 & a_2 & a_3 & . & \bullet & \bullet & \bullet & a_6 \\ b_2 & a_3 & a_4 & . & \bullet & \bullet & \bullet & a_7 \\ . & . & . & . & \bullet & \bullet & \bullet & \bullet \\ b_6 & a_7 & a_8 & \bullet & \bullet & \bullet & \bullet & a_{11} \end{bmatrix}$$

$$A_2 = \frac{1}{D} \begin{bmatrix} a_1 & b_1 & a_3 & . & \bullet & \bullet & \bullet & a_6 \\ a_2 & b_2 & a_4 & . & \bullet & \bullet & \bullet & a_7 \\ . & . & . & . & \bullet & \bullet & \bullet & . \\ a_6 & b_6 & a_8 & . & \bullet & \bullet & \bullet & a_{11} \end{bmatrix}$$

$$A_6 = \frac{1}{D} \begin{bmatrix} a_1 & a_2 & a_3 & . & \bullet & \bullet & \bullet & b_1 \\ a_2 & a_3 & a_4 & . & \bullet & \bullet & \bullet & b_2 \\ . & . & . & . & \bullet & \bullet & \bullet & \\ a_6 & a_6 & a_8 & . & \bullet & \bullet & \bullet & b_6 \end{bmatrix}$$

$$D = \begin{bmatrix} a_1 & a_2 & a_3 & . & \bullet & \bullet & \bullet & a_6 \\ a_2 & a_3 & a_4 & . & \bullet & \bullet & \bullet & a_7 \\ . & . & . & \bullet & \bullet & \bullet & \bullet & . \\ a_6 & a_7 & . & . & \bullet & \bullet & \bullet & a_{11} \end{bmatrix}$$

where

$$a_1 = \sum_{k=1}^{N} X_k^{i-1} \qquad\qquad 1 = 1, 2 \ldots 11$$

$$b_i = \sum_{k=1}^{N} y_k X_k^{i-1} \qquad\qquad i = 1, 2 \ldots 6$$

N = number of data points (X_i, y_i)

X_i = scan numbers and,

y_i = either range or azimuth reports.

A measure of the smoothness or random error in a set of data points is given by the root-mean-square deviation of the measured data points from a curve fitted through them. This deviation may be normalized by the number of data points and the number of terms in the polynomial and is usually given by:

$$S = \sqrt{\sum_{i=1}^{N} \left[y_i - \sum_{j=1}^{6} a_i X_i^{j-1} \right]_I^2}$$

for a fifth order polynomial.

A computer program was written to perform the curve fitting and calculate the deviation. This program was based on a similar one described in Reference 34. This software was interfaced to the interactive graphics program described in Section IV-E. This resulted in an interactive graphics program with which data could be visually scanned and when deemed appropriate, selected tracks or sets of target reports analyzed for range and/or azimuth accuracy.

Figure V-47 presents the tracker output data (30 scans) for one of the 100 tracks used in the study. The track used is marked with an arrow. Plots of range and azimuth vs. scan number for MTD radar report data and beacon report data are presented in Figure V-48. The fitted fifth order curves are drawn in each figure and the RMS deviation is also presented. Figures V-49 through V-51 are histograms of the deviations in range and azimuth for the three data types shown. The mean deviations are also presented. Note that the MTD radar report data indicates that the MTD is beam splitting about 10 to 1 ($.14^o$) while in range, where no interpolation is done, the data has a range error of about 1/3 of a range cell size, Finally, the MTD radar data is at least as accurate as the ATCRBS beacon data as shown in Figures V-49 and V-50.

I. Two Target Resolution

In order to measure the ability of the FPS-18/MTD/ARTS III system to detect‘ and track aircraft which *are* in close temporal and spatial proximity a special set of tests were performed. On September 2, 1975, two controlled aircraft, a
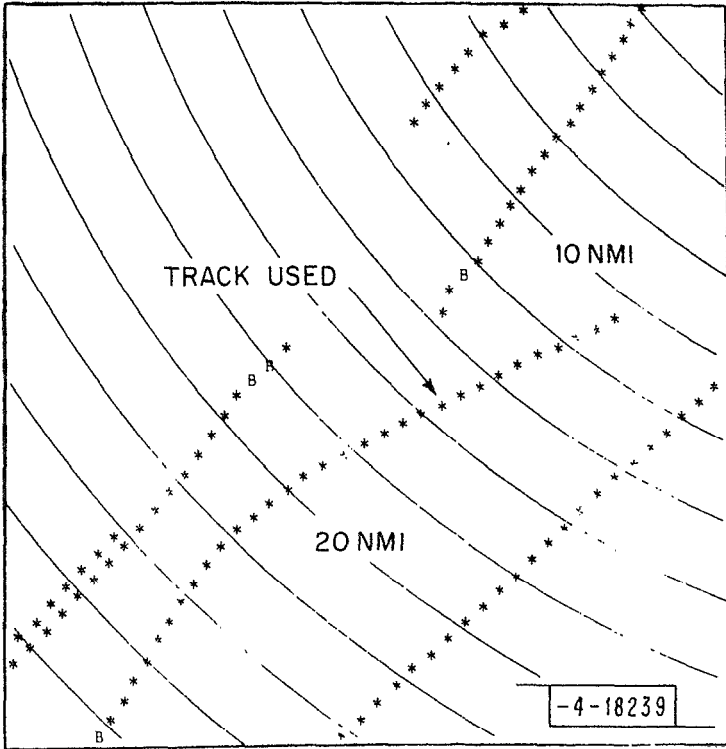
DISPLAY CODE

O RADAR ONLY

B BEACON ONLY

* RADAR AND
   BEACON

? COAST

Fig. V-47.   Sample tracker output: MTD accuracy study.
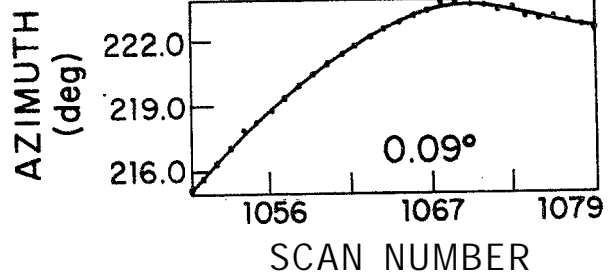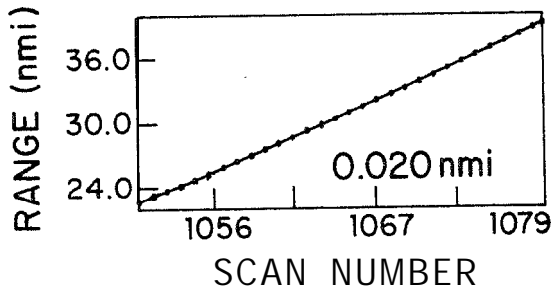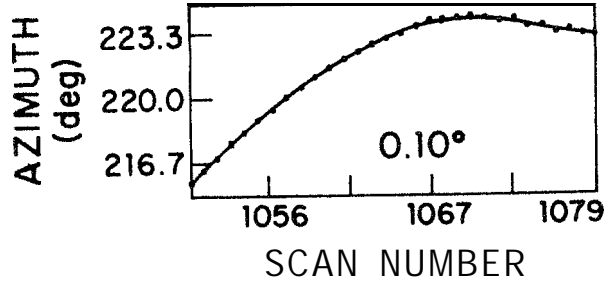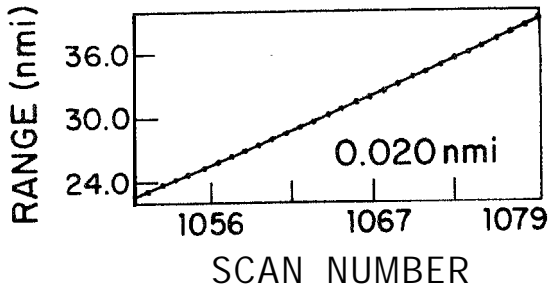
Fig. V-48.   Range and azimuth vs. scan number (measured and fitted);   for
MTD and beacon data.
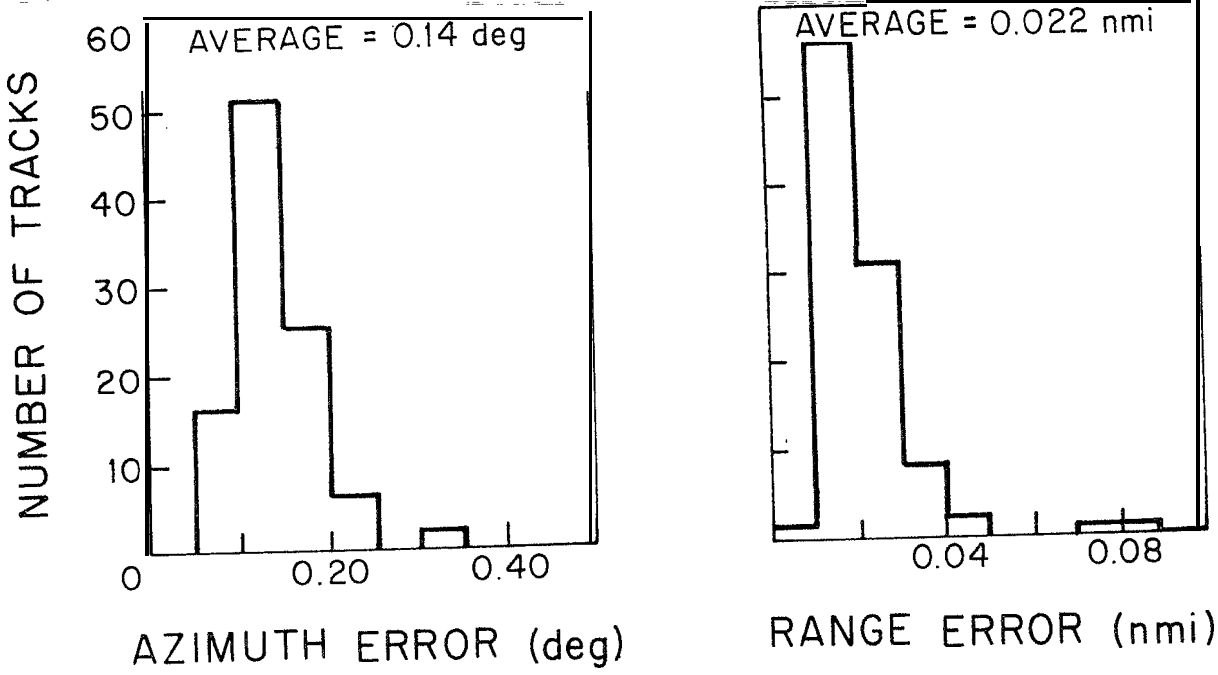
Fig. V-49. MTD report accuracy (100 tracks).,

AVERAGE = 0.17 deg

AVERAGE = 0.024 nmi

NUMBER OF TRACKS

AZIMUTH ERROR (deg)

RANGE ERROR (nmi)
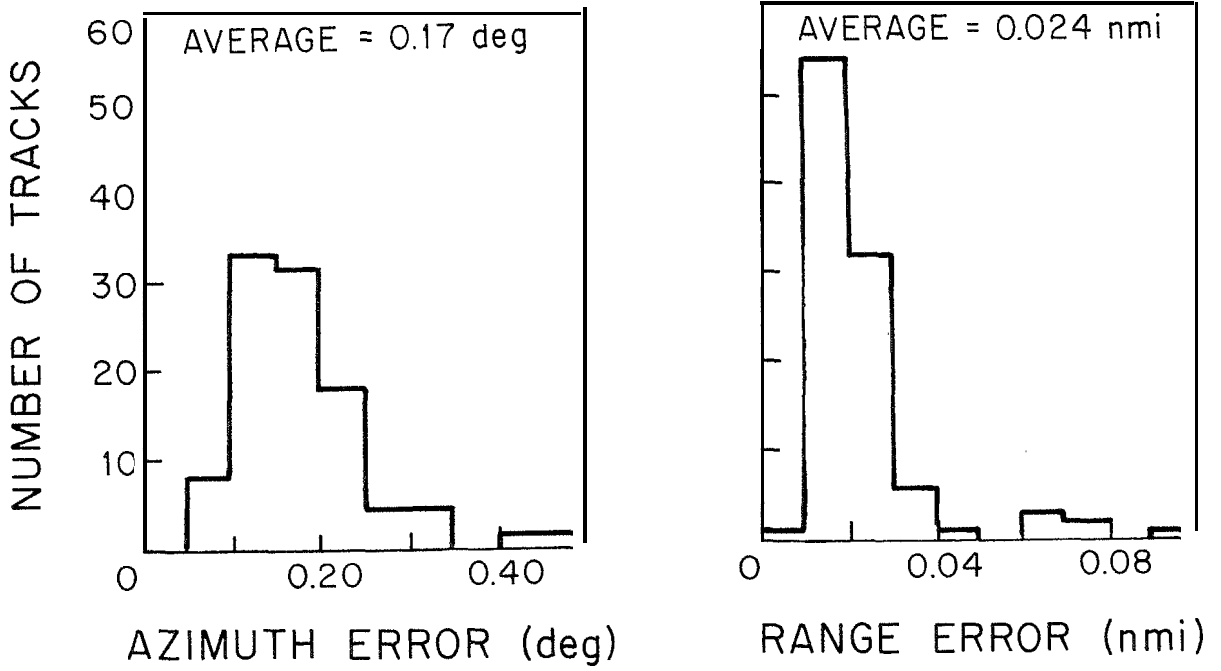
Fig. V-50.   Beacon report accuracy (100 tracks).
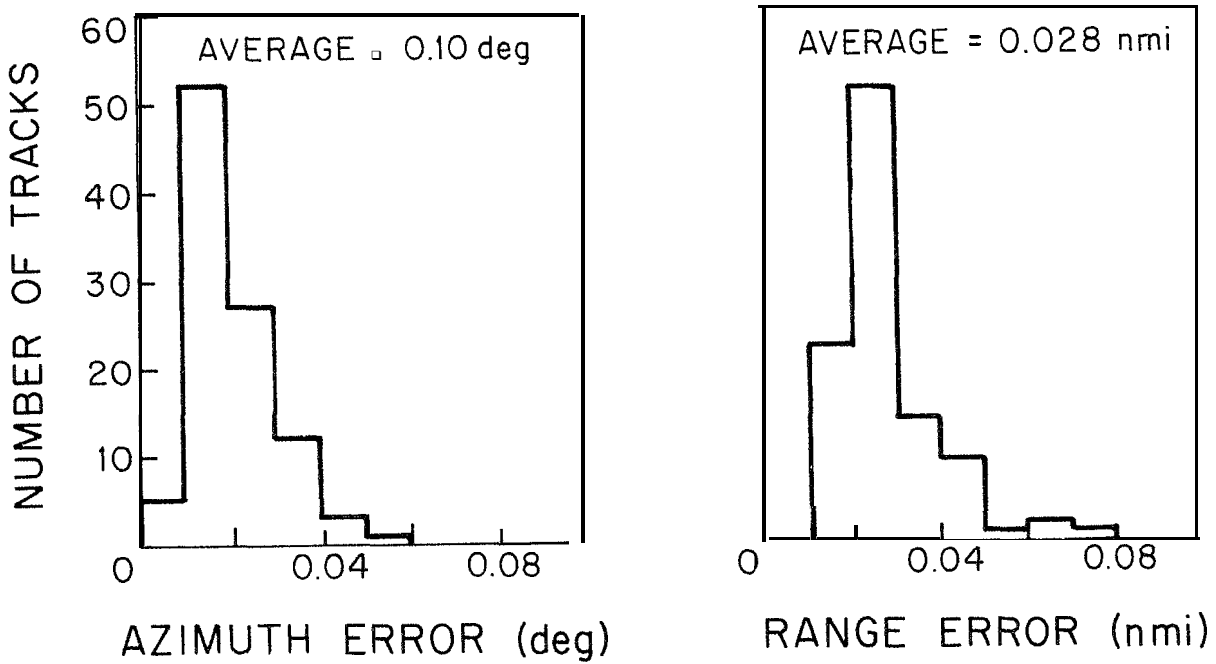
Fig. V-51.   MTD/beacon track report accuracy (100 tracks).

Piper Cherokee and an Aero Commander, flew a two-hour mission at NAFEC. One aircraft flew at an altitude several hundred feet above the other. The Piper Cherokee's course was kept relatively straight while the Aero Commander flew in a crisscross pattern such that the aircraft's paths intercepted each others both temporally and spatially (in range and azimuth). A schematic example of the trajectories is presented in Figure V-52. During the tests the angle with which the two tracks crossed was varied from 0 to 90°.

An example of the detection performance of the MTD is presented in Figure V-53. In this figure the MTD radar reports are displayed. Note that the controlled aircraft cross each other three times. In each case the aircraft are unresolved for at most two radar scans.

Next, the radar only and radar/beacon report data was processed through the ARTS-III tracker and the results were examined. Figures V-54 and 55 present forty scans of automated tracker output for the radar only and radar/beacon data which corresponds to Figure V-53. The radar only tracking results are quite poor whenever the ARTS-III tracker has two tracks whose track windows overlap, thus causing both reports from both tracks to *fall* into both track windows. The ARTS-III tracker gives up and only coasts the track even when the correct choice of reports with tracks is obvious. This tracker deficiency should be fixed because the quality of the radar data input to the tracker is excellent (see Figure V-53). The tracking performance, when beacon data is added, improved dramatically because the beacon codes of each beacon report are used by the tracker to correlate the report with an already established track.

J. Operation with Different Radars

1. Background

The MTD supplies the timing pulses required for the associated radar transmitter/receiver. The radar supplies intermediate frequency signals to the MTD. In addition to the intermediate frequency target echo signals, the MTD, being a coherent processor, requires an intermediate frequency phase reference signal. The MTD was-originally designed to interface with a klystron radar.

150
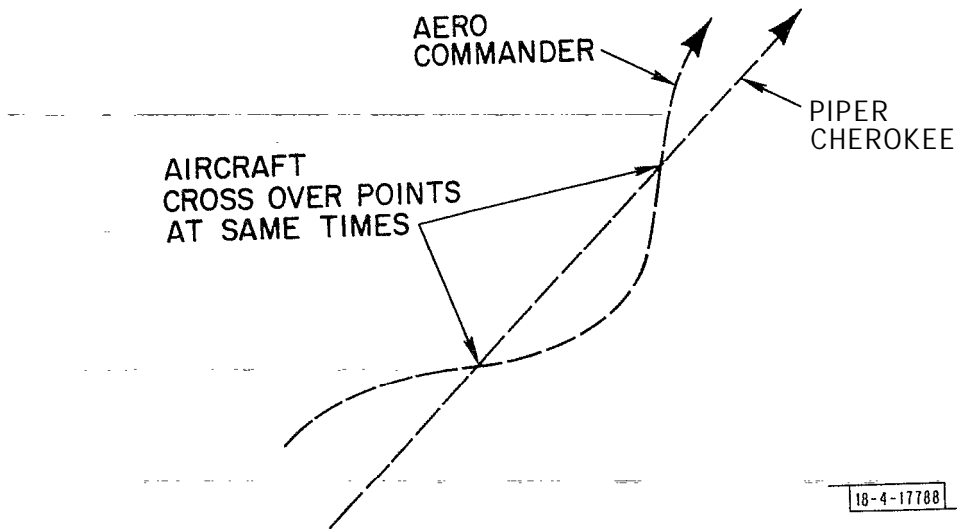
Fig. V-52. Crossing flight paths: test flight of 2 September 1975.

SCAN 1110 TO 1149

Fig. V-53. MTD report data (40 scans) (tests of 2 September 1975).

DISPLAY CODE

0 RADAR ONLY

B BEACON ONLY

° RADAR AND
    BEACON
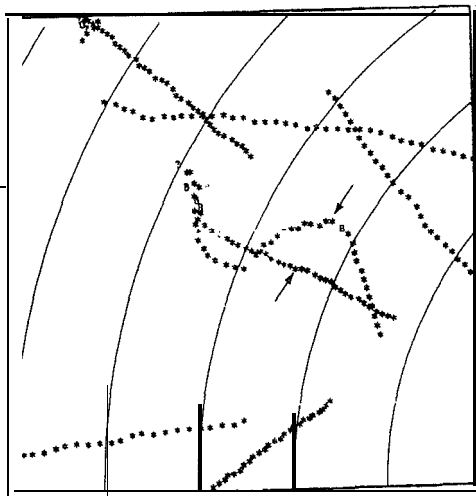
? COAST

(TWO MILE RANGE RINGS)

Fig. V-54. MTD automated tracker output – radar and beacon data (test flight of 2 September 1975).

DISPLAY CODE

0 RADAR ONLY

? COAST
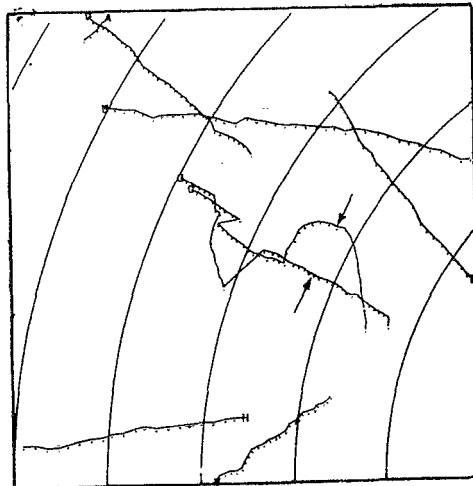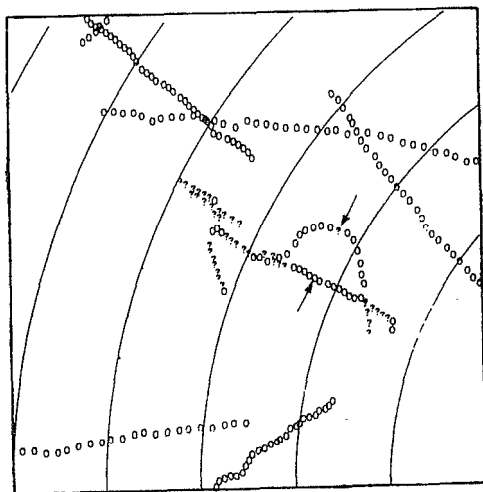
(TWO MILE RANGE RINGS)

Fig. V-55. MTD automated tracker output – radar only data (test flight of 2 September 1975).
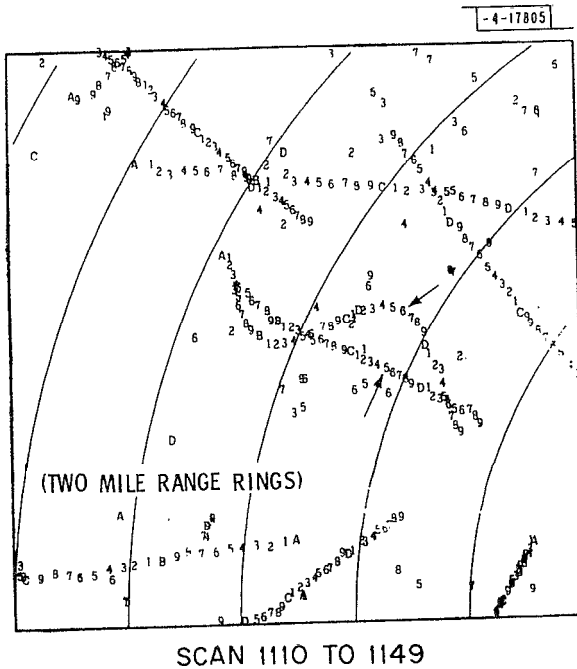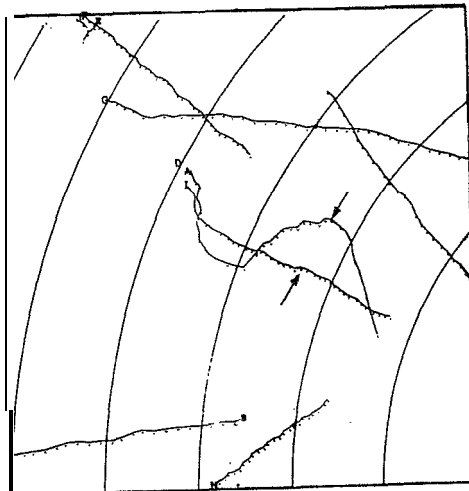
The phase reference signal was generated at the intermediate frequency by a continuous wave oscillator. In the MTD the transmitted pulse was generated by gating and amplifying a 1-microsecond burst of this CW signal. This 1-microsecond pulse of intermediate frequency energy was heterodyned with a continuous wave, S-band oscillator in the radar to provide an S-band pulse at a known phase which could be amplified in the klystron power amplifier and transmitted. This arrangement is not particularly new and is generally known as a synchrodyne radar. The FPS-18 and FPS-20 designed in the early 1950's are synchrodyne radars as is the ASR-8.

Synchrodyne radars have the advantage that the transmitted phase is coherent from one transmitted pulse to the next so that ground clutter from ambiguous ranges (second-time-around clutter) can be dealt with effectively. Klystron pulsed radar transmitters, however, are expensive, bulky and inefficient. By far the majority of operational S-band surveillance radars use magnetron transmitters. Magnetrons are small, inexpensive and relatively efficient. They have the disadvantage that, being pulsed power oscillators, the pulses start at random phase.

Some phase reference must be provided if a coherent system is to be operated from a-magnetron transmitter. Conventionally, this is accomplished by taking a low power sample of the transmitted pulse, heterodyning it against a high frequency local oscillator and-using the resulting intermediate frequency pulse to phase lock an intermediate frequency oscillator. This arrangement has been in use since WW II. The high frequency local oscillator has become generally known as the stalo for stable local oscillators and the coherent intermediate frequency oscillator is known as the coho.

Note that both the synchrodyne and the magnetron radar use high frequency local oscillators (stalos). In most contemporary radars the stalo is a cavity oscillator either vacuum triode or semiconductor. In the ASR series of radars, the stalo imposes the most important limitation on the radar's clutter rejecting capability. Other possible causes of degraded clutter rejecting performance include spurious phase or frequency modulation of the transmitted pulse, random inaccuracies in the phase locking of the cbho (in magnetron radars), timing jitter and-non-linearities in the receiver train.

2.   F P S - 1 8

The MTD was originally designed to interface with a (modified) FPS-18,
see Figure V-56.   The coho is a commercial crystal oscillator that is mounted
with the MTD analog hardware.   The master timing clock for all the digital
hardware is derived from the coho.   To simplify this process, the coho frequency
was set at the 24th harmonic of the range gating frequency.   This turns out to
be slightly less than 31 MHz.

All the intermediate frequency amplifiers in the MTD are wideband amplifiers.
The system noise bandwidth is set by a passive filter in the signal IF channel.
This filter has a 31-MHz center frequency and a passband of about 2.6 MHz.   The
noise bandwidth of the coho channel is restricted by a somewhat wider bandpass
filter, and the burst of 31 TTL pulses that is delivered by the MTD digital
timing is converted into a burst of sinusoidal pulses by yet another bandpass
filter.

3.   ASR-7

The MTD was originally connected to an ASR-7 channel at Lincoln Laboratory
before they were moved to NAFEC.   Some preliminary stability measurements were
made at that time but the move to NAFEC came before the system could be operated
as a radar.

In order to facilitate rapid changeover between the ASR-7 and the FPS-18,
the IF circuits in the former were retuned to a center frequency of 31 MHz.
Slight modification--to the modulator driver circuitry was required so that the
ASR-7 could accommodate the higher PRF required by the MTD.

The coho in the ASR-7 must be turned off shortly (a few microseconds) be-
fore each new transmitter pulse so that the phase locking process always starts
with the oscillator in a quiescent state.   Accordingly, an additional coho
gating pretrigger is required from the MTDOtherwise the ASR-7 and MTD appeared
to be compatible so that mating the two equipments was primarily a matter of
running the necessary cables.   The interface is shown schematically in Figure V-57.

4.   ASR-5

The ASR-5 is very similar to the ASR-7 but uses all vacuum tube elec-
tronics, as opposed to the solid-state circuitry in the ASR-7.   Accordingly,
trigger amplifiers were required to raise the trigger outputs from the MTD to a

154

level which would trigger the vacuum tube circuitry in the ASR-5. The particular
ASR-5 at the TFAST site had been modified with a crystal stablized solid-state
stalo and a PIN diode STC attenuator. It was found that the transmitter modu-
lator circuitry would operate at the MTD interpulse periods with no modification.
The interface between the MTD and the ASR-5 is almost identical to that with the
ASR-7 and is shown on Figure V-57.

    5.   Results

        a.   SGP Results

        The SGP spectral analysis routine which was available at NAFEC pro-
vided a simple and direct *way* of evaluating each radar's potential when connected
to the MTD. The antenna is stopped with the beam directed at some strong isolated
fixed reflector. The SGP range gate timing is then adjusted so that the fixed echo
is in the SGP range *gate*. Finally, the STC attenuator is adjusted so that the
fixed echo is just below the limit level at the A/D converters. The SGP then pro-
vides a graphical display of the sideband power density over the unambiguous
doppler interval. This is derived from 64-point fast Fourier transform calculations.
Radars can be compared directly simply by comparing the SGP output displays from
each radar. If quantitative estimates of clutter rejection as a function of
doppler are desired, the SGP frequency coefficients must be weighted with the
response of the doppler filter in question.

   Some SGP results are shown in Figure V-58. The FPS-18 and ASR-5 results were
measured at NAFEC while the ASR-7 results were measured at Lincoln Laboratory.

        b.   MTD Results

        At NAFEC the MTD has been connected to each of the three radars
and operated into both the Nova display system and the augmented ARTS-III system
at one time or another. Except for those times when clutter is being received
from ambiguous ranges, it is not possible to tell which radar is in use by ob-
serving the PPI display.

  K.   Accuracy of MTD Doppler Velocity Measurements

  Because the MTD employs a doppler filter bank rather than an MTI high-pass
filter, it has the capability of measuring the ~doppler or radial velocity of the
target being detected. The MTD transmits four PRF's. These are sent two per

155
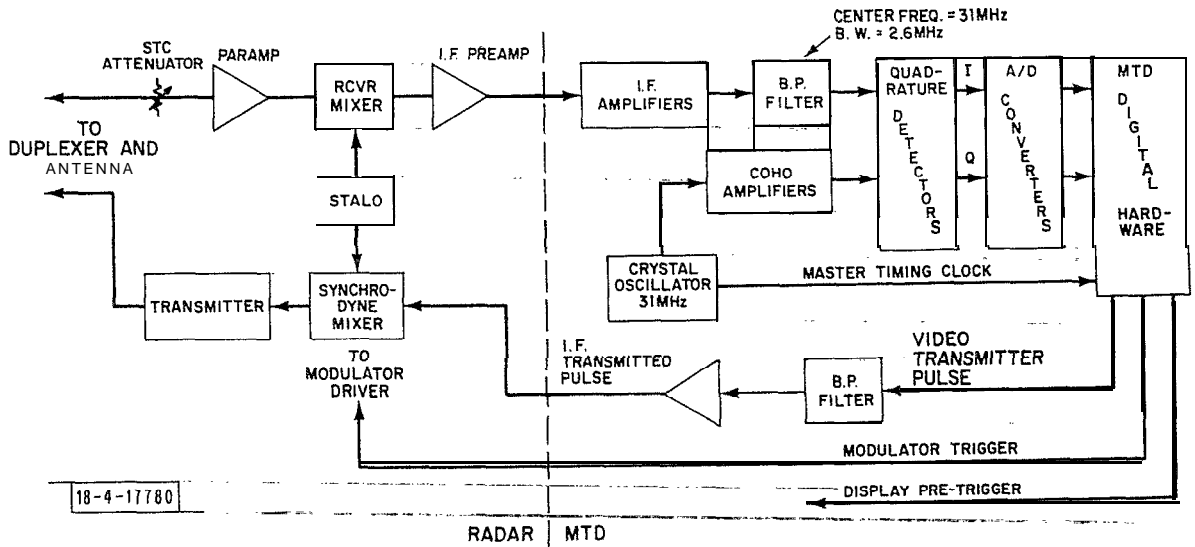
Fig. V-56.. MTD interface with synchrondyne radars.
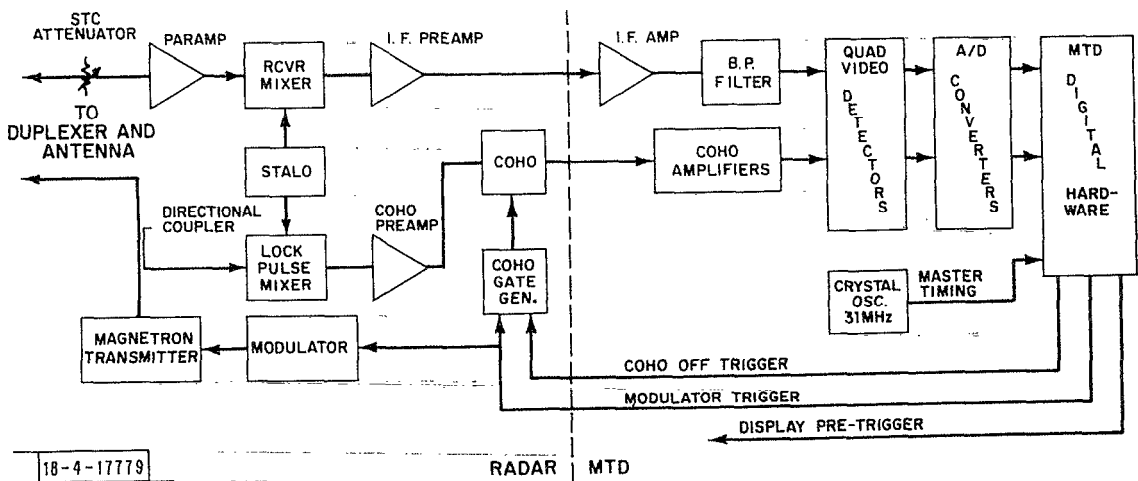
Fig. V-57. MTD interface with magnetron radars.

156
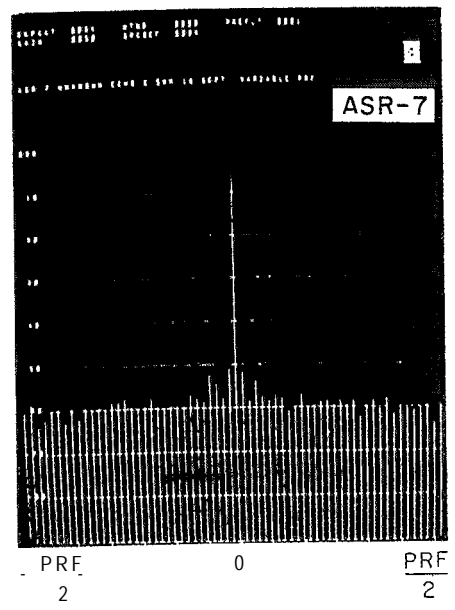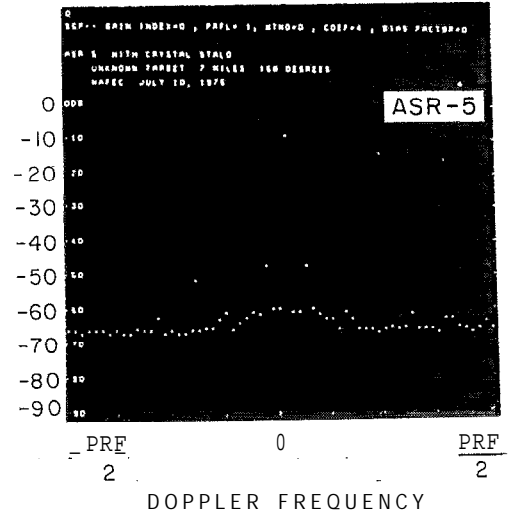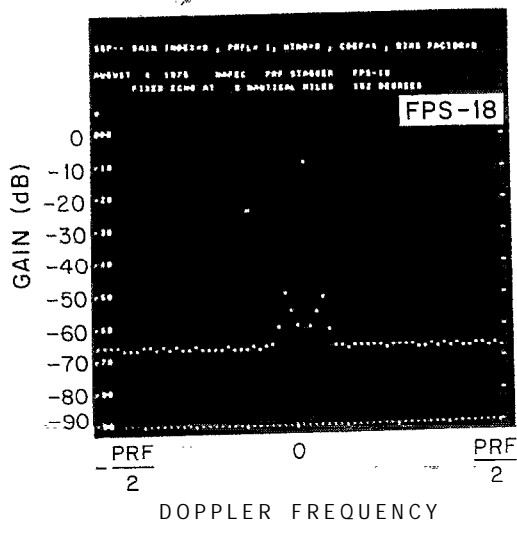
Fig. V-58. Instability spectra with variable PRF (1120, 1380 Hz.).

scan, the two values are alternated between each CPI. The PRF's are changed each scan by 1% to resolve second-time-around targets. The four values of PRF are listed in Table V-1.

TABLE V-1

List of PRF's

	PRF	Blind Speed
even scans	1120.8 Hz	118.8 knots
	1379.4	146.2
odd *scans*	1113.1 Hz	117.9 knots
	1367.7	145.0

The two PRF's used each scan are alternated between every CPI. Since these PRF's have an average blind speed of 132 knots most aircraft radial velocities will be ambiguous if measured using only one PRF. However, since there are transmissions at both PRF's each beamwidth, the radial velocity may be resolved to a multiple of.

$$V_u = \frac{V_B V_A}{V_B - V_A}$$

where V_U = radial velocity

V_B = blind speed of $(PRF)_1$

V_A = blind speed of $(PRF)_2$

For the PRF's used in the MTD, this corresponds to a maximum unambiguous radial velocity of-634 knots. An algorithm has been developed and programmed into the ARTS-III software to calculate the unambiguous radial velocity. The details of the algorithm are given in reference 17. The algorithm does not take into account the differences in PRF's from scan to scan, but instead uses the averages of the high and low PRF's. This introduces an error of three knots in the measurement of radial velocity. A doppler velocity is computed for detection sets when detections occur at both PRF's. When the set has detection(s) from only one' PRF, no computation can be performed and an ambiguous velocity flag is set in the target report.

The relations used in the computation are:

A. $\quad X_1 = \dfrac{X_\phi - Y_\phi}{R}$

B. $\quad X_2 = X_1 + K$ when $X_1 < \phi$

C. $\quad X_2 = X_1 - K$ when $X_1 \geq \phi$

D. $\quad V = \dfrac{X - X_\phi}{-9.62}$

where: $\quad X\phi = \dfrac{D_x}{64}\, f_x,\ Y_\phi = \dfrac{D_y}{64}\, f_y,\ R = 1 - \dfrac{f_x}{f_y},\ \text{and}\ K = \dfrac{f_y}{R}.$

f_y is the average of the lower PRF's

f_x is the average of the higher PRF's

D_y is the interpolated doppler number for the lower ERF (0-63).

D_x is the interpolated doppler number for the higher PRF (0-63).

After computing X_1, K is added to or subtracted from X_1 (dependent on the sign of X_1) to produce X2. From these-two values, the one that is nearest to a multiple of f_x, termed X, is used in the velocity calculation. The sign of the result is retained to define. target motion direction.

$V \geq \phi$ target moving toward radar

$V < \phi$ target moving away from the radar

Figure V-59 presents the measured doppler velocity vs. scan number for the propeller driven Piper Cherokee flown on August 12, 1975. The spikes in Figure V-59 are clearly erroneous values because the aircraft could not undergo such wild accelerations in such short periods of time. The propeller modulations and other noise in the doppler signal give rise to slightly erroneous values of interpolated doppler numbers D_x and D_y. These, in turn, if the errors are large enough cause the algorithm to be off by a multiple of the unambiguous velocity which is equal to 634 knots for this radar. Since it is not known a priori if the return is in error by 634 knots, one must assume that it is if and when the data

159
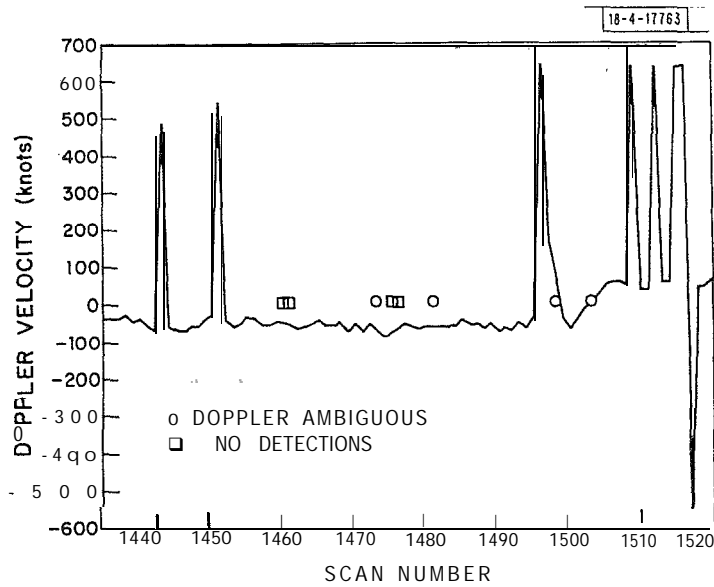
Fig. V-59. Doppler velocity of Piper Cherokee, measured using Univac algorithm (12 August 1975).
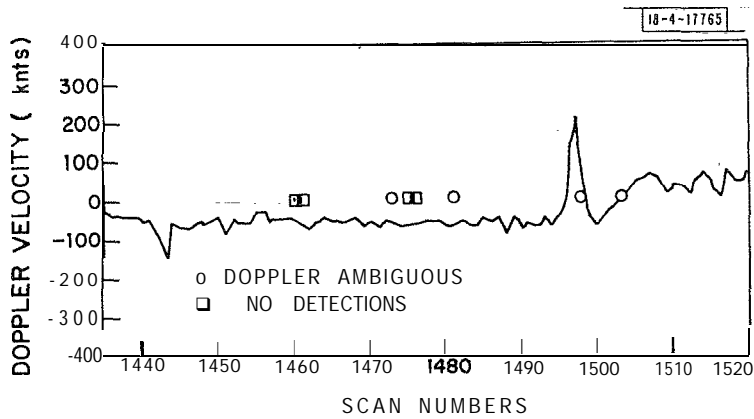
Fig. V-60. Doppler velocity of Piper Cherokee, measured (12 August 1975).

160

is quite useful.   If it is assumed that the aircraft <u>cannot</u> change its radial velocity by more than 500 knots in the 4.7 seconds between scans and the radial velocity in the previous scan has been determined by smoothed rate of change of range measurements, then the data in Figure V-59 takes the form presented in V-60, Except for a few points, these values are in good agreement with the actual values of a radial velocity.

The same analysis was done for an EB-57 jet aircraft.   The measured doppler velocity vs. scan number is presented in Figure V-61.   The data in Figure V-61 is cleaner although there are still some erroneous points due to noise and turbine modulation.   When the additional constraint is added, the data takes the form of Figure V-62.   Here the data is clearly excellent with no substantial deviations from the expected values.   The jitter in radial velocity is about 25 knots.   It should be noted that only a small amount of data has been analyzed in this manner.   More thorough studies of the accuracy of the doppler velocity information should be made to either confirm or modify these conclusions so that reliable doppler velocity information is available for use in the ARTS-III tracker.
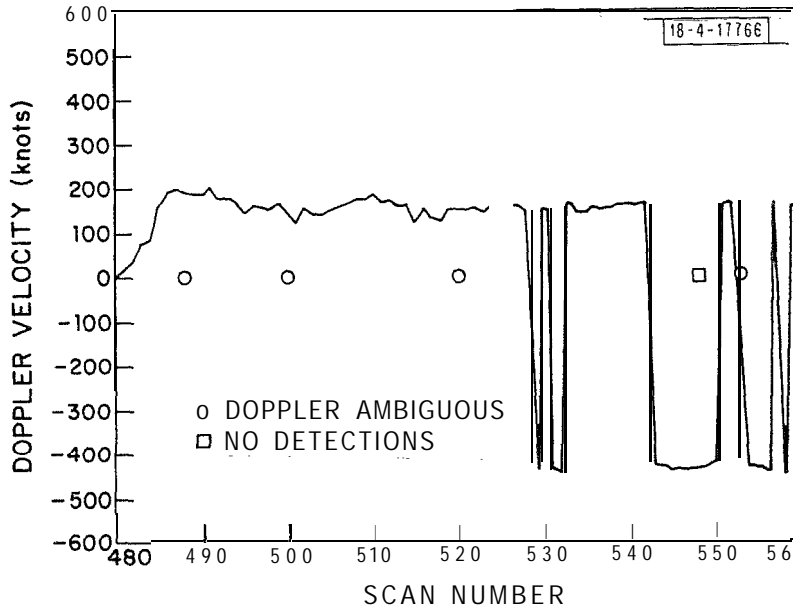
Fig. V-61. Doppler velocity of EB-57 (jet), measured using Univac algorithm.
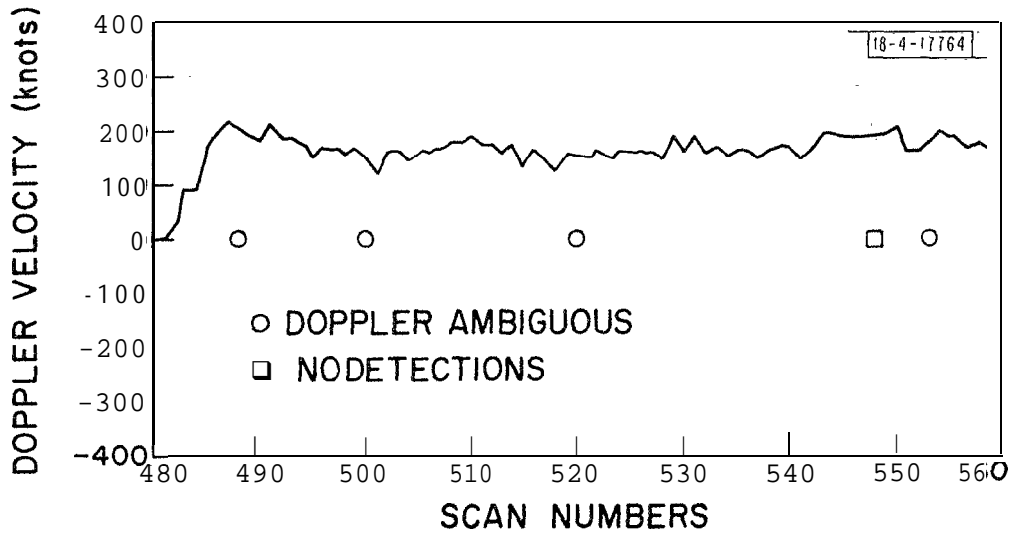
Fig. V-62. Doppler velocity of EB-57 (jet), measured.

162

S-BAND RADAR ENVIRONMENT DOPPLER SPECTRA

A real-time Fourier analysis program, called the Single Gate Processor (SGP), has been written to process data from a single selectable radar range cell. The program was written in NOVA assembly language to run on a NOVA 1220 minicomputer utilizing an Imlac PDS-1 display.

In operation, the complex video sample (corresponding to the radar range cell of interest) from the radar return is digitized and transferred to the NOVA every (1/prf) second. Samples are stored sequentially in one of two (64-sample) core buffers. The 64 samples are processed in a 64-point Fast Fourier Transform (FFT), and the output is converted to a log spectral density. The data is then sent to the Imlac refreshed display, where it is presented in the form of a graph giving the relative levels (in dB) of the spectral density for the single gate time series.

The abscissa represents doppler frequency with zero at the center. The range of unambiguous doppler frequencies spans the horizontal dimension of the display with 0 at the center, positive doppler offsets to the right and negative offsets to the left.

The SGP system has proven to be most useful in testing MTD-equipped radars. It appears to be useful for collecting doppler spectral data from radar echoes. This appendix describes the SGP algorithm and presents some representative SGP periodograms from precipitation, aircraft and what are believed to be bird echoes.

The development of the SGP program has evolved over several years and has been the product of many individuals' work[*]. References 35 through 38 document it sequentially. It should be noted that the later documentation supersedes the earlier when inconsistencies exist. Source tapes for SGP in NOVA assembly *lan-*guage may be obtained from B. G. Laird at Lincoln Laboratory.

---

[*] SGP was originally conceived and executed on a Raytheon 706 computer by P. B. McCorison. He used FFT and magnitude algorithms developed by T.M. Hendricks. This description of the latest revision is lifted bodily from a paper by B. G. Laird and P. R. Kretz who developed it.

1. <u>SGP Overview</u>

    This section provides an overview of SGP in operation. The program,
with its various processing options, is illustrated in block diagram form in
Figure A-l.   SGP may be thought of as having two concurrent, mostly asynchronous
tasks to complete.   The first of these is the process. of accepting a complex (two-
word) sample* via a data channel transfer approximately every 800 µs, and storing
it in the proper location in one of two input buffers.

    The second task, which takes much longer, is the process of processing the 64
complex samples in a full input buffer, performing an FFT on them, and producing
a 64-point spectral display.   As soon as one of the buffers is full, Task #1
switches to filling the second buffer-and Task #2 can begin processing the first
buffer.   Ideally, Task #2 would finish producing the 64-point spectral display in
less than the alotted 51.2 ms (64 x 800 µs), in time to begin handling the full
contents of the second buffer, which Task #1 had meanwhile been filling with new
data.   Task #1 would then switch back filling buffer 1 and so on.   In reality,
Task #1 fills a second buffer long before Task #2 is finished processing the
first; Task #1 is halted until-Task #2 completes, and a portion of the available
radar returns goes unsampled.   This is not serious, time gaps between buffers do
not affect successive spectral results.   However, successive samples in a buffer
must be sequential with a constant sampling rate.

    This suggests that Task #1 must have precedence over Task #2 and be capable
of interrupting Task #2 whenever necessary, with the one exception that Task #2
should be uninterruptable if both input buffers are full.   In addition, Task #1 is
externally triggered in the sense that data transmission to the computer can only

---

*Samples are in the form of two 16-bit two's complement words (two 11-bit A/D.
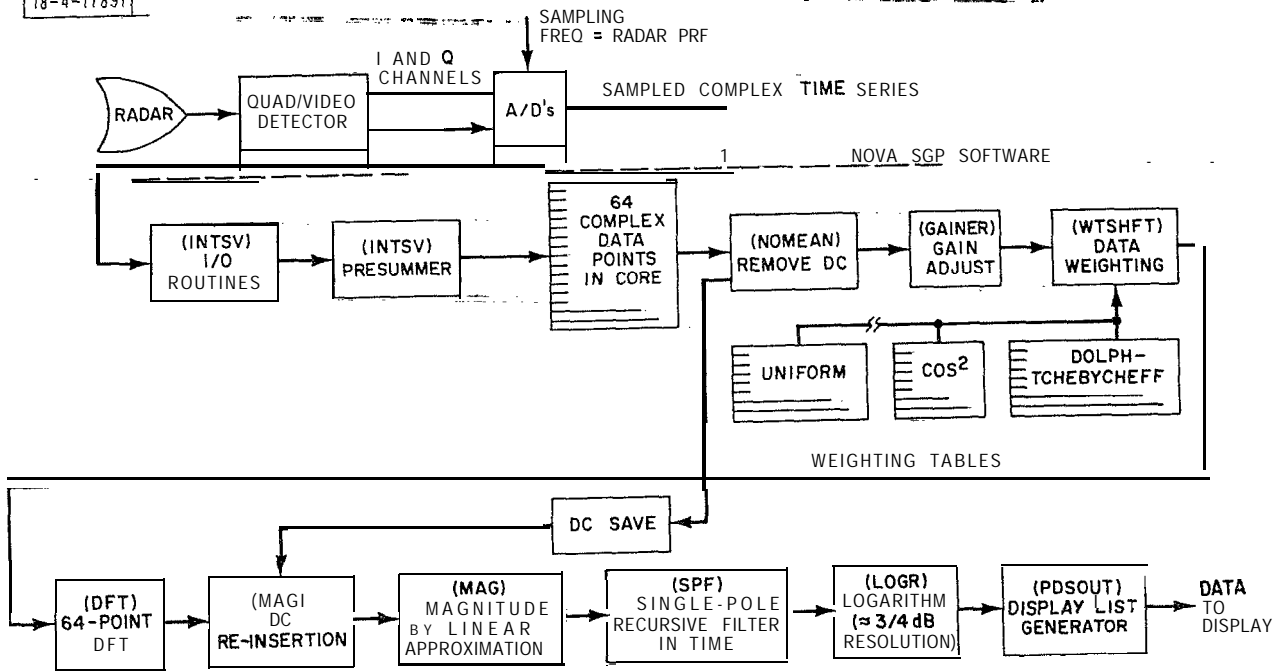samples with sign extended).

Fig. A-1.   SGP system block diagram.

take place upon the arrival of a prf pulse generated by the radar (and appropriately delayed to select the desired range gate). This pulse arrives at the data channel interface to the A/D's every 1/prf seconds (presently 800 μs). However, the transfer of the sample into the computer cannot take place unless the data channel has been properly enabled by a short sequence of instructions from the computer. Before processing through the FFT, the data may be presummed. By presumming we mean the process of converting, for example, 256 successive time samples into 64 time samples by replacing every four samples with an average of the four. This averaging may be done over 1-16 samples. An input buffer is filled-in bit reversed order, as required by the FFT algorithm used in SGP.

Next, Task 82 takes over and the data is prepared for the FFT by removing the DC level from the samples. This is accomplished by determining the mean value of the 64 samples and subtracting it from each sample. A real as well as an imaginary mean is determined, and saved for re-insertion after the FFT and before displaying.

Once the DC value is removed from the data, all data points are multiplied by a gain factor.- This allows for the amplification of comparatively weak AC signals riding on a large DC component (usually the case with radar data) in order to get maximum use of the allowable dynamic range of input data. The gain index is one of the operator controllable variables and allows a gain of from 0 to 60 dB. The DC components subtracted earlier are also scaled by this gain factor in order to prepare them far reinsertion.

The next step in processing the spectral data is weighting of the time series. Weighting functions are used to counteract the spurious high frequency components which appear in the spectra of any finite length DFT. Four different sets of weighting are available; uniform weighting, Dolph-Chebyshev, cosine squared, and cosine fourth power.

The data is now processed by the 64-point in place, decimation in time, FFT algorithm. A forward FFT (from the time domain to the frequency domain) is performed. No provisions have been made to allow SGP to perform an inverse FFT. The complex constants used as multipliers in the butterfly operations have been computed in advance and stored in tables. A modified butterfly is used in order to

prevent overflow (i.e., the data is right-shifted before the addition takes place in the butterfly). Advantage is taken of the fact that due to the unsigned nature of the two accumulator (32-bit) result of the NOVA multiply, using only the high order 16 bits of the result has the effect of right-shifting the *answer* one bit.

After the FFT is performed, the stored DC value is added (after doing appropriate weighting) to the first element of the output buffer from DFT. Magnitudes of the complex numbers are then determined by a method of linear approximation, which has the effect of preserving the dynamic range of the numbers and introduces a maximum error of about 1.5% with an average error or 0.5%. By trial and error it was discovered that two lines (with the break point being 0.445) will closely approximate a complex number between 0 and 1.

The magnitudes of the complex numbers are then integrated with successive 64-point spectra in order to provide a smoother spectral estimate by recursive filtering. The formula used for each point in the display is:

New value to be displayed = Old display value − Old display value/2^N + Present sample/2^N

The 64 output values are converted to a logarithmic scale .and are then sent to the Imlac PDS-1 to be displayed. When the data is being sent the second half of the buffer is sent first,-followed by the first half. This has the effect of placing the 0 frequency information at the center of the spectral display. An option available to the operator allows each data point in this display spectrum to be incremented by an addition of from 0 to 20 dB in increments of 4 dB. This factor is added to all data in the display and generally has-the effect of increasing the relative dynamic range of the data displayed.

2. Precipitation Spectra

Figures A-2 through A-7 present SGP periodograms from precipitation echoes. These were taken with the radar pointed at several different azimuths. The antenna was stationary and linear polarization was employed.

These periodograms were made at NAFEC on 19 March 1974. On that day there was widespread rain, The peak rainfall rate was estimated to be between 1/2" and 1" per hour. Winds were reported to be 30 knots from 140° (relativk'to magnetic North) at the surface, 49 knots from 180° at 6000 ft altitude and 33 knots from 220° at 18000 ft. These pictures represent the widest spectra recorded during the testing period.

167
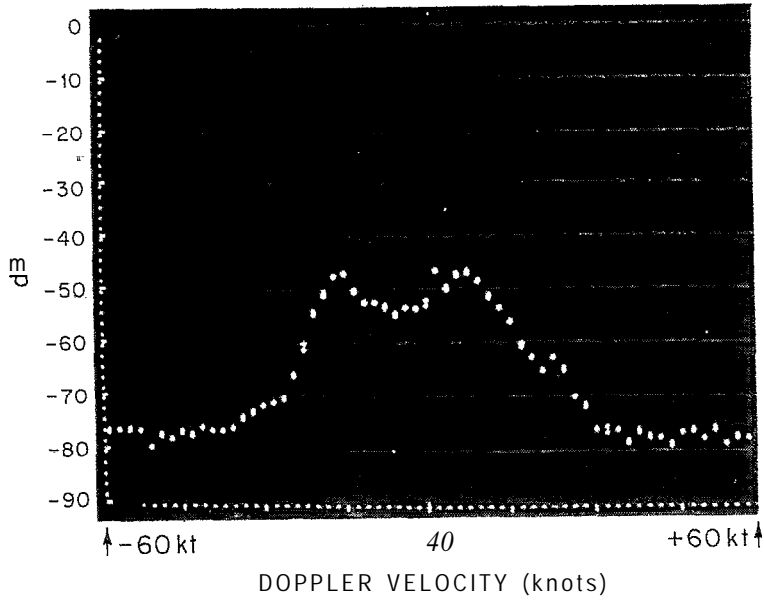
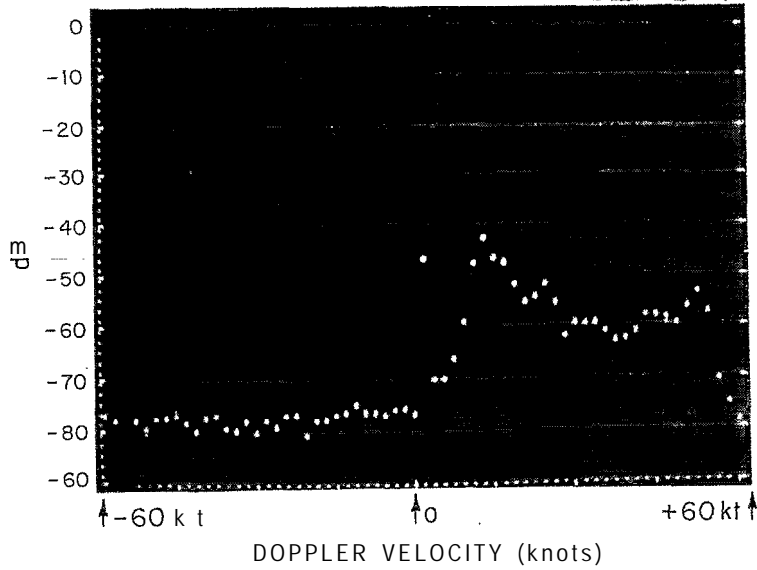Fig. A-2. Precipitation spectrum at azimuth of 90°.

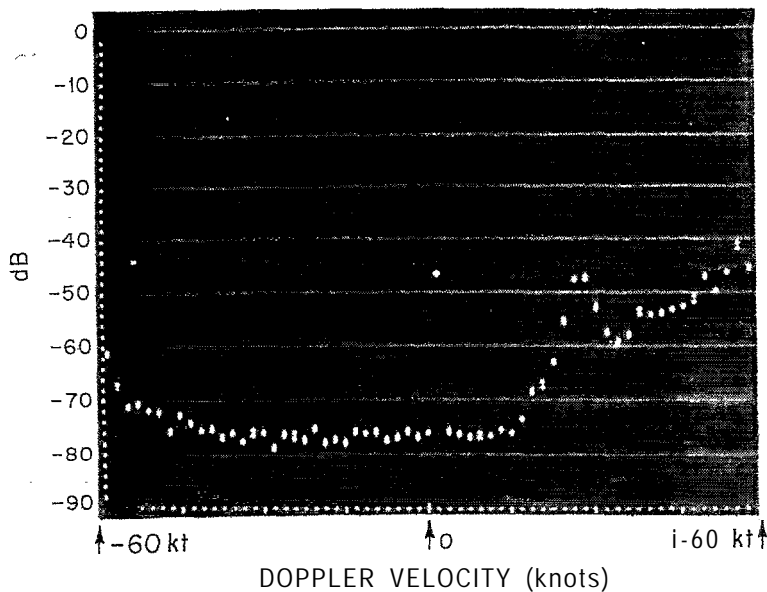Fig. A-3. Precipitation spectrum at azimuth of 130".

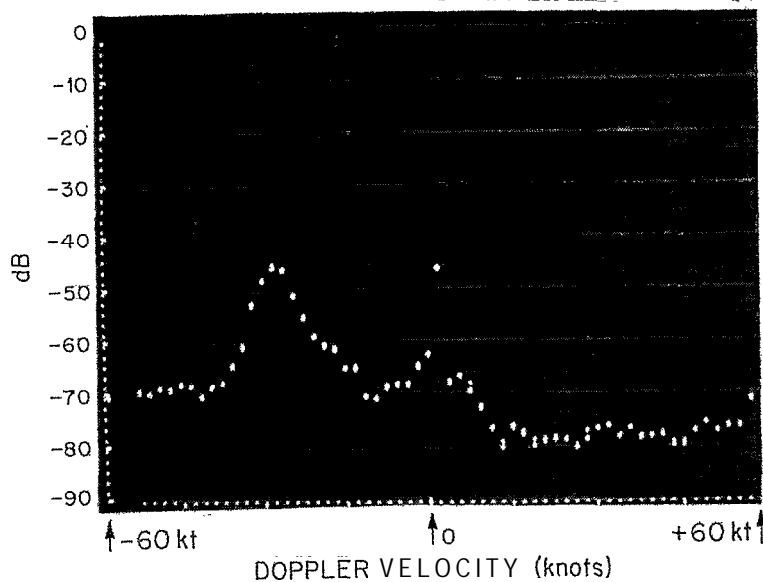Fig. A-4.   Precipitation spectrum at azimuth of 150°.

Fig. A-5.   Precipitation spectrum at azimuth of 300°.
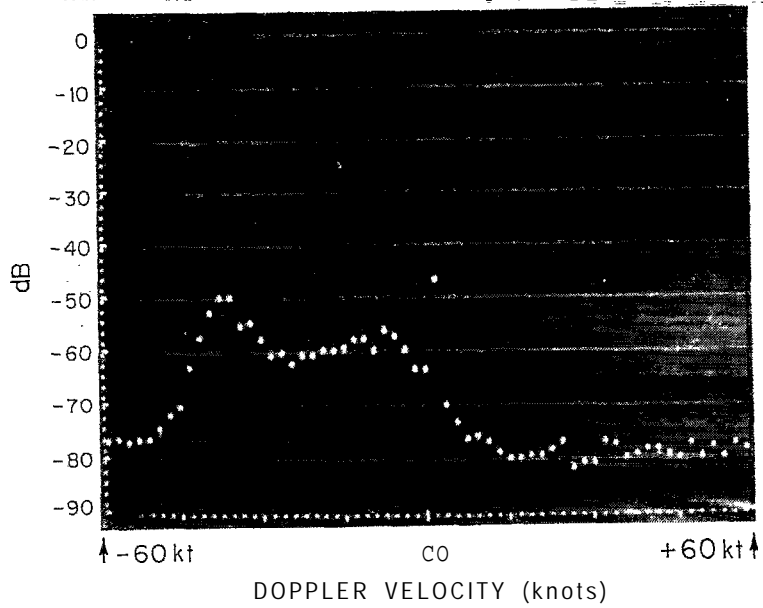
Fig. A-6.   Precipitation spectrum at azimuth of **320°**.
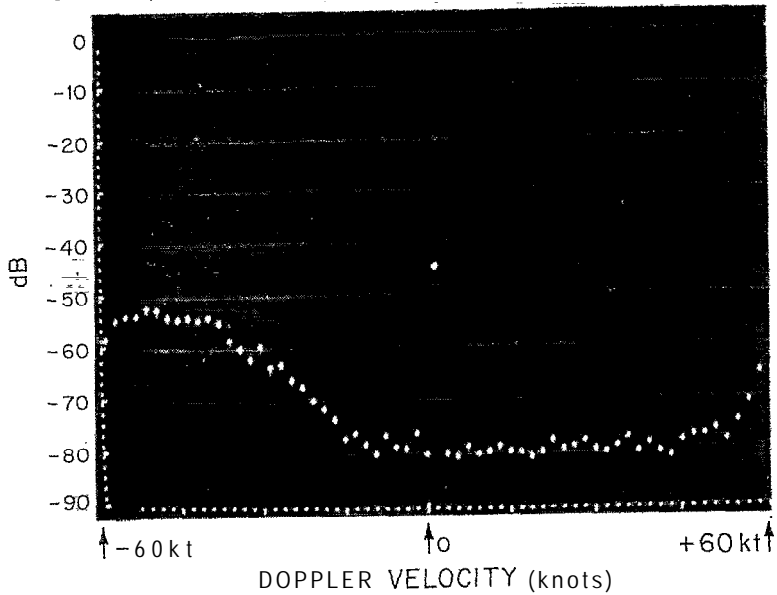
Fig; A-7.   Precipitation spectrum at azimuth of **330°**.

Note that the zero doppler line in all these periodograms appears to be at about -48 dB (or about 30 dB above the noise level). This was caused by DC offset in the analog system and the A/D converters.

3. Angel Spectra

Figures A-8 and A-9 present some periodograms which resulted when the SGP range azimuth cell was positioned over an area known to be frequented by soaring seagulls. The three periodograms in Figure A-8 each show a single rather narrow peak. These are believed to be returns from solitary seagulls at a sanitary landfill near NAFEC. Figure A-9 shows some spectra which are believed to results from several seagulls occupying the range azimuth cell simultaneously. These were taken in the same geographic area.

4. Aircraft Doppler Spectra at S-Band

Several SGP periodograms from aircraft were photographed at Lincoln Laboratory before the MTD was moved to NAFEC. Figures A-10 and A-11 are spectra from an airliner approaching the radar. Figure A-12 is a periodogram from a twin-engine executive transport (Aero Commander) in approach configuration flying essentially toward the radar. Figures A-13 and A-14 are from small, single-engine airplanes gliding, with engines idling, toward the radar.
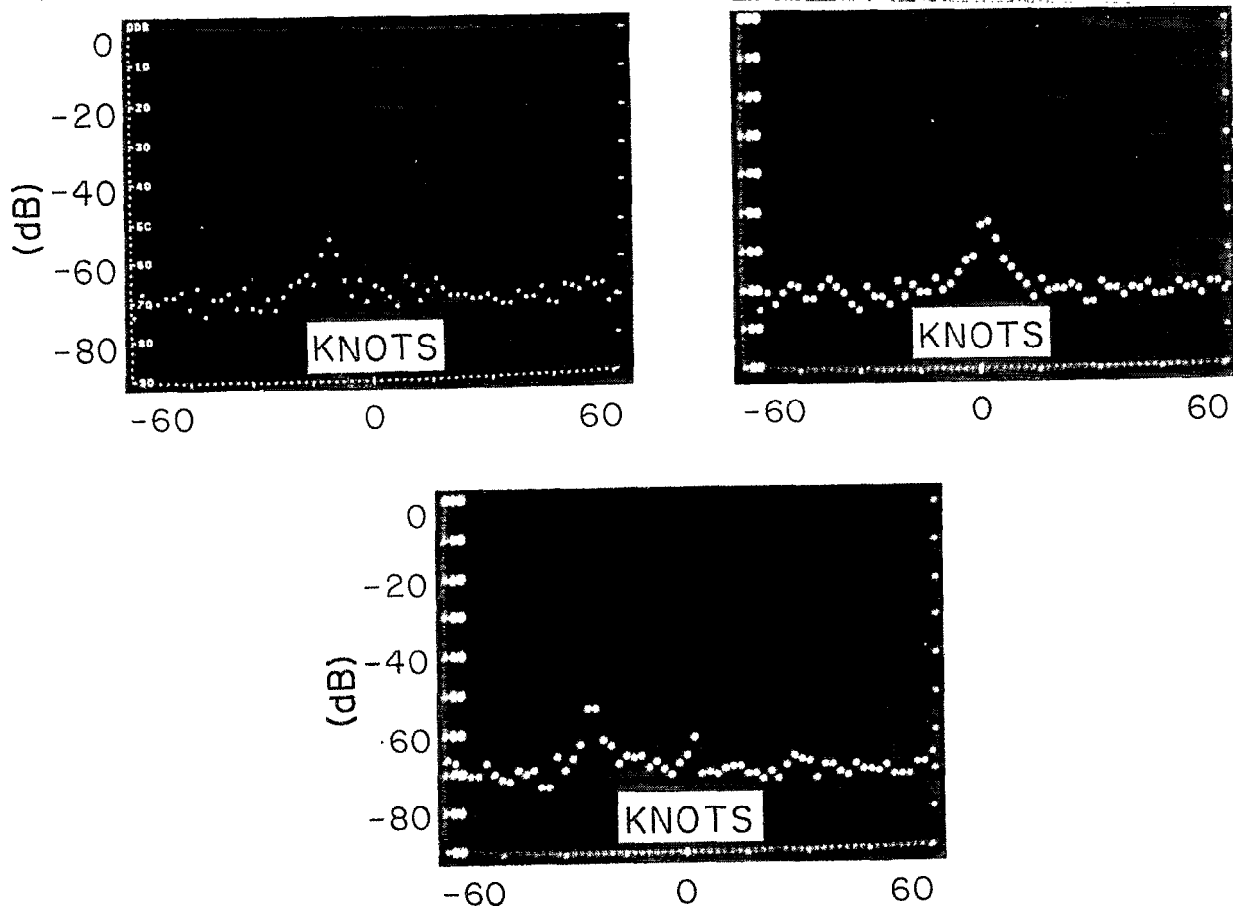
Fig. A-8. SGP doppler spectra of angels (probably solitary soaring seagulls).

Fig. A-9. SGP doppler spectra of angels (probably multiple soaring seagulls).

Fig. A-10.   Airliner approaching radar at traffic pattern speed.

Fig, A-U..   Airliner approaching radar at traffic pattern speed,
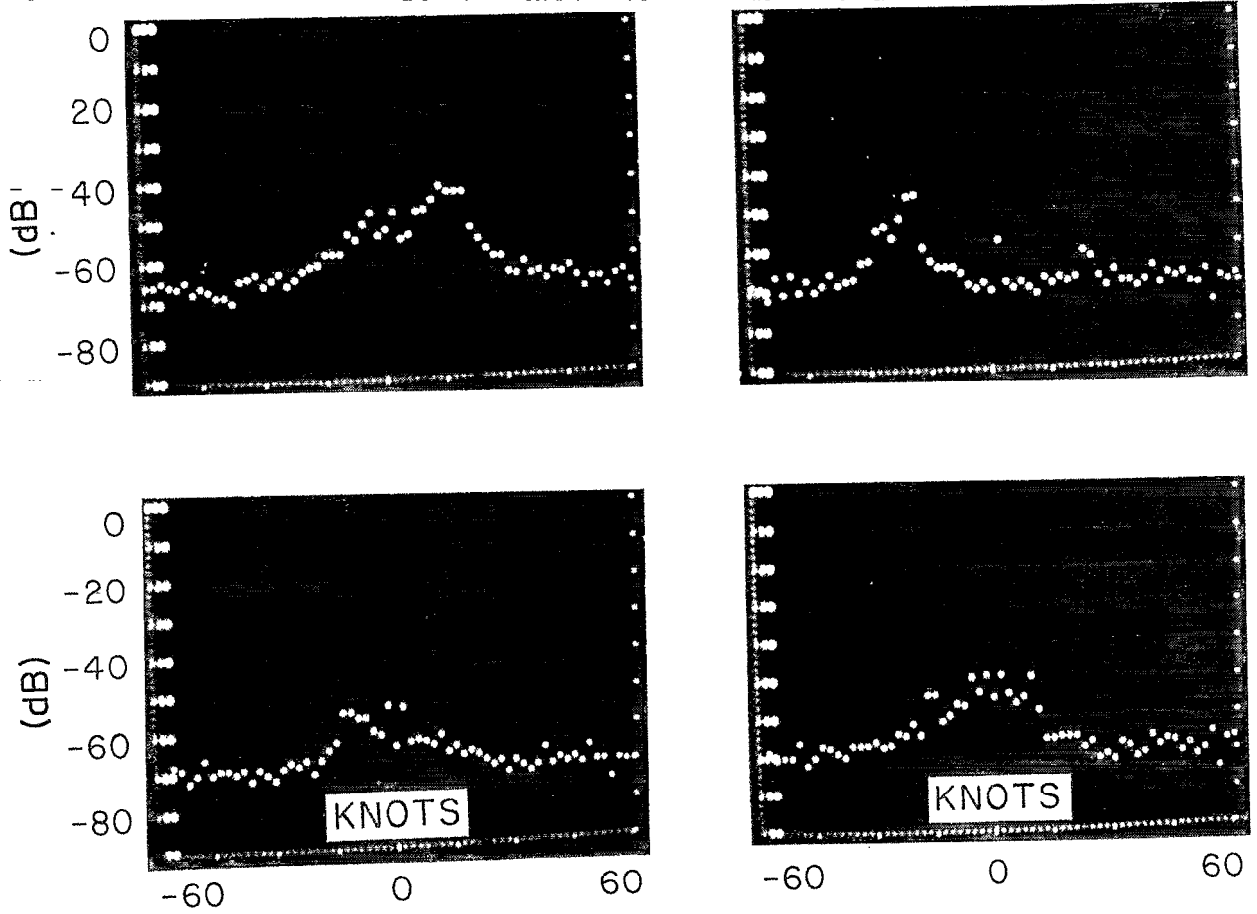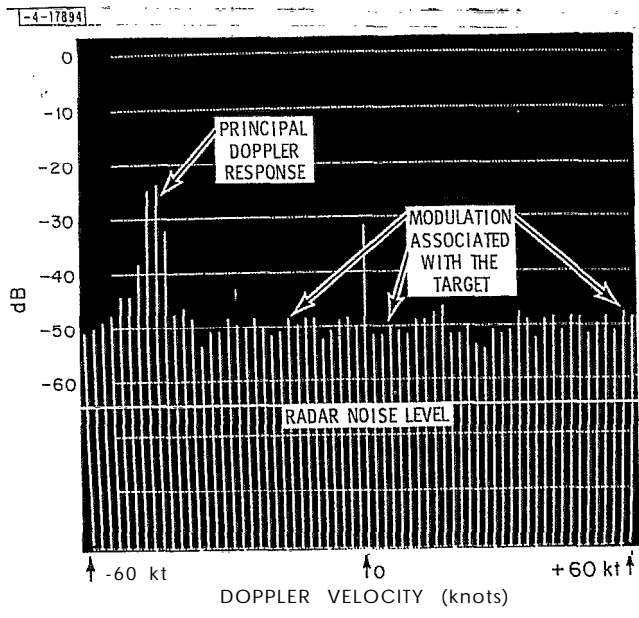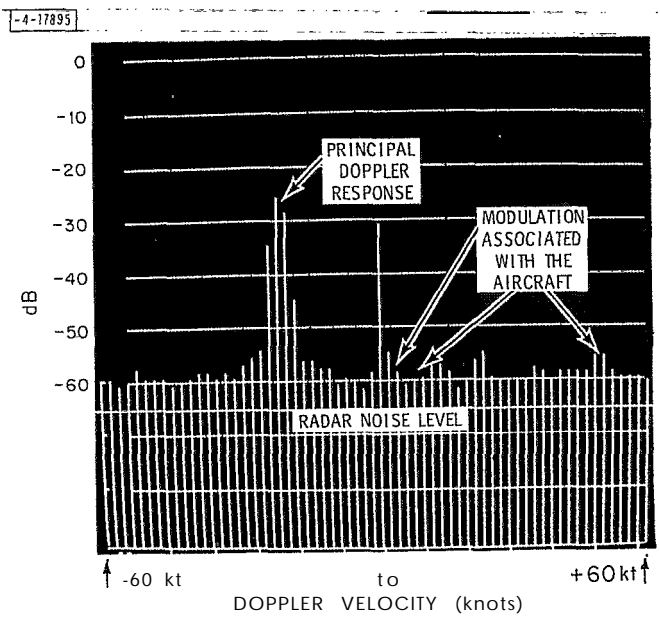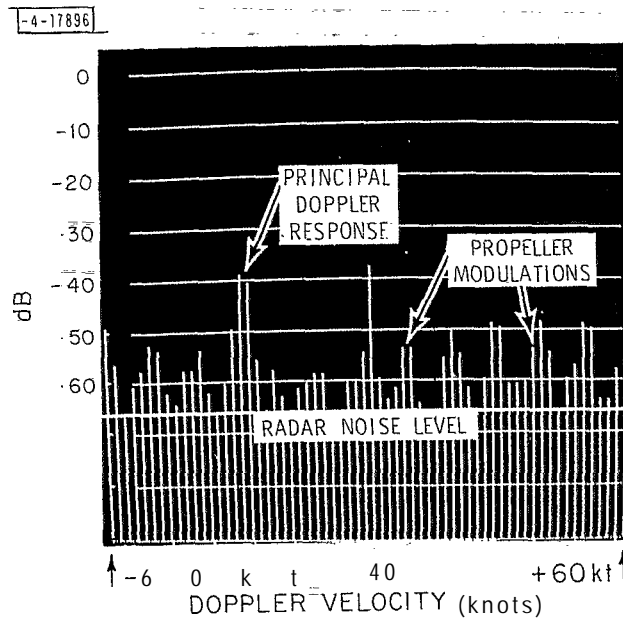
Fig. A-12. Executive twin approaching radar in final approach configuration.
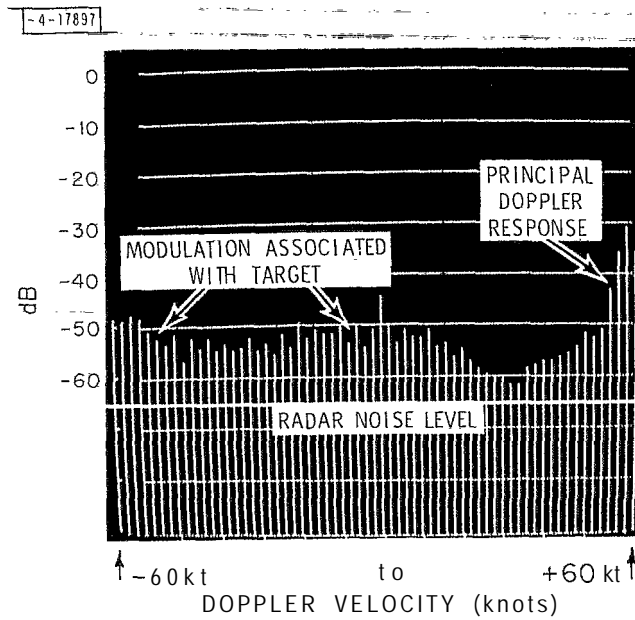
Fig. A-13. Single engine light plan approaching radar on final approach,

175

a minimum range below which two or more steps are called for within a single range resolution element. This minimum range is less than a mile for both the R^3 and R^4.

In practice, the attenuation is set at some initial value before the transmitter pulse and maintained there until the minimum resolvable range is reached. The STC attenuation is then allowed to decrease until it reaches zero. The range at which zero attenuation is reached is a function of the initial attenuation. The STC attenuation vs range curves are presented in Figure B-2. From that figure we determine that for an R^4 curve with an initial value of 60 dB, zero attenuation is reached at a range of 17.5 nmi. Similarly, an R^3 curve with an initial value of .63 dB would reach 0 attenuation at a range of 39.375 nmi.

Nominal ASR-5 antenna parameters are listed below.

Antenna gain (one-way)	34 dB
Waveguide loss	2 dB
Beamwidth	1.4^o

The antenna gain was measured on an antenna range before the antenna was installed at NAFEC. The 2-dB waveguide loss was measured by NAFEC personnel. The value 2 dB was measured between the feed horn and an ASR-5 magnetron output port. The path from the feed horn to the E'PS-18 is almost identical, except for the deletion of a circulator and the addition of a waveguide switch and a diplexer. The antenna was operated tilted up so that the 3-dB (one-way) point was aimed at the horizon. The radar power output was measured at the directional coupler shortly after the clutter data was taken. At that time, it was 29.1 dBW. The MTD duty ratio is approximately .00123, thus the peak power output was approximately 660 kW.

A noncoherent signal was injected into the directional coupler and adjusted until its strength was 37 dB greater than the RMS noise in the IF bandwidth. This signal is equal to -61.9 dBm as referred to the waveguide at the directional coupler. Hence the following tables:
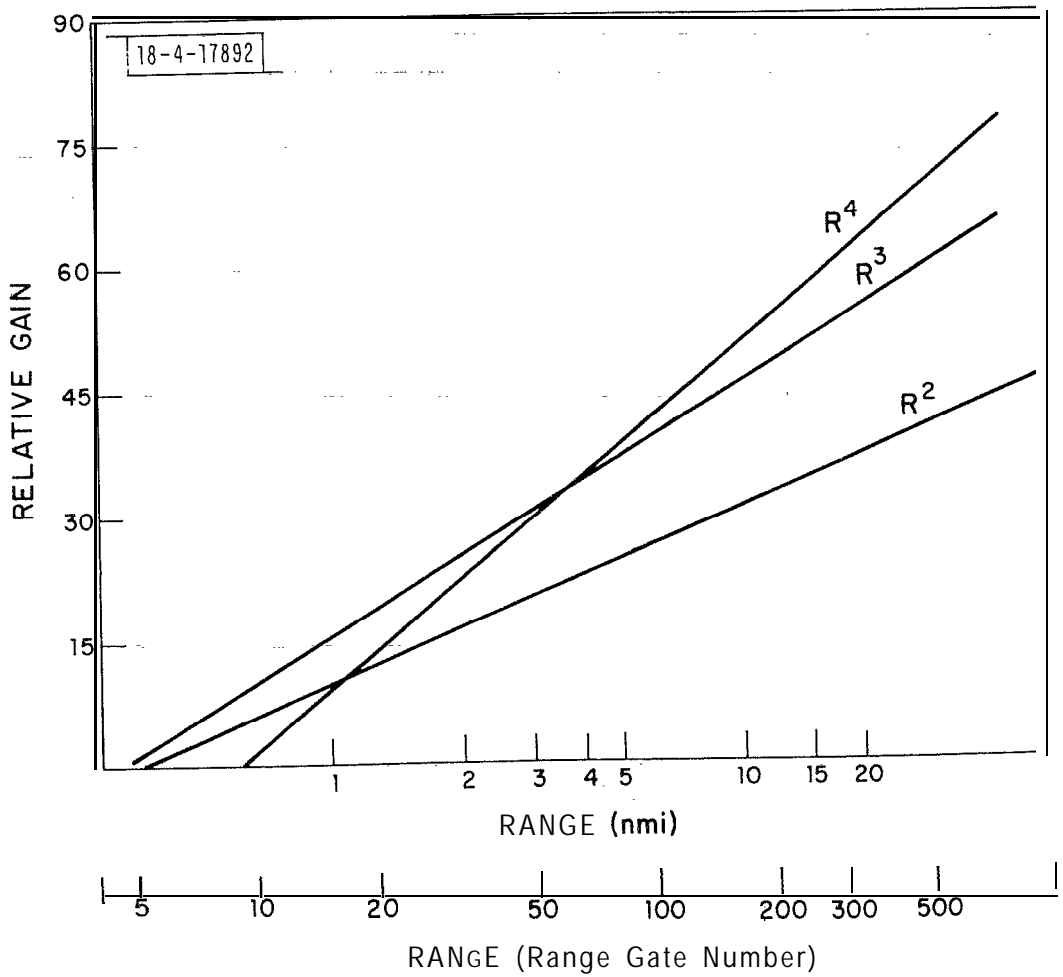
Fig. B-2. Relative gain of STC vs. range.

RADAR PARAMETERS

Gain (on horizon)	31 dB
Loss (one-way)	2 dB
Peak Power	+88.2 dBm
Noise Power	-98.9 dBm

TABLE B-2

σ Values for R^{-4} STC Curve, Initial Value 60 dB (using Equation 1)

Letter	(C/N) dB	σ (dBsm)
G	5 ± 3	-8
H	11 ± 3	-2
I	17 ± 3	$+4$
J	23 ± 3	$+10$
K	29 ± 3	$+16$
L	35 ± 3	$+22$
M	41 ± 3	$+28$

TABLE B-3

σ_o Values for R^{-3} STC Curve, Initial Attenuation 63 dB

Letter	(C/N) dB	σ (dB)$_o$
G	5 ± 3	-48
H	11 "	-42
I	17 "	-36
J	23 "	-30
K	29 I'	-24
L	35 "	-18
M	41 "	-12

There is another uncertainty related to the digital STC curve. Since the STC attenuation varies in 1-1/2 dB steps, there can be a range dependent error of as much as 1-1/2 dB. This error tends to make the clutter returns come in stronger than they would with a continuous STC curve. In addition, there are errors due to-variation in the noise and DC bias levels at the A/D converter inputs.

The clutter values measured this way are estimated to be accurate to within $^{+5}_{-7}$ dB of the indicated value.

The clutter map output was recorded on paper tape at NAFEC and processed into high resolution map outputs from the system.   Figures B-3 through B-6 present these results.   Further, Figure B-7 presents the output of the clutter map as seen on a PPI format display.

Fig. B-3. Range vs. azimuth plot of σ_o at NAFEC site.

Fig. B-4. Range vs. azimuth plot of σ_o (6 dB steps) measured at NAFEC.

Fig. B-5.   Range vs. azimuth plot of σ at NAFEC site.

Fig. B-6. Range vs. azimuth plot of σ at NAFEC site.

FIVE MILE
RANGE RINGS

AREA USED FOR
GROUND CLUTTER
FLIGHT TESTS

Fig. B-7. Ground clutter at NAFEC.

188

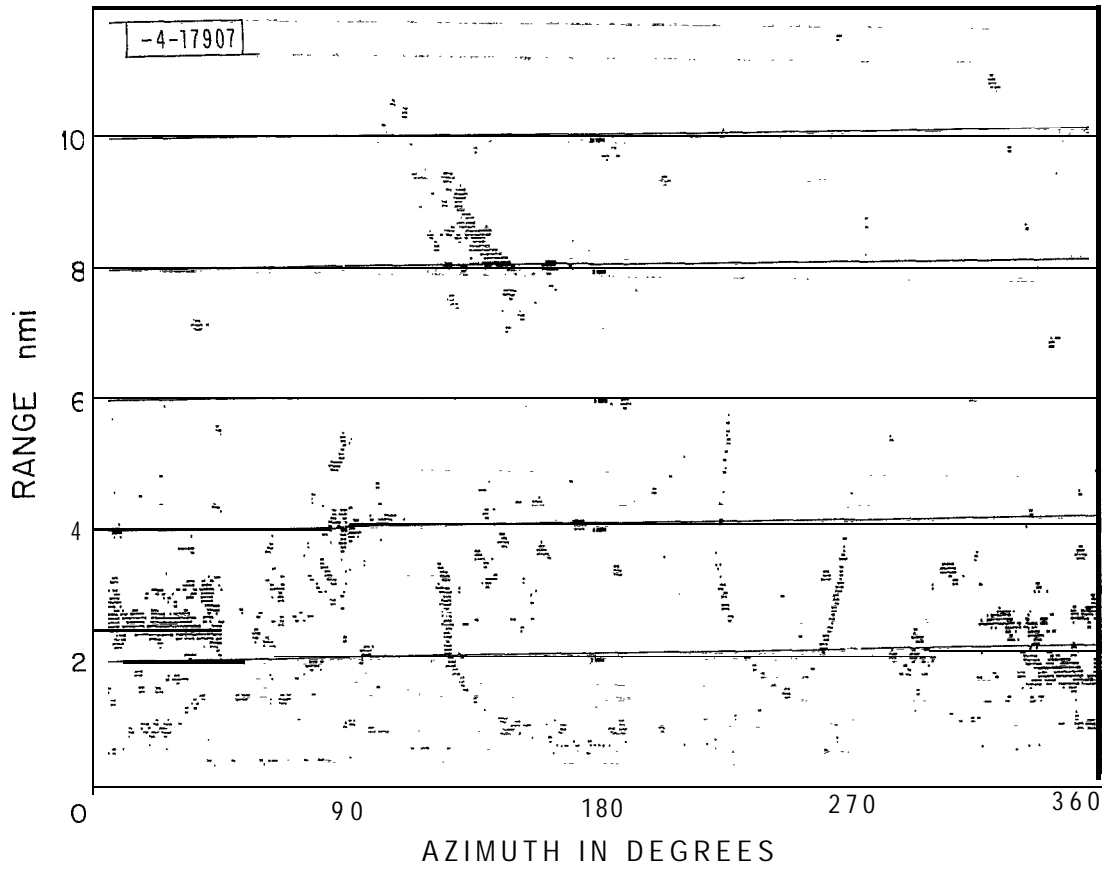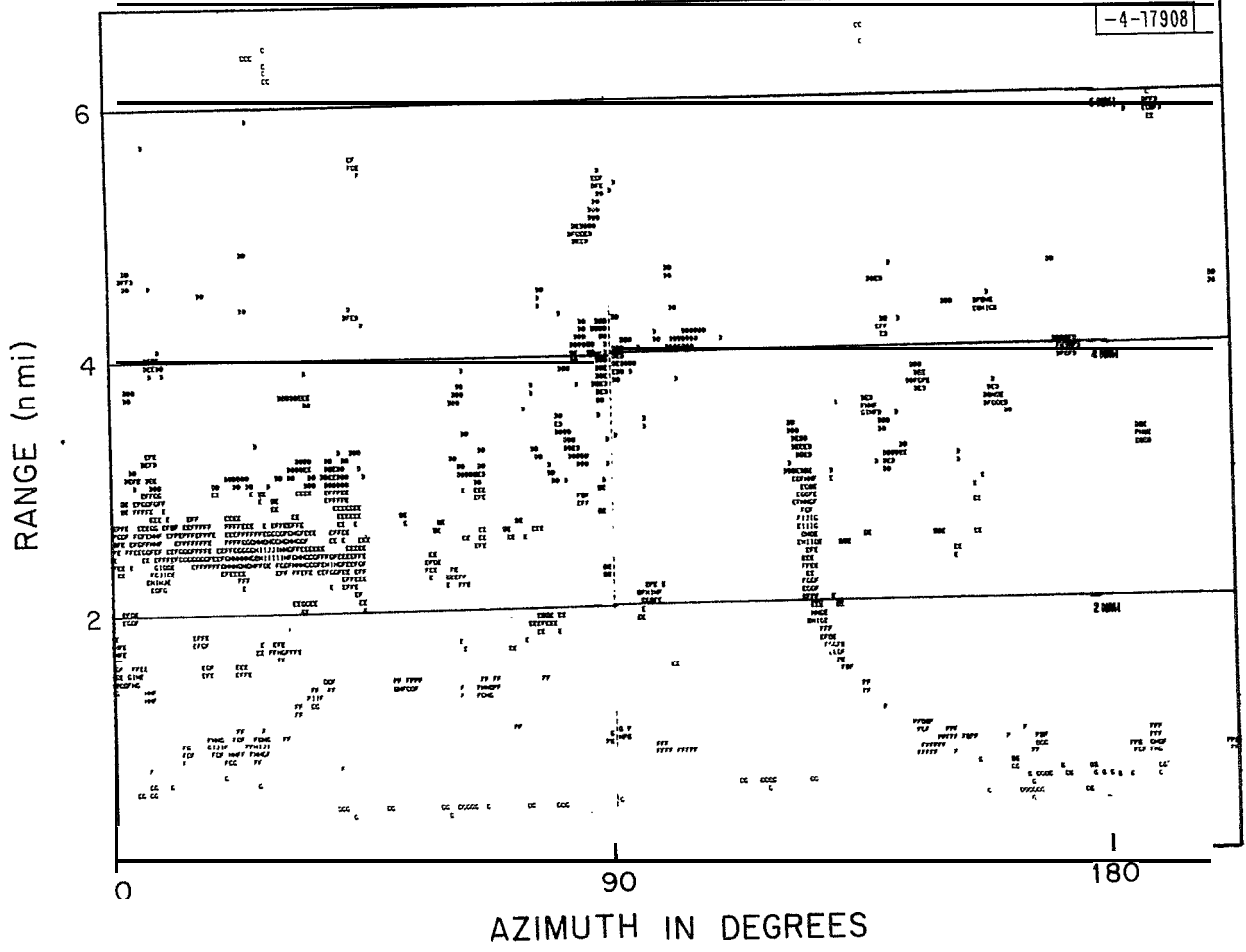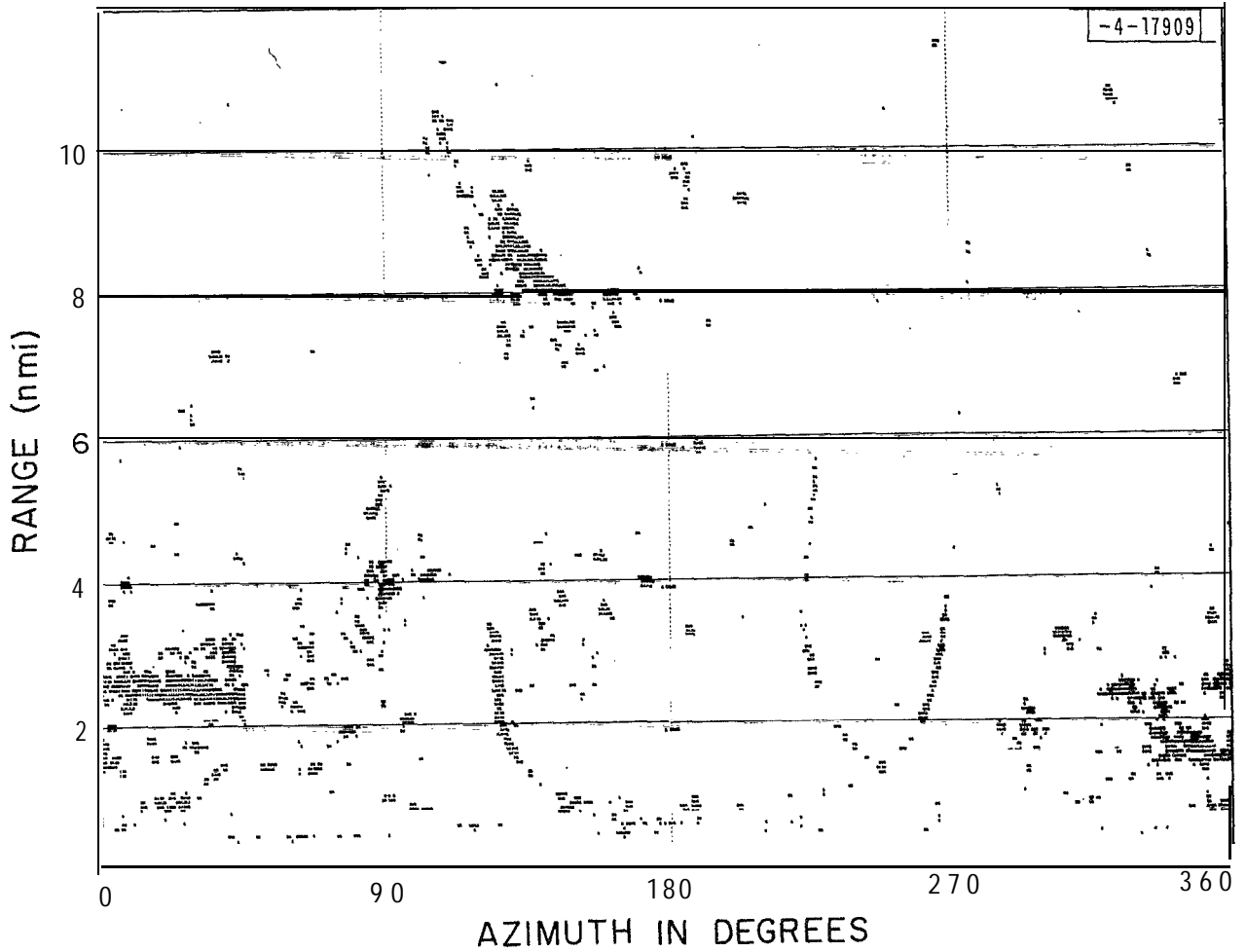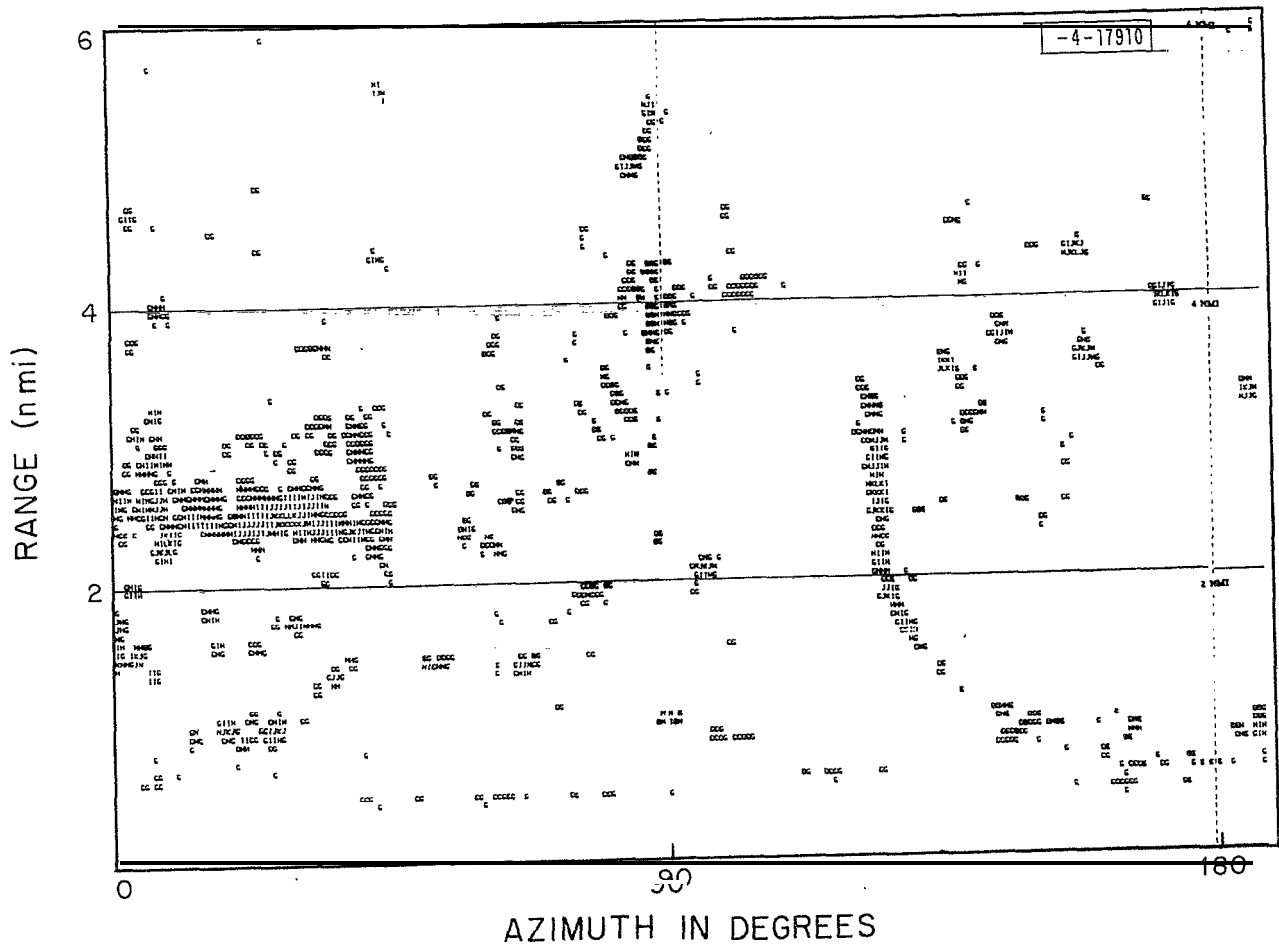# APPENDIX C

THEORETICAL ANALYSIS OF THE FALSE ALARM PERFORMANCE
OF THE MTD IN GAUSSIAN NOISE

1. INTRODUCTION

The effects of quantization on the false alarm rate of the MTD (Moving Target Detector) processor have been calculated. A combination of analytical and numerical techniques were used in the calculation. Simulation or Monte Carlo techniques were not used because the probabilities of false alarm to be calculated were between 10^{-3} and 10^{-6}. Thus, between 108 and 10^{14} trials would have been necessary to measure the probability of false alarm to about 10%. Processing this number of trial events through a simulated MTD would have been extremely costly and time consuming even -considering the size and cost of time on the Laboratory's large, general-purpose computer, an IBM 370 model 168.

The probability of false alarm as a function of RMS noise voltage, filter number, and threshold setting has been calculated. As expected, for RMS noise voltage much greater than 1 A/D least count, the probability of false alarm is constant and independent of both filter number and RMS noise voltage. Also, as the RMS noise voltage approaches 1 A/D least count, the probability of false alarm increases significantly and is not independent of filter number.

The calculation consists of taking Gaussian distributions of known RMS noise voltage, sampling them in the A/D converters, and then propagating them through the MTD using digital convolution techniques. The probability distribution of the noise output from the magnituder (see Figure V-l) is compared with a multiple of the probability distribution of the sum of thirteen samples of the magnitude distribution. This is a type of mean-level thresholding. The resulting P_{fa}, the probability of false alarm per range azimuth doppler cell as a function of RMS noise level, doppler filter number, and threshdlding constant is calculated. The P_{fa} is then related to the false alarm rate predicted for the MTD.

INCREASING RANGE ➡
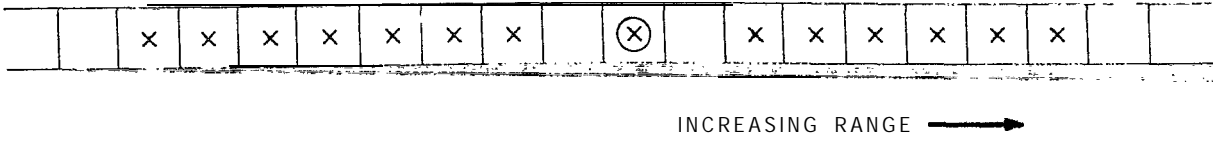
◯   DENOTES CELL TO BE THRESHOLDED

X   DENOTES CELLS SAMPLED TO DETERMINE THRESHOLD ON CELL MARKED ◯

Fig. C-1.   Range cells used in main level thresholding.

2. DETAILS OF ANALYSIS

A. A/D Converters

It is assumed that the noise input to the MTD is white Gaussian noise whose bandwidth is sufficiently broad so that the samples taken at the 2.6 MHz rate will be independent. The noise before the A/D converter has a probability density given by

$$p(v) \, dv = \frac{1}{\sqrt{2\pi}\sigma} \, e^{-\frac{v^2}{2\sigma^2}} \, dv \qquad (1)$$

where: v = noise voltage

σ = RMS noise voltage

$p(v) \, dv$ = probability that the voltage has a value between v and $v+dv$.

The effect of the A/D converters is to transform a continuous voltage distribution into a discrete probability distribution, $f(n)$, which is a sequence, where

$$f(n) = \int_{n-1/2}^{n+1/2} p(v) \, dv = \int_{n-1/2}^{\infty} p(v) \, dv + \int_{n+1/2}^{-\infty} p(v) \, dv \qquad (2)$$

If we define a new variable

$$u^2 = \frac{v^2}{2\sigma^2} \qquad (3)$$

and note that the complementary error function $\text{erfc}(x)$ is given by

$$\text{erfc}(x) = \frac{2}{\sqrt{\pi}} \int_x^{\infty} e^{-u^2} \, du \qquad (4)$$

191

then we observe that equation (2) becomes

$$f(n) = 1/2 \left\{ \text{erfc} \left(\frac{n - 1/2}{\sqrt{2}\sigma}\right) \quad \text{erfc} \left(\frac{n + 1/2}{\sqrt{2}\sigma}\right) \right\} \tag{5}$$

where: $f(n)$ = probability density of the discrete voltage n [*]

n   = noise voltage (discrete quantity)

σ = RMS noise voltage.

B.   Adders

Before the near optimum linear filter (e) (see Figure V-1) there are two adders for summing two adjacent samples of voltage in both the I and Q channel. The probability distribution of a sum of independent random variables may be obtained by convolving the probability distributions of the individual random variables.   The convolution of two Gaussian random variables of equal standard deviation is given by

$$p(N) = \int_{-\infty}^{\infty} \frac{1}{\sqrt{2\pi}\,\sigma} e^{-x^2/2\,\sigma^2} \frac{1}{\sqrt{2\pi}\,\sigma} e^{-(N-x)^2/2\,\sigma^2} dx \tag{6}$$

Combining terms in the exponents, completing the square in the exponents and integrating we get

$$p(N) = \frac{1}{2\sqrt{\pi}\sigma} e^{-N^2/4\,\sigma^2} \tag{7}$$

which is a Gaussian distribution whose standard deviation σ_s (RMS voltage) is given by

$$\sigma_s = \sqrt{2}\sigma \tag{8}$$

where σ_s = RMS noise value of sum of two independent samples

σ = RMS noise value of individual samples before A/D converters (value where measured)

The effect of the adders is accounted for by altering by a factor of $\sqrt{2}$ the value of RMS noise input to the A/D converters.

---

[*] n = 1 is one least count in the A/D converters and set equal to 2 mv for the MTD system.

C. Near Optimum Linear Filter

1. Introduction

In the near optimum linear filter of the MTD (see Figure V-1) 10 complex samples are processed through a near optimum linear filter which consists of a three-pulse MTI canceller, followed by an 8-point FFT, and finally by weighting in the frequency domain.

Let $\tilde{a}_1$, $\tilde{a}_2$ . . . $\tilde{a}_{10}$ * be the complex samples input at-this stage. Then for the ith sample the output of the 3-pulse MTI canceller is given by

$$\tilde{b}_i = \tilde{a}_i - 2\,\tilde{a}_{i+1} + \tilde{a}_{i+2} \qquad\qquad 1 \leq i \leq 8$$

The output of the 8-point Fast Fourier Transform (FFT) is given by

$$\tilde{c}_m = \sum_{n=0}^{7} \tilde{b}_{n+1}\, e^{-j\frac{2\pi mn}{8}} \qquad 0 \leq m \leq 7 \qquad\qquad (10)$$

Finally, the output of the weighting is related to its input by

$$\tilde{d}_p = 1/4\,\tilde{c}_{p-1} + \tilde{c}_p - 1/4\,\tilde{c}_{p+1} \qquad 0 \leq p \leq 7 \qquad (11)$$

where $\tilde{c}_8 \equiv \tilde{c}_o$

thus combining Eq. (9), (10) and (11)

$$\tilde{d}_m = \sum_{m=0}^{7} \left\{_{n+1} - 2a_{n+2} + a_{n+3}\right\} \left\{ -1/4\, e^{-j\frac{\pi}{4}n(m-1)} + e^{-j\frac{\pi}{4}nm} - 1/4\, e^{-j\frac{\pi}{4}n(m+1)} \right\}$$

$$(12)$$

---

*Symbols with the cap "$\sim$" such as $\tilde{a}$, $\tilde{b}$, $\tilde{c}$ denote complex quantities whereas those without the cap denote real quantities.

Equation (12) may be cast into a simpler form

$$\tilde{d}_m = \sum_{n=1}^{10} \tilde{f}_n (m) \; \tilde{a}_n \tag{13}$$

This just states that the filter output is a linear function of the 10 complex samples $\tilde{a}_n$.

If we define $\tilde{G}(m, n)$

$$\tilde{G}(m, n) = -\; 1/4 \; e^{-j \frac{\pi}{4} n(m-1)} + e^{-j \frac{\pi}{4} mn} \; 1/4 \; e^{-j \frac{\pi}{4} n(m+1)} \tag{14}$$

then Eq. (12) becomes

$$\tilde{d}_m = \sum_{n=0}^{7} \left[\tilde{a}_{n+1} - 2 \, a_{n+2} + a_{n+3} \right] G(m, n) \tag{15}$$

and by inspection we see that $\tilde{f}_n(m)$, the complex coefficients of Eq. (13), become

$$\tilde{f}_1 (m) = \tilde{G}(m, 0) \tag{16}$$

$$\tilde{f}_2 (m) = -2 \, \tilde{G}(m, 0) + \tilde{G}(m, 1) \tag{17}$$

$$\tilde{f}_n (m) = \tilde{G}(m, n-3) - 2 \, \tilde{G}(m, n-2) + \tilde{G}(m, n-1) \qquad \text{for } 3 \leq n \leq 8 \tag{18}$$

$$\tilde{f}_9 (m) = \tilde{G}(m, 6) - 2 \, \tilde{G}(m, 7) \tag{19}$$

$$\tilde{f}_{10} (m) = \tilde{G}(m, 7) \tag{20}$$

Equation (13) may be rewritten

$$\hat{d}_m = \sum_{n=1}^{20} g_n(m) \, e_n + j \sum_{n=1}^{20} h_n(m) \, e_n \qquad (21)$$

where $g_n(m) = f_n^R(m)$ $\qquad\qquad$ $1 \leq n \leq 10$

$\qquad\qquad = -f_{n-10}^I(m)$ $\qquad\qquad$ $11 \leq n < 20$ $\qquad\qquad\qquad$ (22)

$h_n(m) = f_n^I(m)$ $\qquad\qquad$ $1 \leq n \leq 10$

$\qquad = f_{n-10}^R(m)$ $\qquad\qquad$ $11 \leq n \leq 20$ $\qquad\qquad\qquad$ (23)

$e_n = a_n^R$ $\qquad\qquad$ $1 \leq n \leq 10$

$\qquad = a_{n-10}^I$ $\qquad\qquad$ $11 \leq n \leq 20$ $\qquad\qquad\qquad$ (24)

and $f_n^R(m) = Re \; \{ f_n(m) \}$

$f_n^I(m) = Im \; \{ f_n(m) \}$

$a_n^R = Re \; \{ a_n \}$

$a_n^L = Im \; \{ a_n \}$ $\qquad\qquad\qquad\qquad\qquad\qquad\qquad\qquad$ (25)

Equation (21) shows the relationship between the output of the near-optimum filter and its input. $g,(m)$ and $h_n(m)$ are the coefficients which the input voltages are multiplied by to obtain the output voltage.

2. Analytical Technique

It is the purpose of this section to show how the discrete probability density of the voltage at the output of the near optimum linear filter may be obtained from the input discrete probability densities and the filter coefficients.

This will be done taking into account the specific truncation techniques of the MTD filter.

Because the I and Q channels are assumed symmetric in every respect and by inspection of equations (21) through (25) we note that the probability density of the real part of the filters output is equal to the probability density of the imaginary part of the filters output. This is due to the symmetry of the input discrete probability densities, in this case, sampled symmetric Gaussian distributions. Thus, it will suffice to calculate only one of the channel's output densities. Also, if a random variable is a sum of M independent random variables, then the probability distribution of the sum is the linear convolution of the probability distributions of the M random variables. For discrete systems the linear convolution may be done using-discrete Fourier transform (DFT) techniques, since the probability density, either real or imaginary part, is a linear combination of random variables which are sampled Gaussians of-known RMS voltage. That is

$$d_m{}^R = d_m{}^I = \sum_{n=1}^{20} g_n(m) \; e_n \qquad 0 \le m \le 7 \qquad (26)$$

This may be rewritten

$$d_m{}^R = d_m{}^I = \sum_{n=1}^{20} r_n(m) \qquad 0 \le m \le 7 \qquad (27)$$

where $d_m{}^R$ = real part of the voltage output of the mth filter

$d_m{}^I$ = imaginary part of the voltage output of the mth filter

$r_n(m) \equiv g_n(m) \; e_n$

Thus, it has been shown that the filter output is the sum of 20 voltages, and the probability density of-the mth filter output is the convolution of the.'20 discrete probability densities of the discrete random variables $r,(m) \equiv g,(m) \; e_n$.

3. Linear Convolution Using the Discrete Fourier Transform*

The linear convolution of two or more sequences may be efficiently calculated by computing their discrete Fourier transforms, multiplying them and then computing the inverse discrete Fourier transform. There exists a highly efficient algorithm for computing the discrete Fourier transform. This algorithm is called the fast Fourier transform algorithm. The multiplication of discrete Fourier transforms followed by an inverse discrete Fourier transform corresponds to a circular convolution of the sequences. Since we are interested in obtaining a linear convolution, we must insure&hat the circular convolution has the effect of a linear convolution.

As an example, let us first consider two N point sequences, $f_1(n)$ and $f_2(n)$, and let $f_3(n)$ denote their linear convolution; i.e.,

$$f_3(n) = \sum_{m=0}^{N-1} f_1(m)\, f_2(n-m) \tag{28}$$

It is straightforward to verify that $f_3(n)$ is of length $2N-1$, that is, it can have at most $2N-1$ non-zero points. If it is obtained by multiplying the discrete Fourier transforms of $f_1(n)$ and $f_2(n)$, then each of these discrete Fourier transforms, $F_1(k)$ and $F_2(k)$, must also have been computed on the basis- of $2N-1$ points. Thus, if we define

$$F_1(k) = \sum_{n=0}^{2N-2} f_1(n)\, W^{-nk} \tag{29}$$

$$F_2(k) = \sum_{n=0}^{2N-2} f_2(n)\, W^{-nk} \tag{30}$$

$$f_3(n) = \frac{1}{(2N-1)} \sum_{k=0}^{2N-2} F_1(k)\, F_2(k)\, W^{nk} \tag{31}$$

with

$$W = e^{j2\pi/(2N-1)} \tag{32}$$

*See Reference 23

Then $f_3(n)$ will be the linear convolution of $f_1(n)$ and $f_2(n)$. A linear convolution would also be achieved if the discrete Fourier transform were computed on the basis of more than 2N-1 points, but would not be achieved if the DFT were computed on the basis of fewer points.

In general, we may wish to convolve two or more sequences of unequal lengths. If $f_1(n)$ has a duration N_1 and $f_2(n)$ has a duration N_2, then their convolution will have length $N_1 + N_2 - 1$. Thus, we need to compute discrete Fourier transforms based on $N \geq N_1 + N_2 - 1$.

Finally, if we wish to convolve M sequences $f_1(n), f_2(n), f_3(n) . . . f_M(n)$, each of length N and each representing a discrete probability density, then their convolution should have length at least NM-1 in order that the convolution be linear and not circular. Thus, we will need to compute the discrete Fourier transforms of P point sequences where P = NM-1.

D. Magnituding

The algorithm used to calculate the magnitude of the I and Q channel voltages is

$$\sqrt{I^2 + Q^2} \quad \text{larger} \left\{ |L| \quad \text{and} \quad 7/8 \ |L| + 1/2 \ |S| \right\} \tag{34}$$

where $|L|$ = larger of $|I|$ and $|Q|$ voltages and

$|S|$ = smaller of $|I|$ and $|Q|$ voltages.

Since this transformation is non-linear, care must be taken in generating the discrete probability density of the magnitude of the voltage out of the mth filter from the probability densities of the voltage from the I and Q channels.

If D(m) is the discrete probability density of the magnitude of the voltage out of the magnituding algorithm for the mth filter, then

$$D_m(p) = \sum_{k=M}^{M} \sum_{R=-M}^{M} d_m^R(k) \ d_m^R(\ell) \tag{35}$$

where k and ℓ are constrained to run only over those values for which

$$p = \text{larger} \left\{ |L| \quad \text{and} \quad 7/8 \ |L| + 1/2 \ |S| \right\} \tag{36}$$

where $|L|$ = larger of $|k|$ and $|\ell|$ and

$|S|$ = smaller of $|k|$ and $|\ell|$.

$d_M^R(k)$ and $d_M^R(\ell)$ are given by equation (12)

E.   Thresholding

Thresholding is done adaptively using a mean-levelthresholding scheme for each range-azimuth-doppler cell. The mean level is measured each scan by sampling 14 Voltage samples. It should be noted that the 14 voltage samples do include the cell to be thresholded; do not include the directly adjacent range cells and do include six range cells on one side and seven range cells on the other side of the cell of interest (see Figure C-l). It is not analytically feasible to calculate directly the propagation of the noise probability distributions through a mean-level thresholding scheme which includes cells to be thresholded, but the probability distribution of a scheme which does include the cell to be thresholded may be related to a similar scheme which does not. A derivation of this relationship is given in the next section. It will be shown in the next section that 13 independent cells should be averaged in the calculation.

In the calculation thresholding is accomplished by taking the sum of 13 samples, multiplying by-one of eight constants, ac, dividing the voltage by 4 and then comparing this voltage with the voltage out of the magnituder. If the voltage out of the magnituder is equal or larger, then a threshold crossing is declared. The multiplicative constant a_c is variable and can take on values of 1, 1 1/8, 1 1/4, 1 3/8, 1 1/2, 1 5/8, 1 3/4 and 1 7/8. These constants determine the value of probability of false alarm for the system. For these values, for high RMS noise, the P_{FA} will fall between approximately 10^{-4} and 10^{-9}".

The probability distribution of the sum of 13 samples of independent noise samples is just the 13-fold convolution of the magnitude distribution $D_m(p)$. This probability distribution of the sum is obtained by taking the discrete Fourier transform of the sequence $D_m(p)$, raising each of the elements of the resulting distribution to the 13th power and then taking the inverse DFT. The DFT's are all done using the FFT algorithm. Thus, if the discrete probability density for the sum of 13 independent samples of $D_m(p)$ is defined as $E_m(p)$, then

$$E_m(p) = DFT^{-1} \left(DFT \ (D_m(p)) \right)^{13} \tag{37}$$

---

*See Reference 26

Thus, we see that the probability of false alarm for the mth doppler cell is given by

$$P_{FA}(m) = \sum_{k=0}^{M'} \sum_{\ell=0}^{M'} D_m(k) \, E_m\left(\frac{a_R \ell}{4}\right) \tag{38}$$

subject to the condition that $\underline{k} \geq \dfrac{a_R \ell}{4}$,

where $D,(h)$ and $E_m(\ell)$ have been defined previously

$$a_R = \frac{4\,a_C}{4 - a_C} \tag{39}$$

a_C is the thresholding constant between 1 and 1 7/8

a_R is used instead of a_C to account for the fact that the cell to be thresholded is being sampled-, as will be shown in the next section.

F.   Relationship Between Mean-Level Thresholds Which Do and Do Not Include the Thresholded Cell

If the thresholded cell is not a member of the sample used to estimate the threshold, then the thresholding criteria is

$$|Y| \geq \frac{a_C}{4} \sum_{i=1}^{N} |y_i| \tag{40}$$

where: $|Y|$ = sample from cell to be thresholded

$|y_i|$ = sample from i^{th} cell not including the cell to be thresholded.

a_C = threshold constant used in the calculation

N = number of cells used to estimate the threshold

But, if the thresholded cell is a member of the sample used to measure the threshold, then the thresholding criteria is

$$|Y| \geq \frac{a_R}{4} \left\{ \sum_{i=1}^{N-1} |y_i| + |Y| \right\} \tag{41}$$

where a_R is the thresholding constant for the experimental MTD case.

Combining Equations (40) and (41) for $N = 14$, we can relate the two thresholding constants used in the experimental MTD, a_R, and in the calculation, a_C.

Thus,

$$a_C = \frac{4\,a_R}{4 - a_R} \tag{42}$$

The values of a_C for the values of a_R used in the MTD are tabulated below

a_C	a_R
1.333	1
1.565	1 1/8
1.818 ..	1 1/4
2.40	1 1/2
2.737	1 5/8
3.111	1 3/4
3.515	1 7/8

3. NUMERICAL TECHNIQUES

A. Computer Program

A Fortran computer program has been written to implement the analytical
approach set forth in Section II.   A separate computer program was used to compute
the filter coefficients given in Equations (24) and (25).   These coefficients form
'five matrices of real numbers whose dimension is 20 by 5.   The 20 corresponds to
the 10 complex samples processed, each of which has a real and imaginary part.
The 5 corresponds to the number of unique filter outputs.   The coefficients for
the 1 and 7, 2 and 6, and 3 and 5 filters are the same.   Five integer numbers are .
needed to describe each of the coefficients because each coefficient is of the
form

$$F(I, J) = A(I, J) + \frac{B(I, J)}{\sqrt{2}} + 1/4 \ C(I,J) + \left\{ D(I,J) + \frac{E(I,J)}{\sqrt{2}} \right\}$$ (43)

where A, B, C, D and E are dimensioned 10 by 5.

Since a special algorithm was used in the MTD for multiplying by $\frac{1}{\sqrt{2}}$
this algorithm was coded in Fortran and was used to generate the probability
distributions of r,(m) in Equation (22).

B. Numerical Errors

The analog Gaussian voltage probability distribution at the input of A/D
converters extends over an infinite range of voltage, $-\infty < v < \infty$.   An exact de-
scription of the discrete probability density obtained by sampling-the Gaussian

distribution would require an infinite length sequence. At some point, the Gaussian sequence must be truncated. The lenght of the input sequence was set such that the sum of the members of the sequence

$$\sum_{n=-M}^{M} f(n) = 1 - \varepsilon \qquad (44)$$

where ε is the input error. The sequence $f(n)$ was truncated when ε was less than 10^{-7}.

Throughout the computer program errors occur caused by round-off in doing the DFT's and inverse DFT's. The DFT's and inverse DFT's were implemented using the fast Fourier transform algorithm. These programs were written in double precision (64-bits) and they introduced an error in the result of about 10^{-16}.

The final error in the calculation was found by adding up the members of the final probability densities given by Equations (35) and (37). The input truncation error was adjusted so that the error in calculation of P_{FA} was always less than 10%.

C. Computational Results

The computer program to calculate P_{FA} was run for values of RMS noise voltage between 0.5 and 20 mV (1/4 and 10 least counts in the A/D converters), for the four unique filters 1 through 4 and for the threshold settings of 1 through 1 7/8.

In the MTD it is convenient to measure the false alarm time; that is the time required to get 100 false alarms. The probability of false alarm for each filter is related to the false alarm time by

$$FAT = \frac{1.29 \times 10^{-3}}{P_{FA}} \qquad (45)$$

where FAT is the time in seconds to get 100 false alarms from one filter and P_{FA} is the probability of false alarm for that filter.

The calculated curves of false alarm time vs RMS noise voltage and filter number are plotted for threshold settings of 1, 1 1/8 and 1 1/4 in Figures C-2, C-3 and C-4.
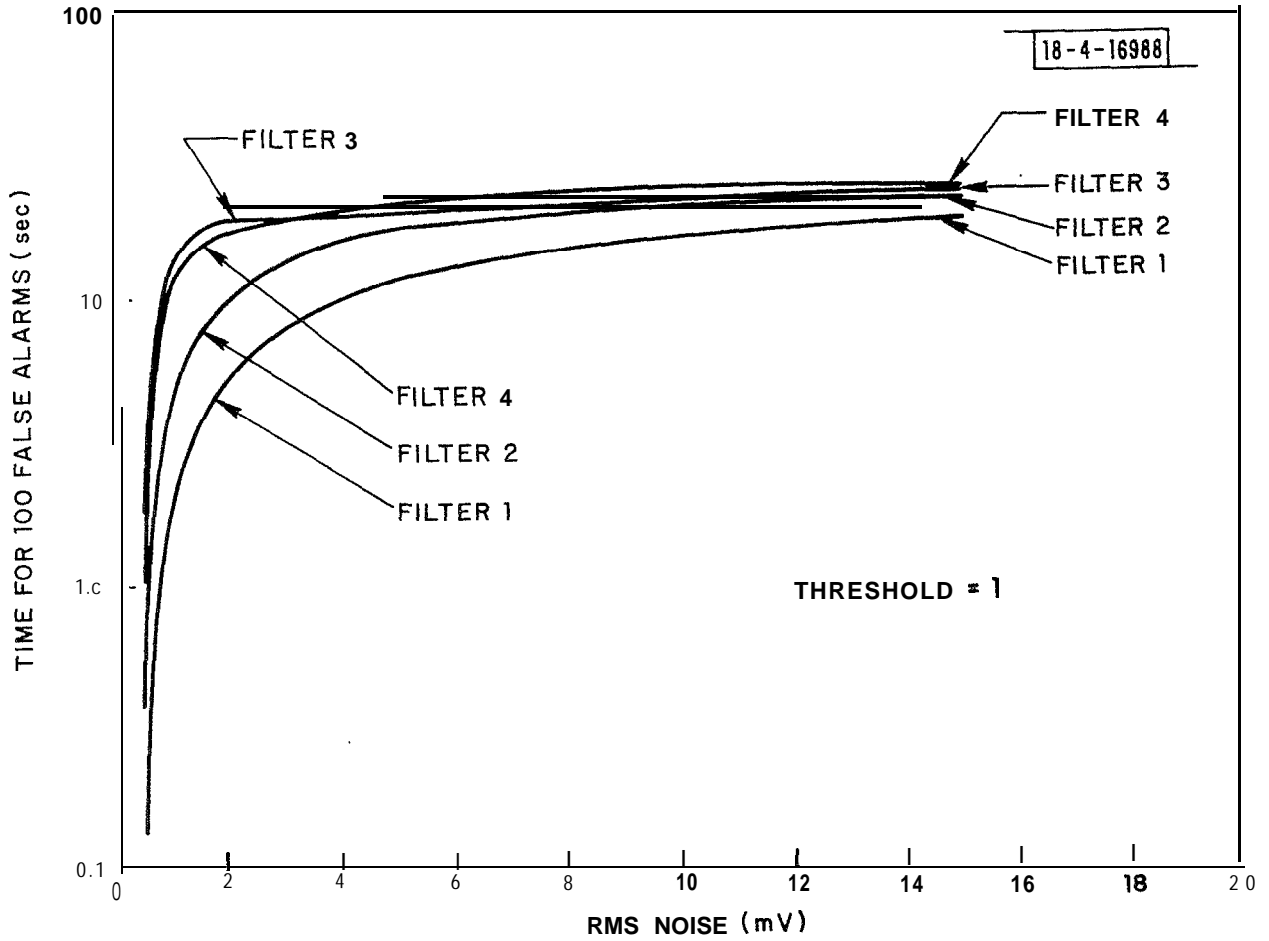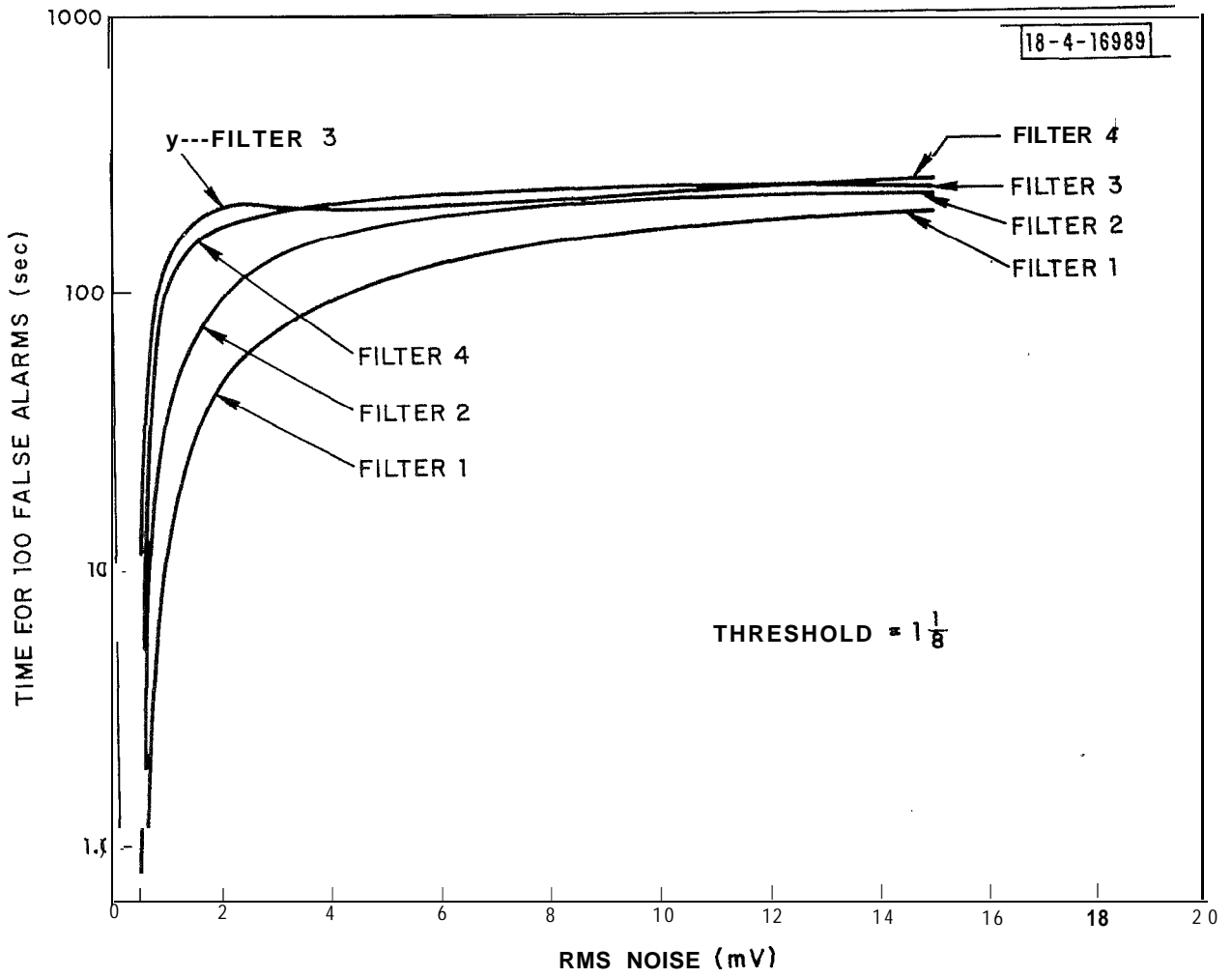
Fig. C-Z. False alarm time vs. rms noise voltage: threshold = 1.

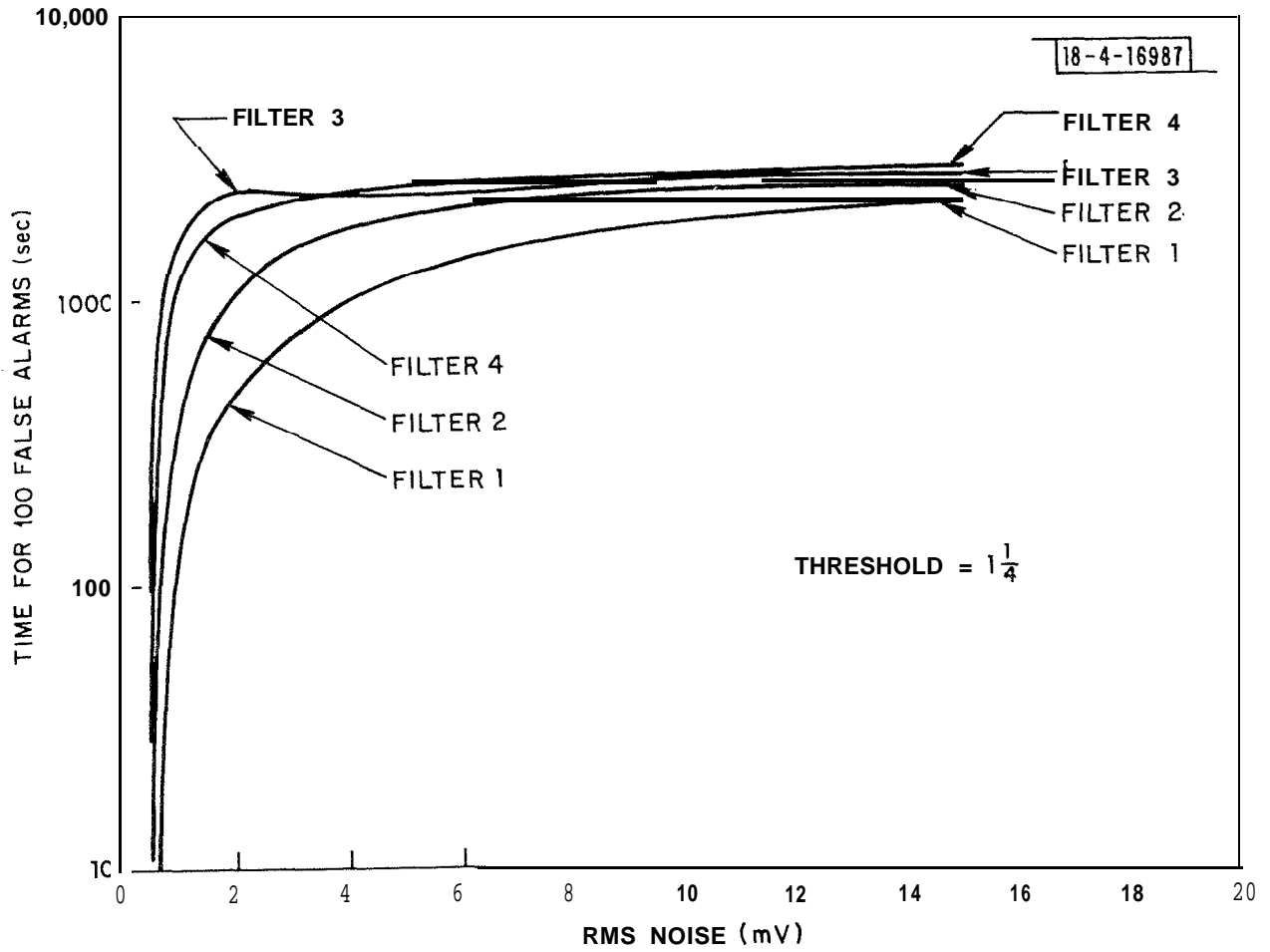Fig; C-3.   False alarm time vs. rms noise voltage: threshold = 1 1/8.

Fig. C-4.   False alarm time vs. rms noise voltage: threshold = 1 1/4.

4. NEW TECHNIQUES FOR ELIMINATION OF THE EFFECTS OF TRUNCATION

The present MTD has quantization effects which are caused by both the A/D converters and truncations within the MTD processor. A study was made to separate the effects caused by these two sources. In order to eliminate the effect of truncation so that only A/D converter effects would cause P_{FA} degradation at low RMS noise; the analysis program was modified in the following manner:

1. The weighting section of the near optimum linear filter was eliminated for simplicity,

2. The multiplies by $1/\sqrt{2}$, which yield truncation errors, were approximated by 3/4. That is, coefficients of the form $a + \dfrac{b}{\sqrt{2}}$ were approximated by 4a + 3b. This necessitated adding two more bits in the 8-point FFT, but at the gain of dynamic range of the processor.

3. Thirteen cells were sampled to calculate the mean voltage and the sampled cells did not include the cell of interest.

With these changes the analysis program was run with no truncation and with the $1/\sqrt{2}$ multiply approximated by

$$\frac{N}{\sqrt{2}} = N \left(\frac{1}{2} + \frac{1}{8} + \frac{1}{16} + \frac{1}{64} + \frac{1}{256} \right) \tag{46}$$

as done in the MTD. The results of these calculations are presented in Figures C-5 and C-6 for filters 1 and 4 at a threshold setting of 1 1/4. In Figure C-5 we see that as much as a 10-dB increase in dynamic range may be added to the processor by adding bits in the processor to avoid truncation effects of the $1/\sqrt{2}$ multiply.
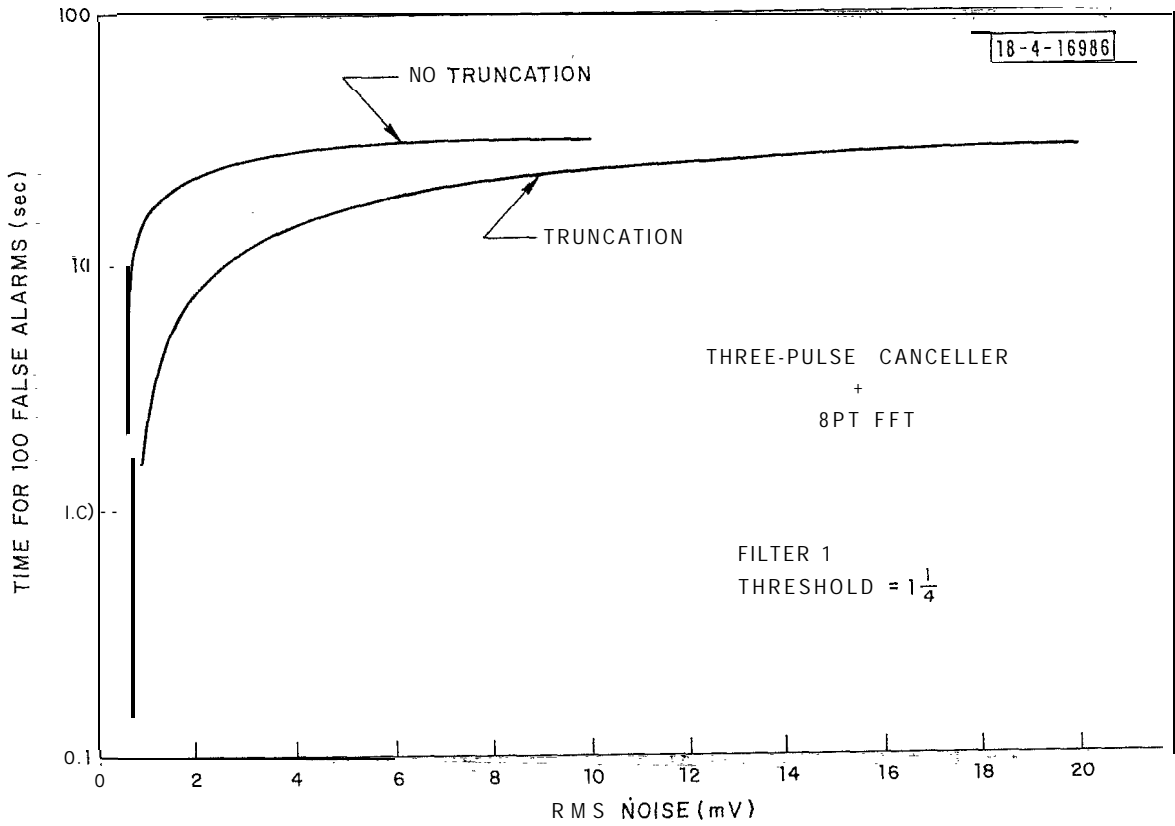
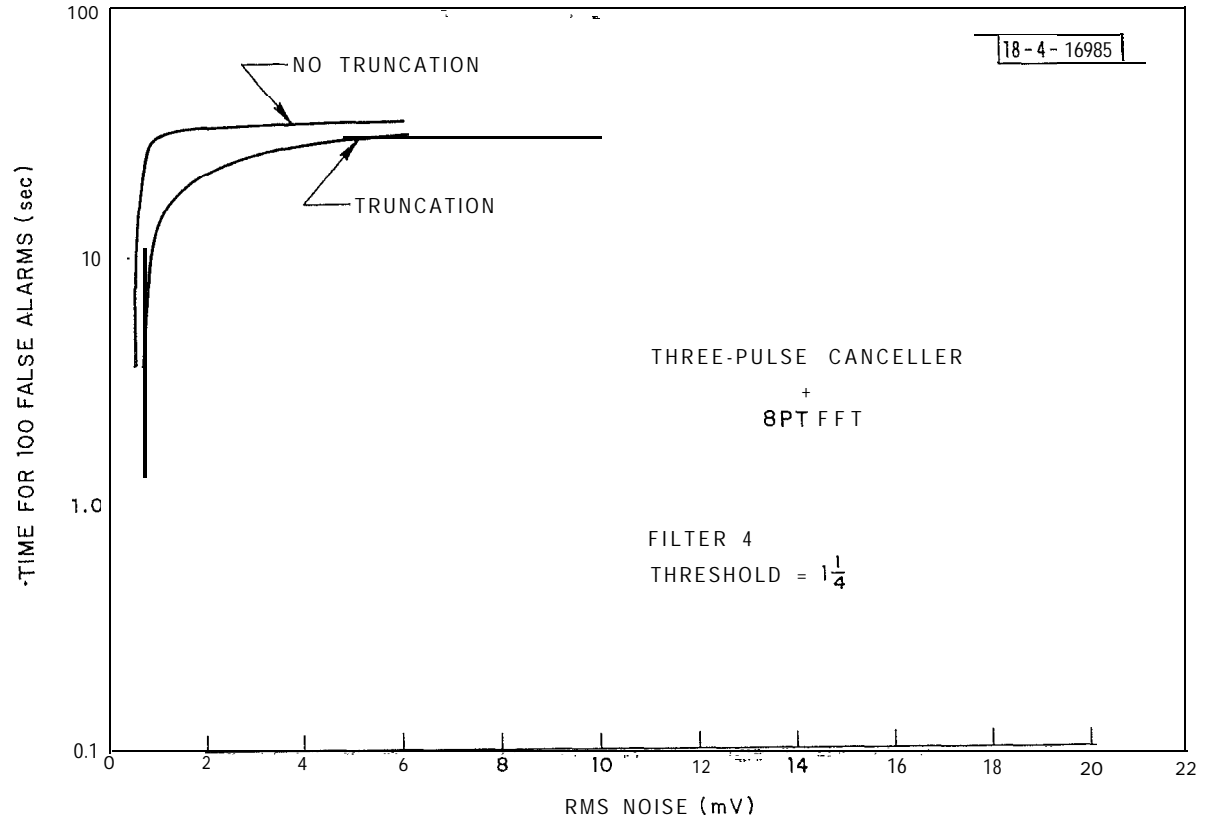Fig. C-5. False alarm time vs. rms noise voltage: filter 1, threshold = 1 1/4.

Fig. C-b.   False alarm time vs. rms noise voltage: filter 4, threshold = 1 1/4.

208

ACKNOWLEDGEMENTS

REFERENCES

1. C. E. Muehe, et al., "New Techniques Applied to Air Traffic Control Radars," Proc. IEEE, Vol. 62, No. 6, pp 716-723 (June 1974).

2. C. E. Muehe, "Digital Signal Processor for Air Traffic Control Radars," NEREM 1974, Boston, Mass. (29-31 October 1974).

3. R. M. O'Donnell, et al., "Advanced Signal Processing for Airport Surveillance Radars," EASCON 1974, Washington, D.C. (October 1974).

4. F. E. Nathanson, Radar Design Principles (McGraw-Hill, 1969).

5. "A Brief Description of the Solid-State ASR-7 Airport Surveillance Radar," Texas Instruments, Inc., (May 1970).

6. J. Croney, "Clutter on Radar Displays, Reduction by Use of Logarithmic Receivers," Wireless Eng., pp 83-96 (April 1956).

7. E. Eastwood, Radar Ornithology (Methuen & Co., London, England, 1967).

8. G. Pollon, "Distribution of Radar Angels," IEEE AES, Vol. AES-8, No. 6 (November 1972).

9. R. E. Richardson, et al., "Elimination of a Type of Natural Clutter in L-band Radars," Technical Report 178, Lincoln Laboratory; M.I.T. (15 April 1958), AD133851.

10. J. R. Barry, et al., "Angel Clutter and the ASR Air Traffic Control Radar," Applied Physics Laboratory, Johns Hopkins University '(Feb. 1973), FAA-RD-73-158.

11. D. F. DeLong, Jr. and E. M. Hofstetter, "On the Design of Optimum Radar Waveforms for Clutter Rejection," IEEE Trans. Informat. Theory, Vol. IT-13, pp 454-463 (July 1967).

12. R. C. Emerson, "Some Pulse Doppler MTI and AMTI Techniques," Report 274, Rand Corp., p 104 (1 March 1954).

13. W. H. Drury, "Improved MTI Radar Signal Processor," Project Report ATC-39, Lincoln Laboratory, M.I.T. (3 April 1975).

14. P. B. McCorison, private communication.

15. K. D. Tschetter, "Coding Description of ARTS Implementation of Lincoln Laboratory Radar and Moving Target Detector," Report PX11136, Rev. A, Sperry Univac (February 1975).

16. R. M. Johnson, Design Data for ARTS Implementation of Lincoln Laboratory Radar and Moving Target Detector, Sperry Univac, PX10512, July 1975.

17. W. B. Davenport and W. L. Root, <u>An Introduction to the Theory of Random Signals and Noise</u>, McGraw Hill, (1958).

18. "Augmented Radar Beacon Tracking Level System Design Specification," Sperry Univac, Defense Systems Division, FAA-RD-74-169 (May 1974).

19. "ARTS-III Augmented Tracking-Study," Sperry Univac, Defense Systems Division, FAA-RD-73-27 (June 1972).

20. H. Moses, "Air Traffic Control Radar Systems Definition Report," FAA-OSEM, FAA-EM-72-1 (March 1972).

21. W. W. Shrader, "Radar Technology Applied to Air Traffic Control," IEEE Trans. on Comm., Vol. COM-21, No. 5, May 1973 (pp. 591-605).

22. P. E. Steichen, et al, "Radar Processing Subsystem of the All Digital Tracking Level System," Sperry Univac, Defense Systems Division, PX-10066, (February 1973).

23. A. V. Oppenheim and R. W. Schafer, <u>Digital Signal Processing</u>, Prentice Hall, (1975).

24. J. A. Cadzow, <u>Discrete Time Systems</u>, Prentice Hall (1973).

25. K. D. Tschetter, "Coding Description for Reduction of MTD Raw Data and MTD/RDAS System Data," Sperry Univac, Defense Systems Division, PX-11135 (February 1975).

26. "ATC Surveillance/Communications Analysis and Planning," Quarterly Technical Summary, FAA-RD-73-75, MIT Lincoln Laboratory, (1 March 1973), pp. 10-15.

27. R. M. O'Donnell, (Private Communication, 1975).

28. E. Peters, MIT Lincoln Laboratory (Private Communication, 1975).

29. L. V. Blake in "Radar Handbook", M. I. Skolnik Editor, McGraw Hill, New York 1970, Sec. 2.4 and 2.6.

30. R. Manasse, "The Application of the Theory of Signal Detectability to Signals with Unknown Polarization and Phase," MIT Lincoln Laboratory Group Report 32-25, 20 August 1956.

31. D. K. Barton, <u>Radar Systems Analysis</u>, Prentice Hall,,.Inc., (1964).

32. "Static Radar Cross-Section of Light Aircraft," Report No. AFSWC-TR-73-46, Radar Target Scatter Division, 6585th. Test Group, Holloman AFB, New Mexico, (December 1973).

33. D. Turnbull in Appendix B ta "Radar Enhancement of Small Aircraft in the Air Traffic Control Sy FAA Report FAA-RD-75-98 (September 1975).

34. P. R. Bevington, "Data Reduction & Error Analysis for the Physical Sciences". (McGraw Hill Book Co. 1969).

35. T. M. Hendricks, private communication.

36. M. A. Schwartz, private communication.

37. How to Use the Nova Computers, Data General Corporation, Southboro, MA (October 1972).

38. B. G. Laird and P. R. Kretz, private communication.

39. C. E. Muehe, (Private Communication, 1974).

40. L. Cartledge, (Private Communication, 1974).